PB96-128087

NATIONAL CENTER FOR EARTHQUAKE ENGINEERING RESEARCH
State University of New York at Buffalo

Experimental and Analytical Investigation of Seismic Retrofit of Structures with Supplemental Damping: Part II - Friction Devices

by

C. Li and A.M. Reinhorn

State University of New York at Buffalo
Department of Civil Engineering
Buffalo, New York 14260

Technical Report NCEER-95-0009

July 6, 1995

This research was conducted at the State University of New York at Buffalo and was partially supported by the National Science Foundation under Grant No. BCS 90-25010 and the New York State Science and Technology Foundation under Grant No. NEC-91029.

50272-101

PB96-128087

REPORT DOCUMENTATION PAGE	1. REPORT NO. NCEER-95-0009	2.	3.

4. Title and Subtitle Experimental and Analytical Investigation of Seismic Retrofit of Structures with Supplemental Damping: Part II - Friction Devices	5. Report Date July 6, 1995
	6.
7. Author(s) C. Li and A.M. Reinhorn	8. Performing Organization Rept. No.
9. Performing Organization Name and Address State University of New York at Buffalo Department of Civil Engineering Buffalo, New York 14260	10. Project/Task/Work Unit No.
	11. Contract(C) or Grant(G) No. (C) BCS 90-25010 (G) NEC-91029
12. Sponsoring Organization Name and Address National Center for Earthquake Engineering Research State University of New York at Buffalo Red Jacket Quadrangle Buffalo, NY 14261	13. Type of Report & Period Covered Technical Report
	14.

15. Supplementary Notes This research was conducted at the State University of New York at Buffalo and was partially supported by the National Science Foundation under Grant No. BCS 90-25010 and the New York State Science and Technology Foundation under Grant No. NEC-91029.

16. Abstract (Limit: 200 words)

This is the second in a series of NCEER technical reports by the authors addressing capabilities and limitations of passive energy dissipation systems through performance comparative studies. Friction devices are considered in this report through a combined experimental and analytical study. The 1:3 scale reinforced concrete frame, the same one used in the first study, was again used for experimental verification. The results show that the retrofit of reinforced concrete structures with friction damping devices can produce satisfactory seismic response. The damping enhancement contributes to the reduction of maximum deformations and only slightly modifies the structural forces transmitted to the foundation.

17. Document Analysis a. Descriptors

b. Identifiers/Open-Ended Terms

Earthquake engineering. Retrofitting. Passive control systems. Energy dissipation. Friction damping devices. Reinforced concrete frames. Shaking table tests. Analytical models. Added damping.

c. COSATI Field/Group

18. Availability Statement	19. Security Class (This Report)	21. No. of Pages
Release Unlimited	Unclassified	240
	20. Security Class (This Page) Unclassified	22. Price

(See ANSI-Z39.18) *See Instructions on Reverse* **OPTIONAL FORM 272** (4-77) (Formerly NTIS-35) Department of Commerce

Experimental and Analytical Investigation of Seismic Retrofit of Structures with Supplemental Damping:

Part II - Friction Devices

by

C. Li[1] and A.M. Reinhorn[2]

July 6, 1995

Technical Report NCEER-95-0009

NCEER Task Numbers 92-3105, 93-3101B and 93-5113

NSF Master Contract Number BCS 90-25010
and
NYSSTF Grant Number NEC-91029

1 Structural Engineer, LoBuono, Armstrong & Associates, a Division of Frederic Harris, Inc., Sacramento, California; formerly Graduate Research Assistant, Department of Civil Engineering, State University of New York at Buffalo
2 Professor, Department of Civil Engineering, State University of New York at Buffalo

NATIONAL CENTER FOR EARTHQUAKE ENGINEERING RESEARCH
State University of New York at Buffalo
Red Jacket Quadrangle, Buffalo, NY 14261

PREFACE

The National Center for Earthquake Engineering Research (NCEER) was established to expand and disseminate knowledge about earthquakes, improve earthquake-resistant design, and implement seismic hazard mitigation procedures to minimize loss of lives and property. The emphasis is on structures in the eastern and central United States and lifelines throughout the country that are found in zones of low, moderate, and high seismicity.

NCEER's research and implementation plan in years six through ten (1991-1996) comprises four interlocked elements, as shown in the figure below. Element I, Basic Research, is carried out to support projects in the Applied Research area. Element II, Applied Research, is the major focus of work for years six through ten. Element III, Demonstration Projects, have been planned to support Applied Research projects, and will be either case studies or regional studies. Element IV, Implementation, will result from activity in the four Applied Research projects, and from Demonstration Projects.

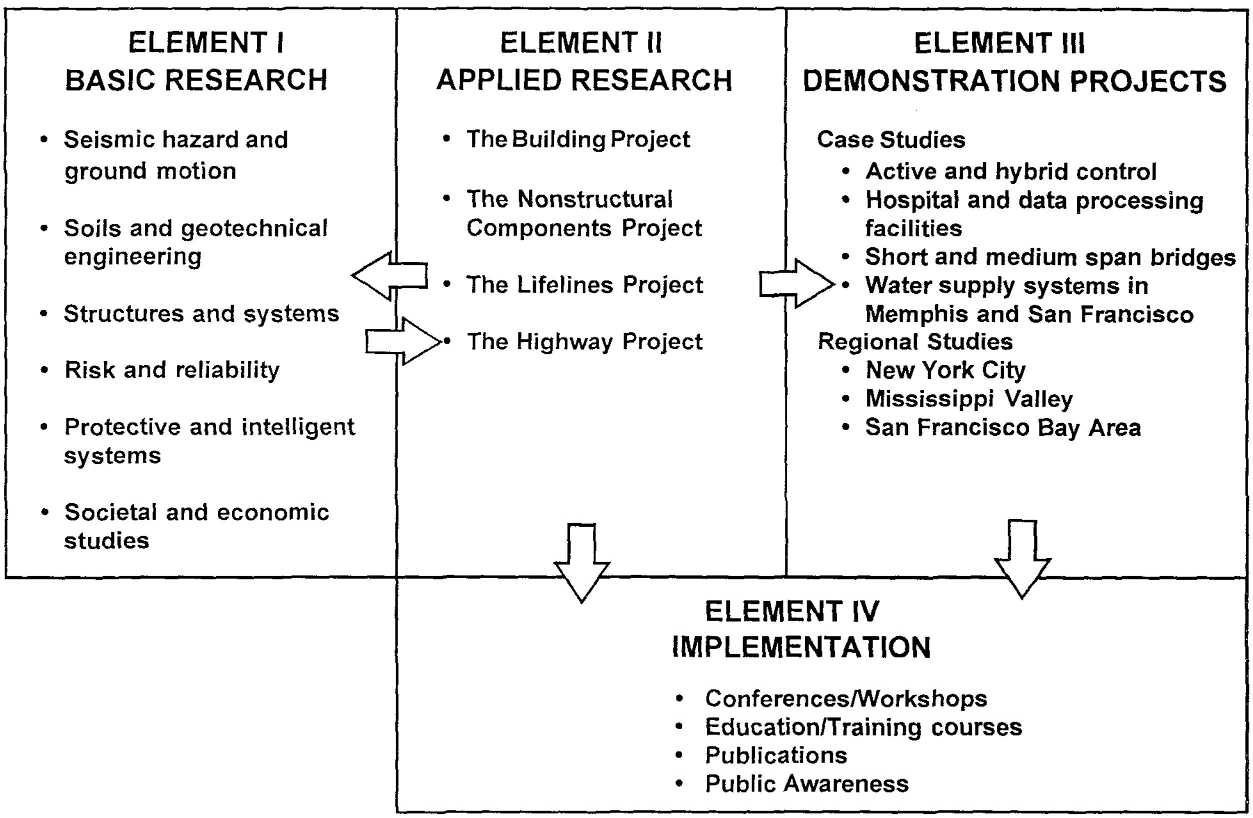

Research in the **Building Project** focuses on the evaluation and retrofit of buildings in regions of moderate seismicity. Emphasis is on lightly reinforced concrete buildings, steel semi-rigid frames, and masonry walls or infills. The research involves small- and medium-scale shake table tests and full-scale component tests at several institutions. In a parallel effort, analytical models and computer programs are being developed to aid in the prediction of the response of these buildings to various types of ground motion.

Two of the short-term products of the **Building Project** will be a monograph on the evaluation of lightly reinforced concrete buildings and a state-of-the-art report on unreinforced masonry.

The **protective and intelligent systems program** constitutes one of the important areas of research in the **Building Project**. Current tasks include the following:

1. Evaluate the performance of full-scale active bracing and active mass dampers already in place in terms of performance, power requirements, maintenance, reliability and cost.
2. Compare passive and active control strategies in terms of structural type, degree of effectiveness, cost and long-term reliability.
3. Perform fundamental studies of hybrid control.
4. Develop and test hybrid control systems.

This is the second in a series of NCEER technical reports by the authors addressing capabilities and limitations of passive energy dissipation systems through performance comparative studies. Friction devices are considered in this report through a combined experimental and analytical study. The 1:3 scale reinforced concrete frame, the same one used in the first study, was again used for experimental verification. The results show that the retrofit of reinforced concrete structures with friction damping devices can produce satisfactory seismic response. The damping enhancement contributes to the reduction of maximum deformations and only slightly modifies the structural forces transmitted to the foundation.

ABSTRACT

The need for structures which function more reliably without damage during severe earthquakes was reemphasized by the behavior of structures during recent earthquakes (Loma Prieta 1989, Northridge 1994, Kobe 1995, etc). The existing structures and often new ones must rely on large inelastic deformations in hysteretic behavior to dissipate the motion's energy, while the capacity to sustain such deformations is limited by previous non-ductile design or limitations of materials. An alternative method to reduce the demand of energy dissipation in the gravity load carrying elements of structures is the addition of damping devices. These devices dissipate most energy through heat transfer and reduce the deformation demands. In inelastic structures the supplemental damping mechanism reduces primarily deformations with small changes in the strength demand. The main benefit of added damping in the inelastic structures is the reduction of the demand for energy dissipation in the gravity load carrying structural members, thus reducing the deterioration of their low cycle fatigue capacity.

An experimental investigation of different damping devices was carried out individually to allow for physical and mathematical modeling of their behavior. A series of shaking table tests of a 1:3 scale reinforced concrete frame incorporating these devices were performed after the frame was damaged by prior severe (simulated) earthquakes.

Several different damping devices were used in this study: (a) viscoelastic, (b) fluid viscous, (c) friction (of two types) and (d) fluid viscous walls. An analytical platform for evaluation of structures integrating such devices was developed and incorporated in IDARC Version 3.2 (Kunnath and Reinhorn, 1994). The experimental and analytical

study shows that the dampers can reduce inelastic deformation demands and, moreover, reduce the damage, quantified by an index monitoring permanent deformations. The structures with friction dampers are able to shift their structural frequencies and increase the energy dissipation with the increase of earthquake intensity to survive a strong earthquake. The general structure's force response is mostly reduced or minimally increased due to the effects of both damping and stiffening. An evaluation of efficiency of dampers using a simplified pushover analysis method was investigated as an alternative method for prediction of structural behavior and design.

This report, second in a series, presents the evaluation of *friction dampers* used as additional braces in reinforced concrete frame structures.

ACKNOWLEDGMENTS

Financial support for this project has been provided by the National Center for Earthquake Engineering Research (Project 923105, 933101B and 935101A). The authors wish to express their gratitude to Tekton Company, Phoenix, Arizona, which manufactured and donated the dampers used in the experiments. Special thanks are given to Mr. Zoltan Kemeny, Senior Engineer of Tekton Company for his invaluable assistances.

The authors wish to acknowledge the dedicated assistance of Mr. Mark Pitman, head of simulation facility, Mr. Dan Walch and Mr. Richard Cizdziel, the senior laboratory technician and the students who took park in the experimental work.

TABLE OF CONTENTS

TABLE OF CONTENTS (cont'd)

TABLE OF CONTENTS (cont'd)

LIST OF ILLUSTRATIONS

LIST OF ILLUSTRATIONS (cont'd)

LIST OF ILLUSTRATIONS (cont'd)

LIST OF ILLUSTRATIONS (cont'd)

LIST OF ILLUSTRATIONS (cont'd)

LIST OF ILLUSTRATIONS (cont'd)

SECTION 1

INTRODUCTION

Many reinforced concrete frame structures, designed according to old standards have deficient nonductile details that make them vulnerable to future seismic events. Based on conventional seismic design practice, a structure is capable to survive a severe earthquake without collapse at the expense of allowing inelastic action in specially detailed critical regions of gravity load carrying members such as columns and beams near or adjacent to the beam-column joints. Inelastic behavior in these regions, though able to dissipate substantial energy, often results in significant damage to the structural members. The inter-story drifts required to achieve significant hysteretic energy dissipation in critical regions are large and usually result in permanent deformations and substantial damage to non-structural elements such as infill walls, partitions, doorways, and ceilings.

An innovative approach for earthquake hazard mitigation was introduced by adding protective devices, non-load bearing, to redistribute the energy within the structure. During a seismic event, the finite energy input is transformed partially into kinetic (movement) and potential (stored) energy and partially dissipated through structure is inherent damping (heat) and through hysteresis in gravity load carrying elements experiencing inelastic deformations. This last energy component, i.e. the hysteretic, is responsible for reducing the structure capacity of carrying gravity loads and its lateral strength or deformation capacities, thus increasing the demand-capacity ratios near collapse. The structural performance can be improved if the total energy input is reduced, or a substantial amount can be dissipated by supplemental damping devices (non-gravity load bearing), and not by the gravity load bearing structural members.

The energy balance equation (Uang and Bertero 1990) can be readjusted to include the effect of damping devices:

$$E_I = E_K + E_S + E_D + E_H + E_{SD} \qquad (1\text{-}1)$$

where $E_I (= \int (m\ddot{u}_t) d\ddot{u}_g)$ is the total input energy, $E_K (= m(\dot{u}_t)^2 / 2)$ is the 'absolute' kinetic energy, $E_S (= (f_s)^2 / 2k)$ is the elastic strain energy in the structure, $E_D (= \int c\dot{u}^2 dt)$ is energy dissipated through structural damping, E_H is the total hysteretic energy dissipated in the structure and E_{SD} is the energy dissipated by supplemental damping devices.

The total absolute energy input, E_I , is the work done by the base shear over the foundation ground movement. This energy contains the inertial forces in the structure, including the response amplifications.

In absence of supplemental damping, the inelastic response and the hysteretic energy demand increase. However, besides the negative effect of increased damage in the structural members, associated with the hysteretic energy dissipation, this increase has a positive effect in softening the structure, thus reducing the inertia forces and the total energy input. This effect is on the base of current seismic design provision which allow for inelastic response. Both energy input reduction and reduction of hysteretic energy demand (thus reducing damage) can be obtained through modern protective devices. The recently developed seismic base isolation (Buckle 1990, Kelly 1991, Mokha et al. 1991) accomplishes the task of reducing the total energy input by filtering the input motion into the structure at its base and by dissipating part of this energy at same location through local damping. The reduction of the energy input reduces the demand for energy dissipation through inelastic action and hysteretic excursions. In most cases inelastic action in the superstructure is avoided completely.

More recently developed devices accomplish redistribution of internal energy, or reduce substantially the total energy input, through active means, such as dampers or active braces (Soong 1990, Reinhorn 1992). These devices, incorporated in complex control systems, act based on "real time" processed information from sensors, which anticipate the further structural movements. Although such systems are extremely efficient in small structures they require additional energy, sometimes unreliable or expensive, in order to produce the energy redistribution in large structures.

Another approach to improve performance and damage control through altering the energy distribution are supplemental damping devices. These mechanical devices are incorporated in the frame of structure and dissipate energy throughout its height. These devices dissipate energy by either yield of mild steel, sliding friction, viscoelastic action in polymeric materials, piston or plate movement within fluid, or fluid transfer through orifices. These systems are the subject of the current research.

1.1 Viscoelastic devices

Viscoelastic dampers, made of bonded viscoelastic layers (acrylic polymers) have been developed by 3M Company Inc. and were used in wind and seismic applications. Examples are the World Trade Center in New York City (110 stories), Columbia SeeFirst Building in Seattle (73 stories), the Number Two Union Square Building in Seattle (60 stories), and General Service Administration Building in San Jose (13 stories). A two-story new school building in Phoenix, Arizona has been constructed in 1992 with its beam to column connections incorporating viscoelastic materials as shown in Fig. 1-1.

The characteristics and suitability of viscoelastic dampers to enhance performance of structures were studied by Lin et al. 1988, Aiken et al. 1990, Chang et al. 1991 and Lobo et al. 1993. Fig. 1-2 shows a typical damper and an installation detail in a steel structure.

The behavior of viscoelastic dampers is controlled by the shear of viscoelastic layers. The acrylic material exhibits solid viscoelastic behavior with storage and loss (stiffness) moduli dependent on frequency and temperature.

In the aforementioned studies, 3M Company's dampers were used. Other devices developed by Lorant Group were studied by Hsu, 1992. Hazama Corp. in Japan developed similar devices using similar materials (Fujita 1991). Shimizu Corporation

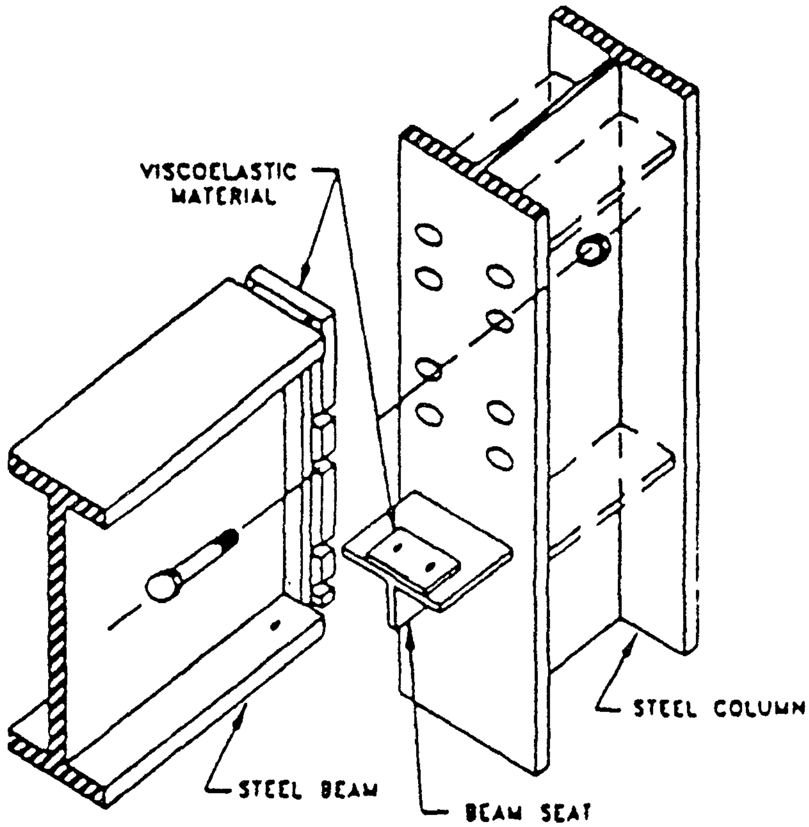

Figure 1-1 Detail of Beam to Column Connection with Viscoelstic Material

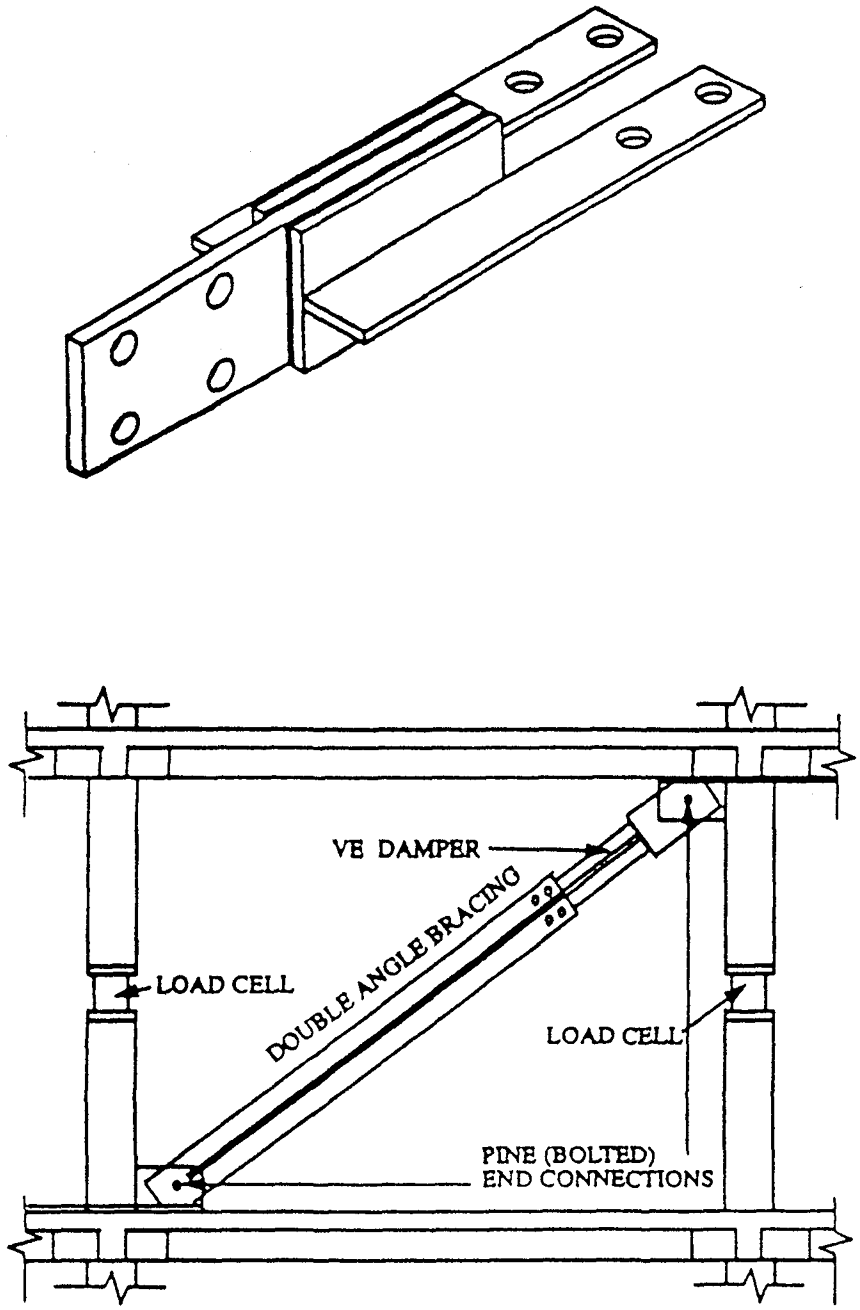

Figure 1-2 Viscoelastic Damper and Installation Detail

developed viscoelastic walls, in which solid thermoplastic rubber sheets are sandwiched between steel plates (Fujita 1991).

The use of dampers in elastic structures was proven efficient, in particular when the inherent damping of the structure is low (Aiken 1990). The use of dampers in inelastic structures, studied by Lobo et al. (1993), Wood et al. (1994) indicate that the viscoelastic material dissipates large amount of energy reducing the demand for hysteretic energy dissipation. In gravity load carrying components, the damping index (equivalent to critical damping in elastic structures) reaches 20% to 22%. However, the overall base shear in the structure has the tendency to increase or only minimally decrease in presence of dampers.

1.2 Viscous walls

Viscous damping walls, consisting of a plate floating in a thin case made of steel plates (the wall) filled with highly viscous fluid (see Fig. 1-3), have been developed by Sumitomo Construction Company, Ltd., and the Buildings Research Institute in Japan. The walls were investigated by Sumitomo Construction Company (Arima, 1988) and were already used in a 78.6 m high, 14 story building at the center of Shizuoka city, 150 km west of Tokyo, Japan. Earthquake simulator tests of a 5 story, reduced-scale building model and a 4-story, full-scale steel frame building embedding such walls have been carried out (Arima, 1988) and the most recently, a three story 1:3 scale reinforced concrete structure has been tested in Seismic Simulation Laboratory at the State

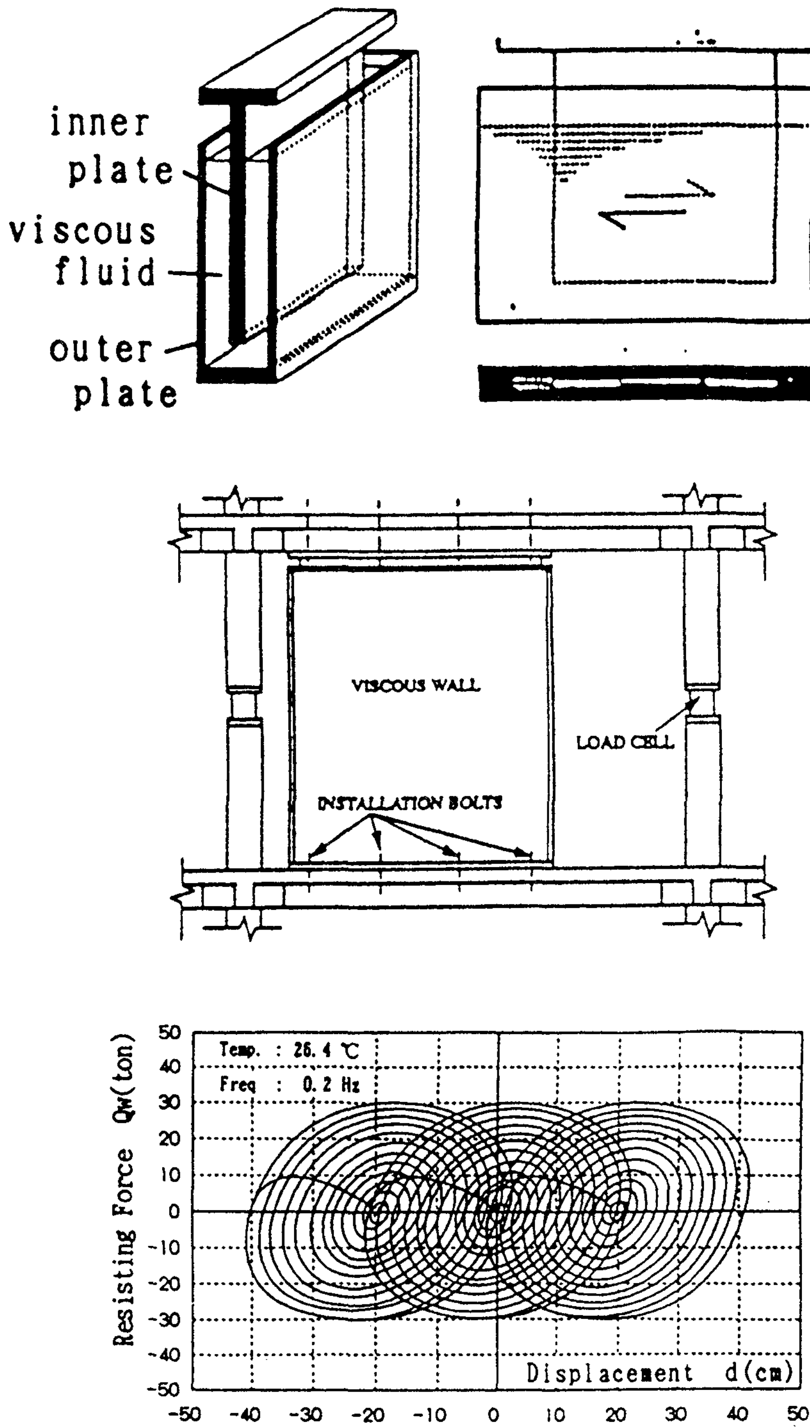

Figure 1-3 Viscous Wall, Installation Detail and Hysteresis Loops (from Miyazaki, 1992)

University of New York at Buffalo (Reinhorn et al. 1994). The devices exhibit nonlinear viscous behavior with stiffening characteristics at high frequencies.

1.3 Fluid Viscous Dampers

Fluid viscous dampers have been used in military for many years because of their efficiency and longevity. This kind of devices operates on the principle of fluid flow through orifices. The construction of this kind of dampers is shown in Fig. 1-4 and the typical force-displacement relationship from test is shown in Fig. 1-5.

The first production usage of a hydraulic damper was in the 75 mm French artillery rifle of 1897. The damper was used to reduce recoil forces and had a stroke of over 18 inches. The modern fluid damping devices are just beginning to emerge in large scale structural construction in recent years. The device possesses linear or nonlinear viscous behavior upon design and is relatively insensitive to temperature changes. The force in a fluid damper may be expressed as:

$$P = C|\dot{u}|^{\alpha} \operatorname{sgn}(\dot{u}) \quad \text{(1-2)}$$

The size of the device is very compact in comparison to force capacity and stroke. Experimental and analytical studies of buildings and bridge structures incorporating the damping devices fabricated by Taylor Devices, Inc., have recently been performed (Constantinou et al. 1993, Reinhorn et al. 1995). Very large reductions of elastic response

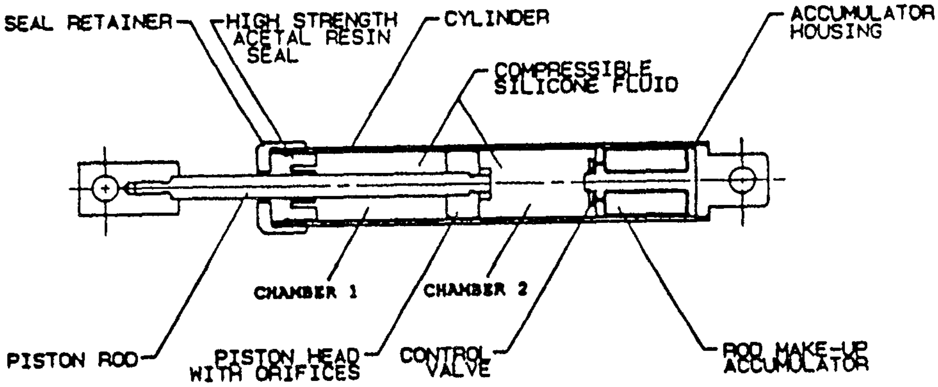

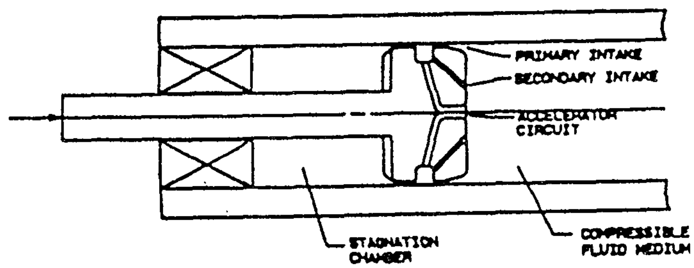

Fluidic Control Orifice

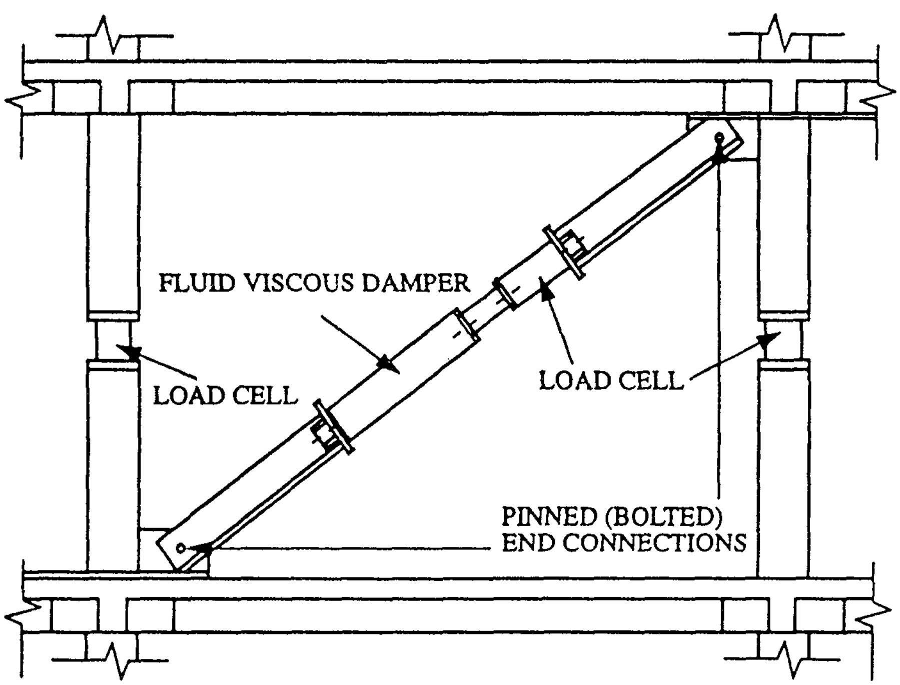

Figure 1-4 Fluid Viscous Damper Construction and Installation Detail

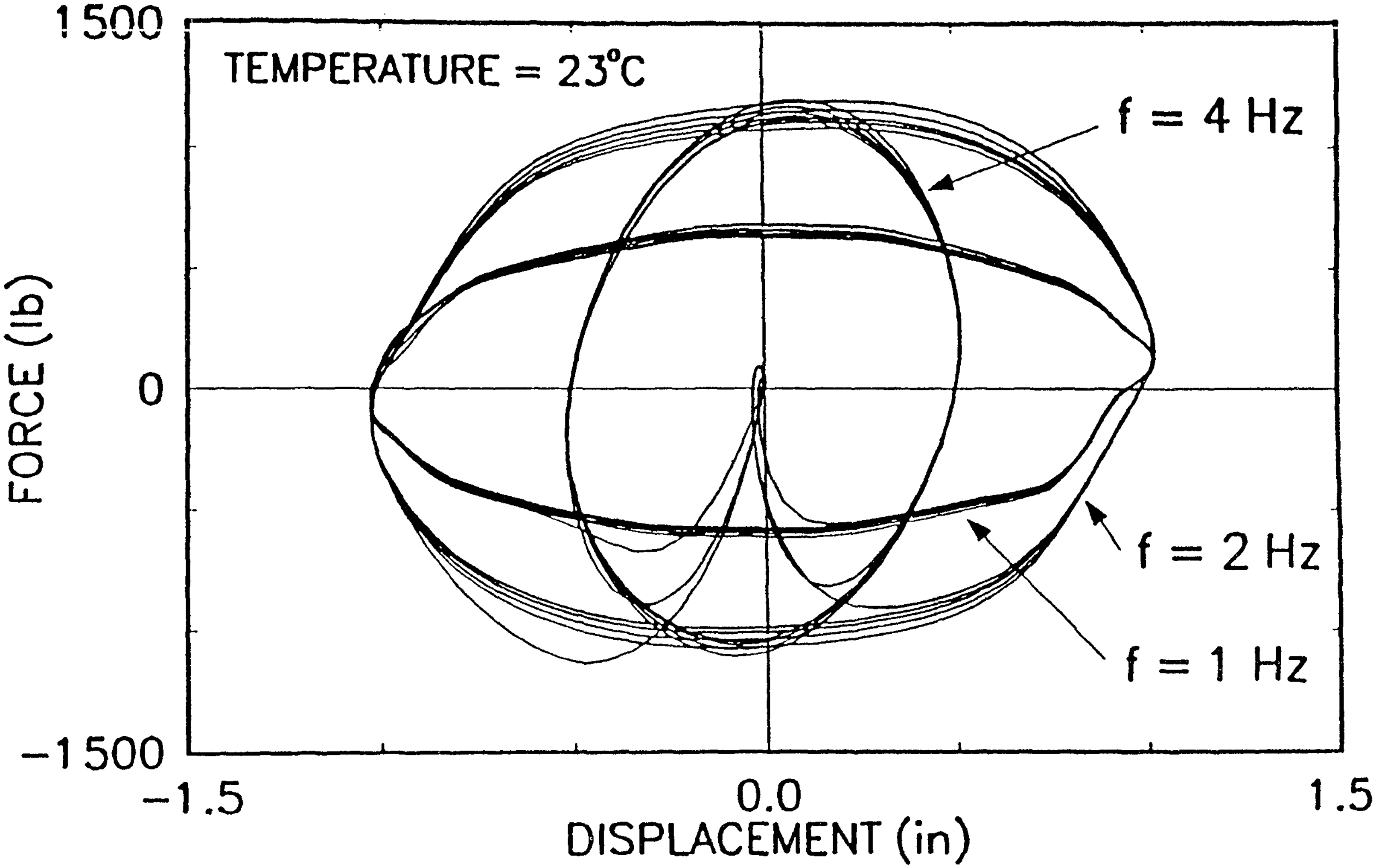

Figure 1-5 Typical Hysteresis Loops of Fluid Viscous Damper

were achieved by the introduction of these devices. The feature of a pure viscous damper that the damping force is out-of-phase with the displacement can be a particularly desirable attribute for passive damping applications to buildings. The Travelers Hotel, a landmark hotel built in the 1920's in Sacramento, California, has been designed with fluid viscous dampers as part of its seismic retrofit scheme. Construction has not yet started.

Nonlinear viscous behavior can be achieved through specially shaped orifice to alter the flow characteristics with fluid speed. Fluid dampers with nonlinear characteristics have been adopted in a number of projects in U.S. recently. The San Bernardino County Medical Center in California is a five building isolated complex utilizing 400 high damping rubber bearings and 233 nonlinear viscous dampers with α=0.5. Furthermore, studies for the seismic retrofit of the suspended part of the Golden Gate bridge in San Francisco concluded that the use of fluid dampers with α=0.75 produce the desired performance (Rodriquez 1994).

1.4 Hysteretic Devices

Hysteretic devices are devices which can dissipate energy through inelastic deformations of their components or friction within their parts or properly designed surfaces.

1.4.1 Friction Devices

There are a variety of friction devices which have been proposed for structural energy dissipation. Usually friction systems generate rectangular hysteresis loops characteristics of Coulomb friction. Typically these devices have very good performance characteristics. and their behavior is not significantly affected by load amplitude, frequency, or the number of applied load cycles. The devices differ in their mechanical complexity and the materials used for the sliding surfaces.

A friction device located at the intersection of cross bracing has been proposed by Pall (1982, 1987) and used in six building in Canada. Fig. 1-6 illustrates the design of this device. When seismic load is applied the interior deforms into a parallelogram and friction is produced at the bolts location. Experimental studies by Filiatrault (1985) and Aiken (1988) confirmed that these friction devices could enhance the seismic performance of structures. The devices provided a substantial increase in energy dissipation capacity and reduced drifts in comparison to moment resisting frames. Reduction in story shear forces were moderate in inelastic structures. However, these forces are primarily resisted by the braces in a controlled manner and only indirectly resisted by the primary structural elements.

Friction devices have been developed and manufactured for many years by Sumitomo Metal Ltd., Japan. The original application of these devices was in railway rolling stock bogie trucks. It is only since the mid of 1980's that the friction dampers have

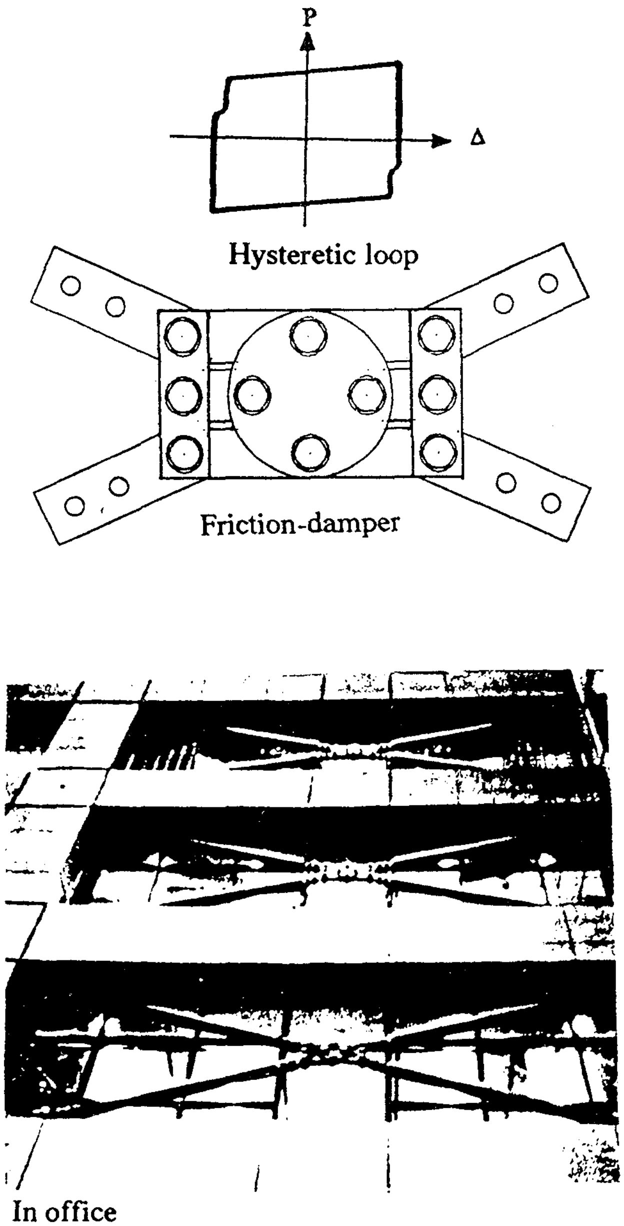

Figure 1-6 Pall Friction Damper, Typical Hysteretic Loop and Application

been extended to the field of structural and seismic engineering. A detailed description of this kind of devices is presented in Section 2.

Recently, a similar type of friction dampers, manufactured by Tekton company, Arizona, was tested in the Seismic Simulation Laboratory at the State University of New York at Buffalo. This type of dampers is made of simple components similar to those by Constantinou and Reinhorn et al. (1991) designed to minimize the cost of manufacturing. The "yielding" force of the damper, i.e. the friction level, can be adjusted through the appropriate torque of bolts that control the pressure on the friction surfaces. A detailed description of this kind of devices is presented in Section 2.

Friction dampers were suggested as displacement control devices for bridge structure with sliding supports (Constantinou, Reinhorn, et al. 1991a, 1991b) made of steel-bronze surface (see Fig. 1-7). The devices can be adjusted to provide a desirable level of resistance and stable energy dissipation in numerous cycles.

Another friction device, proposed by Fitzgerald (1989), utilize slotted bolted connections (SBCs) in concentrically braced connections. Slotted Bolted Connections are modified bolted connections designed to dissipate energy through friction in rectilinear tension and compression loading cycles. Components tests demonstrated stable friction behavior. It may be noted that the sliding interface is that of steel on steel. Very recently Grigorian (1993) tested a slotted bolted connection (see Fig. 1-8) which was nearly identical to the one Fitzgerald (1989) expect for the sliding interface which consisted of

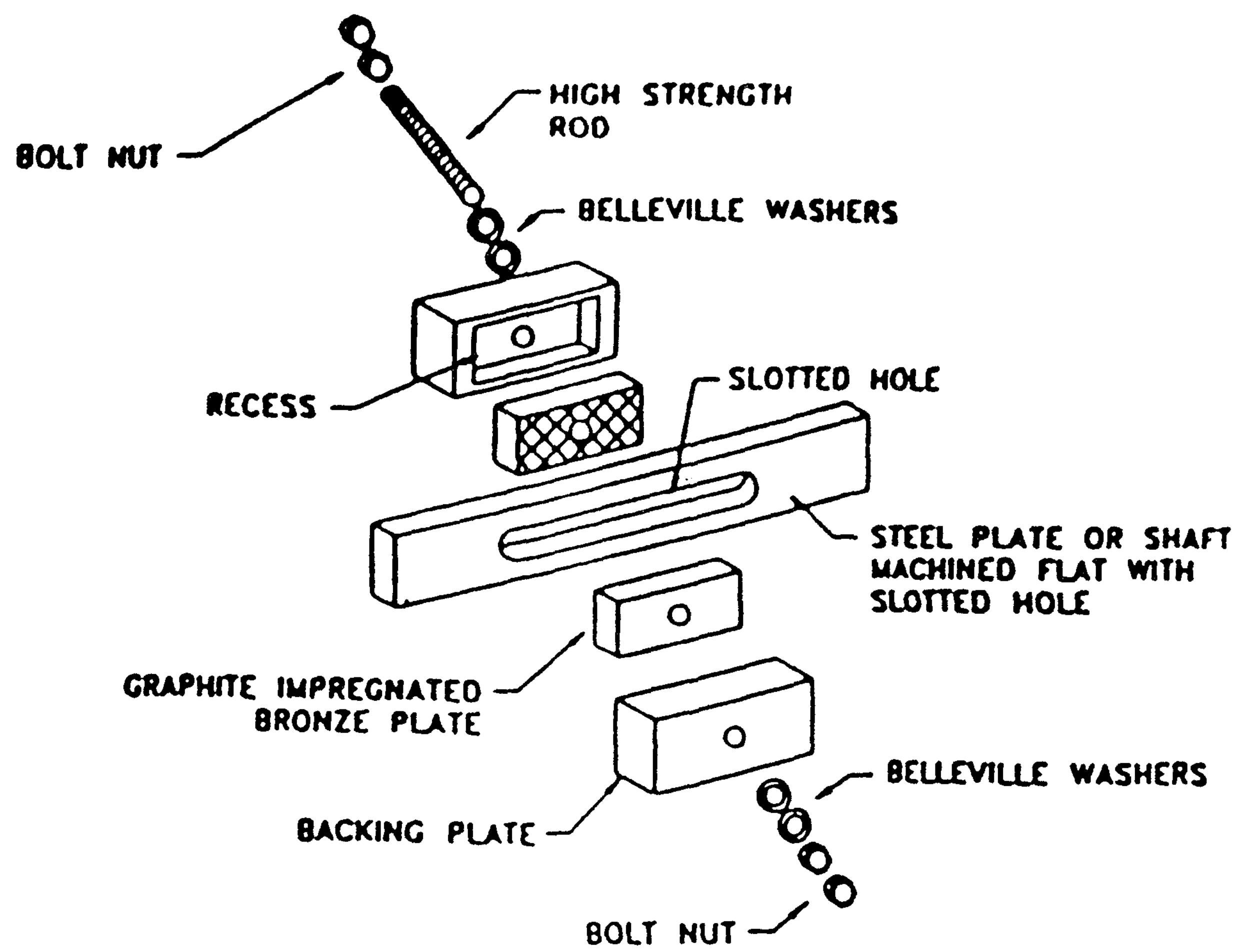

Figure 1-7 Detail of Displacement Controller

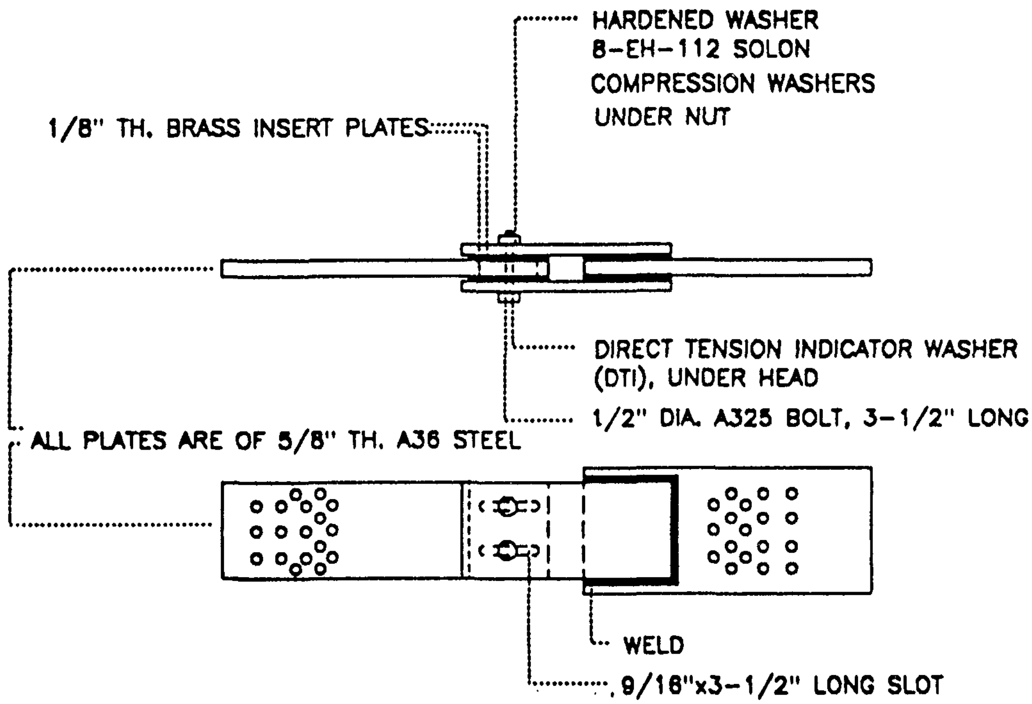

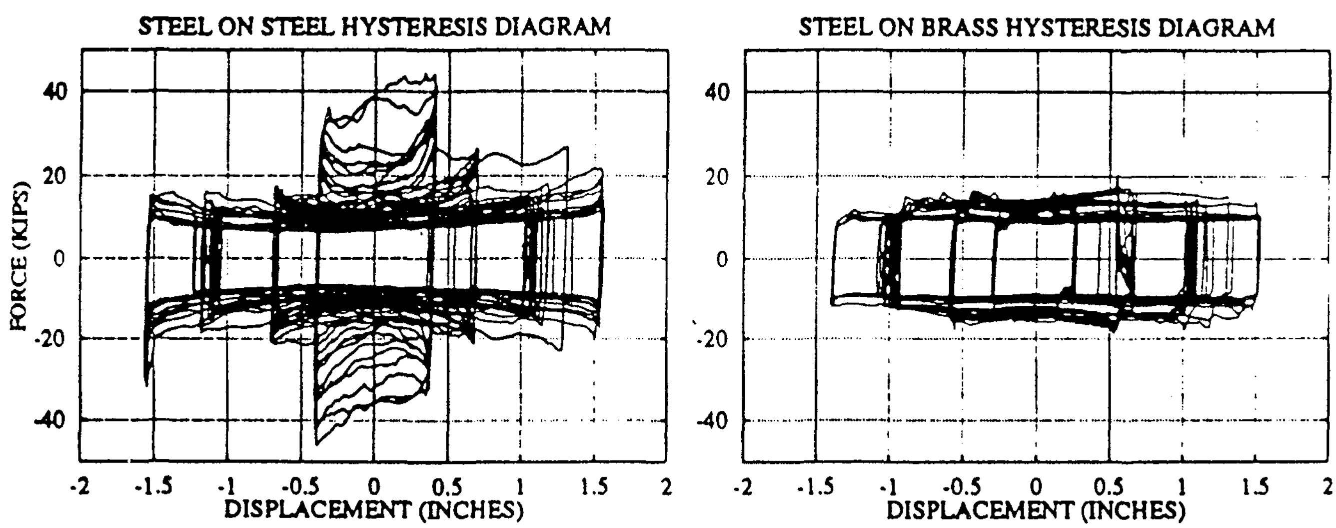

Figure 1-8 Detail of a Slotted Bolted Connection and Hysteresis Behavior

brass in contact with steel. This interface exhibits more stable frictional characteristics than the steel on steel interface.

A more complex friction device (Energy Dissipation Restrain, EDR) combined with self centering capabilities provided by internal springs and end gaps (see Fig. 1-9) was developed by Flour Daniel Corp. (Nims, 1993). This device can develop X type hysteretic loops with restoring capabilities.

All the friction devices described above utilize sliding interfaces consisting of steel-on-steel, brass on steel, graphite impregnated bronze on stainless steel. The composition of the interface is of extraordinary importance for insuring longevity of operation of these devices. Low carbon alloy steels (common steels) will corrode and the interface properties will change with time. Moreover, brass or bronze promote additional corrosion when it is in contact with low carbon steels (BSI, 1979). Only authentic stainless steels with high chromium content do not suffer additional corrosion in contact with brass or steel and could be usedfor long term operation. At the same time Telflon PTFE and steel interface are inert to reciprocal corrosion and have long term stable properties. Moreover, those interfaces have lower friction coefficient and require larger pressure on the interfaces (Tsopelas 1994).

1.4.2 Elastomeric Spring Dampers

A type of single-acting damper device used previously in the railroad and steel industries is studied recently by Pekcan et al. (1995) in the Seismic Simulation Laboratory at the State University of New York at Buffalo. These devices dampers which contain a

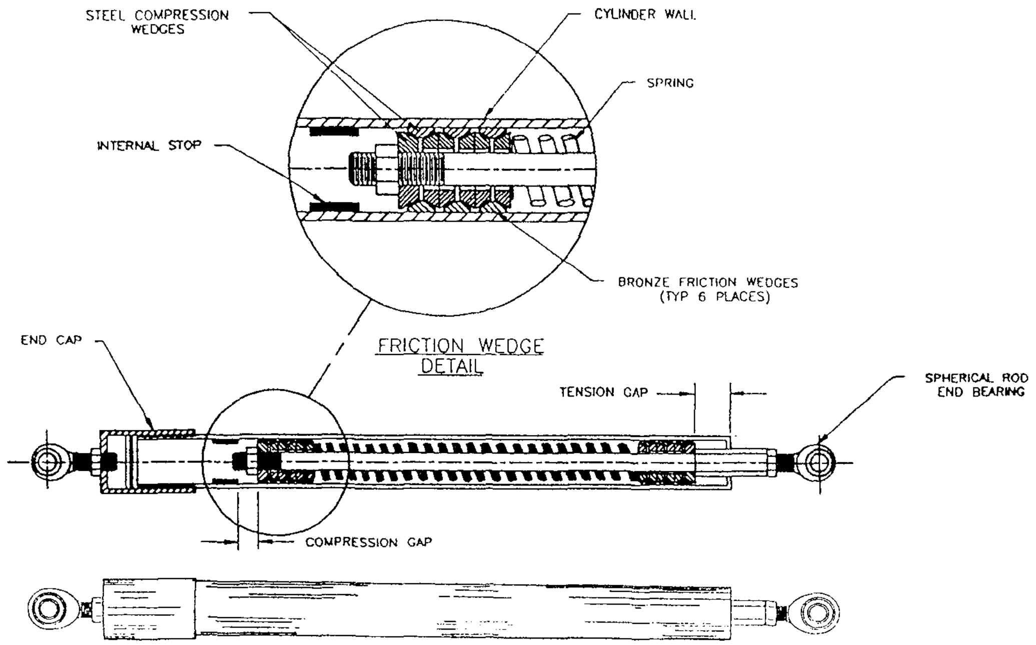

Figure 1 External and Internal Views of Energy Dissipating Restraint

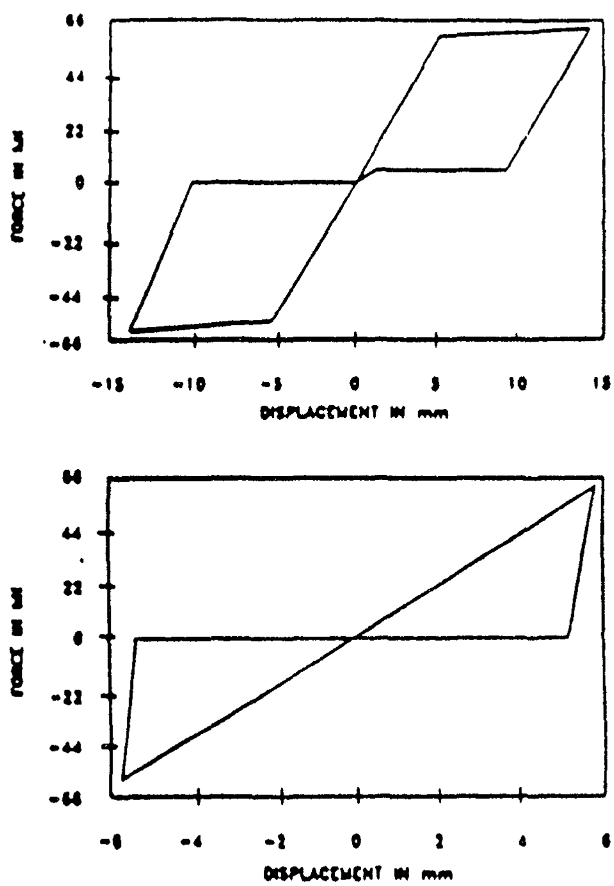

Figure 1-9 Energy Dissipating Restraint and Representative Force-Displacement Loops (from Nims 1993)

silicone-based elastomer, called elastomeric spring, were modified to operate in a double-acting fashion in the study. The dampers can be designed to give both spring and hysteretic behavior. Fig. 1-10 shows the physical arrangement of the double-acting damper and the typical hystereitc loops of the damper.

1.4.3 Metallic Systems

This category of energy dissipation systems takes advantage of the hysteretic behavior of mild steel when deform into their post-elastic range. A wide variety of different types of devices utilizing flexural, shear or extensional deformation mode into the inelastic range. A particularly desirable feature of these system is their stable behavior, long term reliability, and generally good resistance to environmental and temperature factors.

1.4.3.1 Yielding Steel Elements

The ability of mild steel to sustain many cycles of stable yielding behavior has led to the development of a wide variety of devices which utilize this behavior to dissipate seismic energy (Kelly et al. 1972, Skinner et al. 1980, Henry 1978, 1986, Tyler 1983, 1985). Many of these devices use mild steel plates with triangular or hourglass shapes (Tyler 1978, Stiemer et al. 1981) so that the yielding is spread almost uniformly throughout the material. This results in a device which is able to sustain repeated inelastic deformations in a stable manner, avoiding concentrations of yielding and premature failure and buckling of braces, hence, pinched hysteretic behavior does not occur. An energy absorbing device in the form of round mild steel rod with a rectangular shape (Fig.1-11)

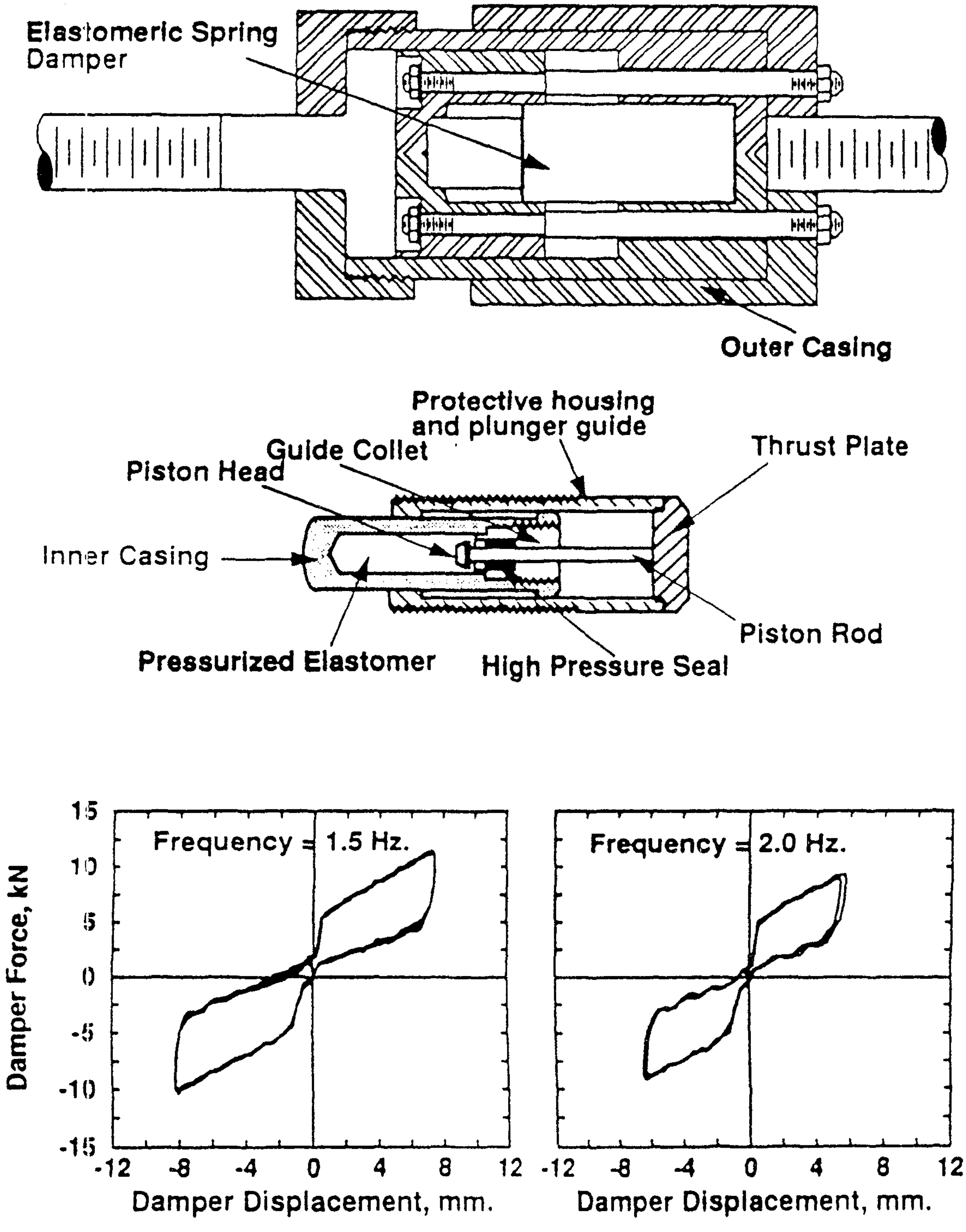

Figure 1-10 Elastomeric Spring Damper and Hysteresis Behavior

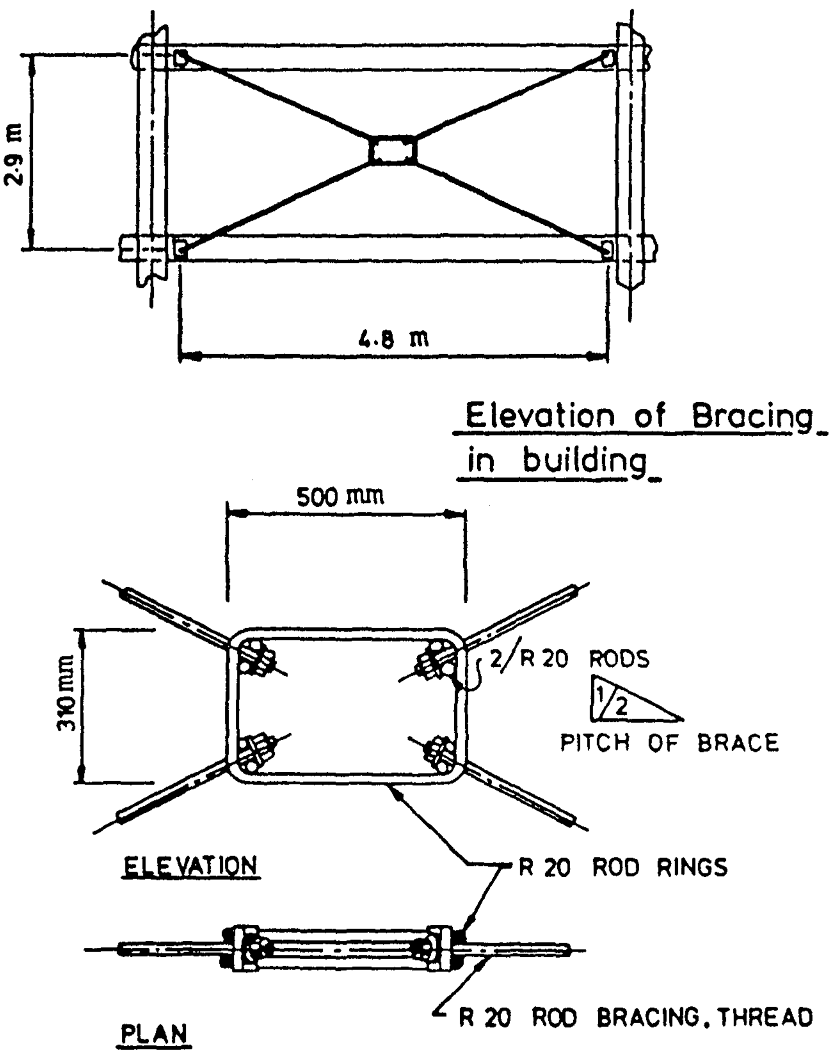

Figure 1-11 Detail of a Yielding Steel Bracing System in a Building in New Zealand

introduced at the intersection of cross bracing, have been developed in New Zealand (Tyler 1978, Skinner 1980). Some of these devices were tested on shaking table at U.C. Berkeley as parts of seismic systems (Kelly 1980). They have been incorporated in a number of buildings in New Zealand and similar ones were widely used in seismic isolation applications in Japan (Kelly 1988).

One such device that uses X-shaped steel plates is the Bechtel Added Damping and Stiffness (ADAS) devices. ADAS elements are an evolution of an earlier use of X-plates, as damping supports for piping systems (Stiemer, et al., 1981). Extensive experimental studies have investigated the behavior of individual ADAS elements and structural systems incorporating ADAS elements (Bergman and Goel, 1987, Whittaker, et al., 1991). The tests showed stable hysteretic performance (Fig. 1-12). ADAS devices had been installed in two bay-story, non-ductile reinforced-concrete building in San Francisco as a part of a seismic retrofit (Fiero et al. 1993), and in two building in Mexico City. The principal characteristics which affect the behavior of an ADAS devices are its elastic stiffness, yielding strength, and yield displacement. ADAS devices are usually mounted as part of a bracing system, which must be substantially stiffer than the surrounding structure elements. The introduction of such a heavy bracing system into a structure may be prohibitive.

Triangular-plate energy dissipaters were originally developed and used as the damping elements in several base isolation applications (Boardman et al. 1983). The triangular plate concept has been extended to building dampers in the form of triangular ADAS, or T-ADAS, element (Tsai and Hong 1992). Component tests of T-ADAS elements and pseudo-dynamic tests of a two-story frame have shown very good results (Fig. 1-13). The T-ADAS device embodies a number of desirable features: no rotational restraint is required at the top of the brace connection assemblage, and there is no potential for instability of the triangular plate due to excessive axial load in the devices.

An energy dissipater for cross-braced structures, which uses mild steel round bars or flat plates as the energy absorbing element, has been developed by (Tyler 1985). This concept has been applied to several industrial warehouses in New Zealand. A number of variations on the steel cross-bracing dissipater concept have been developed in Italy (Ciampi 1991). A 29-story steel suspension building (with floors "hung" from the central tower) in Naples, Italy, utilizes tapered steel devices as dissipaters between the core and the suspended floors.

A six-story government building in Wanganui, New Zealand, used steel-tube energy-absorbing devices in precased concrete cross-braced panels (Matthewson and Davey 1979). The devices were designed to yield axially at a given force level. Recent studies have experimentally and analytically investigated a number of different cladding connection concepts (Craig et al. 1992).

Several types of mild steel energy dissipaters have been developed in Japan (Kajima Corp. 1991, Kobori et al. 1988). So-called honeycomb dampers have been incorporated in 15-story and 29-story buildings in Tokyo. Honeycomb dampers are X-plates (either single plates, or multiple plates connected side by side) that are loaded in plane of the X. (This is orthogonal to the loading direction for triangular or ADAS X-plates). Kajima Corporation has also developed two types of omni-directional steel dampers, called "Bell" dampers and "Tsudumi" dampers (Kobori et al. 1988). The Bell damper is a single-tapered steel tube, and the Tsudumi damper is a double-tapered tube intended to deform in the same manner as an ADAS X-plate but in multiple direction. Bell dampers have been used in a massive 1600-ft long ski-slope structure to permit differential movement between four dissimilar parts of the structure under seismic loading while dissipating energy. Both of these applications are located in the Tokyo area.

Another type of joint damper for application between two buildings has been developed (Sakurai et al., 1992). The devices is a short lead tube that is loaded to deform in shear (Fig. 1-14). Experimental investigations and an analytical study have been undertaken.

Particular issues of importance with metallic devices are the appropriate post-yield deformation range, such that a sufficient number of cycles of deformation can be sustained without premature fatigue, and the stability of the hysteretic behavior under repeated post-elastic deformation.

1.4.3.2 Lead Extrusion Devices (LEDs)

The extrusion of lead was identified as an effective mechanism for energy dissipation in the 1970s (Robinson and Greenbank 1976). LED hysteretic behavior is very similar to that of many friction devices, being essentially rectangular (Fig. 1-9). LEDs have been applied to a number of structures, for increasing the damping in seismic isolation system, and as energy dissipaters within multi-story buildings, In Wellington,

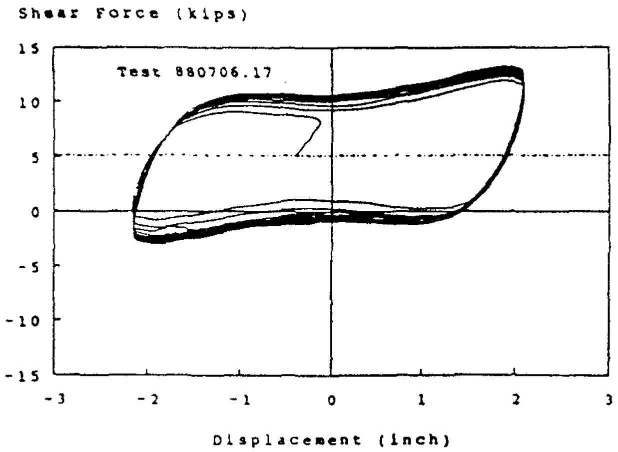

Figure 1-12 **ADAS Devices Hysteresis Loops (from Whittaker, 1991)**

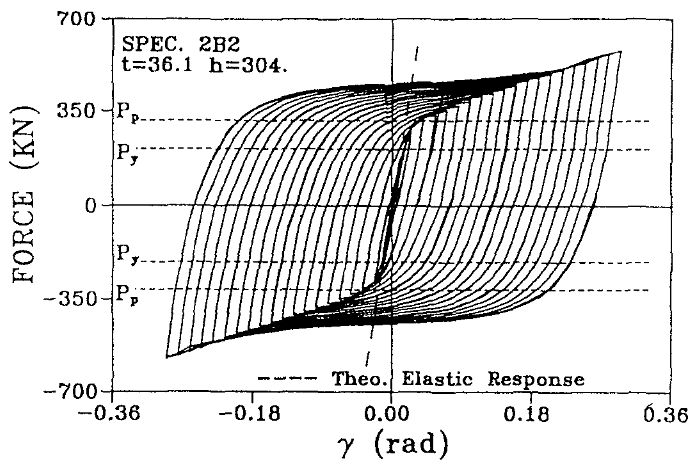

Figure 1-13 **T-ADAS Device Hysteresis Loops (from Tsai, 1992)**

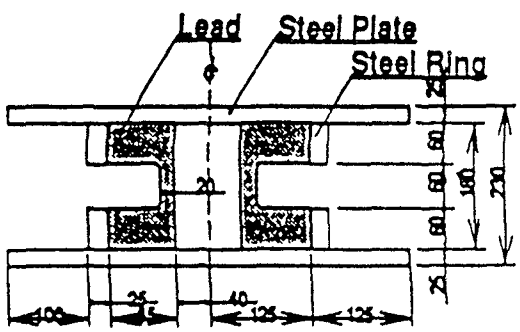

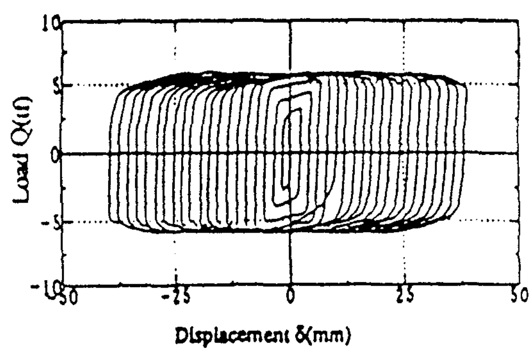

Figure 1-14 Lead Joint Damper and Hysteresis Loops (Sakurai, 1992)

New Zealand, a 10-story, cross -braced, concrete police station is base isolated, with sleeved-pile flexible elements and LED damping elements (Charleson et al. 1987). Several seismically-isolated bridges in New Zealand also utilize LEDs (Skinner et al. 1980). In Japan, LEDs have been incorporated in 17-story and 8-story steel frame buildings (Oiles Corp., 1991). The devices are connected between precased concrete wall panels and the surrounding structural frame.

LEDs have a number of particularly desirable features: their load-deformation relationship is stable and repeatable, being largely unaffected by the number of loading cycles; they are insensitive to environmental factors; and tests have demonstrated insignificant aging effects (Robinson and Cousins 1987) (Fig. 1-15).

1.4.3.3 Shape Memory Alloys (SMAs)

Shape memory alloys have the ability to "yield" repeatedly without sustaining any permanent deformation. This is because the material undergoes a reversible phase transformation as it deforms rather than intergranular dislocation, which is typical of steel. Thus, the applied load induce a crystal phase transformation, which is reversed when the load is removed (Fig. 1-16). This provides the potential for the development of simple devices which are self-centering and which perform repeatably for a large number of cycles.

Several earthquake simulator studies of structures with SMA energy dissipaters have been carried out. At the Earthquake Engineering Research Center of the University of California (Aiken et al. 1992), a 3-story steel model was tested with Nitinol (nickeltitanium) tension devices as part of a cross-bracing system, and at the National Center for Earthquake Engineering Research (Witting and Cozzarelli 1992), a 5-story steel model was tested with copper-zinc-aluminum modes were investigated. Typical hysteresis loops from these tests are shown in Fig. 1-17. Results showed that the SMA dissipaters were effective in reducing the seismic responses of the models.

1.4.3.4 Eccentrically Braced Frame (EBF)

Steel moment-resisting frames have been regarded by structural designers for their earthquake-resistant behavior. However moment-resisting frames tend to be flexible, braced frames are considered as a mean of providing increased structural stiffness. Although Concentrically Braced Frames (CBFs) can easily provide the needed stiffness, the cyclic inelastic behavior of concentrically braced frames is strongly influenced by the cyclic post-buckling behavior of individual braces (Popov et al. 1976). Eccentrically Braced Frames (EBFs) have emerged as a well recognized and widely used structural system for resisting lateral seismic forces. Hysteretic behavior is concentrated in specially designed regions (shear links) of EBF (see Fig. 1-18) and other structural elements are designed according to capacity design principle and intended to remain elastic under all but the most severe excitations. Extensive research has been devoted to EBF (Roeder et al. 1978, Popov et al. 1987, Whittaker et al. 1987) and the concept has seen rapid recognition and acceptance by the structural engineering profession since the inclusion of design rules into seismic code of practice. These braces are using, however, some parts of

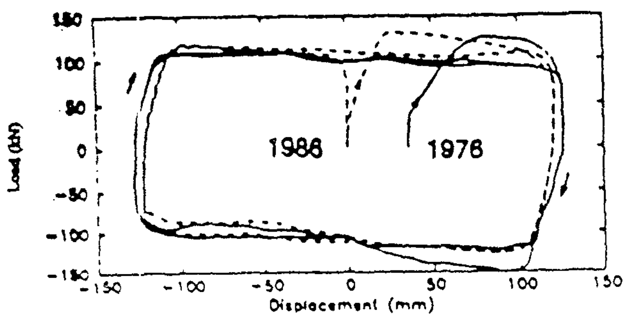

Figure 1-15 LED Hysteresis Loops
(from Robinson, 1987)

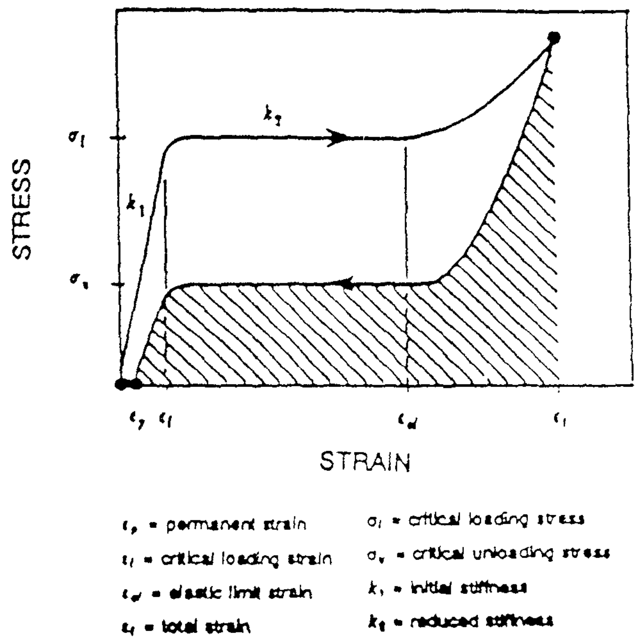

Figure 1-16 SMA Superelastic Hysteresis Behavior
(from Aiken, 1992)

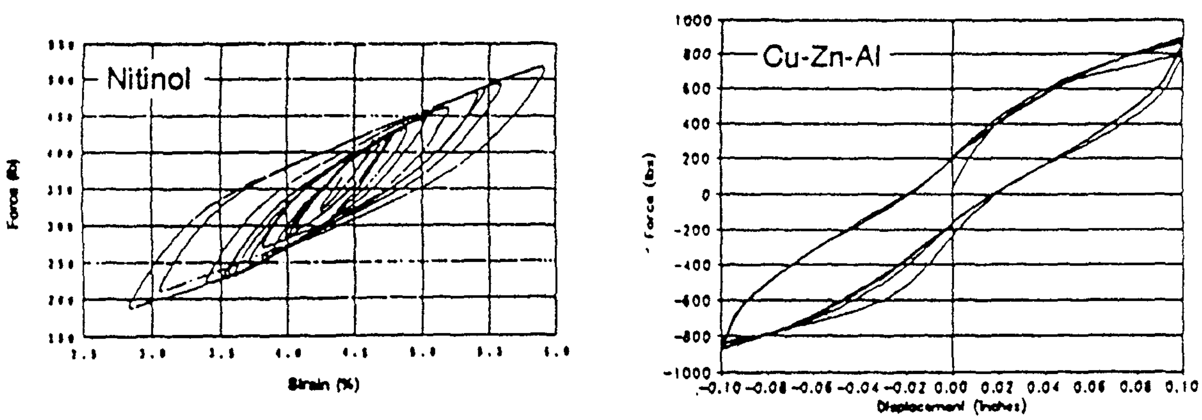

Figure 1-17 NiTi (Tension) and Cu-Zn-Al (Torsion) Hysteresis Loops
(from Aiken, 1992, Witting, 1992)

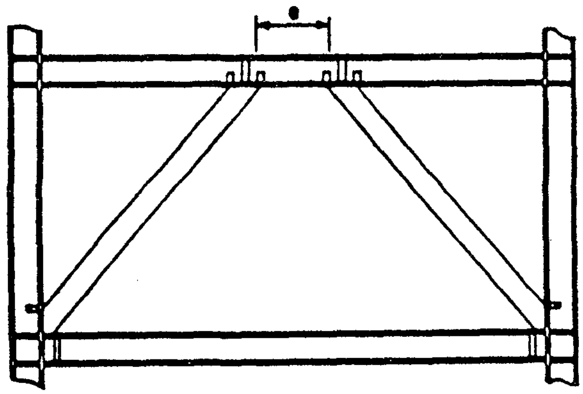

(a) Eccentric K-Brace

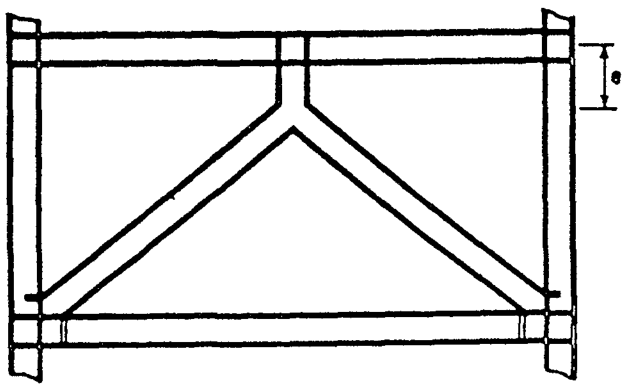

(b) Inverted Y-Brace

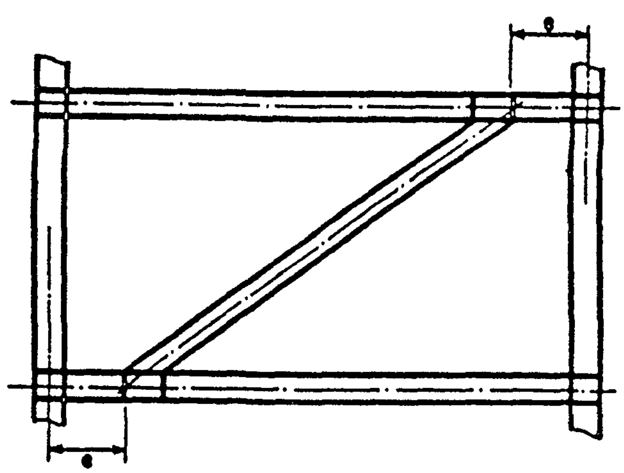

(c) Eccentric D-Brace

Figure 1-18 Different Kind of Eccentrically Braced Element

the gravity load resisting elements which might need to be sacrificed in severe earthquake with implication of substantial damage.

1.5 Code Provision for Design of Structures Incorporating Passive Energy Dissipating Devices

It is imperative for implementation of the technology of energy dissipating devices to have a code design specification. Currently, such code specifications for structures with damping braces do not exist. The absence of such code specification may prevent widespread use of the technology. The existing codes, such as UBC and SEAOC have included provision for design of base isolation systems. Many codes, such as NEHRP, UBC and SEAOC, have included design of EBFs in their provisions. Efforts are made by code agencies (FEMA, ATC, SEAOC) to develop guidelines for use of dampers based on studies of elastic structures.

1.6 Objectives of This Investigation

The research was developed to:

1. investigate experimentally the behavior of friction dampers and structural response when the structural system experiences inelastic deformations.

2. model analytically the friction dampers as part of an inelastic structural model.

3. validate the analytical modeling using experimental data.

4. develop a simplified procedure to estimate the structural seismic demands in presence of dampers

5. determine the contribution of dampers to the changing of the demand-capacity relation (performance index) in severe ground shaking.

SECTION 2

FRICTION DAMPERS

2.1 Description of Tekton Friction Damping Devices

Friction dampers operate as steel shaft sliding between specially design friction pads. The cross sections of a typical Tekton friction damper are shown in Fig. 2-1. The dampers consist of series of adjustable bolts through which one can control the normal force applied to the friction pads. The yield force (break-through friction force) has linear relationship with applied torque on the adjustable bolts. The length of the dampers can be adjusted by pulling or pushing the steel shaft which gives the flexibility for installation.

2.2 Description of Sumitomo Friction Damping Devices

The longitudinal and cross-sections of a typical Sumitomo friction damper are shown in Fig. 2-2. The dampers consist of a series of wedges which act against each other under the load from a compressed spring and apply a normal force to the friction pads. The friction pads slide directly on the inner surface of the steel casing of the device. The friction pads are copper alloy with graphite plug inserts which provide dry lubrication to the unit, ensuring a stable friction force and reducing noise during movement.

For practical applications the devices are incorporated in structural braces or in structural joints with large deformations (see experimental study in Section 4).

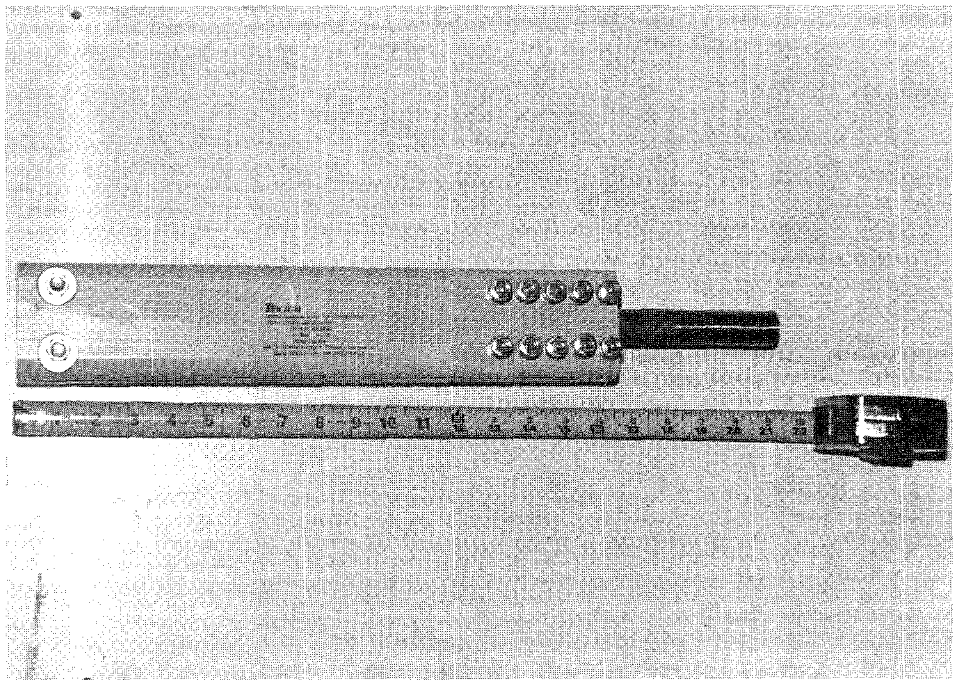

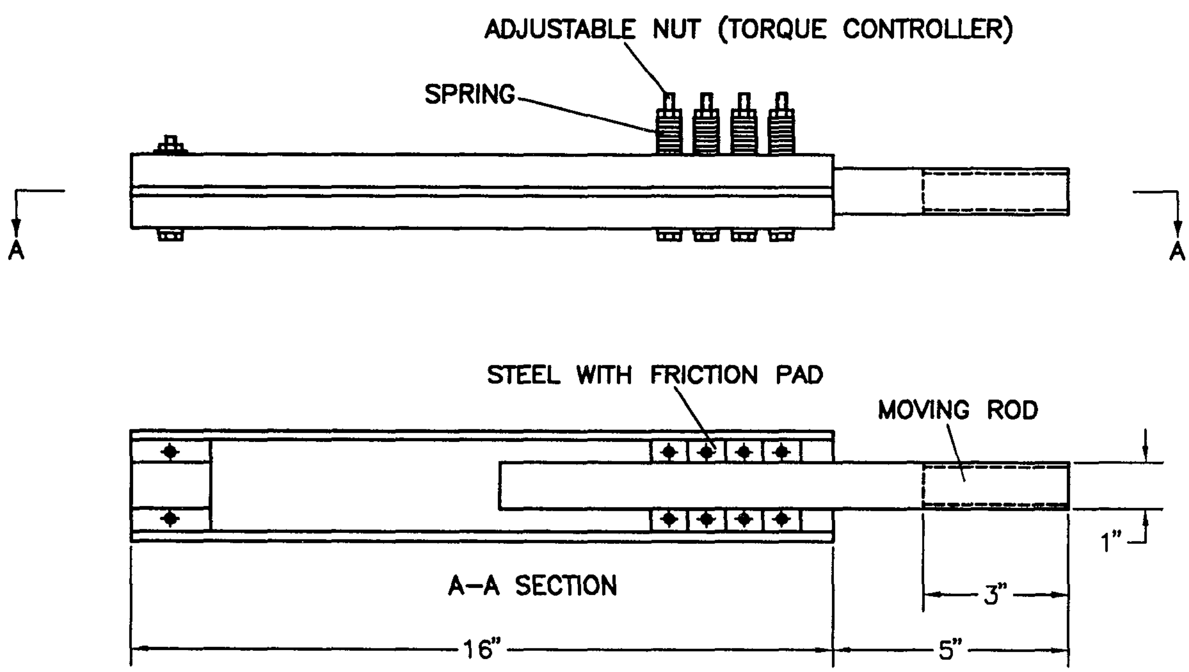

Figure 2-1 Construction of Tekton Friction Damper

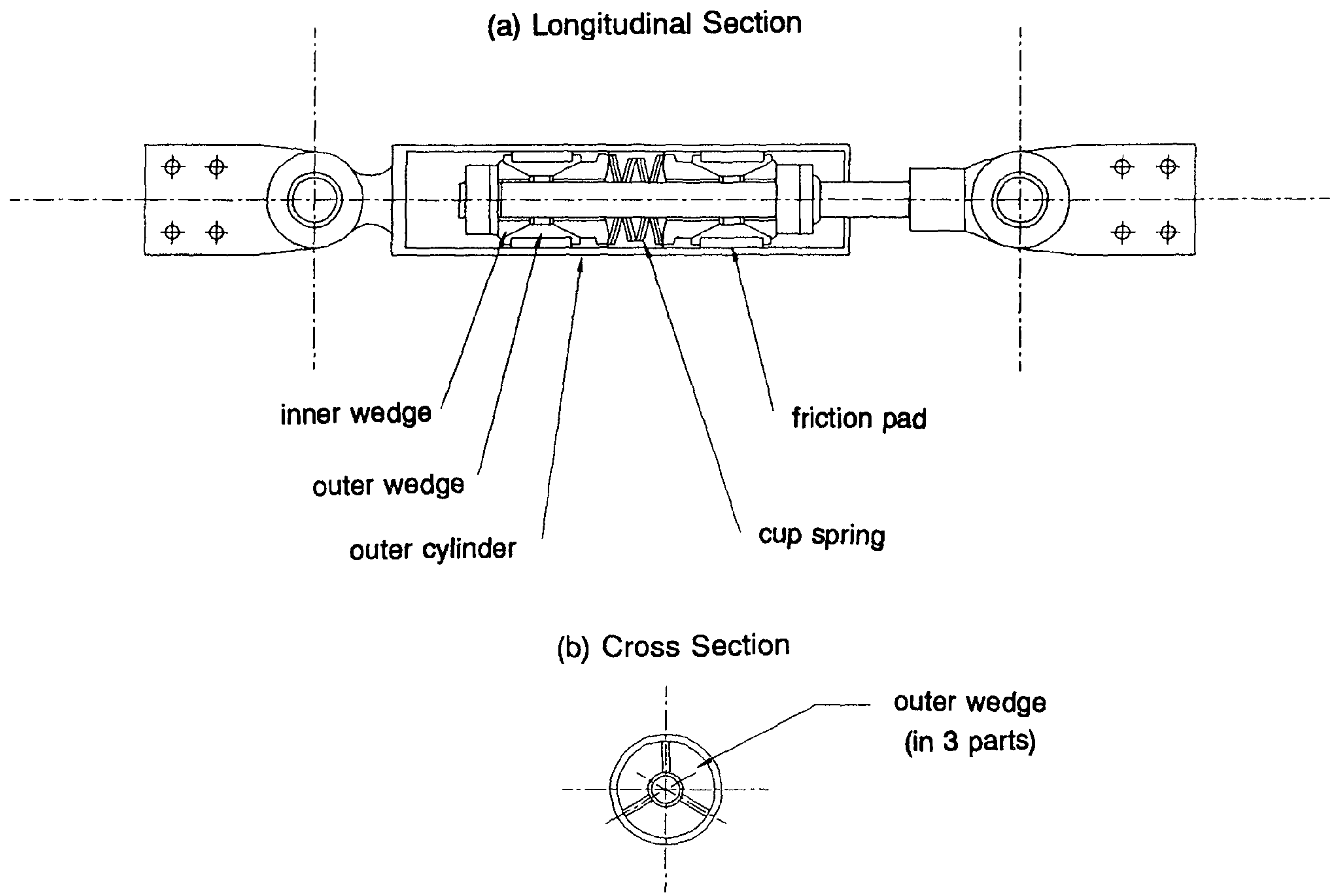

Figure 2-2 Sectional Views of a Sumitomo Friction Damper

2.3 Operation of Dampers

The force in a damper is a result of friction between sliding shaft and friction pads for Tekton friction dampers or between friction pads and the inner surface of the steel casing for Sumitomo friction device. The force in a damper can be defined as two stages, stick and slip, as:

$$F_D = k_D U, \qquad \text{for } |F_D| \leq \mu_{break-away} N \tag{2-1)a$$

$$F_D = \mu_{\min} N, \qquad \text{for } \mu_{\min} N \leq |F_D| < \mu_{break-away} N \text{, after sliding occurred.} \tag{2-1)b$$

where F_D is damper force, k_D is the stiffness of the damper, U is the deformation of the dampers, N is the normal force between steel shaft and friction pads (between friction pads and the inner surface of the steel casing for Sumitomo friction device), $\mu_{breakaway}$ is the maximum static friction coefficient and μ_{min} is the friction coefficient at sliding stage.

2.4 Testing of Damping Devices

Six Tekton friction devices were tested under frequencies 1 Hz, 2 Hz, 3 Hz and 4 Hz, and six Sumitomo friction devices were tested under frequencies 1 Hz, 1.5 Hz and 2 Hz. Each test consist of 20 cycles of harmonic (sinusoidal) motion. The devices were constructed for the retrofit of a reinforced concrete structural model. These devices were tested on a MTS testing machine using a series of harmonic displacements and the resisting forces were measured simultaneously. The purpose of the testing was to confirm the correct setting of slip force and to identify any dependency of the force-displacement behavior on the loading frequency, temperature and number of loading cycles. The testing results are shown in Fig. 2-3, 2-4 and Table 2-1. The testing results show that the properties of the dampers are nearly independent on frequency, temperature and number of cycles.

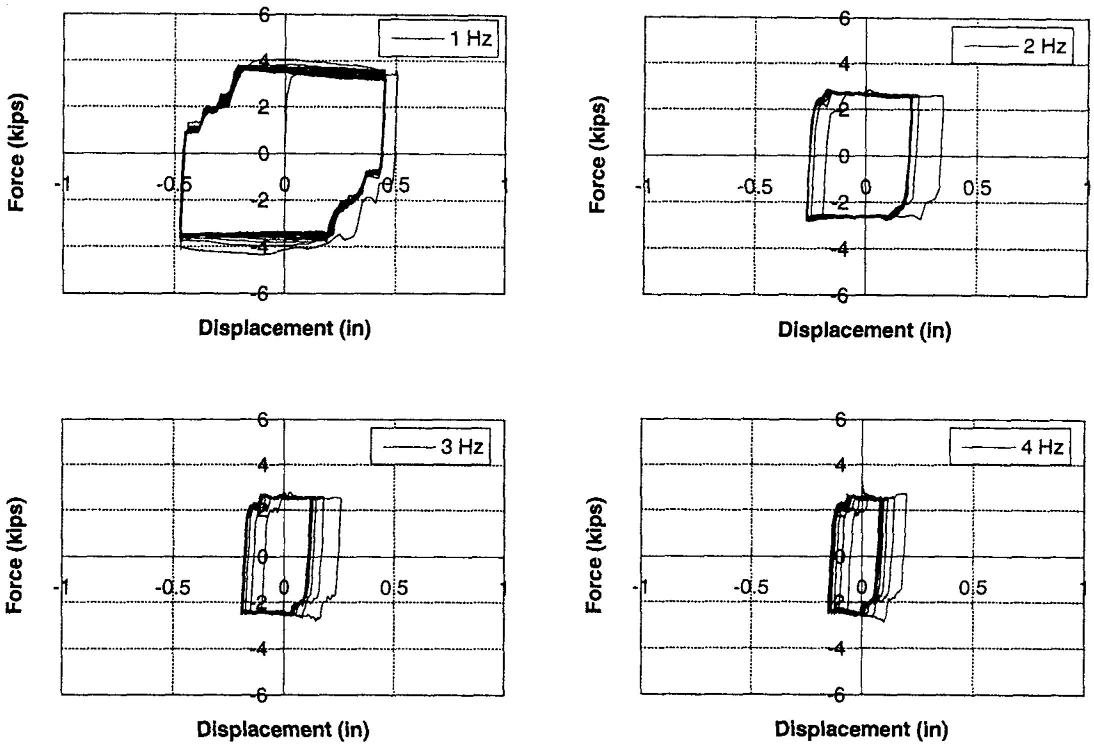

Figure 2-3 Test Results of Tekton Friction Damper for Various Frequencies

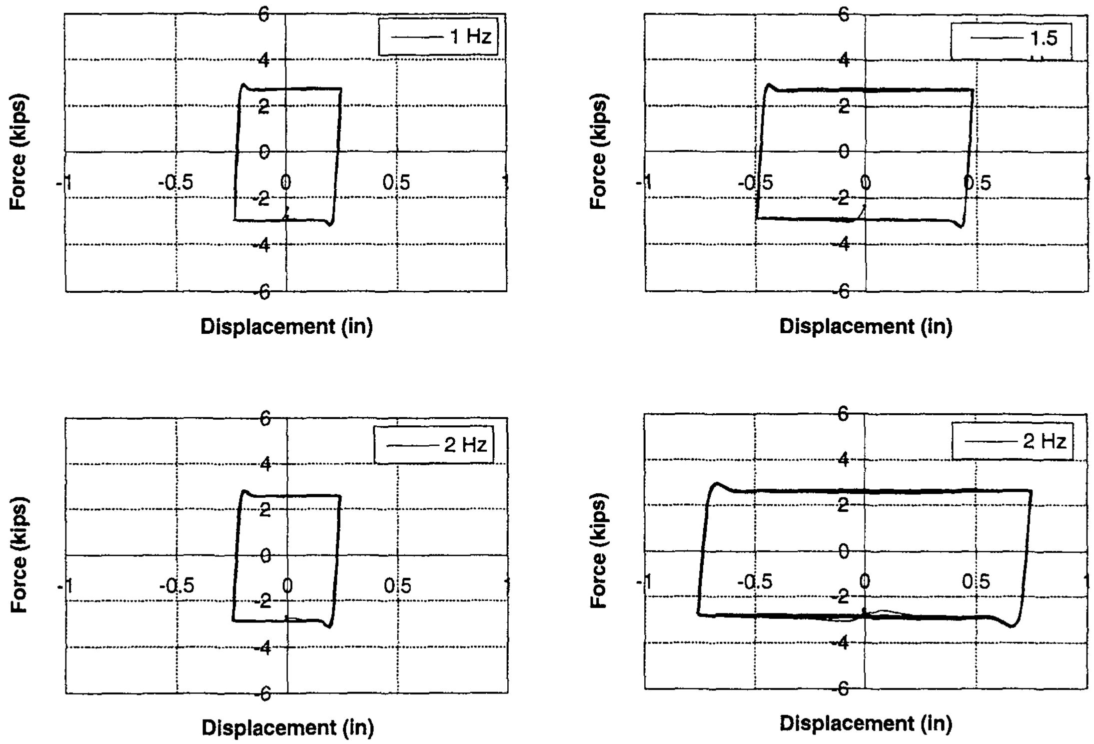

Figure 2-4 Test Results of Sumitomo Friction Damper for Various Frequencies

Table 2-1 Tekton and Sumitomo Friction Damper Component Test Results

Damper type (1)	Test # (2)	Damper # (3)	Frequency (Hz) (4)	Max. Force (kips) (5)	Max. displ. (in) (6)	# of cycles (7)	Location in model (8)
Tekton Friction	1	1	2	2.8	0.47	20	2nd*, East
	2	2	2	3.2	0.47	20	1st, West
	3	3	2	3.2	0.47	20	3rd, East
	4	4	2	3.2	0.47	20	1st, East
	5	5	2	3.1	0.47	20	3rd, West
	6	6	2	2.8	0.47	20	2nd, West
Sumitomo Friction	1	1	2	3.0	0.75	20	3rd, West
	2	2	2	2.9	0.75	20	3rd, East
	3	3	2	3.0	0.75	20	1st, East
	4	4	2	2.9	0.75	20	2nd, West
	5	5	2	2.8	0.75	20	2nd, East
	6	6	1.5	3.0	0.25	20	1st, West
	7	6	1.5	3.0	0.5	20	
	8	6	1.5	3.0	0.75	20	
	9	6	2	3.0	0.25	20	
	10	6	2	3.0	0.755	20	
	11	6	2.5	3.0	0.25	20	
	12	6	2.5	3.0	0.75	20	

SECTION 3

ANALYTICAL MODELING OF FRICTION DAMPERS

3.1 Mathematical Modeling

The shape of the force versus displacement loop of friction dampers is mostly rectangular with smooth corners as shown in the experimental results of Section 2.

3.1.1 Bouc-Wen's Model

A friction damper force $F_D(t)$ can be represented as:

$$F_D = k_0(\alpha U + (1-\alpha)ZU_y) \quad \text{(3-1)}$$

where k_0 is the initial stiffness, α is the ratio of post-yielding stiffness to initial pre-yielding stiffness, U is the relative deformation in the damper, U_y is the yield displacement of the damper and Z is a nondimensional quantity given by:

$$\dot{Z} = \left(\dot{U} / U_y\right)\left\{A - Z^{\eta}\left[\gamma \operatorname{sgn}\left(\dot{U}Z\right) + \beta\right]\right\} \quad \text{(3-2)}$$

in which η is a parameter controls the transition shape from elastic range to yielding range. The value of this parameter can be increased to achieve near-bilinear behavior rather than smooth bilinear behavior (η=2 in this study). When $A/(\beta+\gamma)=1$ the model reduces to model of viscoplasticity (Constaintinou et al. 1990b, Ozedemir and Kelly 1976). The damper force F_D can be calculated using semi-implicit Runge-Kutta method (Rosenbrook

1964) as in Section 5.2.2.1 in detail. To increase the computation speed, Reichman and Reinhorn, 1994 solved a close form solution for Eq. (3-1) and (3-2) for η=2. The nondimentional parameter Z is obtained as:

$$Z = (a/b) f\left[ab\left(U/U_y\right) + c\right] \qquad \text{(3-3)}$$

where, $a = \sqrt{A}$; $b = \sqrt{\gamma + \beta Sgn\left(\dot{U}Z\right)}$; c=constant of integration, equal to displacement at a previous branch, while f[] is a function described as follows:

$$f[\ ] = \begin{cases} \tanh[\ ] & for\ \mathrm{sgn}\left(\dot{U}Z\right) > 0;\quad b^2Z^2 < a^2 \\ \coth[\ ] & for\ \mathrm{sgn}\left(\dot{U}Z\right) > 0;\quad b^2Z^2 > a^2 \\ \tan[\ ] & for\ \mathrm{sgn}\left(\dot{U}Z\right) < 0 \end{cases} \qquad \text{(3-4)}$$

The function f[] controls the branch of the hysteretic loop, when $\mathrm{sgn}(\dot{U}Z) > 0$, loading, occurs and when $\mathrm{sgn}(\dot{U}Z) < 0$ unloading. The integration constant c keeps record of the last transition point from one branch to the other.

3.1.2 Coulomb Friction-Viscous Damping Model (Reichman and Reinhorn 1994)

The friction damper force can be described in three stages and can be represented as a combination of three components: a linear rise, coulomb component and viscous damping component:

$$F_D = k_j U + c_j \dot{U} + \mu_j N \qquad \text{(3-5)}$$

where F_D is the damper force, N is the normal force, k_j , c_j and μ_j are the stiffness, equivalent damping and friction coefficient at various stages of computation (see Fig. 3-1) as follows:

(a) Stick stage

$For\ j = 1\ (i.e.\ when\ |F| \leq \mu_{break-away} N)$:

$k_1 = k_0$, $c_1 = 0$ and $\mu_1 = 0$

(b) Transition stage

$For\ j = 2\ \left(i.e.\ \mu_{\min} N \leq |F| \leq \mu_{\max} N\right)$, after sliding occurred, then

$k_2 = 0$, $\mu_2 = \mu_{min}$, $c_2 = c_{eq}$

$$c_{eq} = N(\mu_{\max} - \mu_{\min}) / \dot{U}_{\lim it}$$

where $\dot{U}_{\lim it}$ is a constant depending on surface properties and it can be obtained by inverting the exponent "a" in the model by Mokha et al. (1989). This "velocity" is usually between 2-4 in/sec. It should be noted that N is variable with time and therefore c_{eq} is also a time dependent variable.

(c) Sliding stage

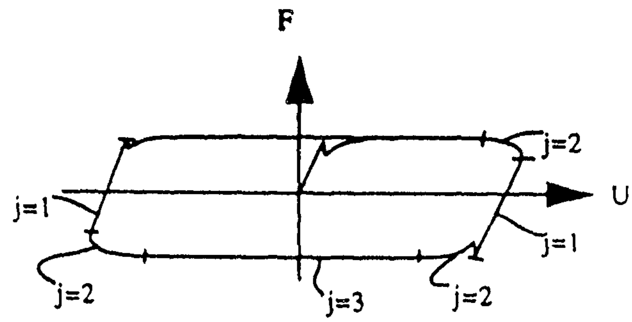

Figure 3-1 Various Stages of Coulomb Friction-Viscous Damping Model (from Reichman and Reinhorn 1994)

The above stage applies when sliding occurs at velocities greater than the limit, $|\dot{U}| \geq \dot{U}_{\lim it}$. For velocities larger than $\dot{U}_{\lim it}$, then stage three, (j=3), applies:

$k_3 = 0$, $c_3 = 0$, and $\mu_3 = \mu_{max}$.

If the friction force drops below the μ_{min} N the system is transferred back to the first stage (j=1).

This model is able to represent in addition to the stick-slip condition, the smooth transition observed between slip and stick stages. The smooth transition in reality and in the analytical procedure, reduces instability and the influence of very high modes resulting from abrupt transition from slip to stick. It is noted that by varying the normal force , N, in the damper, the device can develop variable reaction. Such device can be used as part of a motion control scheme as a semi-active device.

3.1.3 Modeling of Tested Dampers

The dampers tested in this experimental study are "frequency independent. The dampers are calibrated to provide approximately 3.2 kips friction force, as shown in Table 2.1. The dampers are modeled using Bouc-Wen's model in further analytical studies and compared with the Coulomb friction-viscous damping model. It should be noted that the dampers produce a substantial energy dissipation, while also change the behavior of a structure from a moment resisting frame to a braced frame. Their effect in the structure cannot be assessed from their individual mechanical properties only. A complete analytical model of the super-structure including also the above devices is necessary for the overall system evaluation (see Section 5).

SECTION 4

EXPERIMENTAL STUDY OF RETROFITTED STRUCTURE

EARTHQUAKE SIMULATOR TESTING

4.1 Retrofit of Damaged Reinforced Concrete Model

A three story 1:3 scale model structure with lightly reinforced concrete frames, damaged by prior testing with moderate and severe earthquake (Bracci et al. 1992a, 1992b) was retrofitted by conventional concrete jacketing of interior columns and joint beam enhancements and was damaged again by several severe earthquakes (Bracci et al. 1992c). The same structure was further used to assess the possibility of retrofit of damaged frames with supplemental dampers installed in braces attached to the concrete joints. The study was developed to assess efficiency and structural interaction of various types of dampers, i.e.:

(a) viscoelastic dampers of 3M Company (Lobo et al. 1993, Shen et al. 1993).

(b) fluid viscous damper of Taylor Devices Inc. (Reinhorn et al. 1995)a.

(c) friction dampers of Tekton Co. and Sumitomo Co. (This report).

(d) viscous walls of Sumitumo Construction Co. (Reinhorn et al. 1995)b.

The objectives of the retrofit was (a) to reduce overall damage progression in severe episodes of earthquakes; (b) to provide data for analytical modeling of inelastic structures equipped with dampers of hysteretic behavior and (c) to determine the force transfer in the retrofitted structures and its local effects.

The description of the model, the supplemental dampers and the testing program are described in this section.

4.2 Structure Model for Shaking Table Study

The structure was a three story 1:3 scale reinforced concrete frame structure original only for gravity loads without any special seismic provisions. The model was scaled from a prototype using mass simulation (Bracci et al. 1992a) The structural model had a floor weight of 120 kN (27,000 lbs). The structure had 50.8 mm (2 in) thick slabs supported by 76.2x172.4 mm (3x6 in) beams supported by 101.6x101.6 mm (4x4 in) columns before retrofit (see Fig. 4-1 and 4-2). After the conventional retrofit the interior columns were increased to 152.4x152.4 mm (6x6 in) by concrete jacketing with longitudinal post-tensioned reinforcement and with a column capital at each floor obtained by a fillet of joint connection (see Fig. 4-3 and 4-4).

The columns were symmetrically reinforced using 1.2%, total reinforcement ratio, and the beams had 0.8% positive reinforcement along entire beam and 0.8% negative reinforcement ratio above the supports. Detail of reinforcement and material properties can be found in Bracci et al. 1992a. A summary of this information is included in Appendix A for sake of completion.

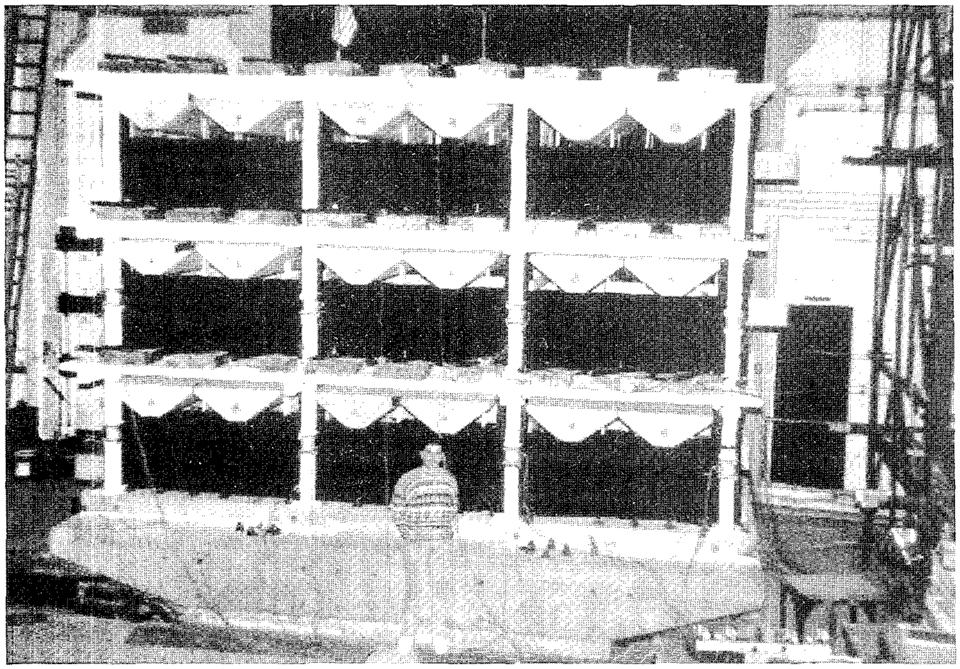

a. Before Conventional Retrofit

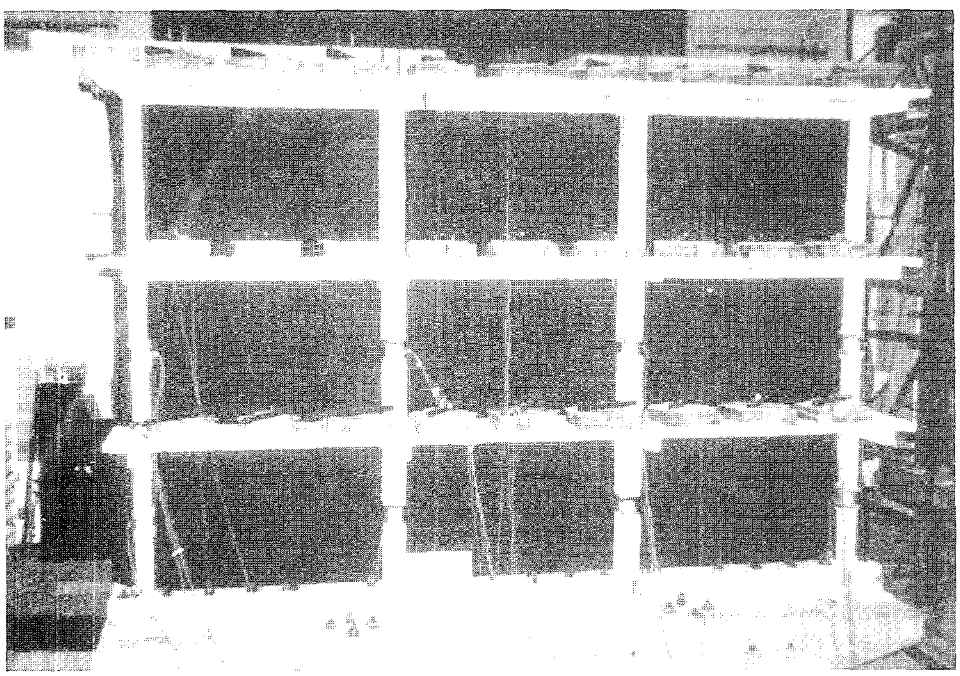

b. After Conventional Retrofit of Columns

Figure 4-1 Perspective View of 1:3 scale R/C Frame Structure

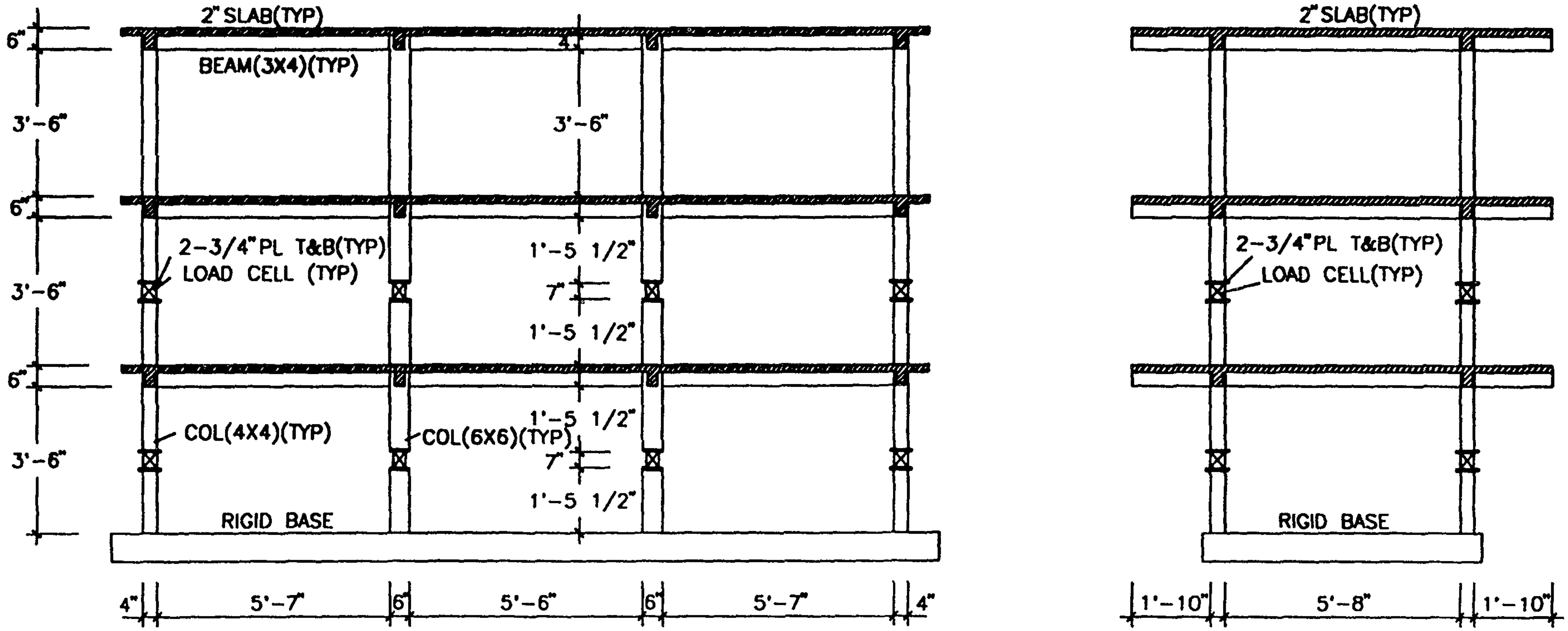

Figure 4-2 Building Dimensions and Location of Local Measuring Devices in Columns

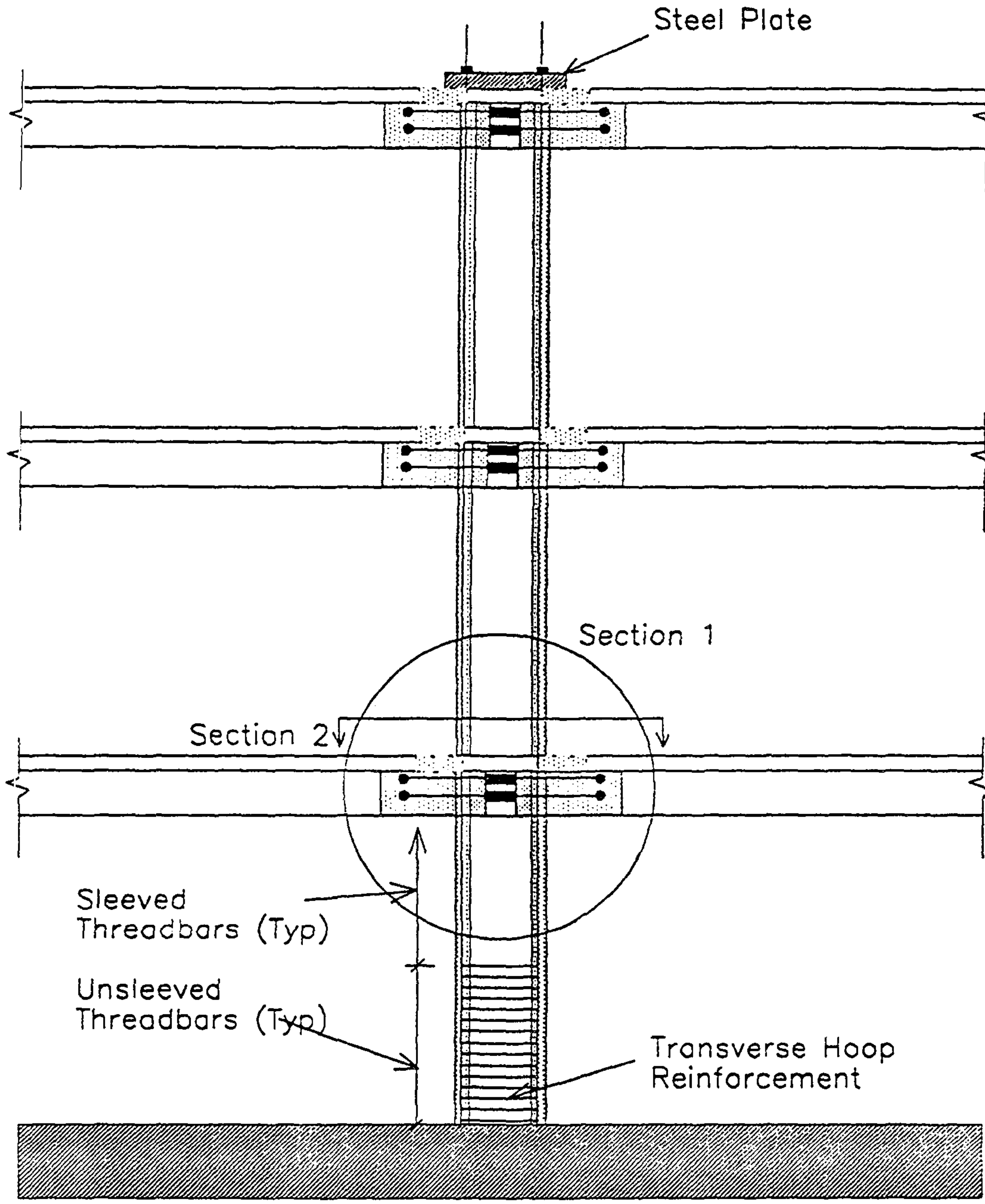

Elevation

Figure 4-3 Conventional Retrofit by Jacketing of Interior Columns

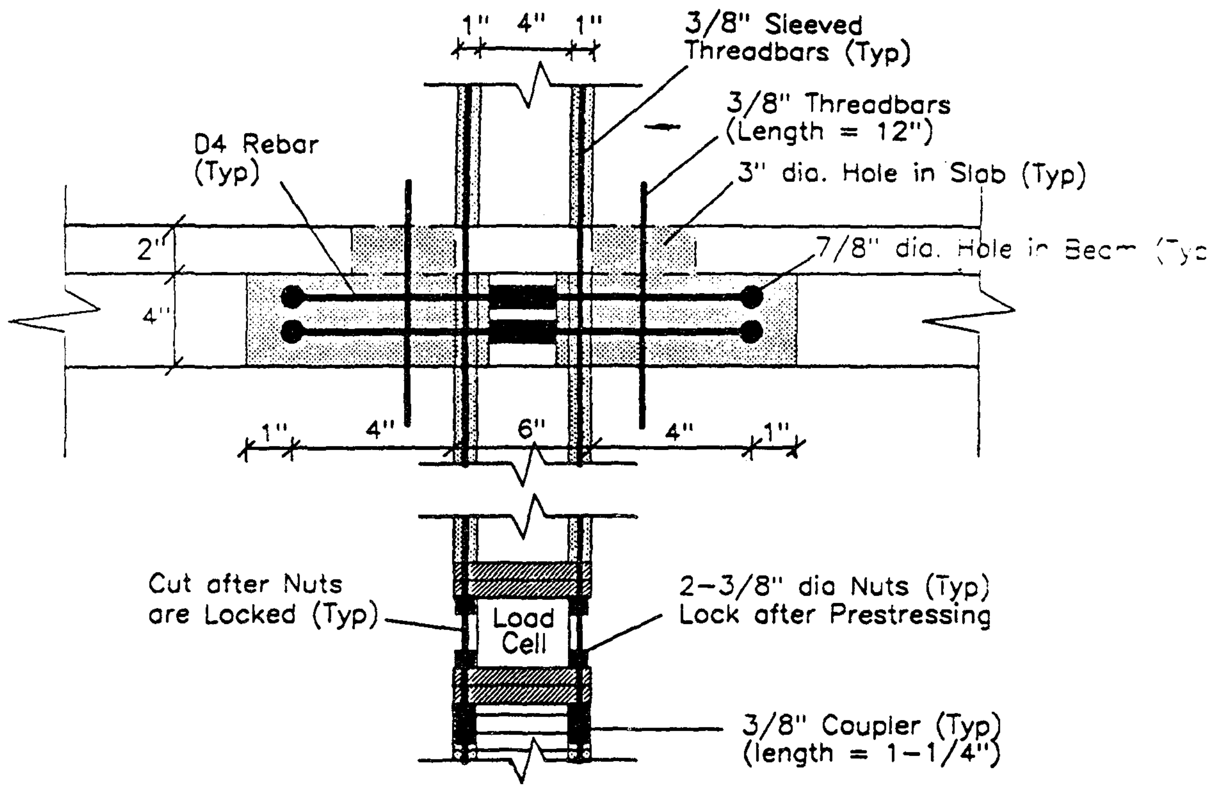

Section 1

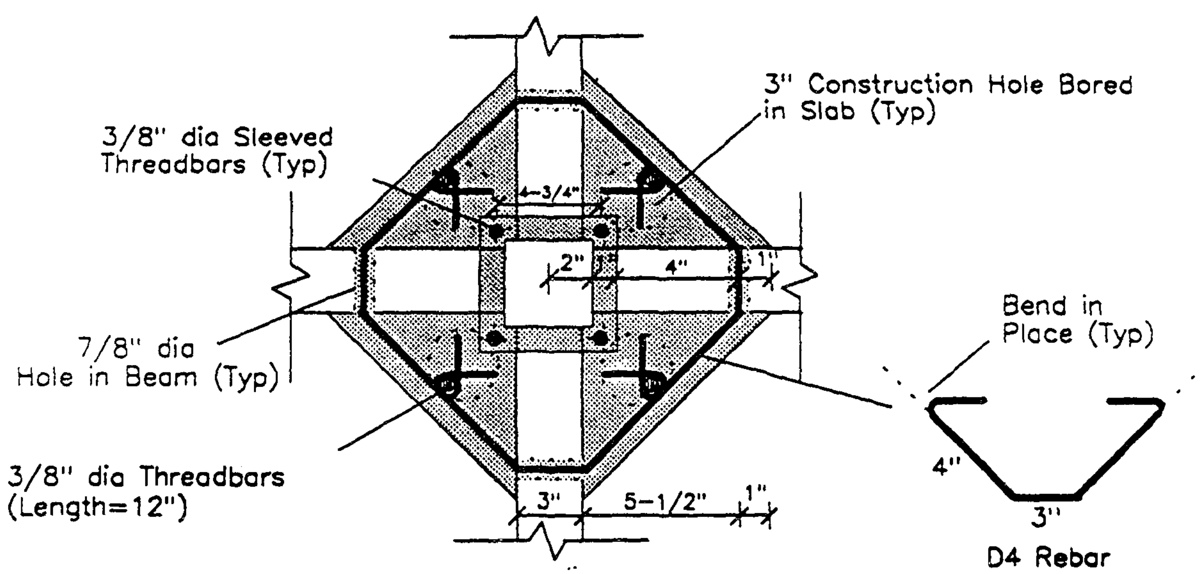

Section 2

Figure 4-4 Detail of Conventional Retrofit with Concrete Jacketing and Joint Fillet

Table 4-1a Moment Capacities of Structural Sections (units kips in)

		Columns				Beams			
		Interior		Exterior		Interior		Exterior	
		Moment	Curvature	Moment	Curvature	Moment	Curvature	Moment	Curvature
(1)	(2)	(3)	(4)	(5)	(6)	(7)	(8)	(9)	(10)
Original Structure									
3rd floor	Top	22	0.01900	18	0.023	30	0.0155	30	0.0155
	Bottom	22	0.01900	18	0.023	80	0.0100	80	0.0100
2nd floor	Top	29	0.01400	22	0.020	30	0.0155	30	0.0155
	Bottom	29	0.01400	22	0.020	80	0.0100	80	0.0100
1st floor	Top	36	0.01100	28	0.017	30	0.0155	30	0.0155
	Bottom	36	0.01100	28	0.017	80	0.0100	80	0.0100
After Conventional Retrofit									
3rd floor	Top	130	0.00048	18	0.015	50	0.0155	30	0.0155
	Bottom	130	0.00048	18	0.015	80	0.0550	80	0.0550
2nd floor	Top	130	0.00048	22	0.019	50	0.0155	30	0.0155
	Bottom	130	0.00048	22	0.019	80	0.0550	80	0.0550
1st floor	Top	130	0.00048	28	0.025	50	0.0155	30	0.0155
	Bottom	70	0.00041	28	0.025	80	0.0550	80	0.0550

1 kips = 4.45 kN, 1 in = 25.4 mm.

Table 4-1b Shear Capacities of Structural Sections (units kips)

	Columns		Beams	
	Interior	Exterior	Interior	Exterior
(1)	(2)	(3)	(4)	(5)
Original Structure				
3rd floor	0.978	0.800	2.619	2.619
2nd floor	1.280	0.978	2.619	2.619
1st floor	1.600	1.244	2.619	2.619
After Conventional Retrofit				
3rd floor	5.770	0.800	2.619	2.619
2nd floor	5.770	0.978	2.619	2.619
1st floor	5.770	1.244	2.619	2.619

1 kips = 4.45 kN

The moment and shear capacities of the sections before and after retrofit are listed in Table 4-1a and 4-1b. The moment capacities were calculated based on data in the Appendix A. It should be noted that the cracking and yielding of a section reduce the moment of inertia of sections and therefore only a fraction of the gross stiffness is active during a seismic event (Bracci et al. 1992b).

The structure was subjected to earthquake simulated motion using the shaking table at University of Buffalo. Moderate (peak ground acceleration PGA 0.2g) and severe episodes (PGA=0.3g) were used to verify the seismic behavior and the efficiency of structure suffered damage near collapse (90%, based on a damage index normalized to a unit which means collapse), the conventionally retrofitted structure suffered less damage, in repairable range. The original structure displayed a soft-column-side-sway mechanism. The conventionally retrofitted structure developed a safer beam-side-sway mechanism, which explains the reduced damage.

However, the structure developed inelastic behavior and damage. Therefore the structure was further retrofitted as presented in the next section.

4.3 Retrofit with Supplemental Friction Dampers

The structure was retrofitted with additional damping braces in the middle bay of each frame at all floors as shown in Fig. 4-5 and 4-6. The structure was also retrofitted with additional damping braces on 1st and 2nd floor only and retrofitted with additional damping braces on 1st floor only. The different configurations are shown in Fig. 4-7. In the following contents, the model with friction dampers or the model with 6 friction

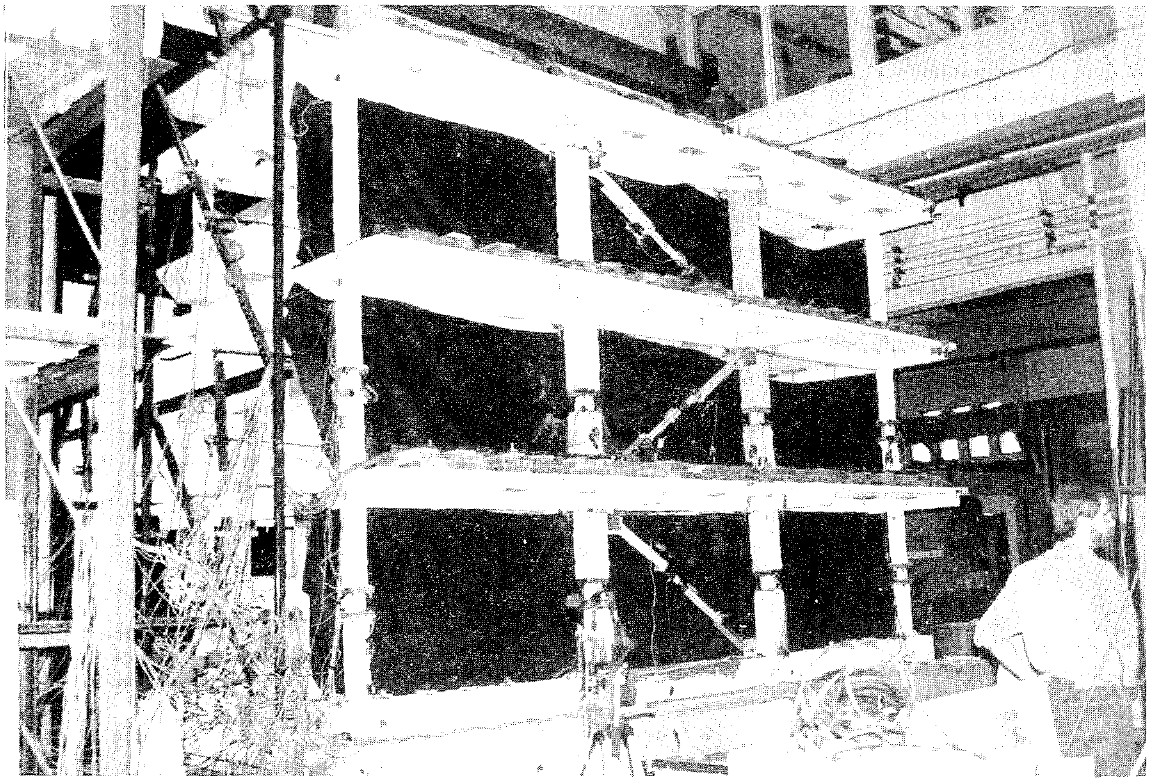

(a) with Tekton Friction Dampers

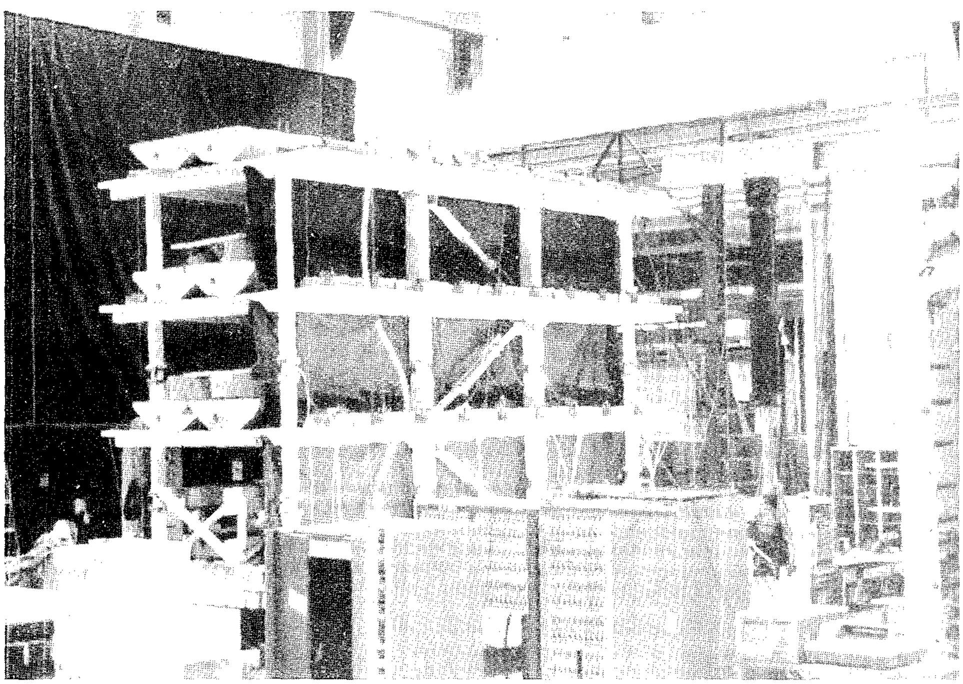

Figure 4-5 Perspective View of the Frame with Installed Damping Devices

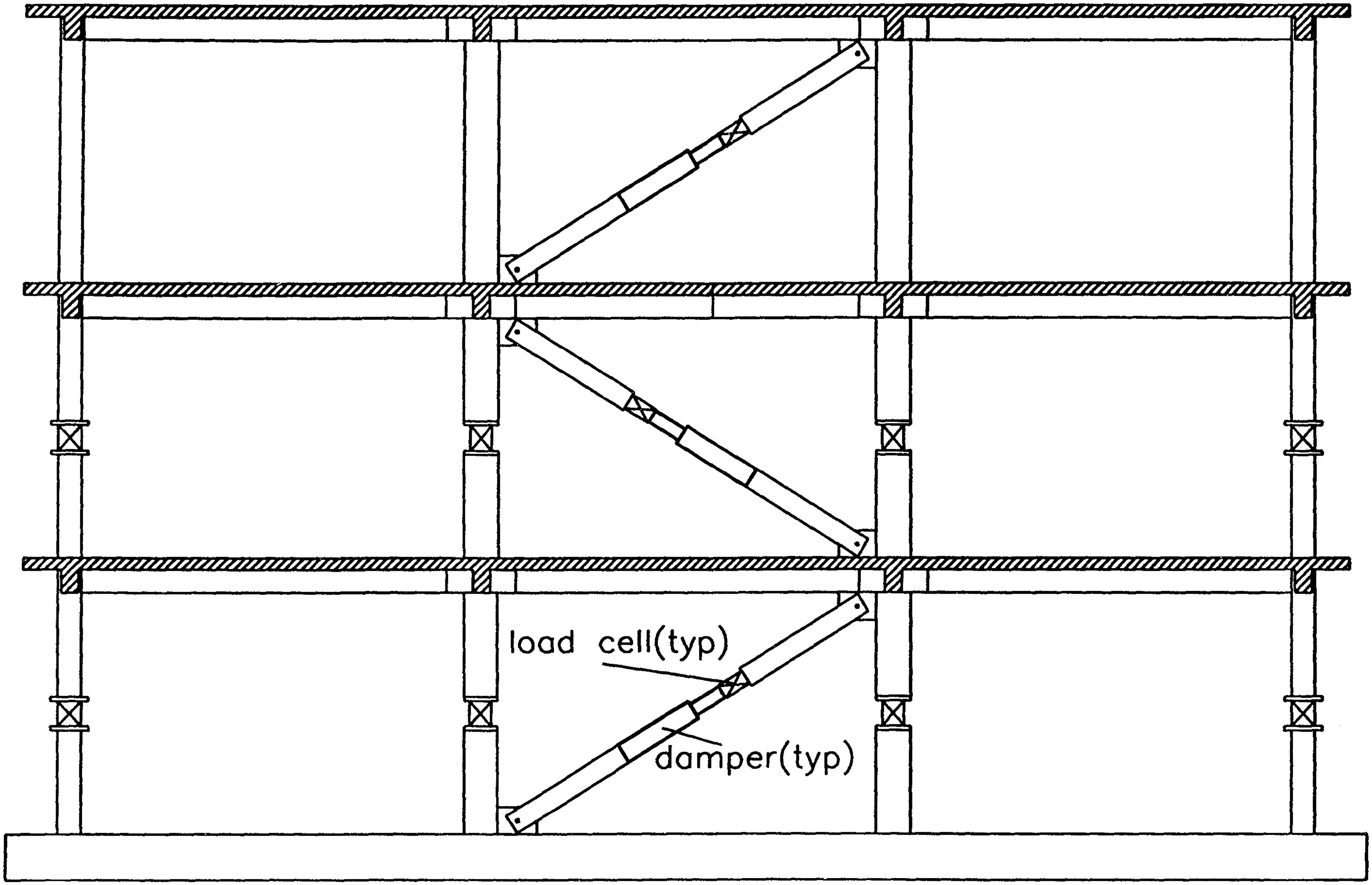

Figure 4-6 Location of Dampers and Measuring Devices

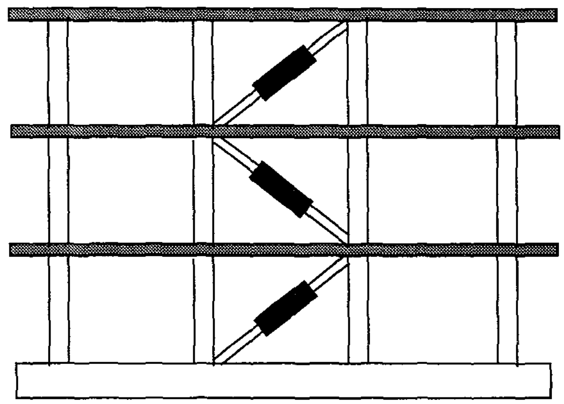

(a) Configuration of the model with 6 dampers (2 dampers each floor)

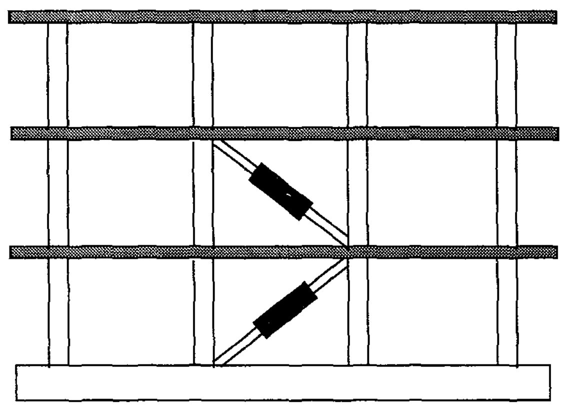

(b) Configuration of the model with 4 dampers (2 dampers each floor, 1st and 2nd floor only)

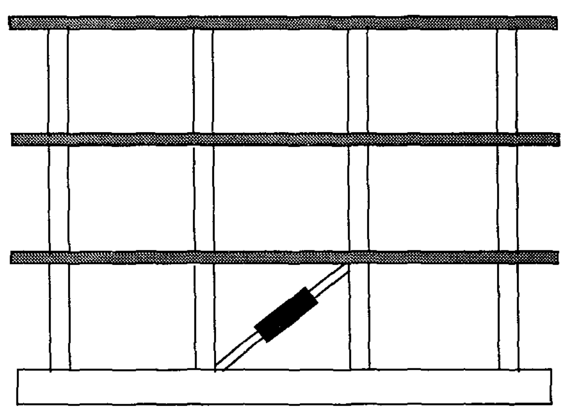

(c) Configuration of the model with 2 dampers at first floor only

Fig. 4-7 Different configurations of the tested model

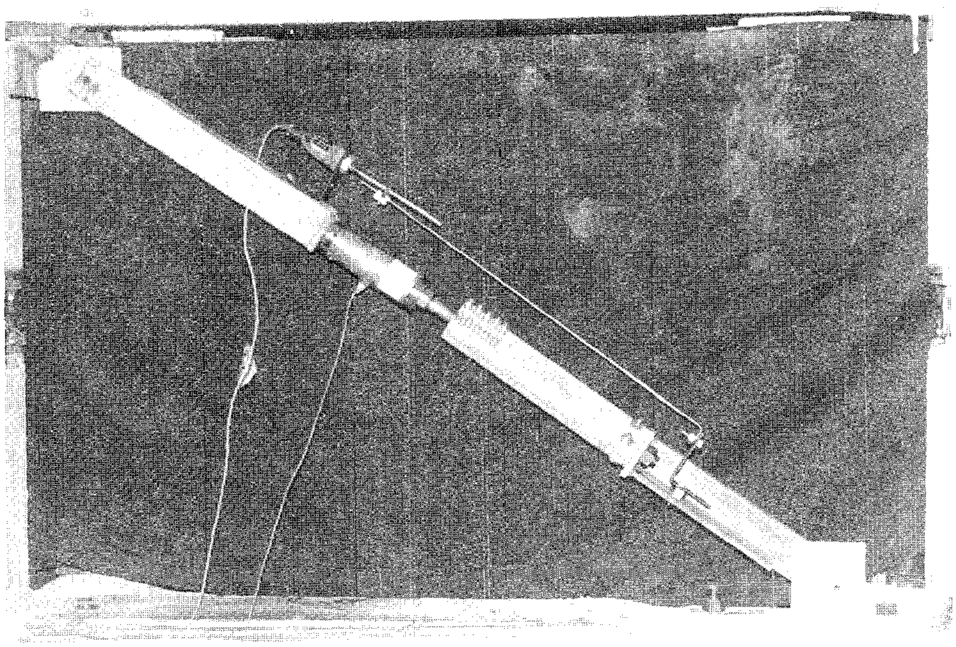

Figure 4-8 Perspective View of Tekton Frictın Dampers Installed in the Mid-bay of the Frame

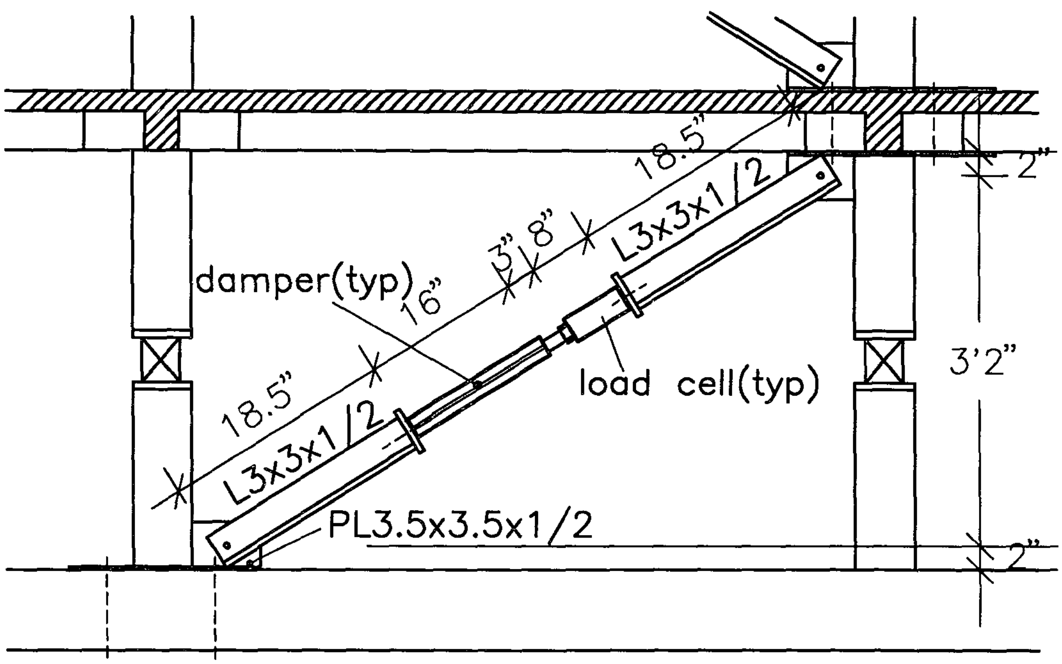

Figure 4-9 Installation Detail of a Tekton Frictin Damper Installed in the Mid-bay of the Frame

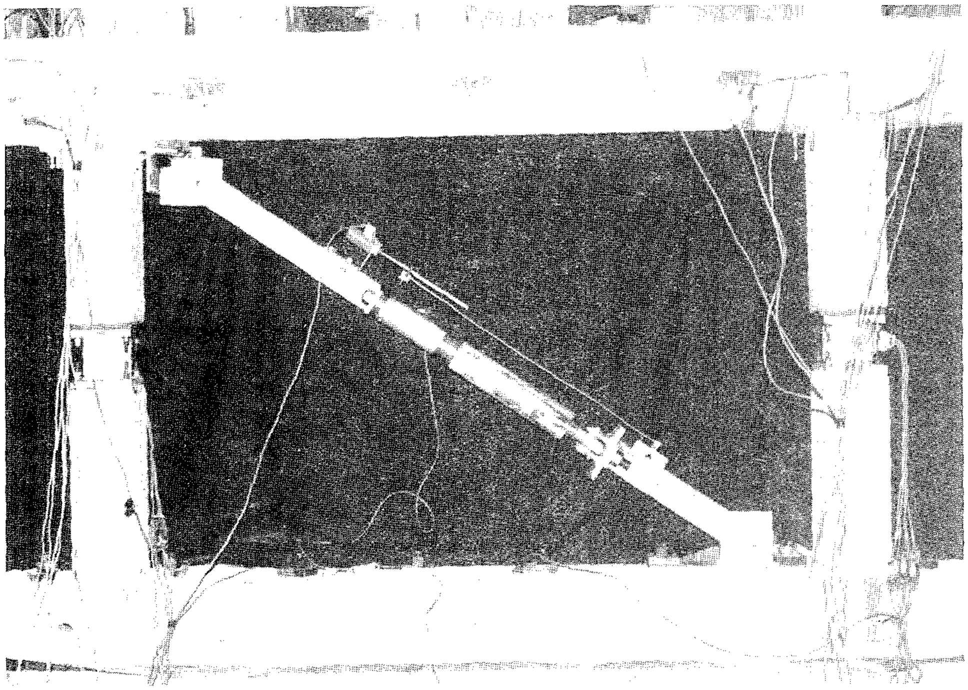

Figure 4-10 Perspective View of Sumitomo Frictin Dampers Installed in the Mid-bay of the Frame

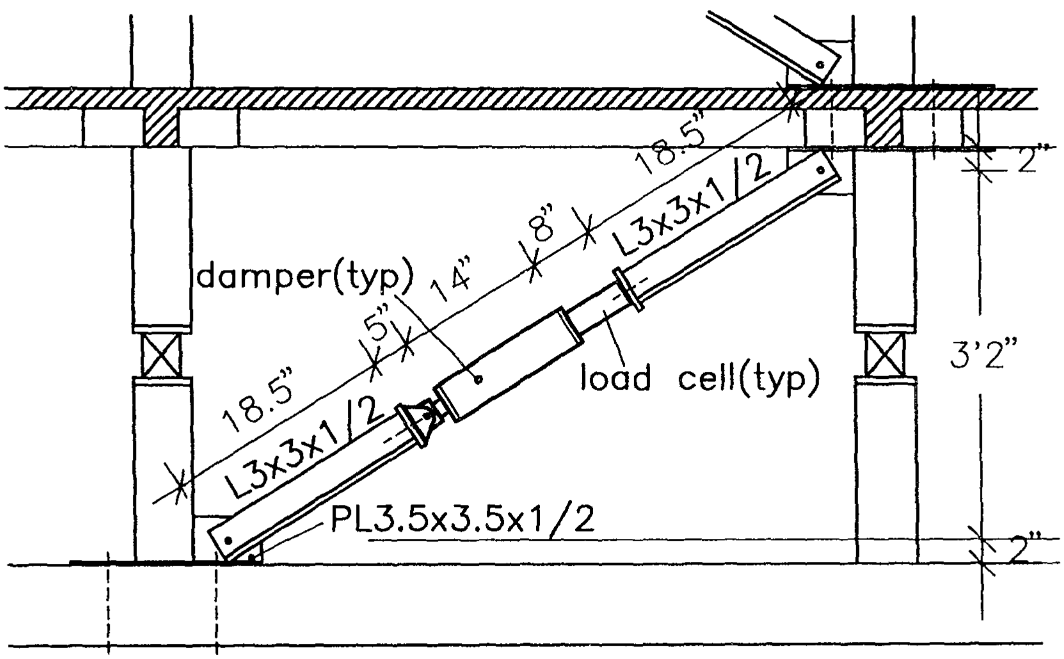

Figure 4-11 Installation Detail of a Sumitomo Friction Damper Installed in the Mid-bay of the Frame

dampers refers to configuration (a) in Fig. 4-7. The model with 4 dampers refers to configuration (b), and the model with 2 dampers refers to configuration (c). The details of the braces are shown in Fig. 4-8 and 4-9 for Tekton devices and Fig. 4-10 and 4-11 for Sumitomo devices.

The braces were connected to the floors at base and top of columns and transferred loads to the joint through the beams and the fillet joint (see Fig. 4-9 and 4-11). The braces consist of an A36 L6x6x1/2" steel angle connected through 1/2 in diameter bolts to allow for a pinned connection at its ends.

4.3.1 Friction Dampers

The dampers installed in the brace were specially designed by Tekton Company and Sumitomo Company for the structure model as shown in Fig. 2-1 and 2-2. The structure model incorporated with Tekton friction dampers was tested after the model incorporated with Sumitomo friction dampers. The friction force of the dampers were calibrated to about 3.2 kips. The damper was connected to the brace using a load cell with a capacity of 30,000 lbs. The Tekton friction dampers (presented in Section 2) were installed in the structure as follows: #4 and #2 at first floor, #1 and #6 at second floor, and #3 and #5 at third floor, where the first ones in the pairs indicate east frame of the structure (see damper properties in Table 2-1), and the similar arrangement of Sumitomo friction dampers can be seen in Table 2-1. Efficiency of using dampers was investigated by using dampers on lower floor only.

The damper construction can prevent rotations between its two ends which is suitable to prevent buckling in the brace assembly.

4.4 Instrumentation

The structure was instrumented with motion and force transducers to monitor the force transfer within the structure. A series of accelerometers were installed horizontally at each floor and at its base. Five directional load cells measuring axial loads, shear forces in two directions, bending moments in two directions were installed in the mid-height of each column of east frame at first and second floor (see Fig. 4-2). For detailed description of load cells see Bracci et al. 1992a. The braces were instrumented with an axial load cell and a longitudinal displacement transducer (see Fig. 4-6) to measure the movement in the damper.

The structure was placed on the shaking table at SUNY/Buffalo. The shaking system was monitored for displacements, velocities and accelerations in horizontal, vertical and rocking directions. A total of 83 channels of data were recorded during each earthquake.

The instrumentation consisting of load cells, displacement transducers and accelerometers is detailed in APPENDIX B with a list of monitored channels and their corresponding descriptions are given in Table 4-2. A total of 83 channels were monitored.

Table 4-2 List of Channels (with reference to Fig. B-1)

CHANNEL	NOTATION	INSTRUMENT	RESPONSE MEASURED
1	AH1	ACCEL	Longitudinal accel. - on the base, east side
2	AH2	ACCEL	Longitudinal accel. - on the base, west side
3	AH3	ACCEL	Longitudinal accel. - 1st floor, east side
4	AH4	ACCEL	Longitudinal accel. -1st floor, west side
5	AH5	ACCEL	Longitudinal accel. - 2nd floor, east side
6	AH6	ACCEL	Longitudinal accel. -2nd floor, west side
7	AH7	ACCEL	Longitudinal accel. - 3rd floor, east side
8	AH8	ACCEL	Longitudinal accel. -3rd floor, west side
9	AV1	ACCEL	Vertical accel. - on the base, north east side
10	AV2	ACCEL	Vertical accel. - 1st floor, north east side
11	AV3	ACCEL	Vertical accel. - 2nd floor, north east side
12	AV4	ACCEL	Vertical accel. - 3rd floor, north east side
13	AV5	ACCEL	Vertical accel. - 1st floor, south east side
14	AV7	ACCEL	Vertical accel. - 2nd floor, south east side
15	AV8	ACCEL	Vertical accel. - 3rd floor, south east side
16	AT1	ACCEL	Transverse accel. - on the base, east side
17	AT2	ACCEL	Transverse accel. - 1st floor, east side
18	AT3	ACCEL	Transverse accel. - 2nd floor, east side
19	AT4	ACCEL	Transverse accel. - 3rd floor, east side
20	D1	DT	Longitudinal accel. - on the base, east side
21	D2	DT	Longitudinal accel. - on the base, west side
22	D3	DT	Longitudinal accel. - 1st floor, east side
23	D4	DT	Longitudinal accel. - 1st floor, west side
24	D5	DT	Longitudinal accel. - 2nd floor, east side
25	D6	DT	Longitudinal accel. - 2nd floor, west side
26	D7	DT	Longitudinal accel. - 3rd floor, east side
27	D8	DT	Longitudinal accel. - 3rd floor, west side
28	N1	LOAD CELL	Axial force - 1st floor exterior column
29	MX1	LOAD CELL	Moment in N-S plan - 1st floor exterior column
30	MY1	LOAD CELL	Moment in W-E plan - 1st floor exterior column
31	SX1	LOAD CELL	Shear in N-S plan - 1st floor exterior column
32	SY1	LOAD CELL	Shear in W-E plan - 1st floor exterior column

ACCEL= Accelerometer, DT= Displacement Transducer; Longitudinal = North-South Direction

Table 4-2 (Cont'd)

CHANNEL	NOTATION	INSTRUMENT	RESPONSE MEASURED
33	N2	LOAD CELL	Axial force - 1st floor interior column
34	MX2	LOAD CELL	Moment in N-S plan - 1st floor interior column
35	MY2	LOAD CELL	Moment in W-E plan - 1st floor interior column
36	SX2	LOAD CELL	Shear in N-S plan - 1st floor interior column
37	SY2	LOAD CELL	Shear in W-E plan - 1st floor interior column
38	N3	LOAD CELL	Axial force - 1st floor interior column
39	MX3	LOAD CELL	Moment in N-S plan - 1st floor interior column
40	MY3	LOAD CELL	Moment in W-E plan - 1st floor interior column
41	SX3	LOAD CELL	Shear in N-S plan - 1st floor interior column
42	SY3	LOAD CELL	Shear in W-E plan - 1st floor interior column
43	N4	LOAD CELL	Axial force - 1st floor exterior column
44	MX4	LOAD CELL	Moment in N-S plan - 1st floor exterior column
45	MY4	LOAD CELL	Moment in W-E plan - 1st floor exterior column
46	SX4	LOAD CELL	Shear in N-S plan - 1st floor exterior column
47	SY4	LOAD CELL	Shear in W-E plan - 1st floor exterior column
48	N5	LOAD CELL	Axial force - 2nd floor exterior column
49	MX5	LOAD CELL	Moment in N-S plan - 2nd floor exterior column
50	MY5	LOAD CELL	Moment in W-E plan - 2nd floor exterior column
51	SX5	LOAD CELL	Shear in N-S plan - 2nd floor exterior column
52	SY5	LOAD CELL	Shear in W-E plan - 2nd floor exterior column
53	N6	LOAD CELL	Axial force - 2st floor interior column
54	MX6	LOAD CELL	Moment in N-S plan - 2st floor interior column
55	MY6	LOAD CELL	Moment in W-E plan - 2st floor interior column
56	SX6	LOAD CELL	Shear in N-S plan - 2st floor interior column
57	SY6	LOAD CELL	Shear in W-E plan - 2st floor interior column
58	N7	LOAD CELL	Axial force - 2st floor interior column
59	MX7	LOAD CELL	Moment in N-S plan - 2st floor interior column
60	MY7	LOAD CELL	Moment in W-E plan - 2st floor interior column
61	SX7	LOAD CELL	Shear in N-S plan - 2st floor interior column
62	SY7	LOAD CELL	Shear in W-E plan - 2st floor interior column
63	N8	LOAD CELL	Axial force - 2nd floor exterior column
64	MX8	LOAD CELL	Moment in N-S plan - 2nd floor exterior column

Table 4-2 (Cont'd)

CHANNEL	NOTATION	INSTRUMNET	RESPONSE MEASURED
65	MY8	LOAD CELL	Moment in W-E plan - 2nd floor, exterior column
66	SX8	LOAD CELL	Shear in N-S plan - 2nd floor, exterior column
67	SY8	LOAD CELL	Shear in W-E plan - 2nd floor, exterior column
68	DF1E	LOAD CELL	Damper force - 1st floor, east side
69	DF2E	LOAD CELL	Damper force - 2nd floor, east side
70	DF1W	LOAD CELL	Damper force - 1st floor, west side
71	DF2W	LOAD CELL	Damper force - 2nd floor, west side
72	DD1E	DT	Damper displacement - 1st floor, east side
73	DD2E	DT	Damper displacement - 2nd floor, east side
74	DD1W	DT	Damper displacement - 1st floor, west side
75	DD2W	DT	Damper displacement - 2nd floor, west side
76	DLAT	DT	Lateral displacement on shaking table
77	ALAT	ACCEL	Lateral acceleration on shaking table
78	DVRT	DT	Vertical displacement on shaking table
79	AVRT	ACCEL	Vertical acceleration on shaking table
80	FORCE_W	LOAD CELL	Accuator force - west side
81	FORCE_E	LOAD CELL	Accuator force - east side
82	VFRC_SE	LOAD CELL	Vertical accuator force - South east side
83	VFRC_NE	LOAD CELL	Vertical accuator force - North east side

ACCEL= Accelerometer, DT= Displacement Transducer.

4.5 Experimental Program

The study was performed using simulated ground motion of two types: (I) white noise excitations in horizontal direction to identify structural properties of the structure at various stages of testing and to verify functionality of instrumentation; different levels of white noise excitations were used to identify structural properties when dampers were at stick state and at sliding state, and (ii) various levels of simulated historical earthquakes scaled to produce elastic and inelastic response in the structure. The structure was tested with and without dampers for comparison sakes. The testing schedule is presented in Table 4-3a and 4-3b. The tests without dampers (tests #32 through #48) were done at lower maximum levels than the tests with dampers, to permit further repairing and testing (without necessity to repair extensive damage).

A total of 28 earthquake simulation tests were performed for the structure model with six Tekton friction dampers (two each floor), with four Tekton friction dampers (two each floor at first and second floor), with two Tekton friction dampers at first floor and bare frame. Nine earthquake simulation tests were performed for the structure model with six Sumitomo friction dampers (two each floor). The simulated ground motion included Taft N21E 1952, El-Centro S00E 1940, Hachinohe 1964, Pacoima Dam S16E 1971, and Mexico City N90E 1985. The tests were performed using the horizontal components only. The simulated requirements for a 1:3 scale structure using artificial mass simulation dictated a reduction of the time interval for the horizontal accelerogram of $1{:}\sqrt{3}$. The

Table 4-3a Shaking Table Experimental Program - Sumitomo Friction Dampers

test # (1)	motion (2)	PGA(g's) (3)	no. of dampers (4)	file name (5)	date (1993) (6)	structural frequencies (Hz) (7)			notes (8)
1	white noise	0.050	0	FLOWA5A	March 5				1
2	white noise	0.050	0	FLOWA50	March 5	1.62	6.94	14.37	
3	128% taft N21E	0.200	0	FLOTA20	March 5	1.31	6.56	14.37	
4	white noise	0.050	0	FLOWB50	March 5	1.62	7.00	14.50	
5	86% el-centro S00E	0.300	0	FLOEA30	March 5	1.31	6.12	14.00	
6	white noise	0.050	0	FLOWC50	March 5	1.62	6.95	14.43	
7	white noise	0.050	6	FRWWA50	March 16	2.81	9.62	16.06	
8	128% Taft N21E	0.200	6	FRWTA20	March 16				2
9	white noise	0.050	6	FRWWB50	March 17	3.00	10.80	17.31	
10	128% Taft N21E	0.200	6	FRWTB20	March 17	2.00	3.70	8.31	3
11	white noise	0.050	6	FRWWC50	March 17	3.25	11.12	18.16	
12	192% Taft N21E	0.300	6	FRWWTA30	March 17	1.81	9.37	15.94	3
13	white noise	0.050	6	FRWWD50	March 17	3.19	10.81	18.62	
14	256% taft N21E	0.400	6	FRWTA40	March 17	1.25	1.81	8.19	3
15	white noise	0.050	6	FRWWE50	March 17	3.18	10.81	18.62	
16	white noise	0.050	6	FRWWF50	March 18	3.18	10.81	18.62	
17	86% el-centro S00E	0.300	6	FRWEA30	March 18	2.37	9.56	16.56	
18	white noise	0.050	6	FRWWG50	March 18	3.18	10.81	18.21	
19	131% hachinohe	0.300	6	FRWHA30	March 18	2.31	9.31	17.31	
20	white noise	0.050	6	FRWWH50	March 18	3.12	10.81	18.31	
21	26% pacoima S16E	0.300	6	FRWPA30	March 18	2.50	8.81	17.81	
22	white noise	0.050	6	FRWWI50	March 18	3.19	10.81	18.31	
23	59% Mexico city N90	0.100	6	FRWMA10	March 18	2.87	8.69	17.75	
24	white noise	0.050	6	FRWWJ50	March 18	3.18	10.81	18.31	
25	117% Mexico city N90	0.200	6	FRWMA20	March 18	2.87	7.75	18.31	
26	white noise	0.050	6	FRWWK50	March 18	3.12	10.81	18.31	

Notes: 1. pretest; 2. Setup problem of braces (transverse vibration); 3. Connection problem of Teposonic on dampers.

Table 4-3b Shaking Table Experimental Program - Tekton Friction Dampers

test # (1)	motion (2)	PGA(g's) (3)	no. of dampers (4)	file name (5)	date (1994) (6)	structural frequencies (Hz) (7)			notes (8)
1	white noise	0.025	6	TFWWA02	June 1st	3.34	11.35	19.07	1
2	white noise	0.150	6	TFWWA15	June 1st	3.03	10.06	23.78	1
3	128% taft N21E	0.200	6	TFWTA20	June 1st	2.09	9.67	16.61	1
4	white noise	0.150	6	TFWWB15	June 1st	3.04	10.06	23.78	1
5	192% taft N21E	0.300	6	TFWTA30	June 1st	1.95	8.59	16.00	1
6	white noise	0.150	6	TFWWC15	June 1st	3.14	10.84	23.78	1
7	256% taft N21E	0.400	6	TFWTA40	June 1st	1.37	5.66	8.59	1
8	white noise	0.150	6	TFWWD50	June 1st	3.14	10.84	24.10	1
9	86% el-centro S00E	0.300	6	TFWEA30	June 1st	1.35	5.66	8.59	1
10	white noise	0.150	6	TFWWE15	June 1st	3.14	10.84	24.10	1
11	131% hachinohe	0.300	6	TFWHA30	June 1st	1.37	5.66	8.59	1
12	white noise	0.150	6	TFWWF15	June 1st	3.14	10.84	24.10	1
13	26% pacoima S16E	0.300	6	TFWPA30	June 1st	1.37	5.66	8.59	1
14	white noise	0.150	6	TFWWG15	June 1st	3.14	10.84	24.10	1
15	59% Mexico city N90	0.100	6	TFWMA10	June 2nd	3.54	11.72	18.33	1
16	white noise	0.150	6	TFWWH15	June 2nd	3.10	10.40	24.00	1
17	117% Mexico city N90	0.200	6	TFWMA20	June 2nd	3.54	11.72	18.33	1
18	white noise	0.150	6	TFWWI15	June 2nd	3.00	9.08	20.69	1
19	white noise	0.100	4	TF4WA10	June 2nd	3.03	7.93	14.26	2
20	32% taft N21E	0.050	4	TF4TA05	June 2nd	3.00	7.43	14.10	2
21	white noise	0.100	4	TF4WB10	June 2nd	3.03	7.93	14.26	2
22	128% taft N21E	0.200	4	TF4TA20	June 2nd	1.32	5.43	8.12	2
23	white noise	0.100	4	TF4WC10	June 2nd	3.03	7.93	14.26	2
24	86% el-centro S00E	0.300	4	TF4EA30	June 2nd	1.32	5.43	8.12	2
25	white noise	0.050	2	TF2WA05	June 6th	2.09	8.20	13.01	3
26	32% taft N21E	0.050	2	TF2TA05	June 6th	2.09	8.20	13.01	3
27	white noise	0.050	2	TF2WB05	June 6th	2.09	8.20	13.01	3
28	128% taft N21E	0.200	2	TF2TA20	June 6th	1.37	6.25	13.28	3
29	white noise	0.050	2	TF2WC05	June 6th	2.08	8.11	12.92	3
30	86% el-centro S00E	0.300	2	TF2EA30	June 6th	1.37	6.25	13.28	3
31	white noise	0.050	2	TF2WD05	June 6th	2.09	8.20	13.01	3
32	white noise	0.050	0	DBFWE05	June 7th	1.29	5.30	11.77	
33	32% taft N21E	0.050	0	DBFTB05	June 7th	1.17	4.88	12.11	
34	white noise	0.050	0	DBFWF05	June 7th	1.29	5.30	11.77	
35	128% taft N21E	0.200	0	DBFTB20	June 7th	0.98	4.88	11.00	
36	white noise	0.050	0	DBFWG05	June 7th	1.29	5.42	11.77	
37	86% el-centro S00E	0.300	0	DBFEB30	June 7th	0.78	5.27	10.74	
38	white noise	0.050	0	DBFWH05	June 7th	1.29	5.47	11.74	

Notes: 1. two dampers each floor; 2. two dampers each floor for 1st and 2nd floors; 3. two dampers only at 1st floor.

acceleration, displacement and velocities and response spectra of the shaking table simulated motion are shown in Fig. 4-12 through 4-21.

4.6 Identification of Structure Properties

A few levels (0.025g, 0.1g and 0.15g) of narrow band (0-25) white noise excitations were used to shake the structure in order to identify initial stiffness of structure before and after each severe shaking. The low level dynamic properties, periods and mode shapes were determined as described below.

4.6.1 Experimental Identification of Dynamic Characteristics of Model

The structure is assumed to behave linearly elastic at low amplitude levels. The increased structural response is therefore:

$$\ddot{U}_i(\omega) = \left(\sum_{j=1}^{N} \phi_{ij} H_j(\omega) \Gamma_j \right) \ddot{U}_g(\omega) \quad \text{...(4-1)}$$

where $\ddot{U}_i(\omega), \ddot{U}_g(\omega)$ indicate the Fourier transforms of the absolute acceleration response (at d.o.f i) and the base excitation, respectively, $H_j(w)$ indicates the complex frequency absolute acceleration response function:

$$H_j(\omega) = \frac{r_j^{\,2} + 2\xi_j r_j i}{\left(1 - r_j^{\,2}\right) + 2\xi_j r_j i} \quad \text{...(4-2)}$$

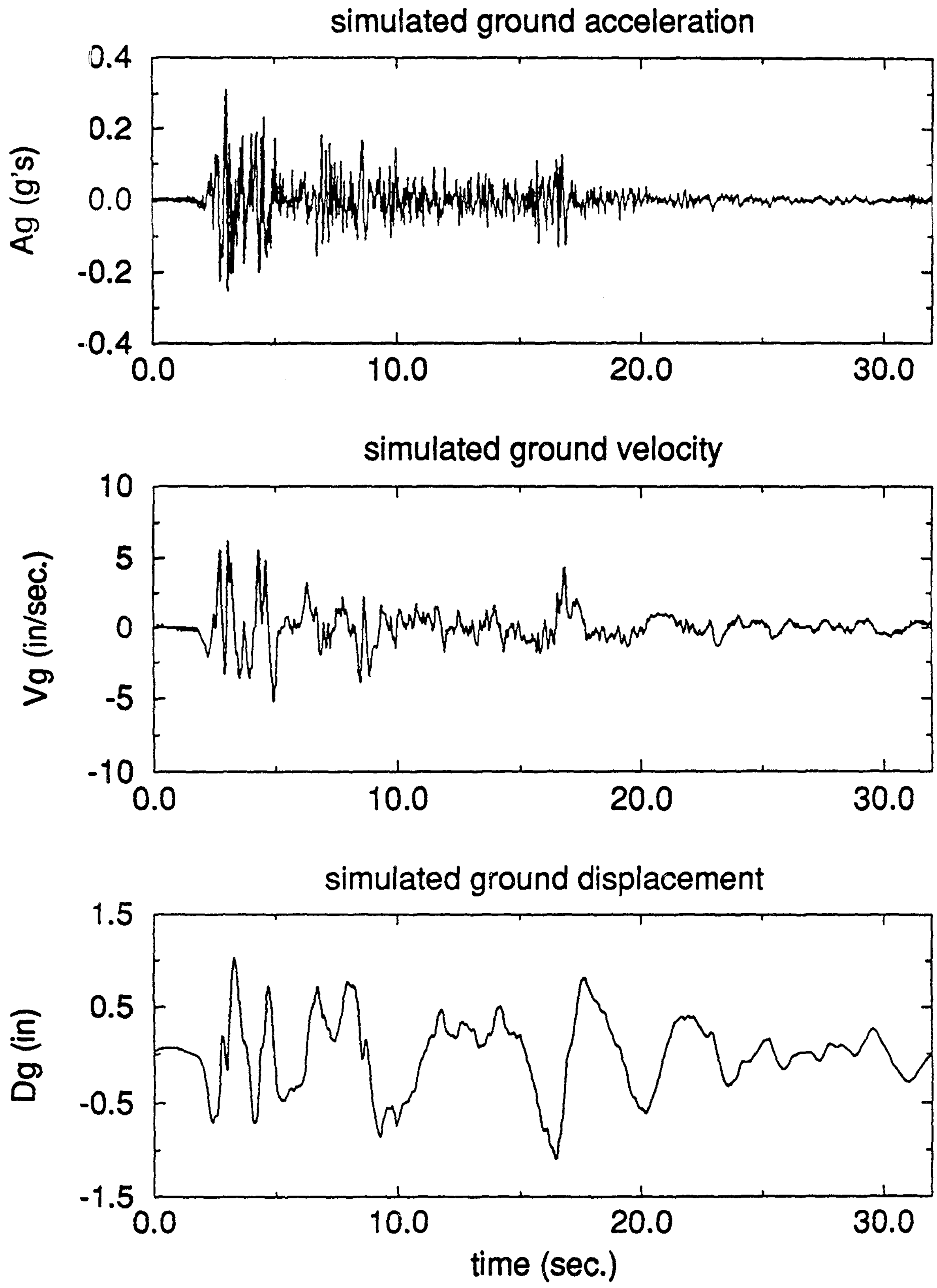

Figure 4-12 Simulated Ground Motion El-Centro S00E Scaled to PGA 0.3g ($t_m = t_p/\sqrt{3}$)

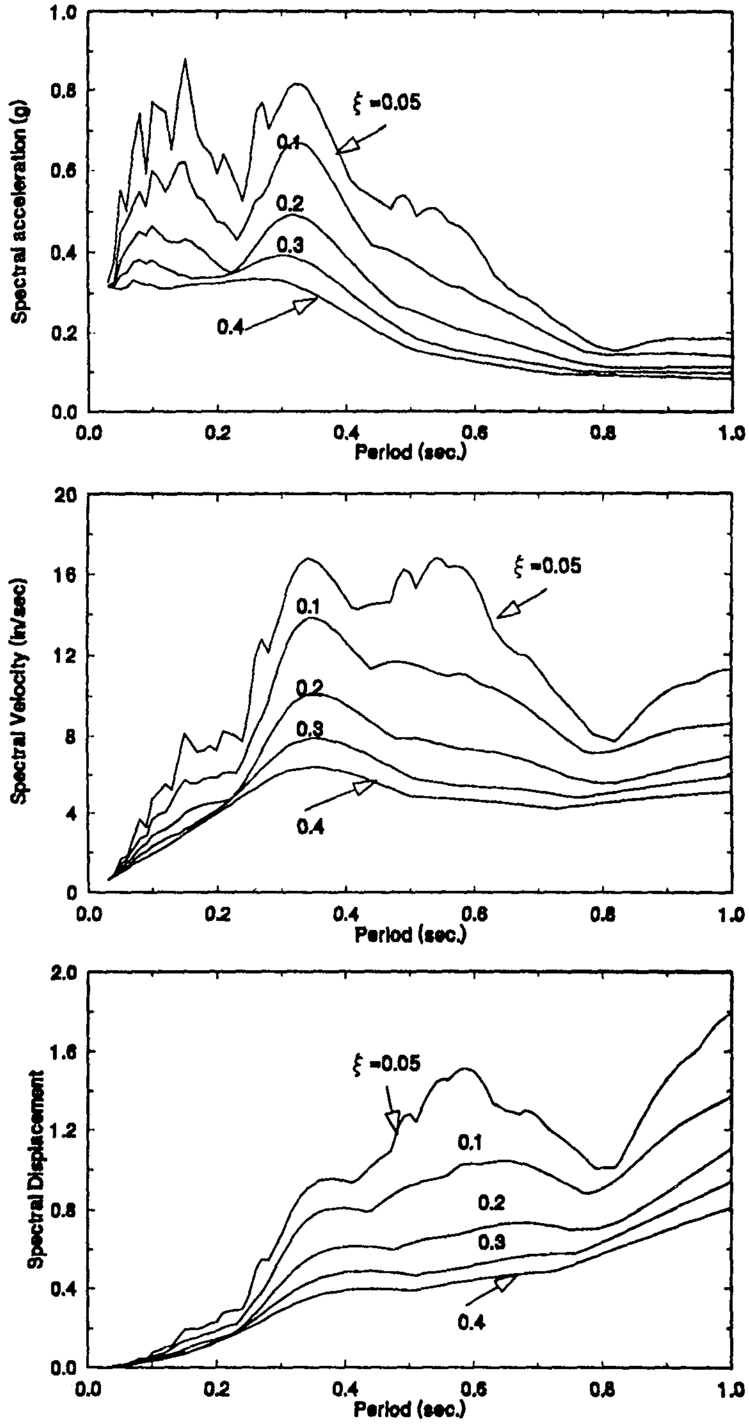

Figure 4-13 Elastic Response Spectra of Simulated El-Centro Earthquake PGA 0.3g

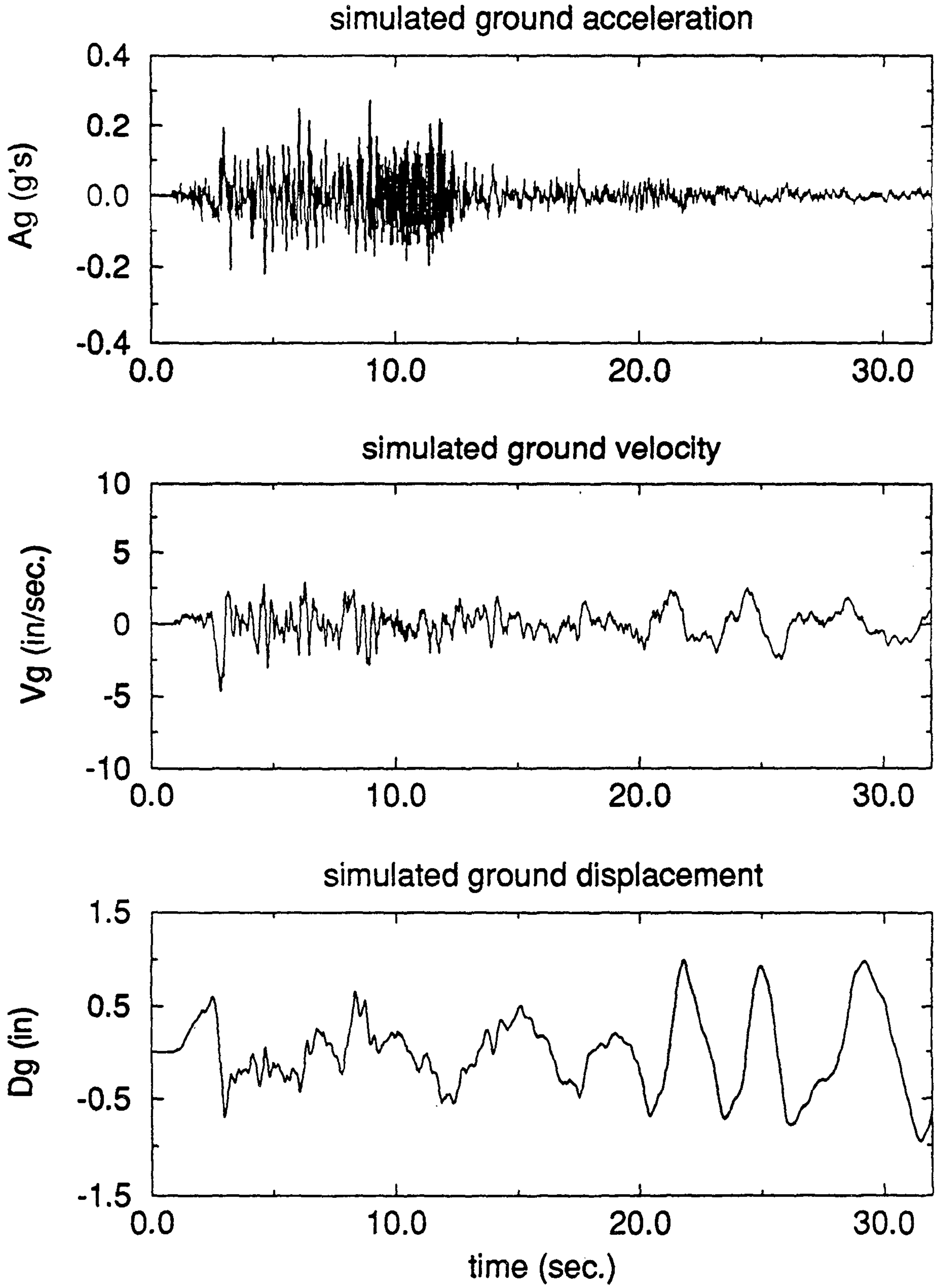

Figure 4-14 Simulated Ground Motion Taft N21E Scaled to PGA 0.2g ($t_m = t_p/\sqrt{3}$)

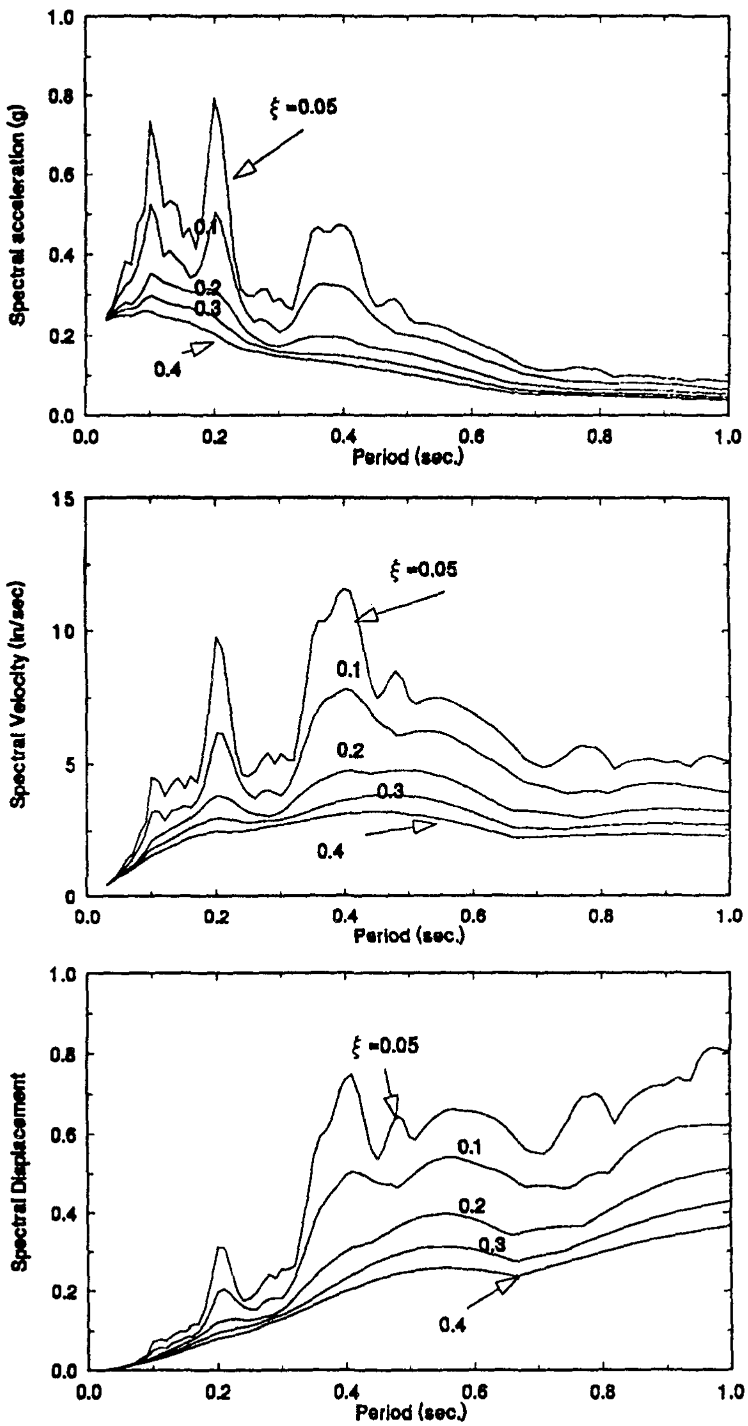

Figure 4-15 Elastic Response Spectra of Simulated Taft N21E Earthquake PGA 0.3g

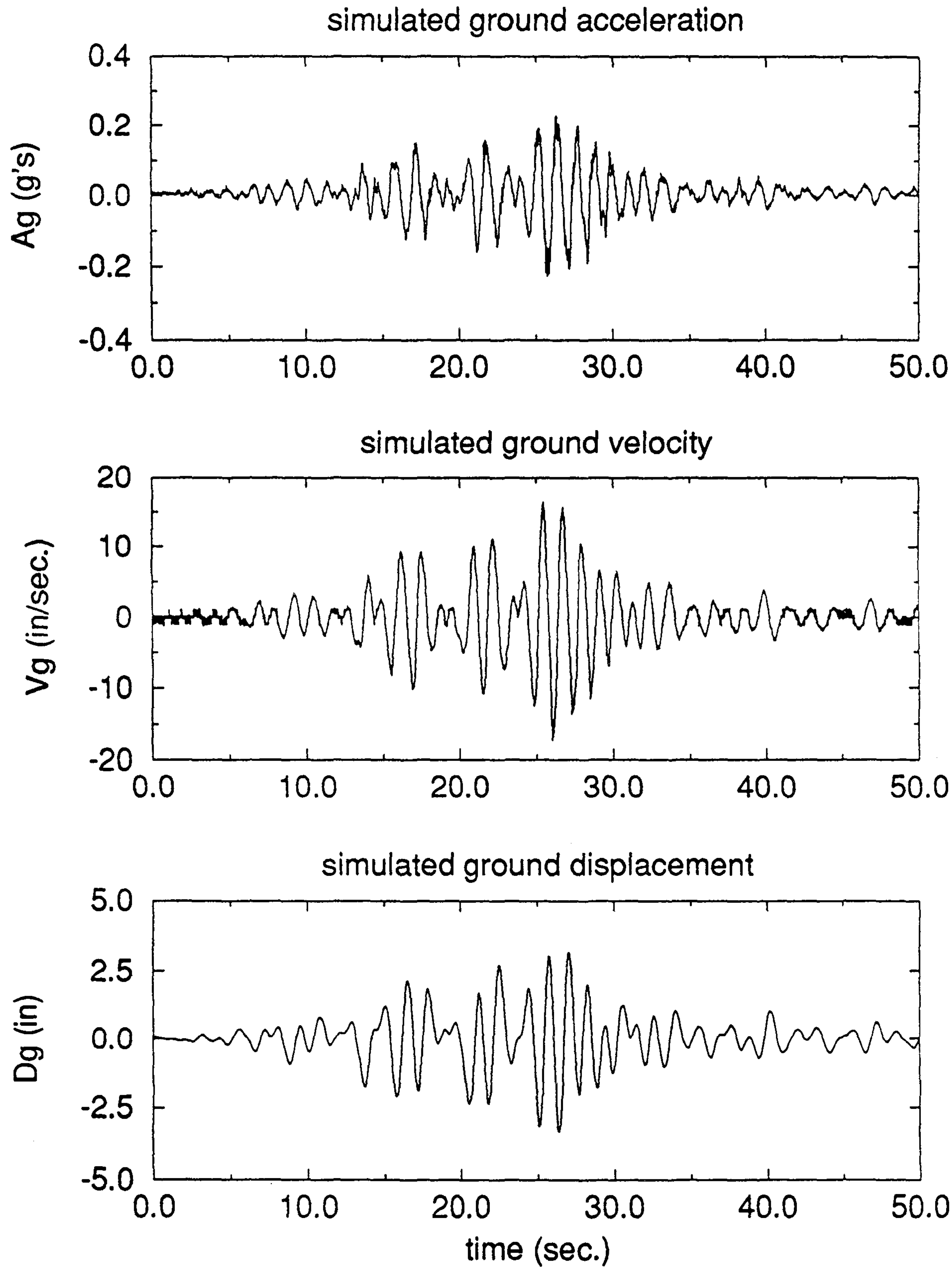

Figure 4-16 Simulated Ground Motion Mexico City N90W Scaled to PGA 0.2g ($t_m = t_p/\sqrt{3}$)

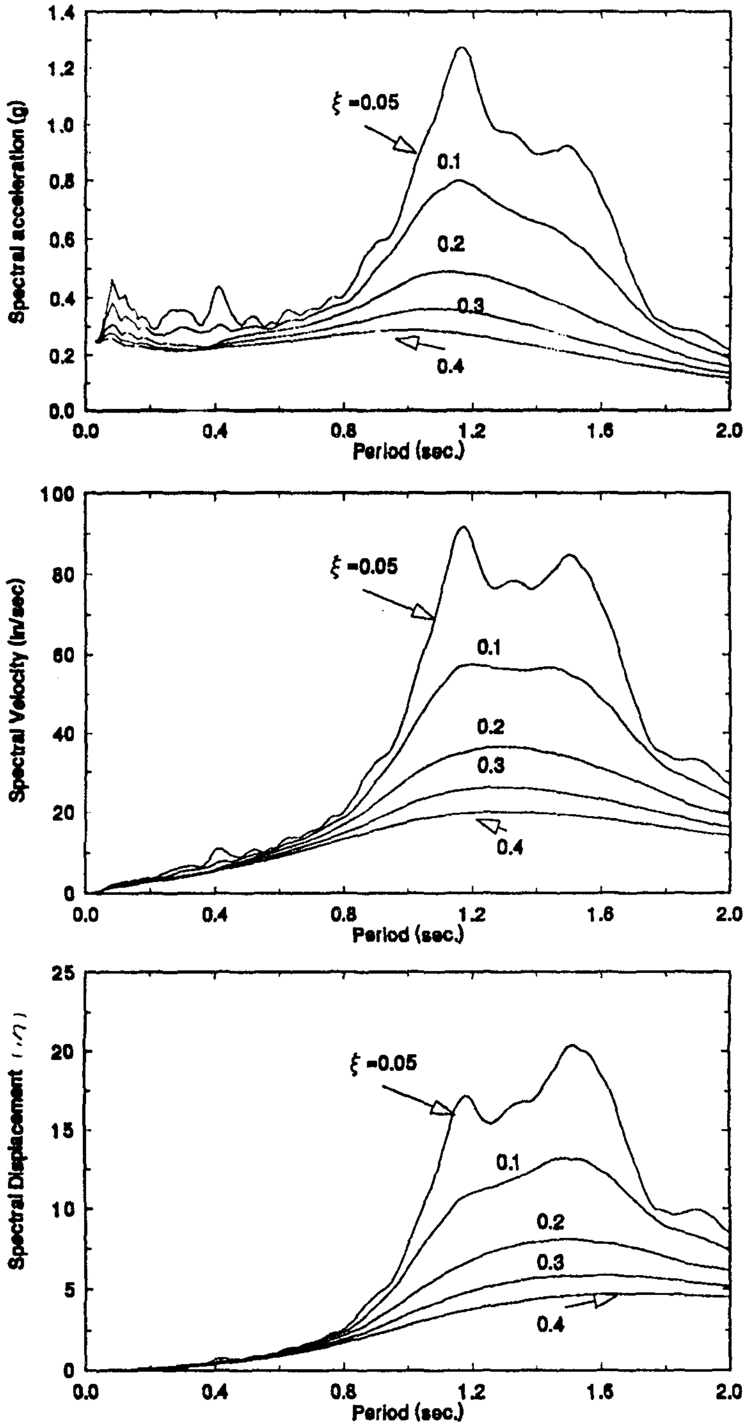

Figure 4-17 Elastic Response Spectra of Simulated Mexico City Earthquake PGA 0.2g

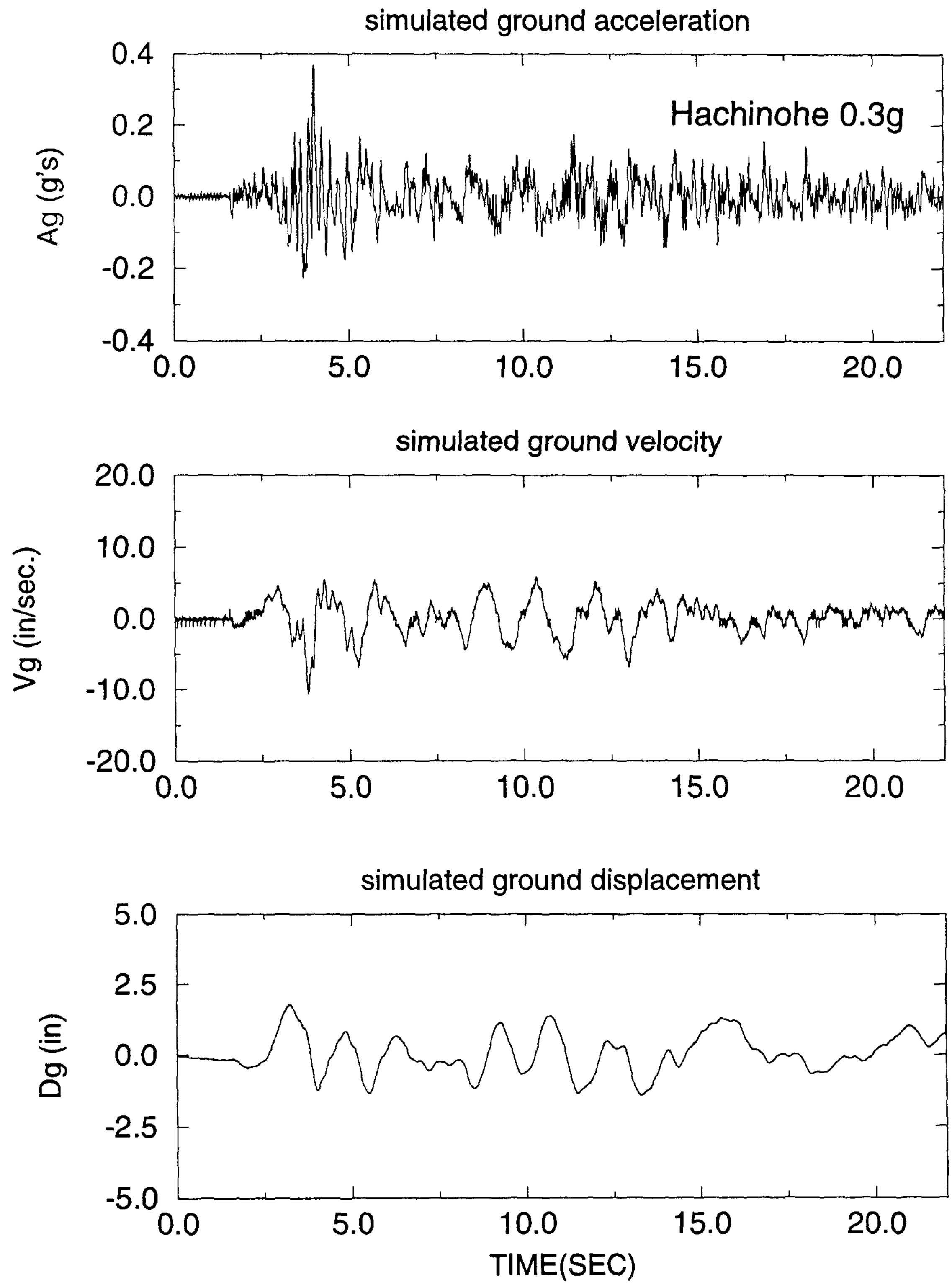

Figure 4-18 Simulated Ground Motion Hachinohe N00S Scaled to PGA 0.3g

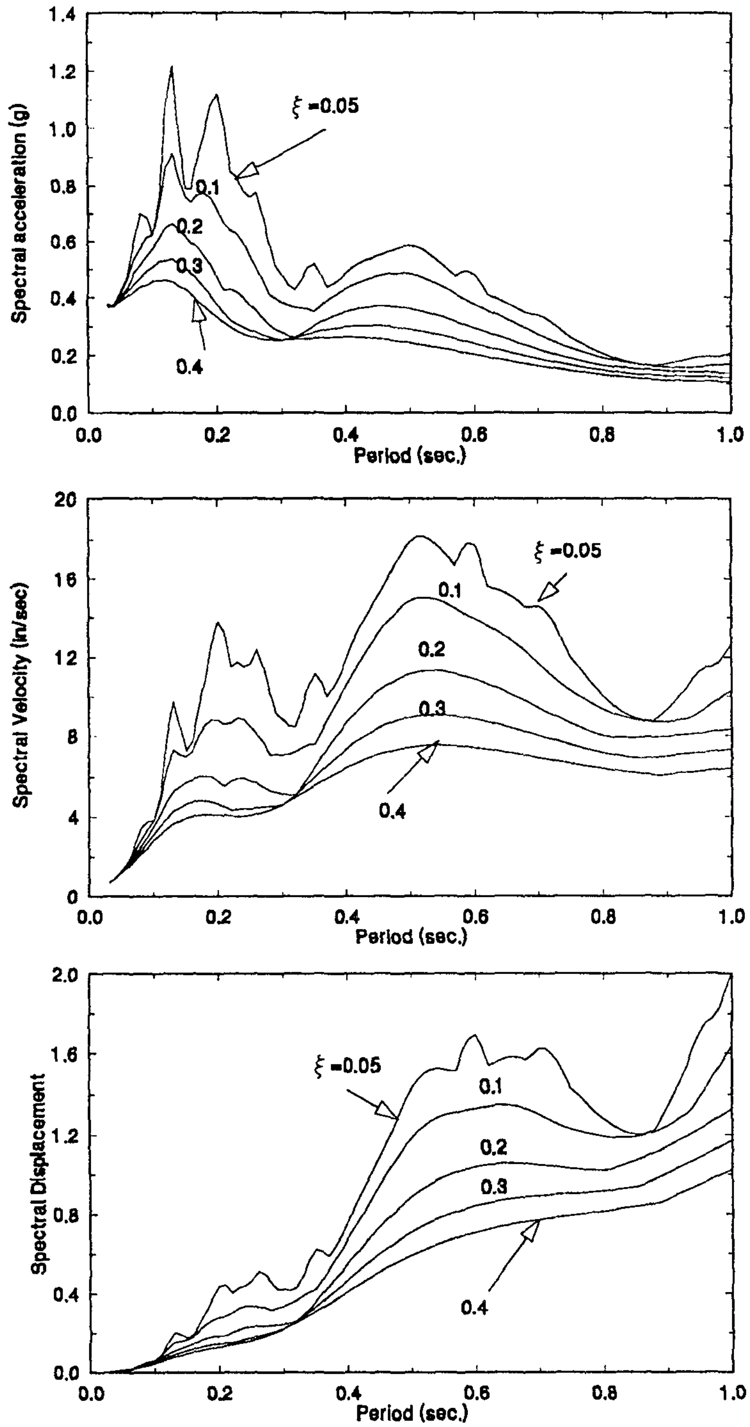

Figure 4-19 Elastic Response Spectra of Simulated Hachinohe N00S Earthquake PGA 0.3g

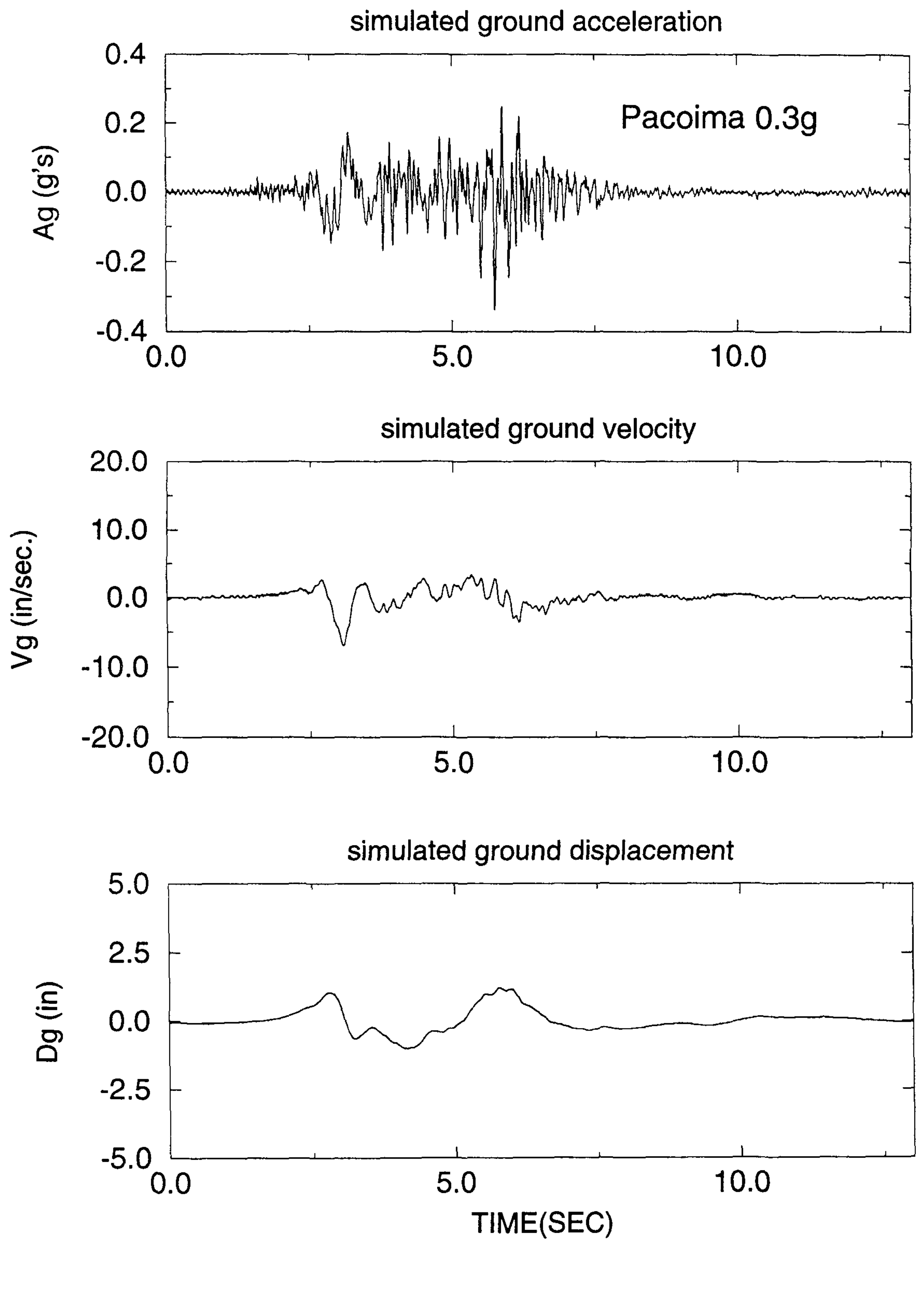

Figure 4-20 Simulated Ground Motion Pacoima S16E Scaled to PGA 0.3g

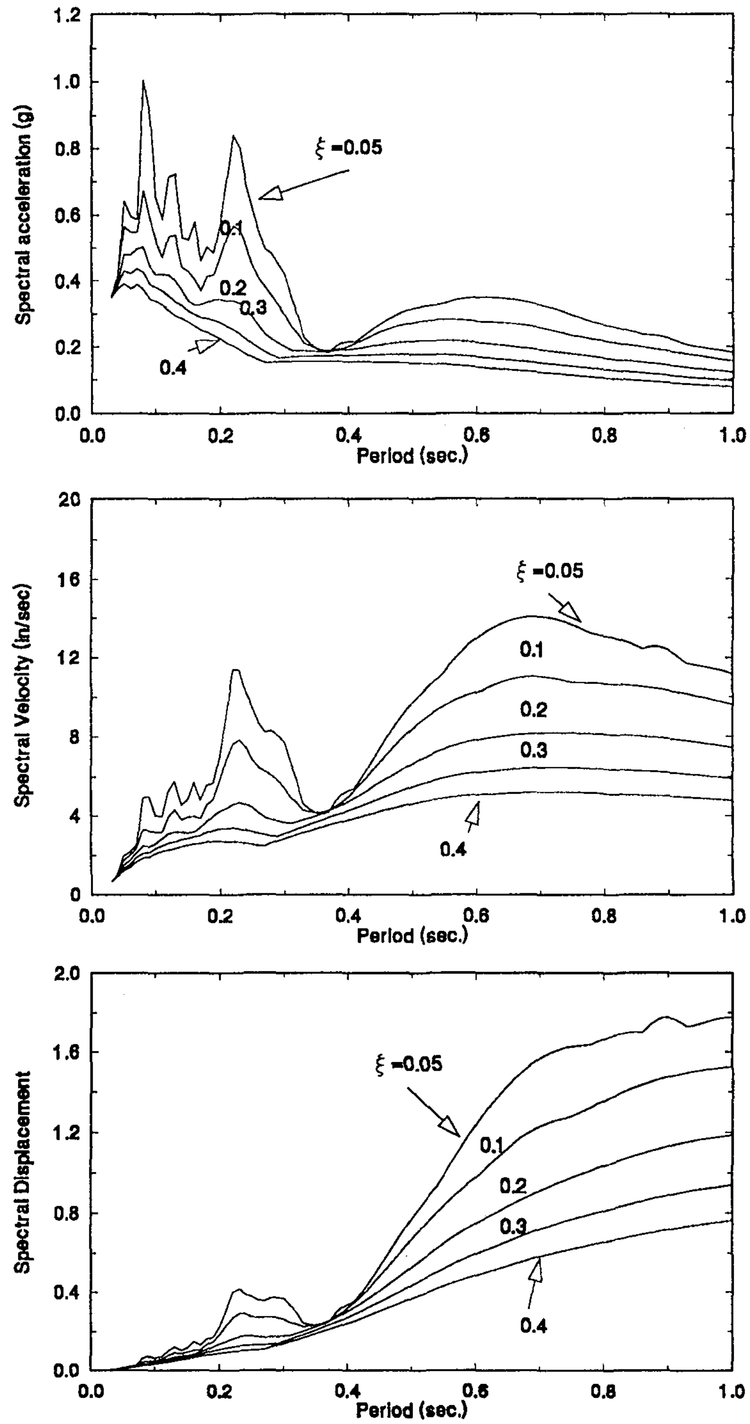

Figure 4-21 Elastic Response Spectra of Simulated Pacoima S16E Earthquake PGA 0.3g

where $r_j = \omega / \omega_j$ is the model frequency ratio for mode j, and $i = \sqrt{-1}$. In Eq. (4-1) ϕ_{ij} is the j-th mass (m) normalized mode shape for the i-th floor (DOF) satisfying the condition,

$$\sum_{i=1}^{N} \phi_{ij}^{2} m_i = 1, \quad (for\ j = 1, N) \qquad (4\text{-}3)$$

and Γ_j is the modal participation factor:

$$\Gamma_j = \sum_{i=1}^{N} \Phi_{ij} m_i \qquad (4\text{-}4)$$

For well separated modes. as obtained in the response of this structure, the acceleration response transfer function, which is defined as:

$$T_{ai}(\omega) = \ddot{U}_i(\omega) / \ddot{U}_g(\omega) \qquad (4\text{-}5)$$

is obtained at a resonant peak from single mode, k, contribution from Eq. (4-1) for $\left(H_j(\omega_k) \to 0, \quad for\ \omega_k \neq \omega_j\right)$:

$$T_{ai}(\omega) = \Phi_{ik} H_k(\omega_k) \Gamma_k \qquad (4\text{-}6)$$

The ratio of modal shapes are obtained from ratio of transfer functions from Eq. (4-6):

$$\phi_{ik} / \phi_{jk} = T_{ai}(\omega_k) / T_{aj}(\omega_k) \qquad (4\text{-}7)$$

At the peak obtained for frequency ω_k , the absolute value of the complex frequency response function from Eq. (4-2) for $r_k = 1$ is obtained as:

$$\left|H_k(\omega_k)\right| = \frac{\sqrt{1+4\xi_k^{\,2}}}{2\xi_k} \qquad \text{(4-8)}$$

Combining Eq. (4-6) and (4-8) the damping ratio ξ_k can be derived:

$$\xi_k = \left(2\sqrt{\left(\frac{T_{ai}(\omega_k)}{\phi_{ik}\Gamma_k}\right)^2 - 1}\right)^{-1} \qquad \text{(4-9)}$$

The damping ratio can be obtained from a recording at any degree of freedom i.

From the identification above, using the orthogonality conditions, the stiffness matrix of the structure can be obtained:

$$\mathbf{K} = \mathbf{M}\mathbf{\Phi}_n\Omega\mathbf{\Phi}_n^{\,T}\mathbf{M} \qquad \text{(4-10)}$$

in which $\mathbf{M}$ is the mass matrix and $\mathbf{\Omega}$ is:

$$\Omega = diag\left(\omega_1^{\,2}, \omega_2^{\,2}, \ldots, \omega_n^{\,2}\right)$$

while $\mathbf{\Phi}_n$ is the mass normalized modal shapes matrix obtained identification using Eq. (4-7) and (4-3) ($\mathbf{\Phi}^T\mathbf{M}\mathbf{\Phi} = \mathbf{I}$). The system matrices can be reduced to *mxm*, if only m modes are retained in the analysis.

Assuming that the damping matrix also satisfies the orthogonality conditions, it can be expressed as:

$$\mathbf{C} = \mathbf{M}\Phi_n \zeta \Phi_n^T \mathbf{M} \quad \text{(4-11)}$$

where the modal damping matrix ζ is:

$$\zeta = diag[2\xi_1\omega_1, 2\xi_2\omega_2, \ldots, 2\xi_n\omega_n]$$

ξ_i= i-th mode damping ratio

ω_i = i-th natural frequency (rad/sec)

where ξ_i are the damping ratio obtained from Eq. (4-9) for each mode k with a modal frequency ω_k.

At high level of excitation the structure becomes inelastic and the above properties cannot be obtained. However, as an indicator of structure changes the "equivalent" dynamic properties can be defined in a similar manner using Eq. (4-7), (4-9) and (4-12) with the data obtained from the pseudo-transfer function, $PT_{ai}(\omega)$, calculated from Eq. (4-5). It should be noted that while Fourier Transform of the excitation $\ddot{U}_g(\omega)$ remains constant during the response, the Fourier Transfer of the response $\ddot{U}_i(\omega)$ is only a "form of an average" of the inelastic response depending on the length of the record. The dynamic properties for the severe shaking were determined according to the above, as an indicator of the response.

4.6.2 Dynamic Characteristics of Structure

The dynamic characteristics of the structure were determined by the aforementioned identification method as indicated by the results in this section.

4.6.2.1 Structure without Supplementary Dampers

The story transfer functions of structure without dampers have small damping and well separated modes (see Fig. 4-22). The peaks occur precisely at the natural frequencies of the model are identified from low level white noise tests as following:

$$\mathbf{f} = \begin{Bmatrix} 1.56 \\ 7.03 \\ 14.06 \end{Bmatrix} \quad \text{(Hz)}$$

The mode shape matrix

$$\Phi = \begin{bmatrix} 1.00 & -0.79 & -0.55 \\ 0.84 & 0.36 & 1.00 \\ 0.48 & 1.00 & -0.79 \end{bmatrix} \left(\textit{or mass normalized} \begin{bmatrix} 2.72 & -2.25 & -1.50 \\ 2.28 & 1.03 & 2.72 \\ 1.30 & 2.85 & -2.15 \end{bmatrix} \right)$$

Thus the stiffness matrix can be calculated from Eq. 4-10 as following:

$$\mathbf{K} = \begin{bmatrix} 137.92 & -175.26 & 63.69 \\ -175.26 & 295.51 & -194.17 \\ 63.69 & -194.17 & 255.21 \end{bmatrix}$$

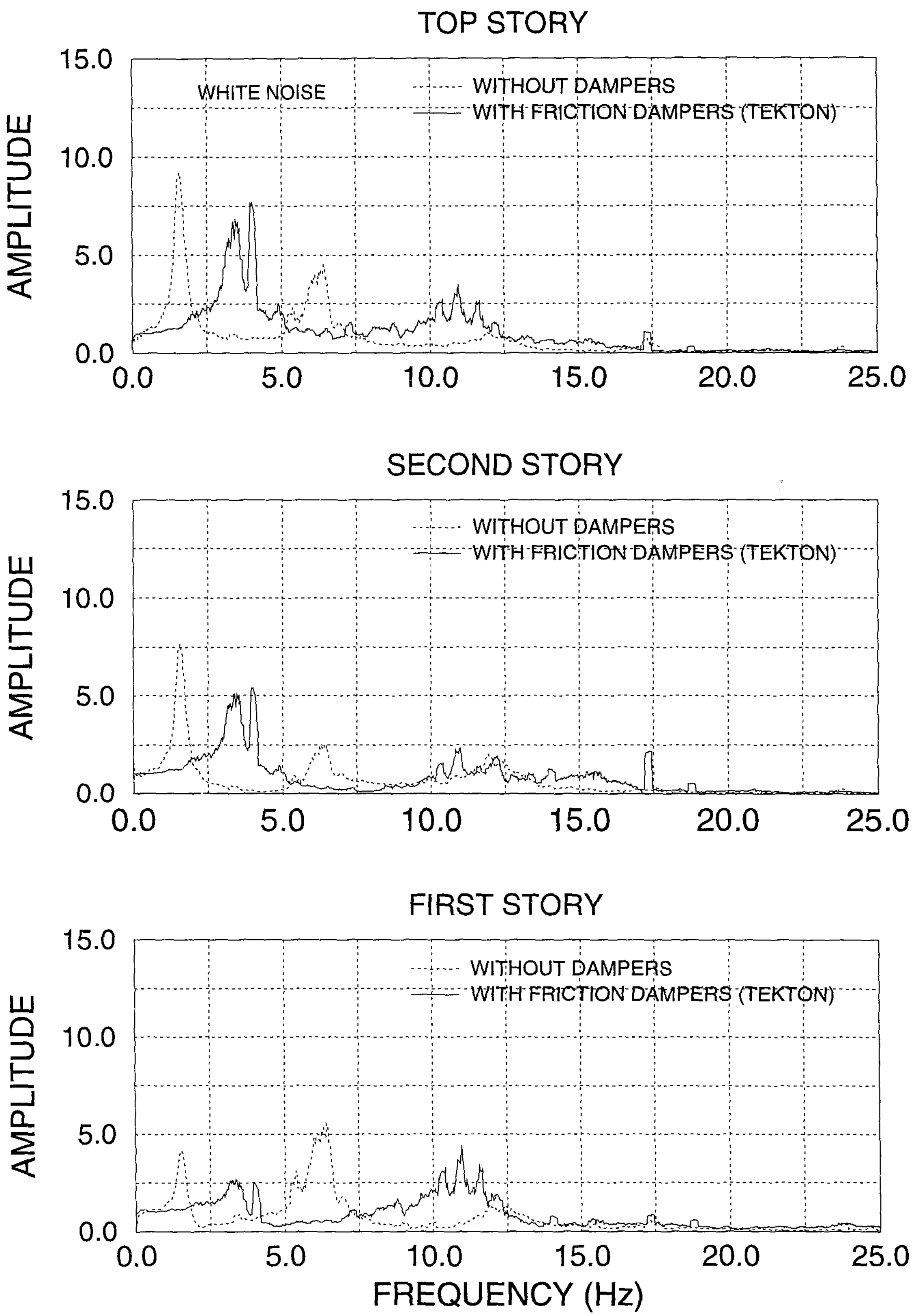

Figure 4-22 Transfer Function from White Noise Ground Motion (with and w/o Tekton Friction Dampers)

4.6.2.2 Structure with Supplementary Dampers

The structure was stiffened significantly after the friction damping devices were installed. From the transform function of white noise excitation (Fig. 4-22 and 4-23), the nature frequencies of the model with friction dampers can be identified as follows:

For the structure with Tekton friction dampers:

$$\mathbf{f} = \begin{Bmatrix} 3.33 \\ 11.00 \\ 17.30 \end{Bmatrix} (\text{Hz})$$

and the mode shape matrix

$$\mathbf{\Phi} = \begin{bmatrix} 1.00 & -0.78 & -0.47 \\ 0.75 & 0.52 & 1.00 \\ 0.39 & 1.00 & -0.43 \end{bmatrix} \left(\textit{or mass mormalized} \begin{bmatrix} 2.89 & -2.15 & -1.50 \\ 2.17 & 1.43 & 3.19 \\ 1.13 & 2.75 & -1.37 \end{bmatrix} \right)$$

Thus the stiffness matrix can be calculated by Eq. 4-10 as following

$$\mathbf{K} = \begin{bmatrix} 256.48 & -335.81 & -12.34 \\ -335.81 & 647.61 & -155.92 \\ -12.34 & -155.92 & 288.53 \end{bmatrix}$$

For the structure with Sumitomo dampers:

$$\mathbf{f} = \begin{Bmatrix} 3.32 \\ 11.30 \\ 17.60 \end{Bmatrix} (\text{Hz})$$

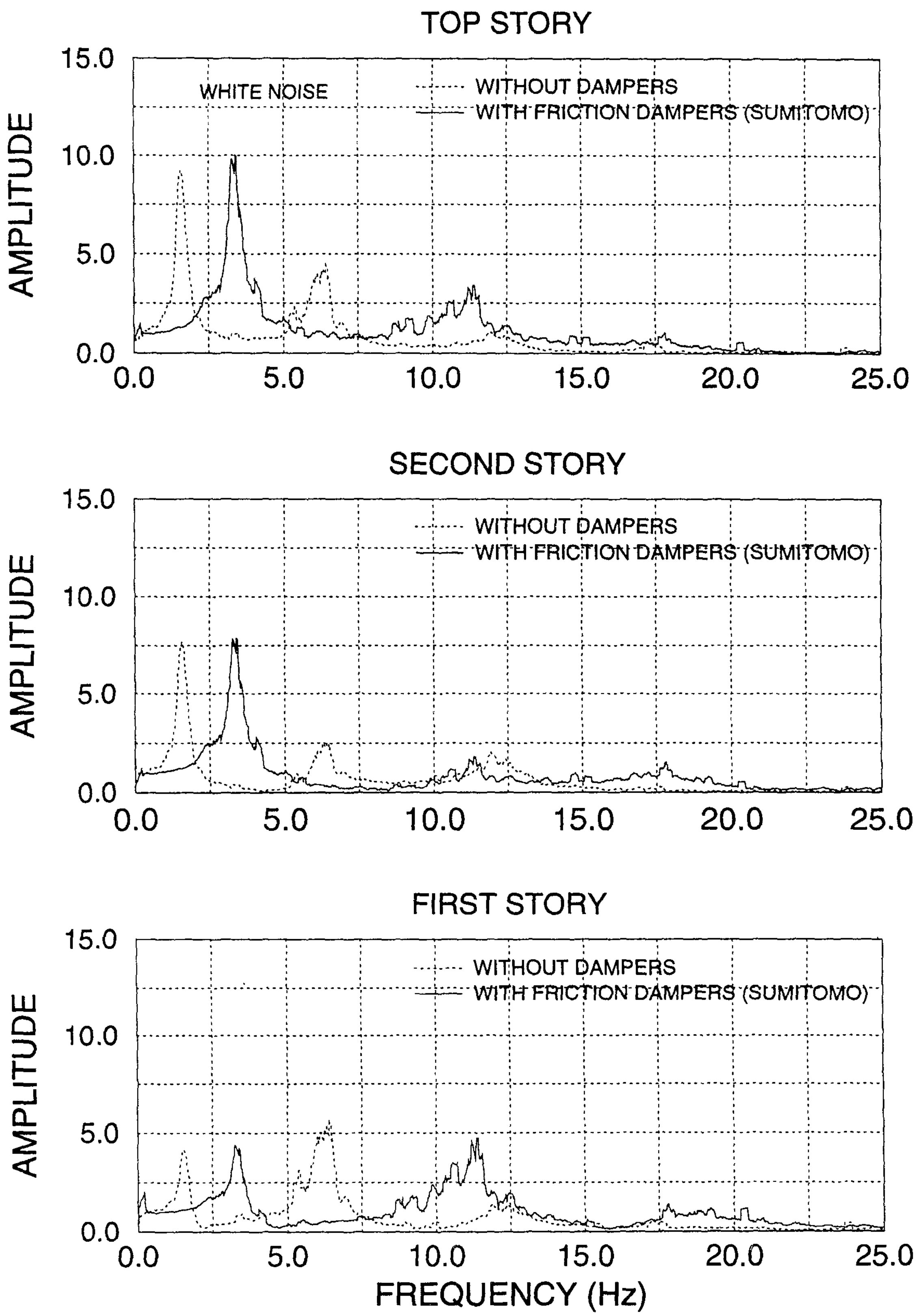

Figure 4-23 Transfer Function from White Noise Ground Motion (with and w/o Sumitomo Friction Dampers)

and the mode shape matrix

$$\mathbf{\Phi} = \begin{bmatrix} 1.00 & -0.74 & -0.54 \\ 0.78 & 0.49 & 1.00 \\ 0.39 & 1.00 & -0.90 \end{bmatrix} \left(or\, mass\, mormalized \begin{bmatrix} 2.85 & -2.09 & -1.01 \\ 2.22 & 1.39 & 2.61 \\ 1.11 & 2.83 & -2.35 \end{bmatrix} \right)$$

Thus the stiffness matrix can be calculated by Eq. 4-10 as following

$$\mathbf{K} = \begin{bmatrix} 186.34 & -216.23 & 2.87 \\ -216.23 & 466.42 & -265.12 \\ 2.87 & -265.12 & 531.37 \end{bmatrix}$$

A summary of the dynamic characteristics of the structure derived from the severe shaking (see Fig. 4-24 and 4-25) is presented in Table 4-4. It should be noted that the fundamental period of the structure at low level of shaking is reduced significantly when dampers are installed, which indicates that the braces and the dampers stiffen the structure. In fact the moment resisting frame becomes a braced frame at low deformations, before the devices slip, however, the apparent period of the structure during severe shaking is 130% larger than at the low level shaking. This can be attributed to the frequent slip of dampers and the softening effect during the inelastic response of the structure.

The damping increases at and severe shaking approximately 5 times, but increases little at low amplitude shaking.. The increase in damping at severe shaking is attributed in part to the inelastic response of structure and in part due to the increase in energy dissipation at lower amplitude in the added dampers.

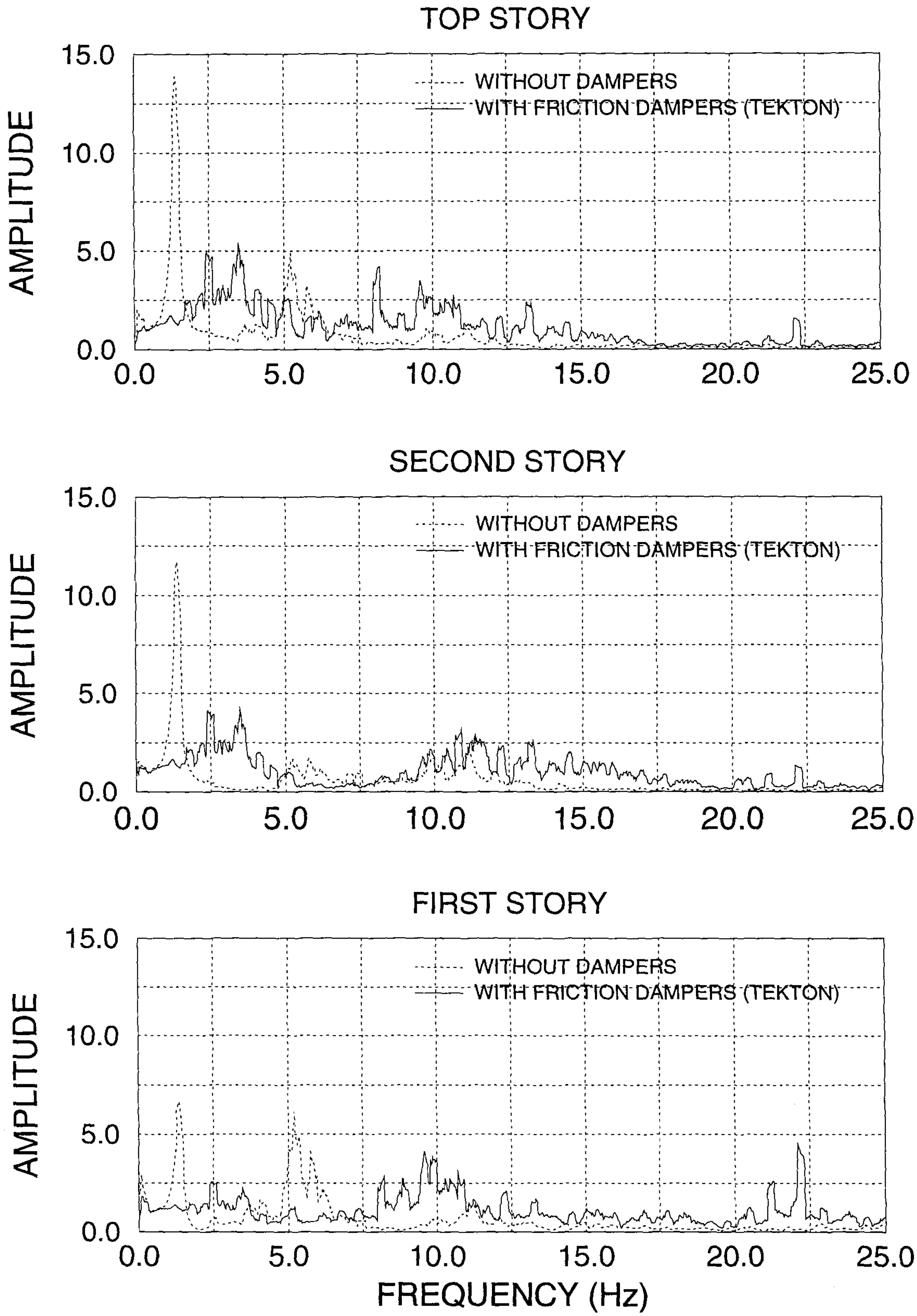

Figure 4-24 Transfer Function from El-Centro 0.3g Ground Motion (with and w/o Tekton Friction Dampers)

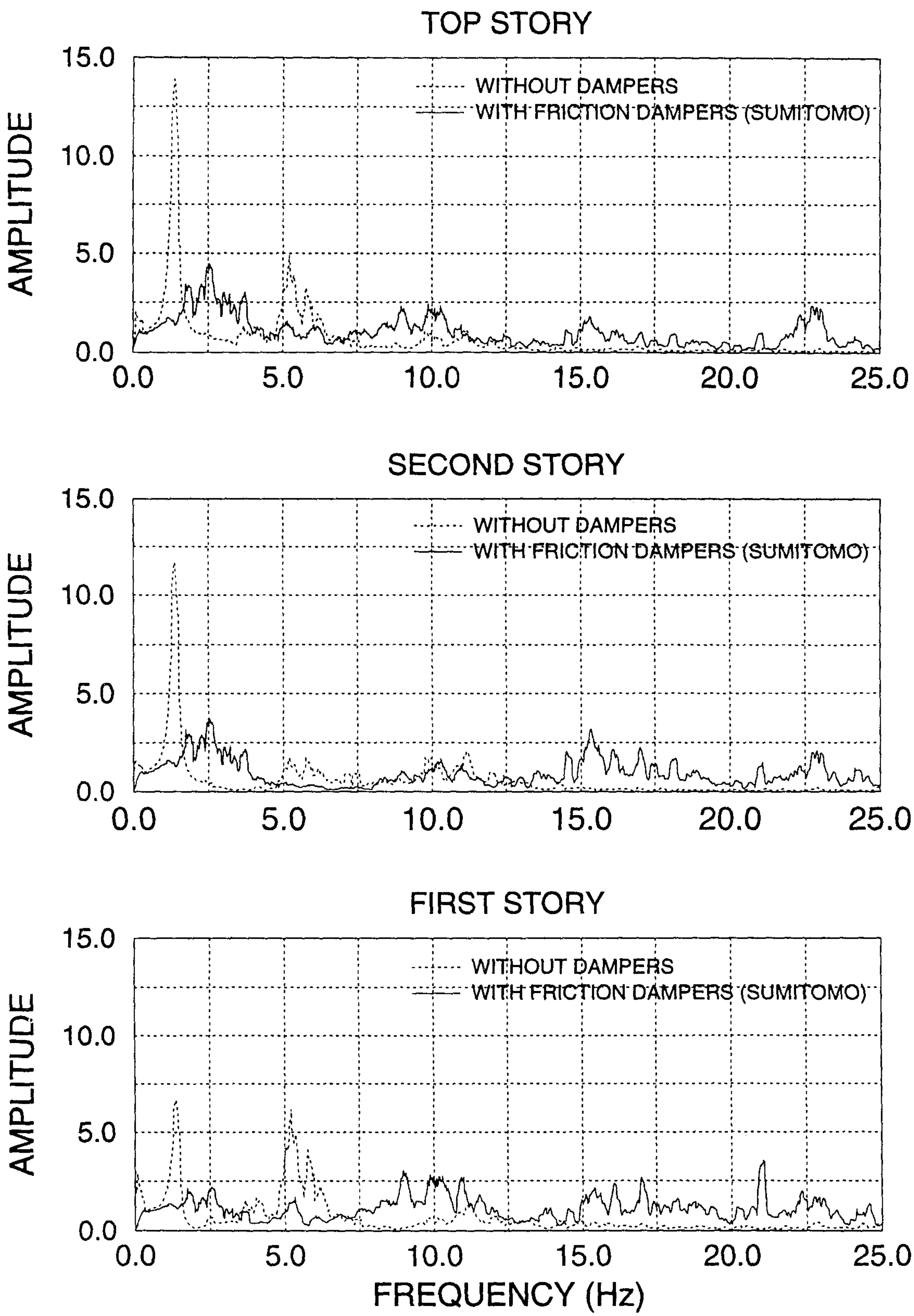

Figure 4-25 Transfer Function from El-Centro 0.3g Ground Motion (with and w/o Sumitomo Friction Dampers)

Table 4-4 Dynamic Characteristics of the Structure

Ground motion	PGA(g's)	Damping (% of critical)			Fundamental period / Frequency (second) / (Hz)	
		Low amplitude testing	Strong motion testing	Approximated analytically	Low amplitude testing	Strong motion testing
(1)	(2)	(3)	(4)	(5)	(6)	(7)
Without dampers						
El-Centro S00E	0.3	3	6	6	0.62 / 1.61	0.76 / 1.31
Taft N21E	0.2	3	5	5	0.62 / 1.61	0.76 / 1.31
With Fluid Dampers (Taylor)						
El-Centro S00E	0.3	16	28	26	0.53 / 1.88	0.62 / 1.61
Taft N21E	0.2	16	26	25	0.50 / 2.00	0.55 /1.81
With Friction Dampers (Sumitomo)						
El-Centro S00E	0.3	7	23	28	0.31 / 3.22	0.42 / 2.38
Taft N21E	0.2	7	26	22	0.31 / 3.22	0.50 / 2.00
With Viscous Damping Walls						
El-Centro S00E	0.3	50	46	44	0.25 / 4.08	0.27 / 3.70
Taft N21E	0.2	49	47	44	0.25 / 4.08	0.27 /3.70

Low amplitude testing - white noise testing before and after simulated ground motion testing.
Strong motion testing - simulated ground motion testing indicated in column (2).
Approximated analytically - according to Lobo et al., 1993.

The equivalent modal damping $\xi_{TOT,k}$ can be estimated for a mode k according to Lobo et al. (1993):

$$\xi_{TOT,k} = \Delta\xi_k + \xi_k\left(1 - \alpha_i + \alpha_i^{\,2} - \alpha_i^{\,3} + \cdots\right) \qquad (4\text{-}12)$$

where $\Delta\xi_k$ is the damping increase due to added damping devices:

$$\Delta\xi_k = \frac{1}{2\omega_k}\left(\Phi_k^{\,T}\Delta C \Phi_k\right) \qquad (4\text{-}13)\text{a}$$

or simply:

$$\Delta\xi_k = \frac{1}{2\omega_k}\sum_i c_i\left(\phi_{ik} - \phi_{i-1,k}\right)^2 \cos\theta_i \qquad (4\text{-}13)\text{b}$$

while ξ_k is the original damping the structure without dampers and

$$\alpha_k = \frac{1}{\omega_k^{\,2}}\sum \Delta k_i\left(\phi_{ik} - \phi_{i-1,k}\right)^2 \cos^2\theta_i$$

and c_i is the equivalent damping constant of friction dampers at ith degree of freedom. The equivalent damping constant c_i of friction damping device can be determined by matching the energy dissipation of the friction device with viscous damping device. Assume the slip force of the friction damper is F_{iy} and the spectral displacement in the damping device is S_d. For any test of viscous damper at a frequency Ω around structural fundamental frequency and an amplitude u_0, if the area included in one hysteretic loop W_d (energy dissipated in one cycle) is equal to $F_{iy}S_d$, we can calculate the equivalent damping constant as:

$$c_i = \frac{F_{iy}S_d}{\pi\Omega u_0^{\ 2}} \quad \text{...(4-14)}$$

where Φ_k and ω_k are the vector k in the modal shapes matrix and the frequency for the undamped structure, respectively.

The approximated values calculated according to the above are listed in Table 4-4 to capture damping increase in the severe shaking.

4.7 Seismic Response

The experimental results of the model without dampers and with different dampers configurations demonstrate clearly the benefits provided by friction damping devices. The comparisons of time history response of structure model with and without dampers are shown in Fig. 26 to 4-33 (El-Centro 0.3g ground motion). Time histories responses of structure model under other ground motions are presented in Fig. 4-44 to 4-51 for reference. The peak response at various levels of shaking is summarized in Table 4-5a and 4-5b. The forces in the structural components are shown in Fig. 4-52. The efficiency of using dampers only in lower floors can be easily seen for the tested model, but further detailed consideration should be taken for different structures. As can be seen in the test with two dampers at first floor only, the drift at second floor may be larger than that at first floor (Taft 0.2g) or close to that at first floor (El-Center 0.3g test). The shear force at

Table 4-5a Maximun Response of Structure Model with Tekton Friction Dampers

model	PGA		story drift			displ. top story	story shear			first story response					
	target	achiev	1st	2nd	3rd		1st	2nd	3rd	all column shear	single damper force	single interior col.shear	single exterior col. shear	single interior col. axial force	single exterior col. axial force
	(g's)		(in)	(in)	(in)	(in)	(kips)	(kips)	(kips)	(kips)	(kips)	(kips)	(kips)	(kips)	(kips)
(1)	(2)	(3)	(4)	(5)	(6)	(7)	(8)	(9)	(10)	(11)	(12)	(13)	(14)	(15)	(16)
	Taft N21E														
without	0.05	0.05	0.14	0.12	0.07	0.31	4.23	3.31	2.14	4.23	-	1.32	0.72	0.57	0.73
dampers	0.20	0.21	0.69	0.42	0.23	1.27	14.82	11.02	7.00	14.82	-	3.34	1.05	2.03	2.50
	El-Centro S00E														
	0.30	0.29	0.67	0.45	0.24	1.32	14.65	10.70	6.88	14.65	-	3.34	1.03	1.68	2.63
	Taft N21E														
	0.20	0.19	0.21	0.17	0.06	0.44	12.56	9.53	5.75	6.91	3.99	1.87	0.24	5.60	7.98
	0.30	0.31	0.40	0.31	0.13	0.82	13.37	12.73	7.66	8.69	4.16	2.45	0.70	6.66	8.73
with	0.40	0.48	0.59	0.48	0.21	1.26	16.58	16.92	10.07	11.84	4.31	3.01	0.96	5.47	14.43
6 friction	El-Centro S00E														
dampers	0.30	0.32	0.47	0.30	0.13	0.88	15.39	11.84	9.13	9.84	4.33	2.73	0.82	5.19	9.88
(2 dampers	Hachinohe														
each floor)	0.30	0.32	0.69	0.44	0.21	1.32	18.39	15.57	9.53	13.60	4.47	3.48	1.01	5.79	18.64
(Tekton)	Pacoima S16E														
	0.30	0.25	0.22	0.15	0.07	0.43	12.45	10.62	5.85	7.12	4.43	1.92	0.37	4.15	6.32
	Mexico city N90														
	0.10	0.12	0.16	0.10	0.05	0.30	10.83	7.69	4.44	5.49	4.68	1.40	0.25	3.28	4.34
	0.20	0.25	2.12	0.78	0.30	3.17	28.21	19.95	10.51	20.85	4.66	5.12	1.74	6.57	26.77
with	Taft N21E														
4 dampers	0.20	0.23	0.14	0.17	0.15	0.45	11.11	9.69	7.05	4.69	5.49	1.00	0.21	5.73	7.66
(2 each floor,	El-Centro S00E														
1st and 2nd)	0.30	0.32	0.40	0.24	0.17	0.77	12.20	10.36	8.46	6.48	4.70	1.67	0.48	5.57	10.70
with	Taft N21E														
2 dampers	0.20	0.23	0.22	0.26	0.18	0.64	9.55	8.24	6.72	4.80	4.48	1.10	0.27	4.10	8.85
at 1st floor	El-Centro S00E														
only	0.30	0.35	0.39	0.34	0.21	0.84	11.40	9.90	7.20	7.45	4.52	1.60	0.48	3.93	13.98

Table 4-5b Maximum Response of Structure Model with Sumitomo Friction Dampers

model	PGA	story drift			displ. top story	base shear	first story response					
		1st	2nd	3rd			all column shear	single damper force	single interior col.shear	single exterior col. shear	single interior col. axial force	single exterior col. axial force
units	(g's)	(in)	(in)	(in)	(in)	(kips)	(kips)	(kips)	(kips)	(kips)	(kips)	(kips)
(1)	(2)	(3)	(4)	(5)	(6)	(7)	(8)	(9)	(10)	(11)	(12)	(13)
	Taft N21E											
without dampers	0.20	0.62	0.33	0.26	1.02	15.17	15.17	-	3.41	0.95	2.35	2.81
	El-centro S00E											
	0.30	0.86	0.44	0.36	1.53	19.17	19.17	-	4.32	1.32	2.30	3.76
	Taft N21E											
with 6 friction dampers (2 dampers each floor) (Sumitomo)	0.20	0.26	0.18	0.14	0.50	12.65	8.27	3.22	2.28	0.44	3.62	1.51
	0.30	0.53	0.35	0.21	1.00	17.54	12.66	3.14	3.27	0.87	5.69	2.65
	0.40	0.66	0.44	0.28	1.24	19.41	14.86	3.46	3.64	1.02	6.71	3.29
	El-centro S00E											
	0.30	0.57	0.30	0.26	1.03	18.82	14.70	3.53	3.56	0.88	11.92	6.93
	Hachinohe											
	0.30	0.78	0.44	0.34	1.39	20.33	15.51	3.22	4.04	1.39	5.68	4.32
	Pacoima S16E											
	0.30	0.30	0.19	0.22	0.58	13.49	8.65	3.82	2.34	0.58	5.29	1.93
	Mexico city N90											
	0.10	0.16	0.10	0.22	0.40	10.84	6.65	3.09	1.75	0.30	4.19	0.94
	0.20	1.32	0.62	0.67	2.15	27.54	23.00	5.28*	5.12	1.80	6.33	5.13

*the stoke limit of the damper was exceeded.

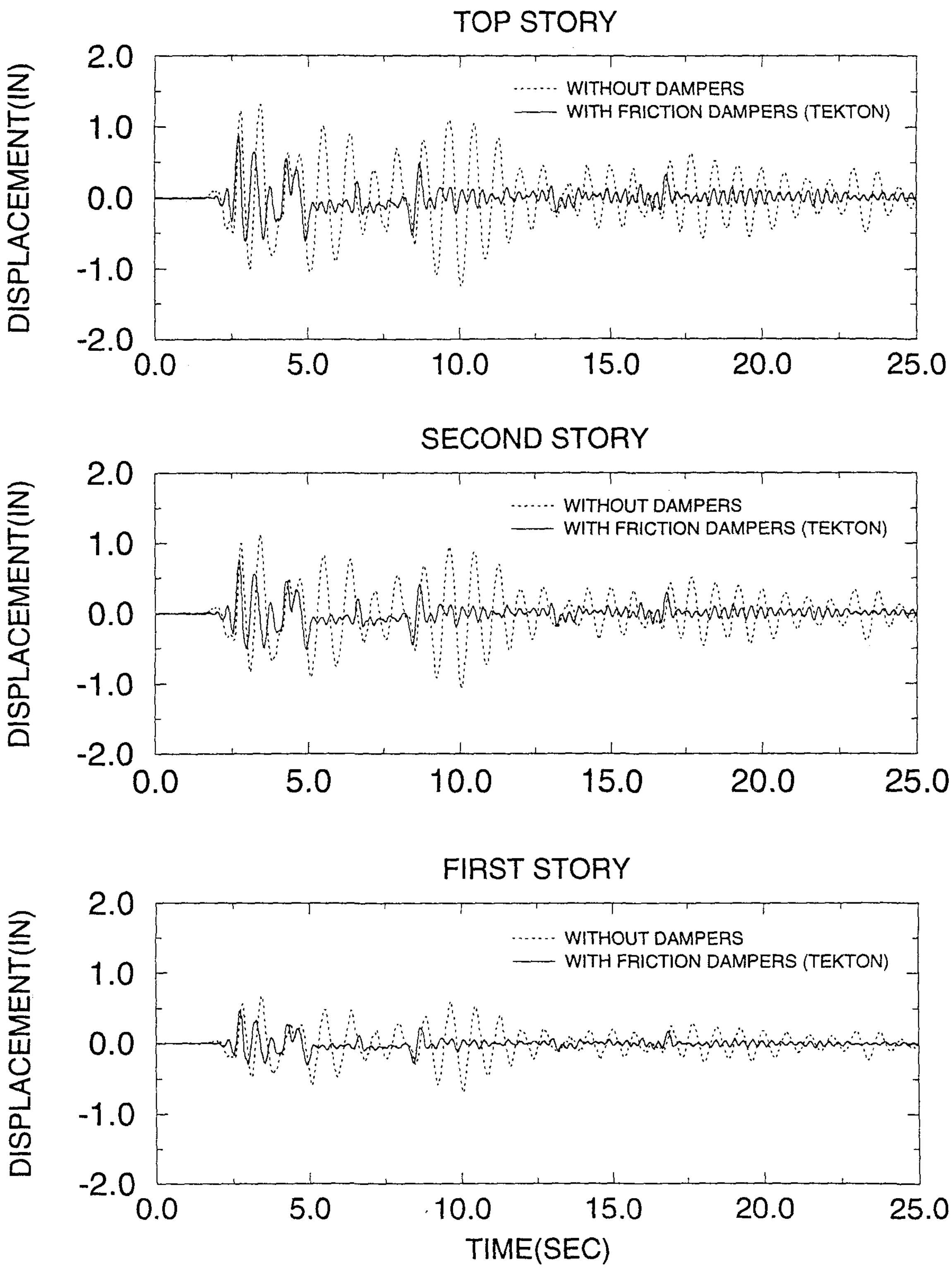

Figure 4-26 Comparison of Displacement Response History for Structure without and with Six Tekton Friction Dampers, from El-Centro Earthquake PGA 0.3g Test

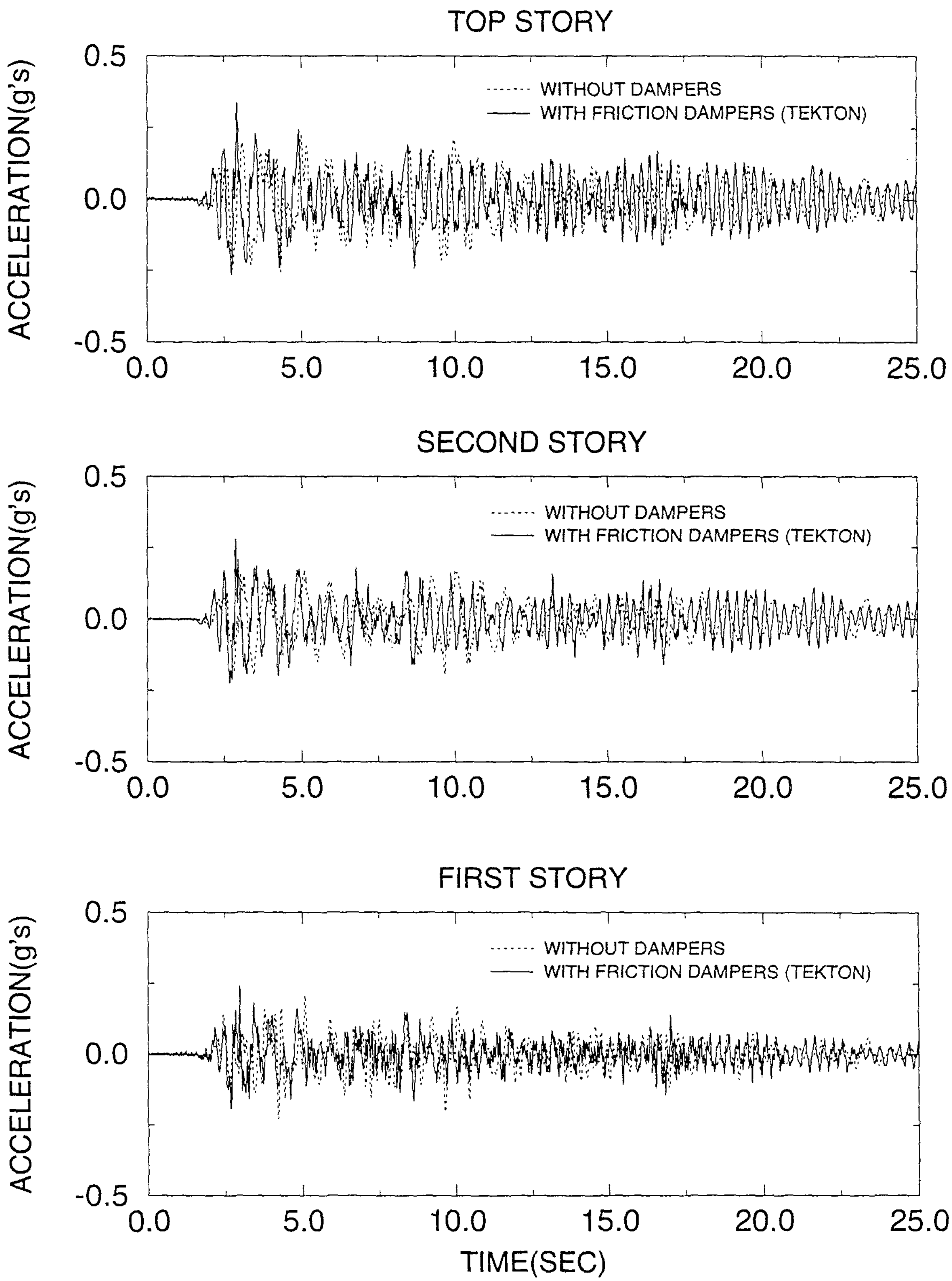

Figure 4-27 Comparison of Acceleration Response History for Structure without and with Six Tekton Friction Dampers, from El-Centro Earthquake PGA 0.3g Test

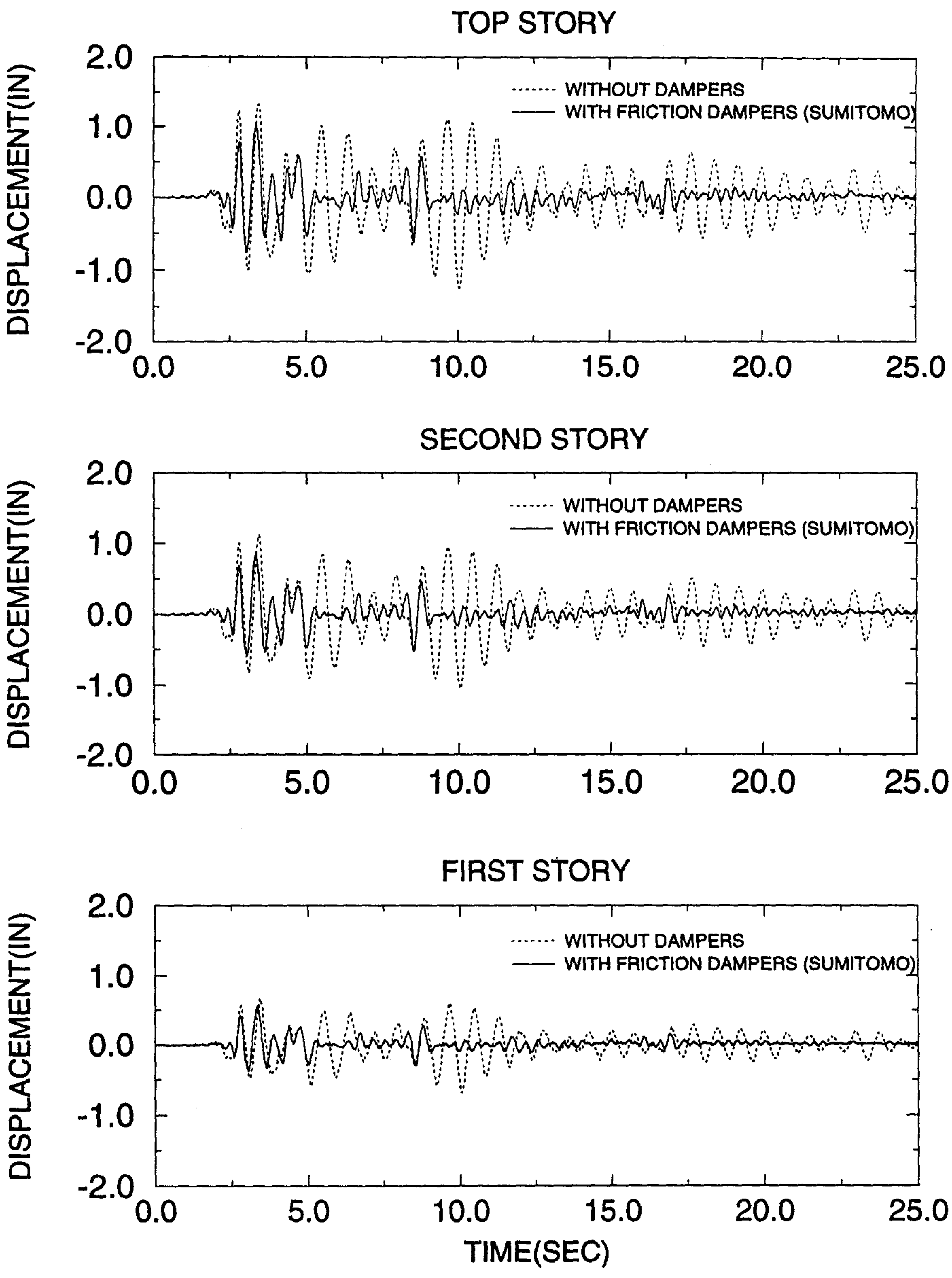

Figure 4-28 Comparison of Displacement Response History for Structure without and with Six Sumitomo Friction Dampers, from El-Centro Earthquake PGA 0.3g Test

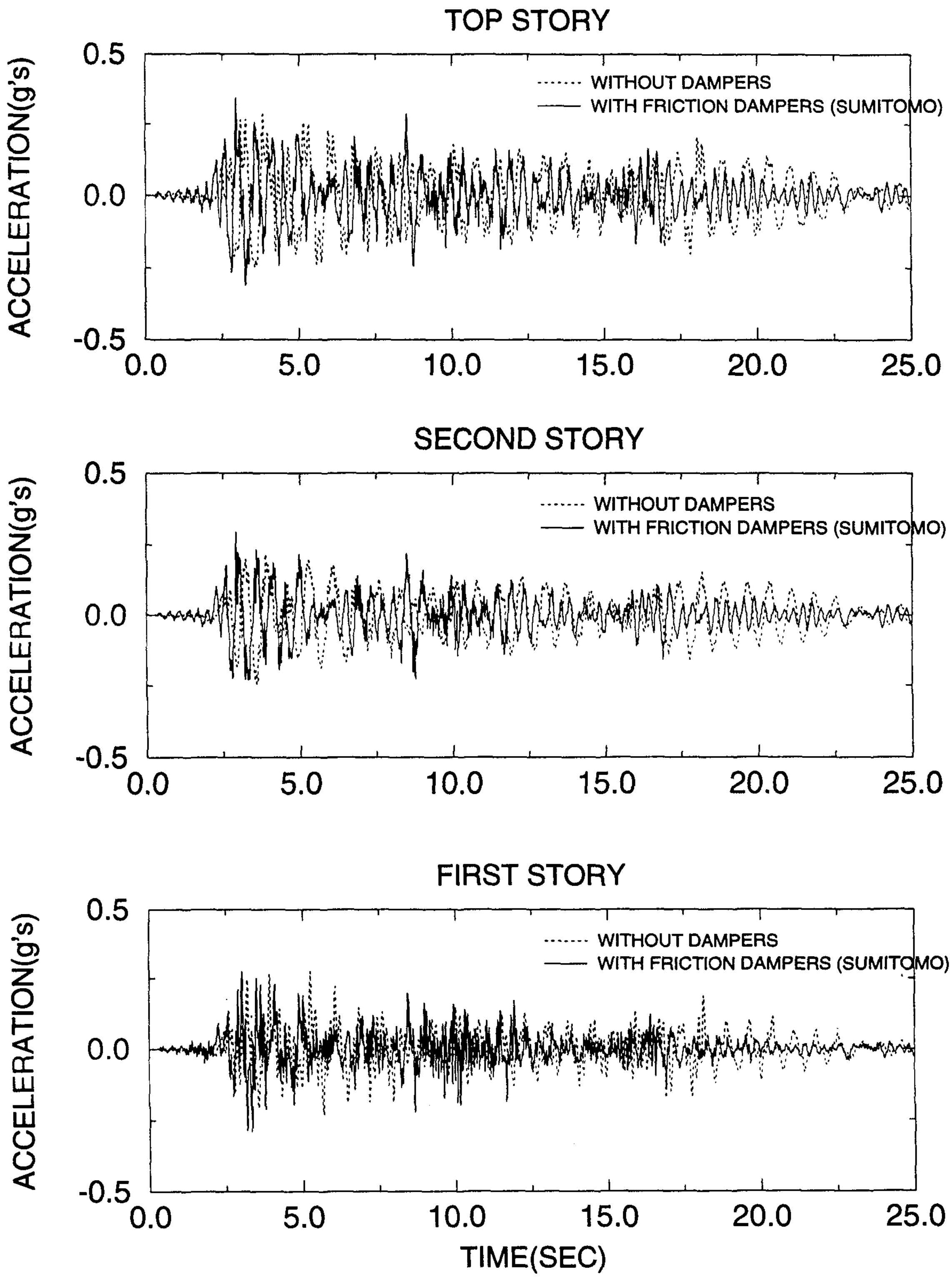

Figure 4-29 Comparison of Acceleration Response History for Structure without and with Six Sumitomo Dampers, from El-Centro Earthquake PGA 0.3g Test

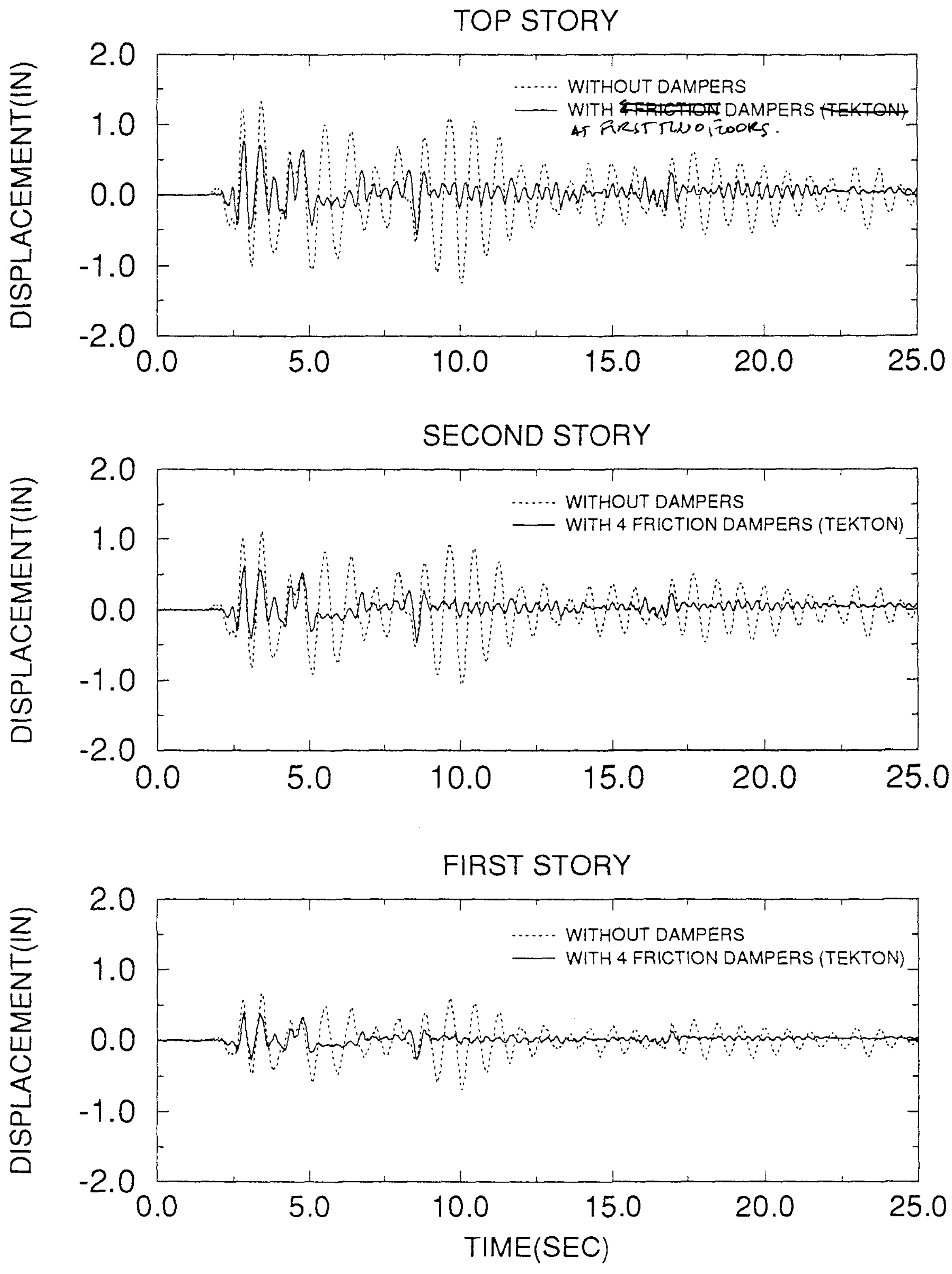

Figure 4-30 Comparison of Displacement Response History for Structure without and with Four Tekton Friction Dampers, from El-Centro Earthquake PGA 0.3g Test

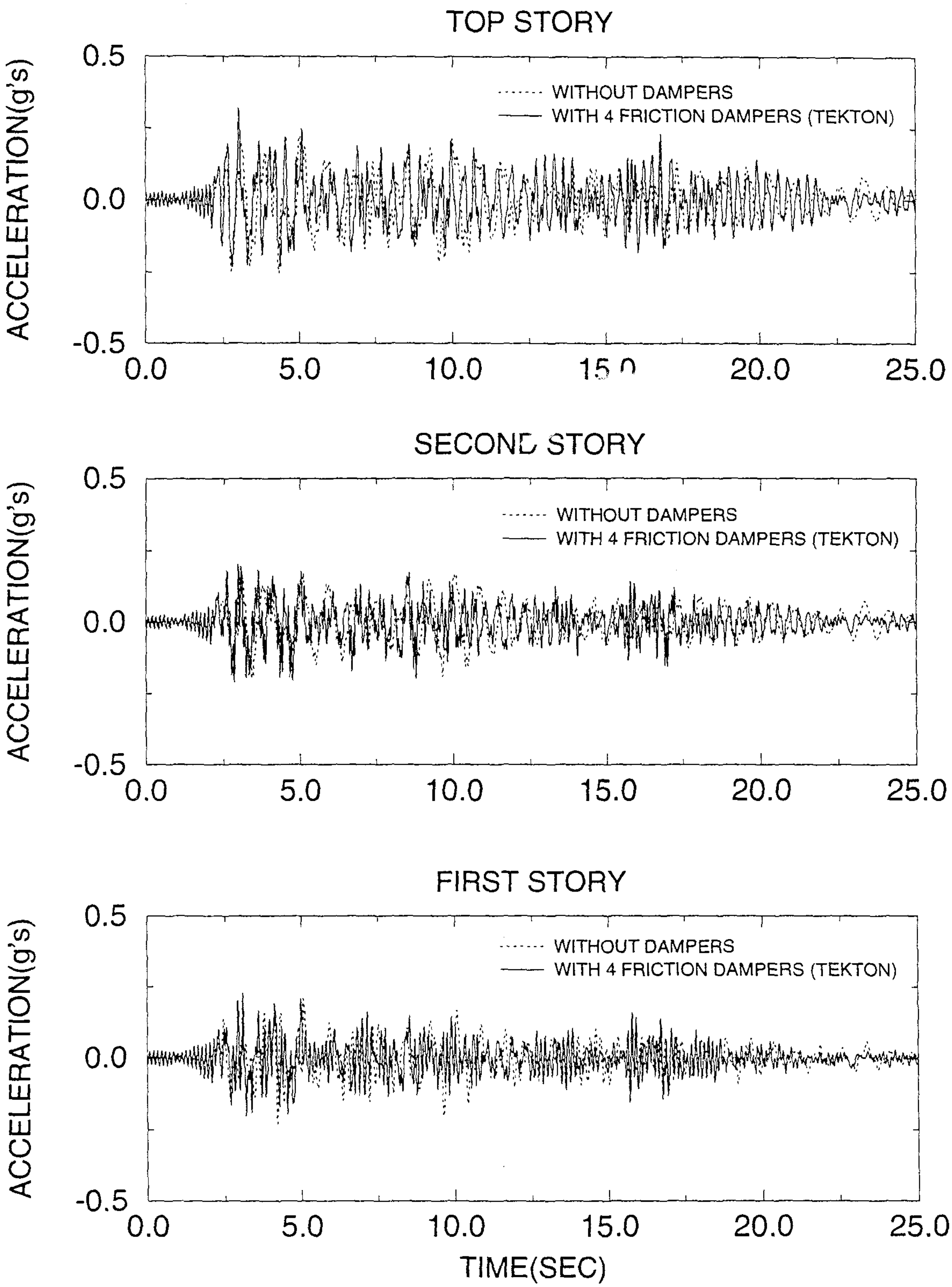

Figure 4-31 Comparison of Acceleration Response History for Structure without and with Four Tekton Friction Dampers, from El-Centro Earthquake PGA 0.3g Test

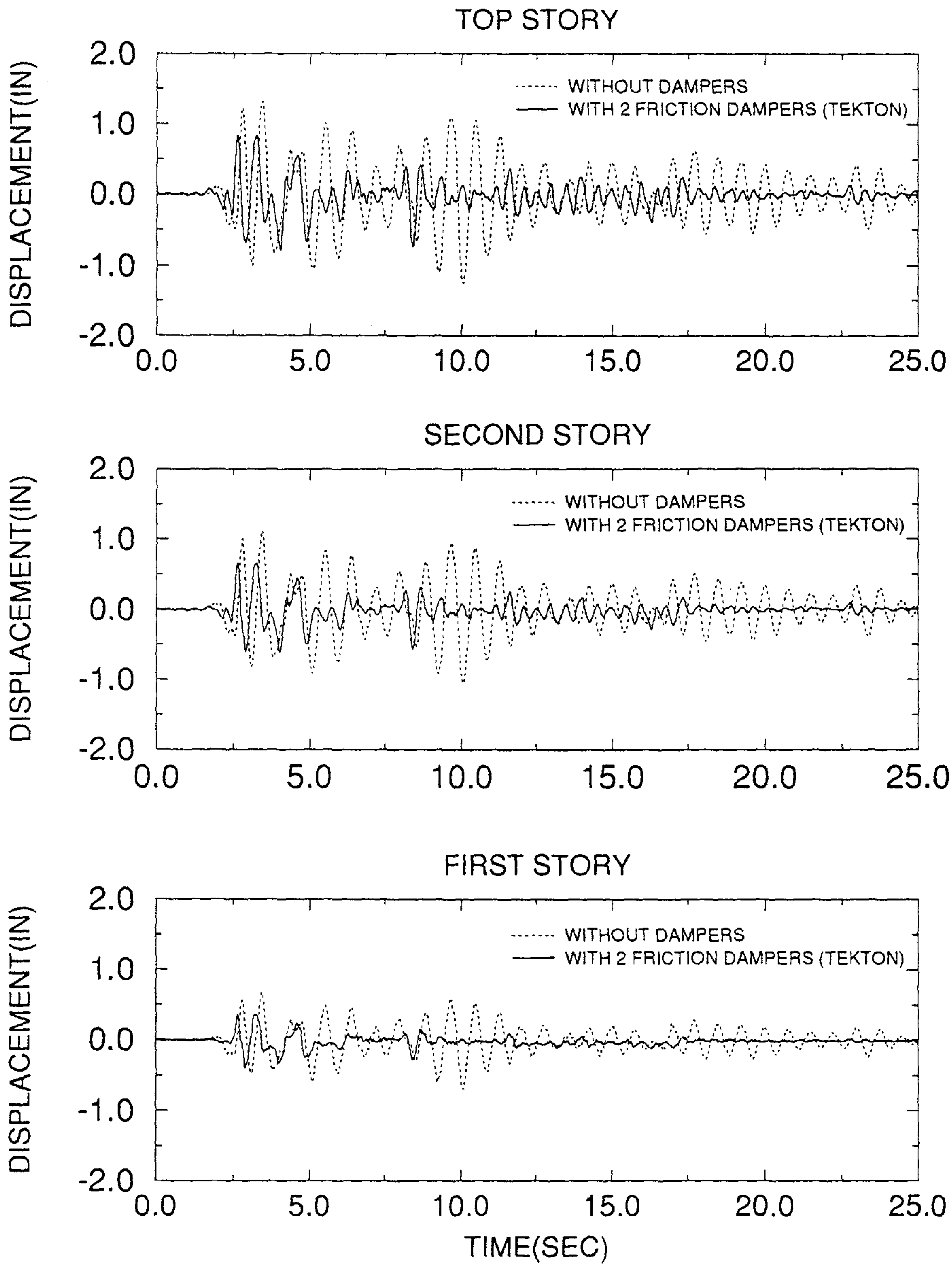

Figure 4-32 Comparison of Displacement Response History for Structure without and with Two Tekton Friction Dampers, from El-Centro Earthquake PGA 0.3g Test

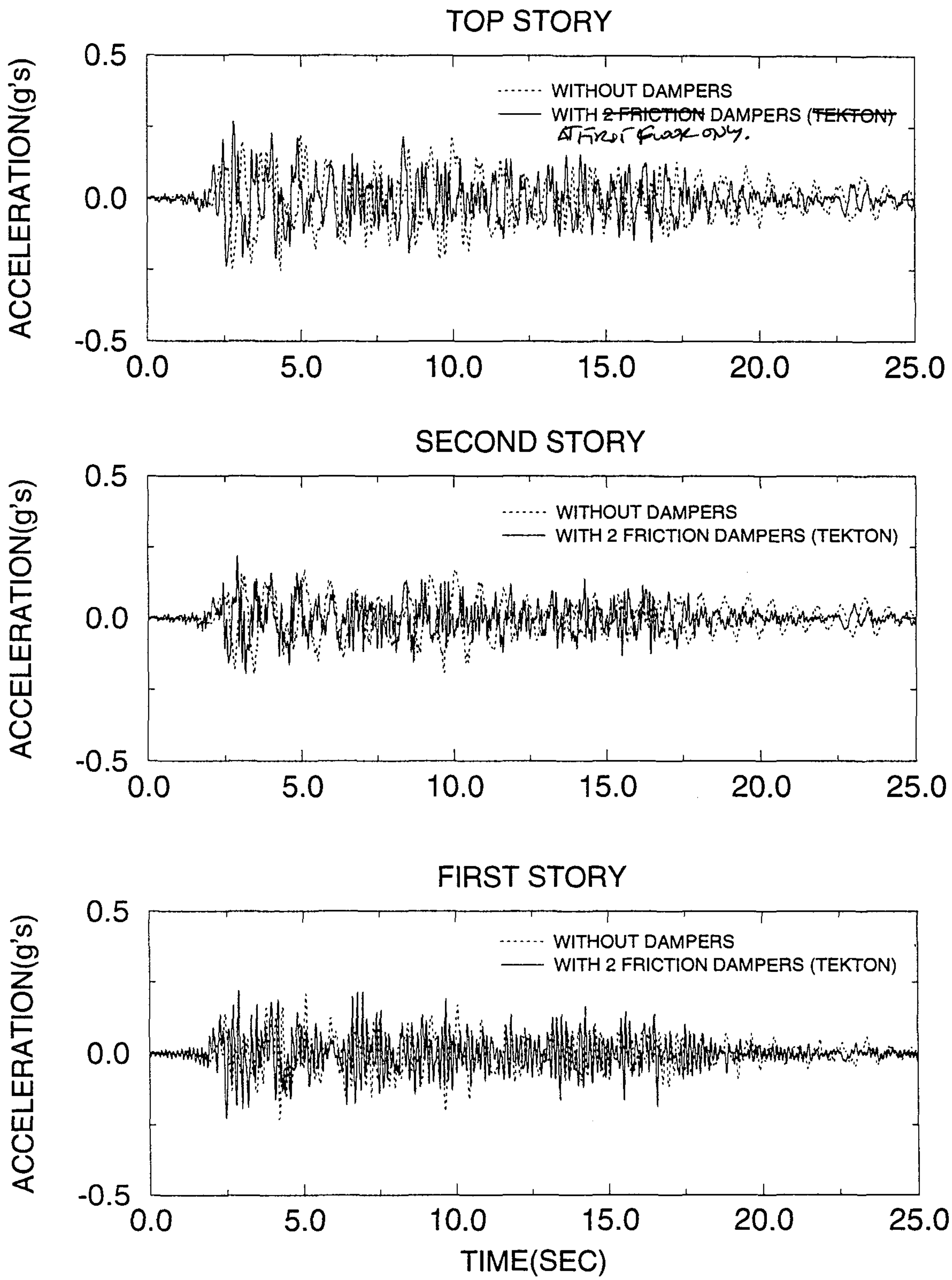

Figure 4-33 Comparison of Acceleration Response History for Structure without and with Two Tekton Friction Dampers, from El-Centro Earthquake PGA 0.3g Test

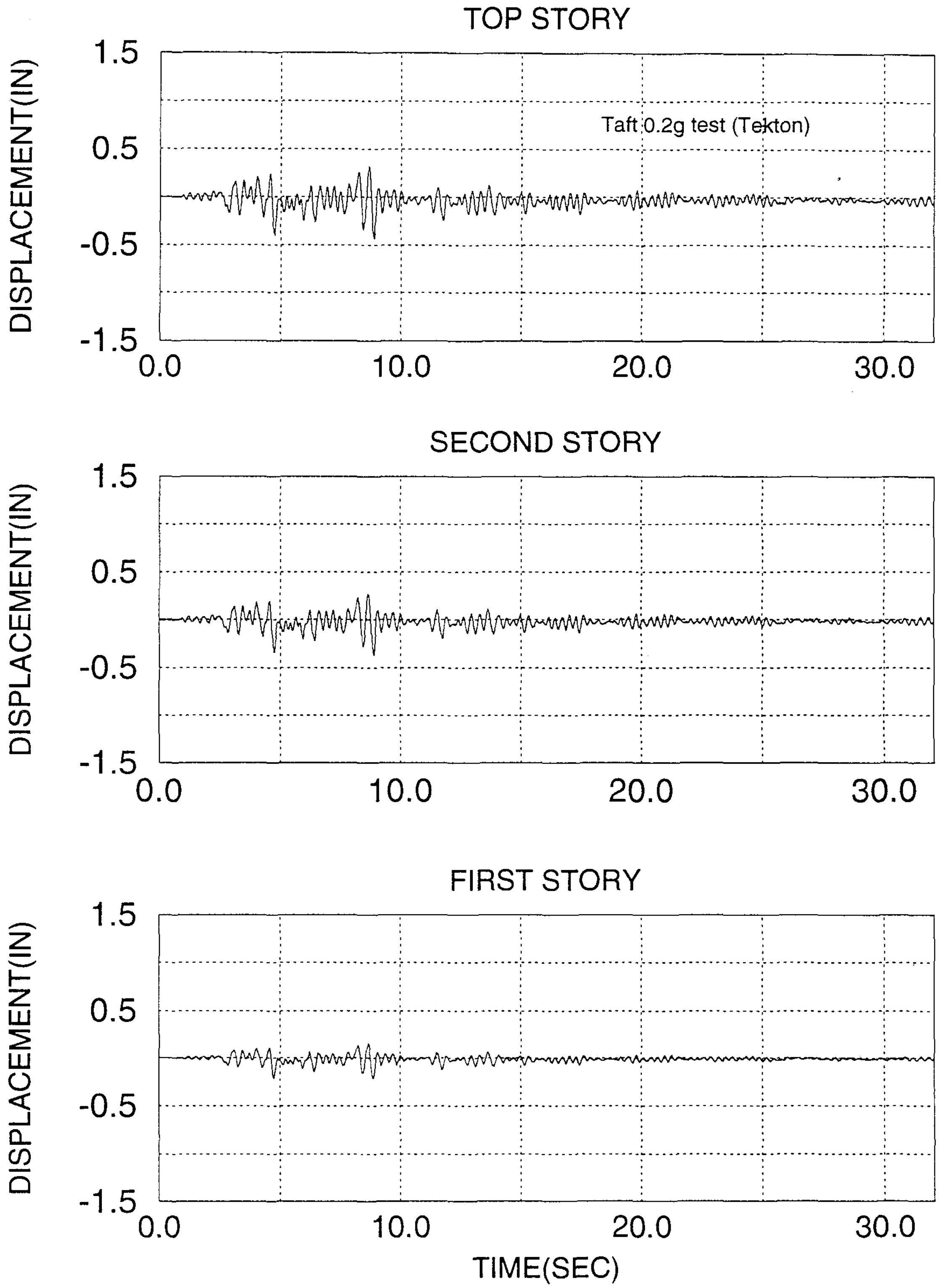

Figure 4-34 Displacement Time History Response of the Model with Six Tekton Friction Dampers, Taft Earthquake PGA 0.2g

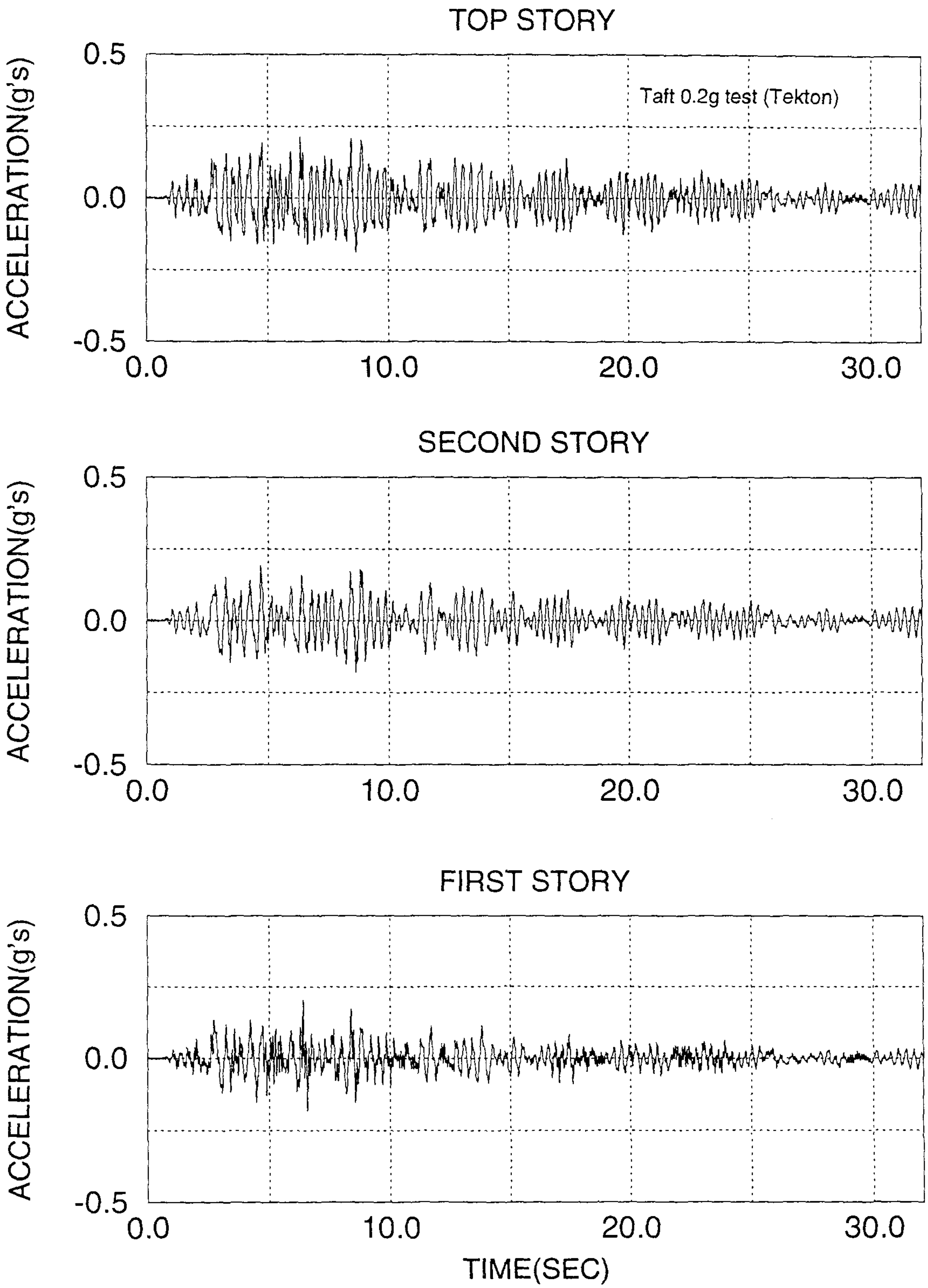

Figure 4-35 Acceleration Time History Response of the Model with Six Tekton Friction Dampers, Taft Earthquake PGA 0.2g

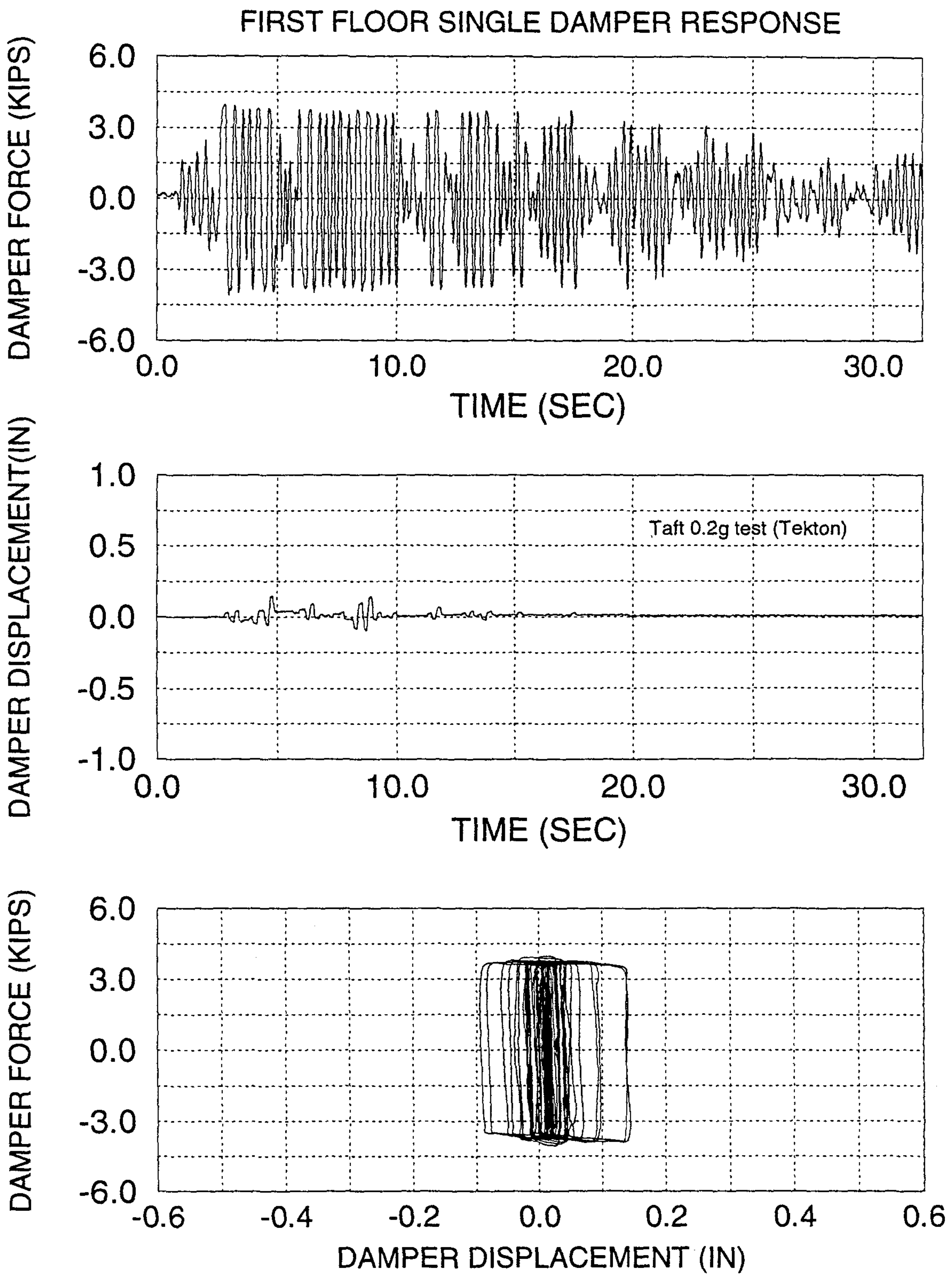

Figure 4-36 First Floor Single Damper Response, Taft Earthquake PGA 0.2g

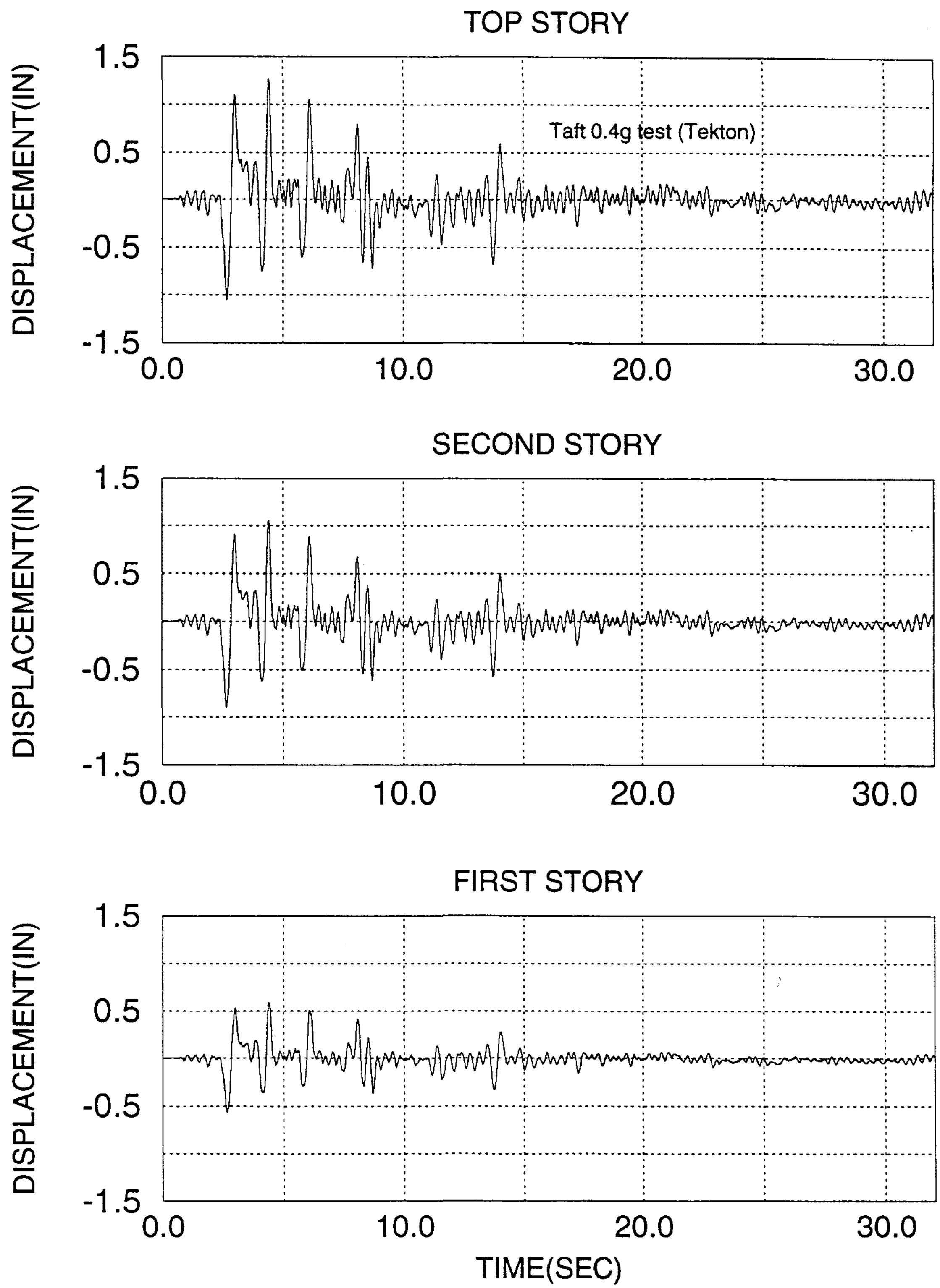

Figure 4-37 Displacement Time History Response of the Model with Six Tekton Friction Dampers, Taft Earthquake PGA 0.4g

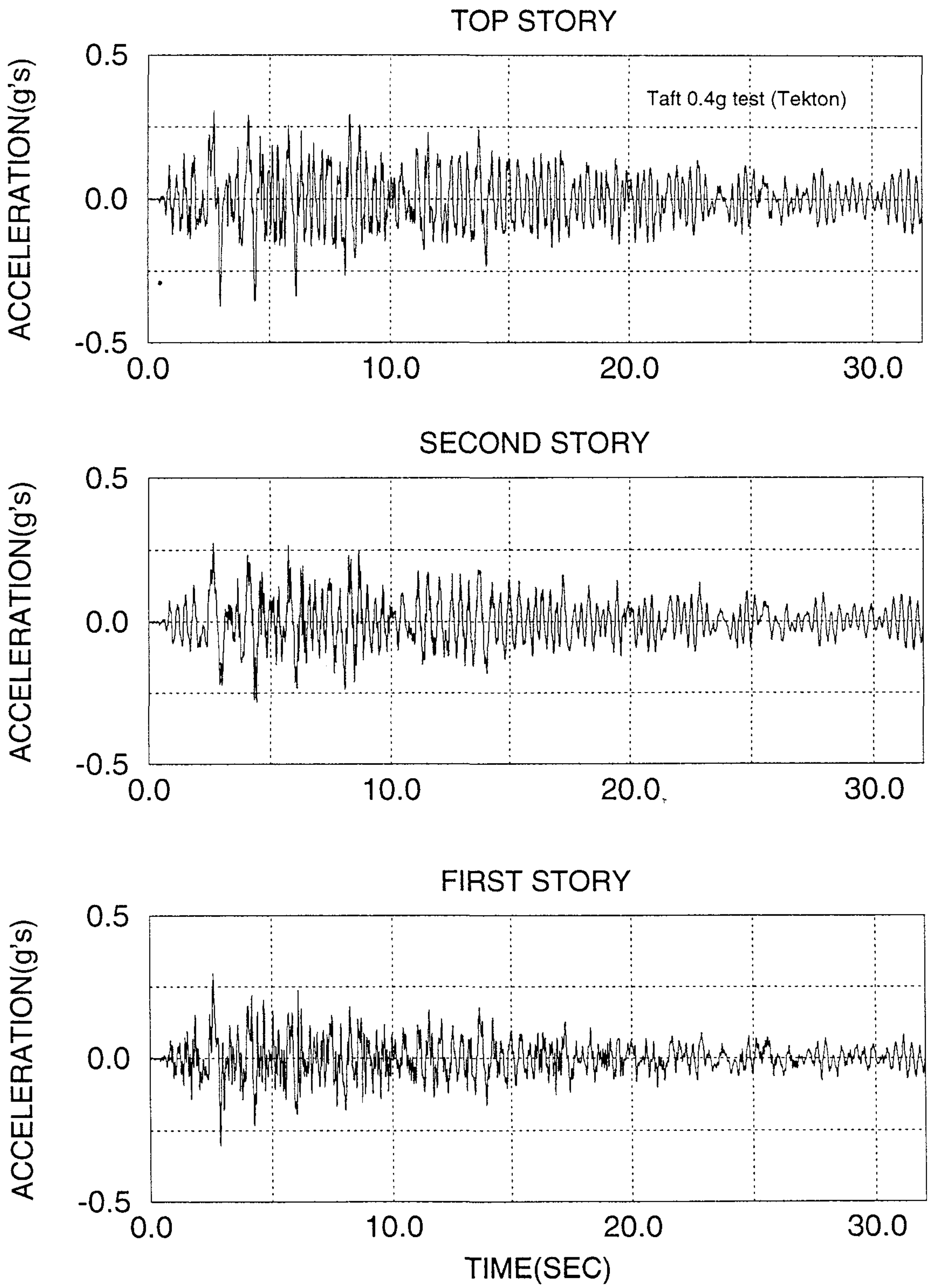

Figure 4-38 Acceleration Time History Response of the Model with Six Tekton Friction Dampers, Taft Earthquake PGA 0.4g

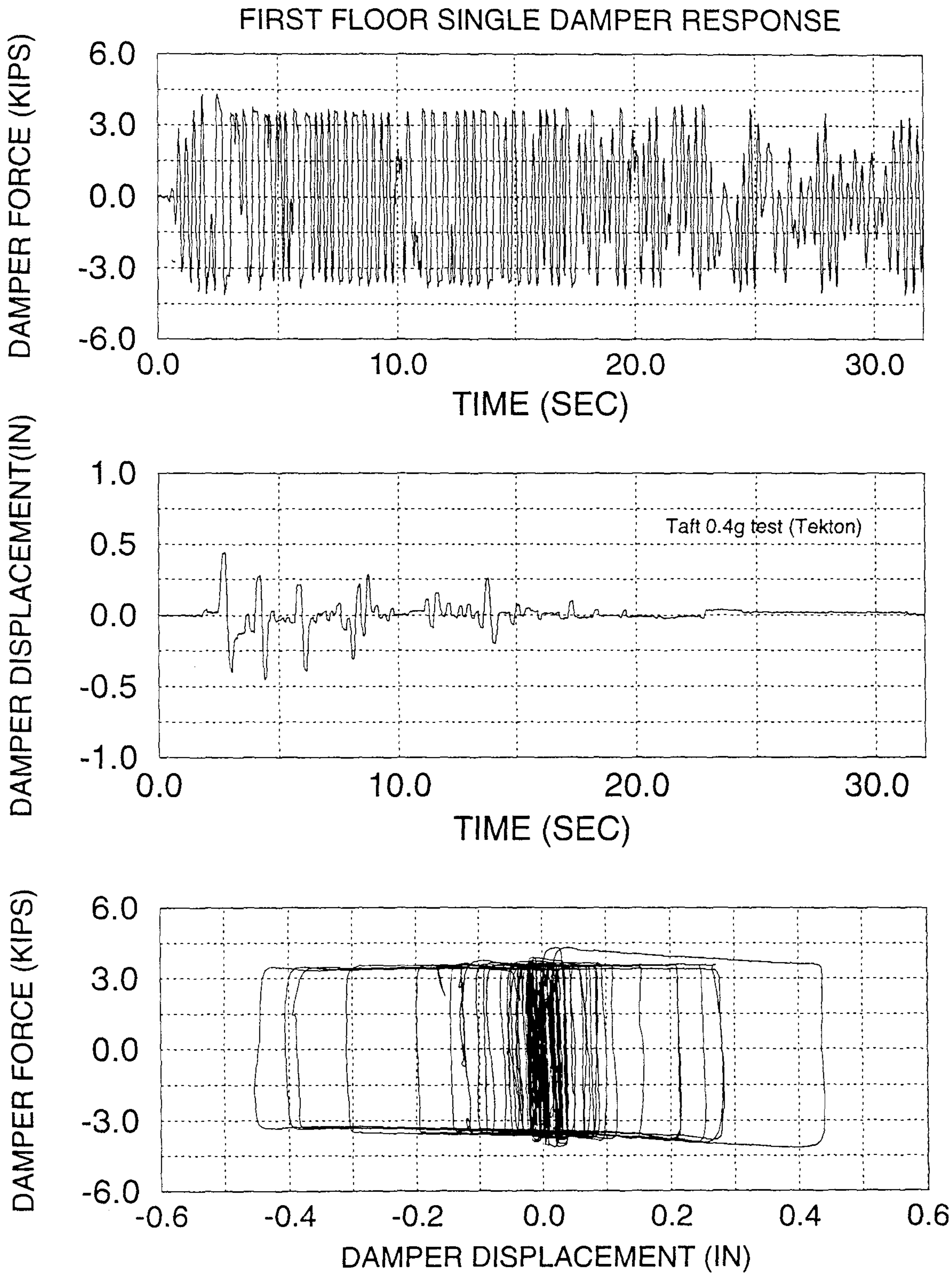

Figure 4-39 First Floor Single Damper Response, Taft Earthquake PGA 0.4g

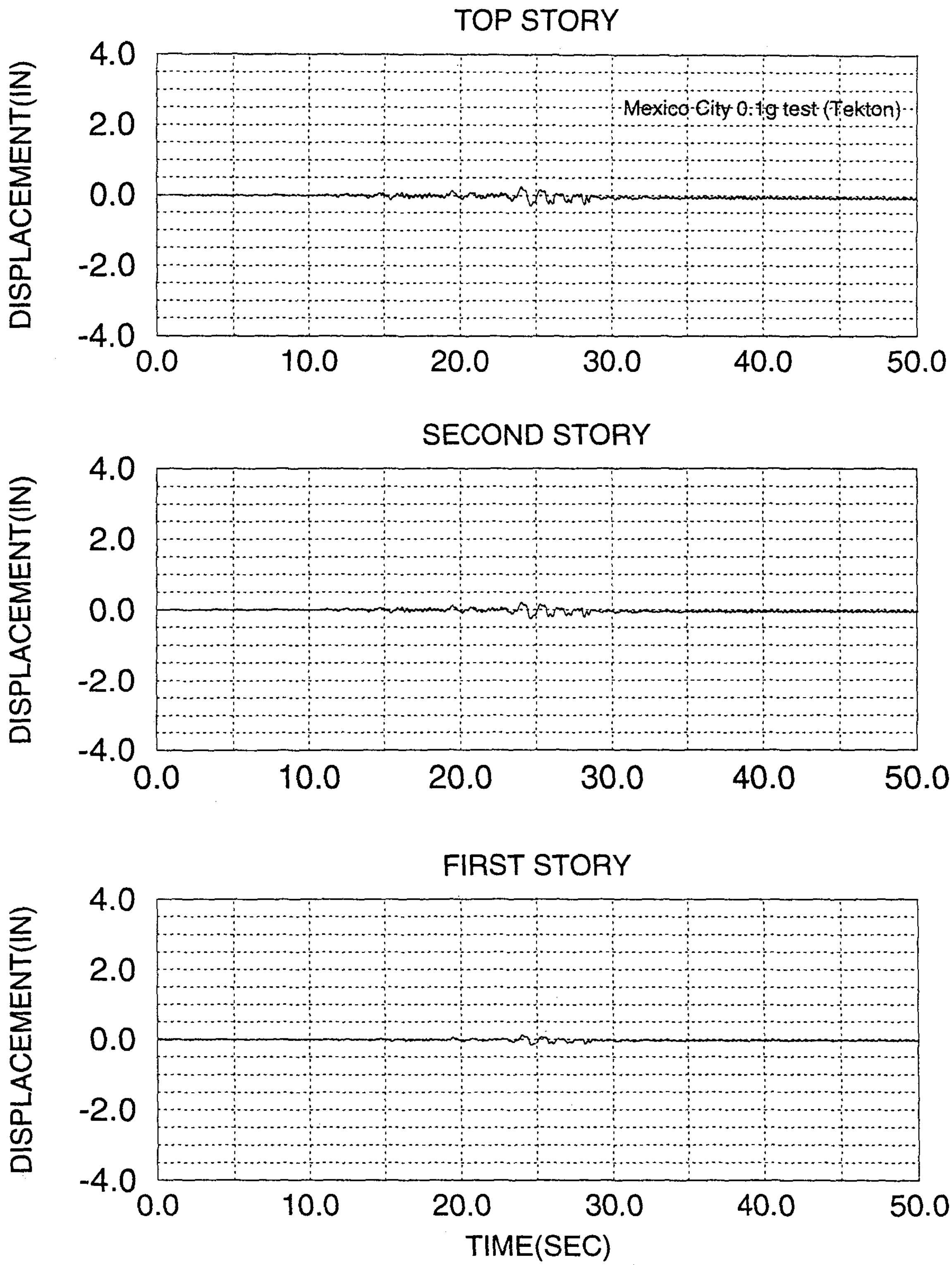

Figure 4-40 Displacement Time History Response of the Model with Six Tekton Friction Dampers, Mexico City Earthquake PGA 0.1g

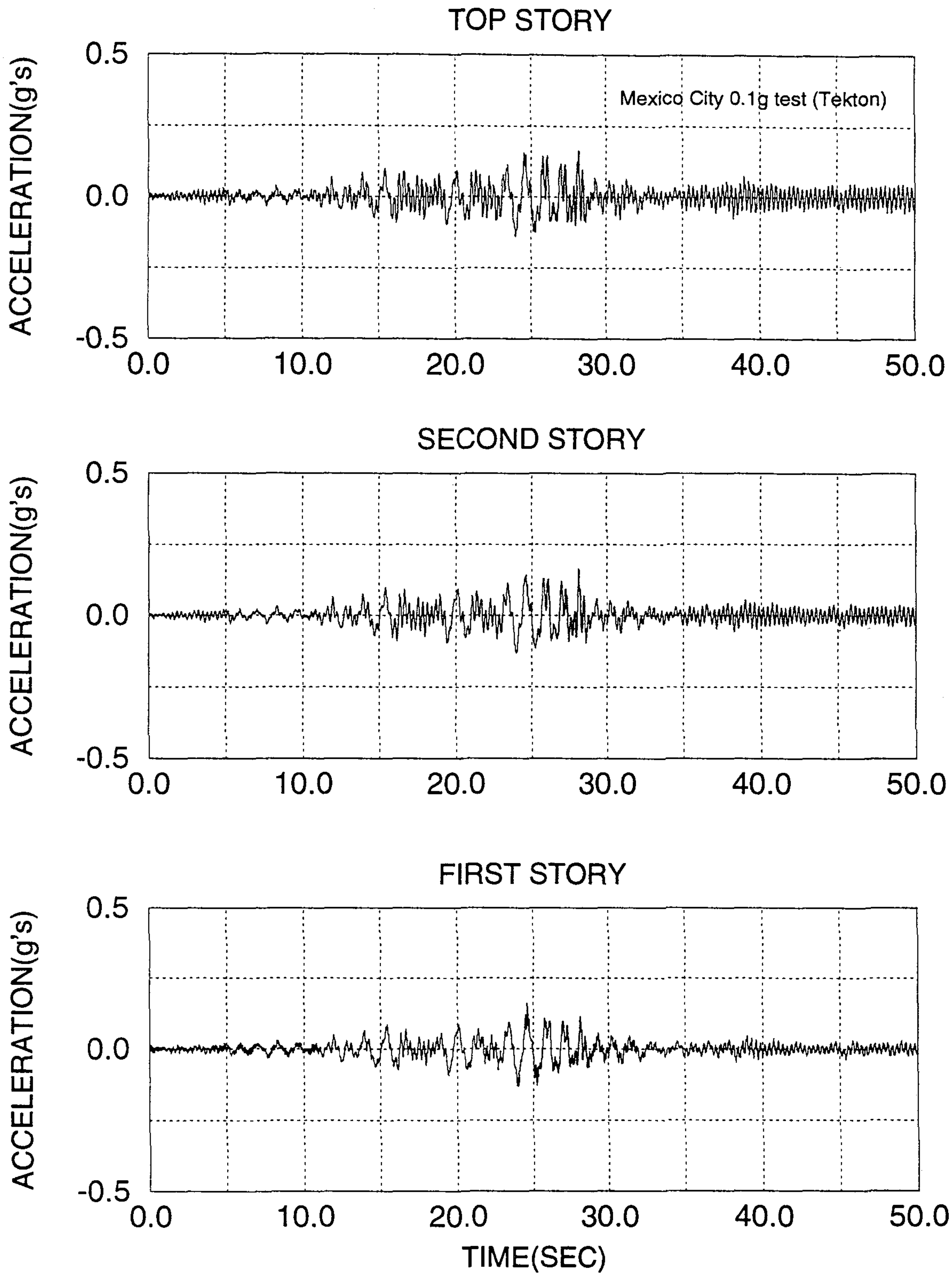

Figure 4-41 Acceleration Time History Response of the Model with Six Tekton Friction Dampers, Mexico City Earthquake PGA 0.1g

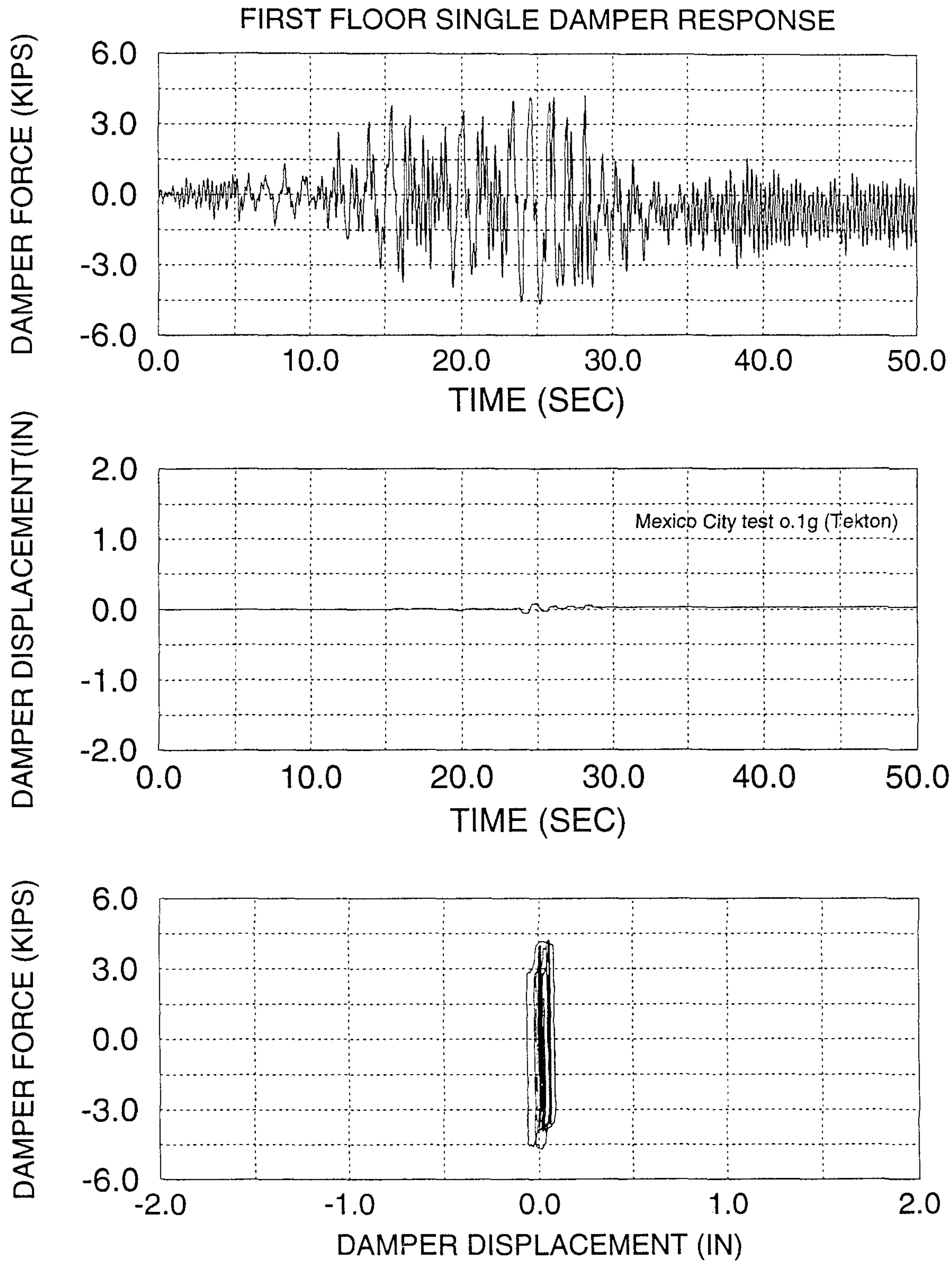

Figure 4-42 First Floor Single Damper Response, Mexico City Earthquake PGA 0.1g

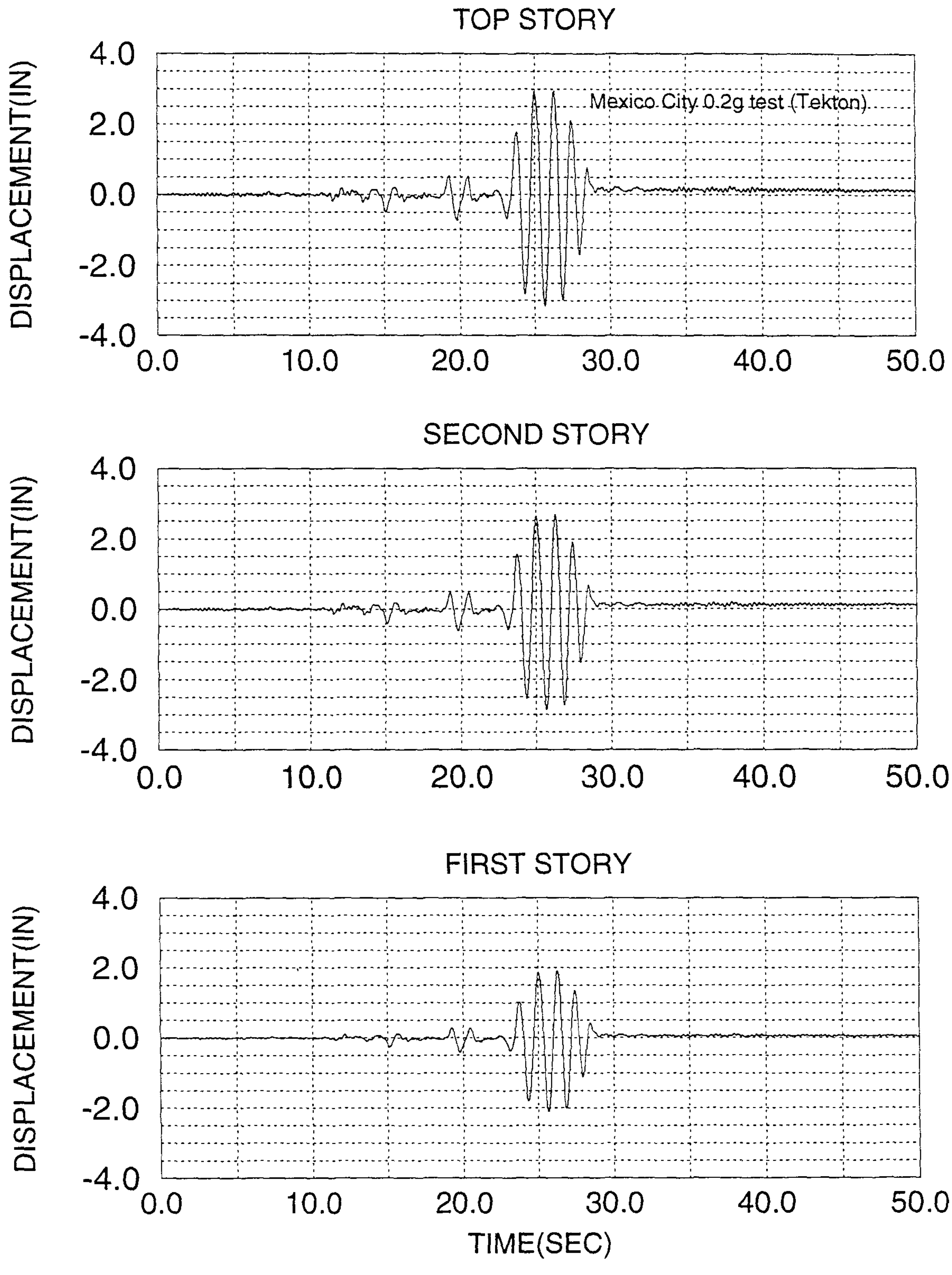

Figure 4-43 Displacement Time History Response of the Model with Six Tekton Friction Dampers, Mexico City Earthquake PGA 0.2g

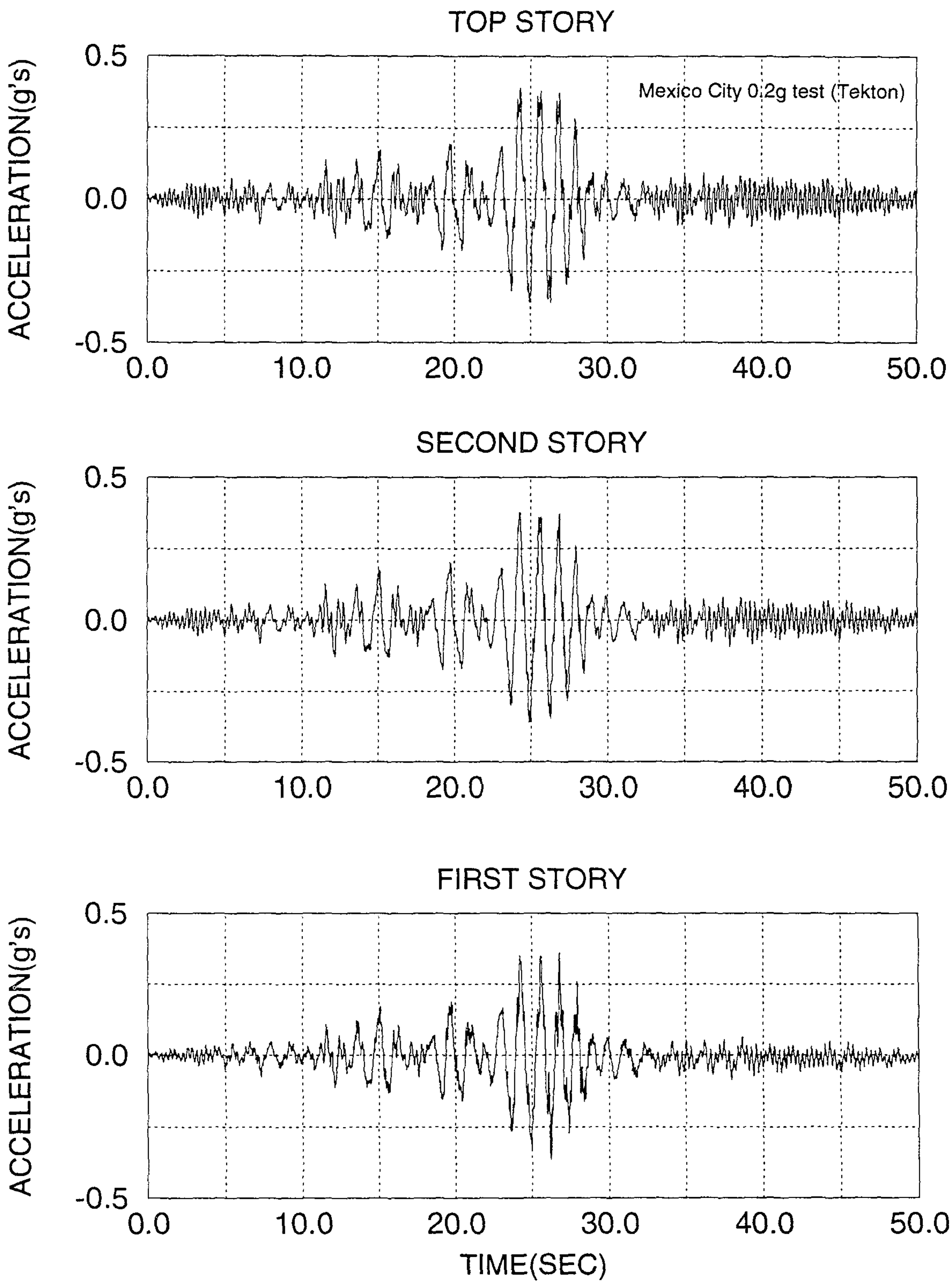

Figure 4-44 Acceleration Time History Response of the Model with Six Tekton Friction Dampers, Mexico City Earthquake PGA 0.2g

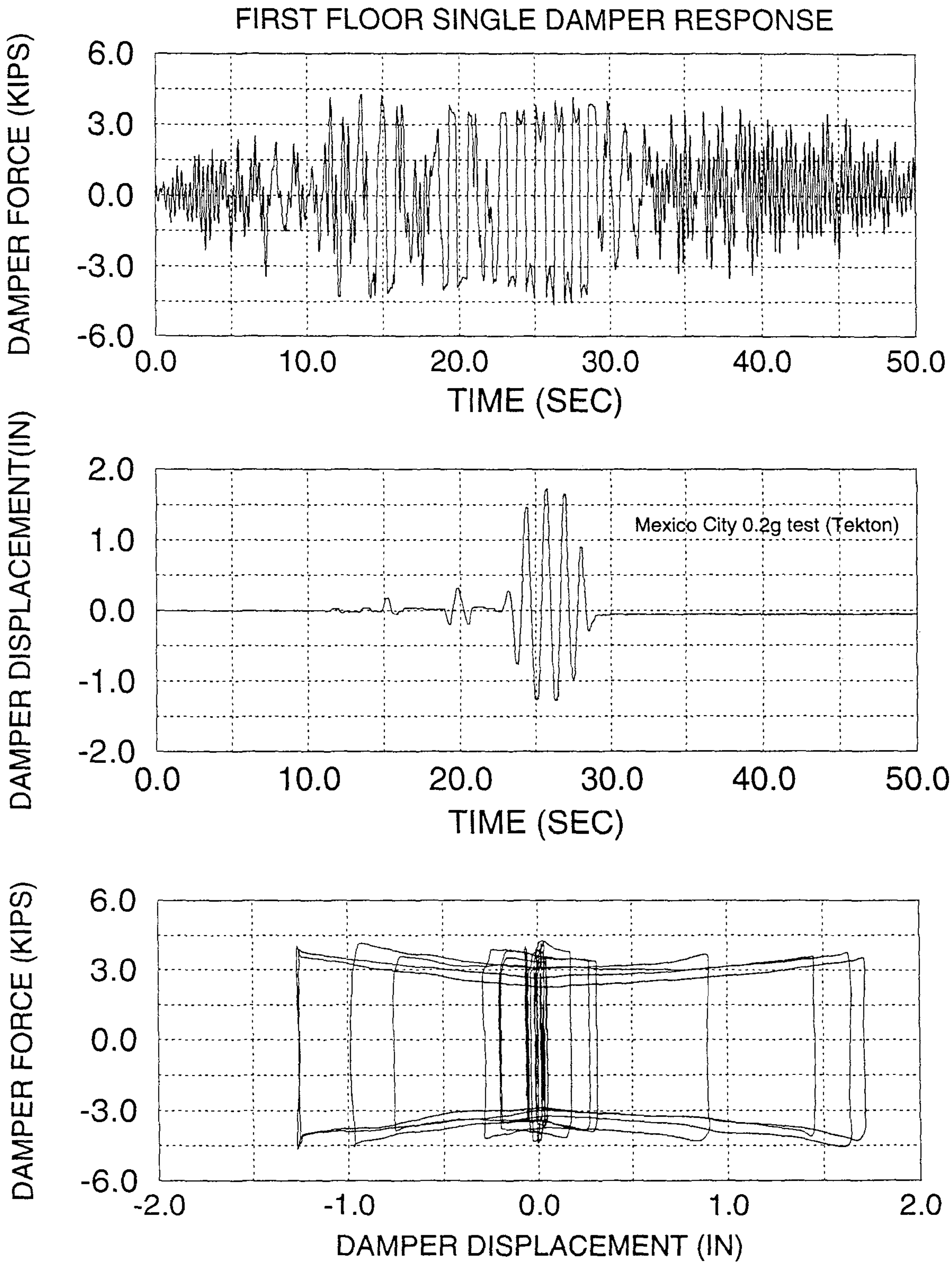

Figure 4-45 First Floor Single Damper Response, Mexico City Earthquake PGA 0.2g

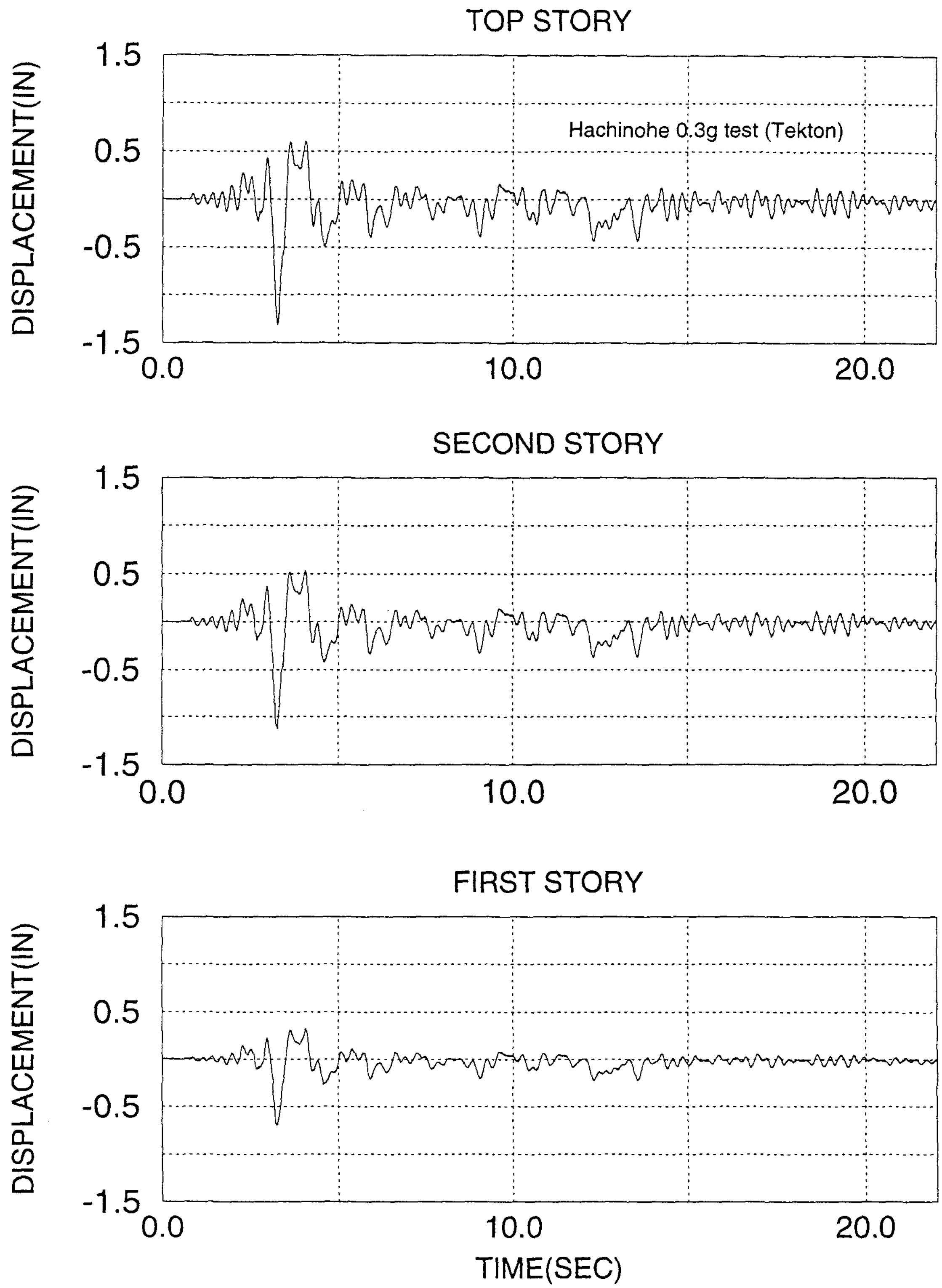

Figure 4-46 Displacement Time History Response of the Model with Six Tekton Friction Dampers, Hachinohe Earthquake PGA 0.3g

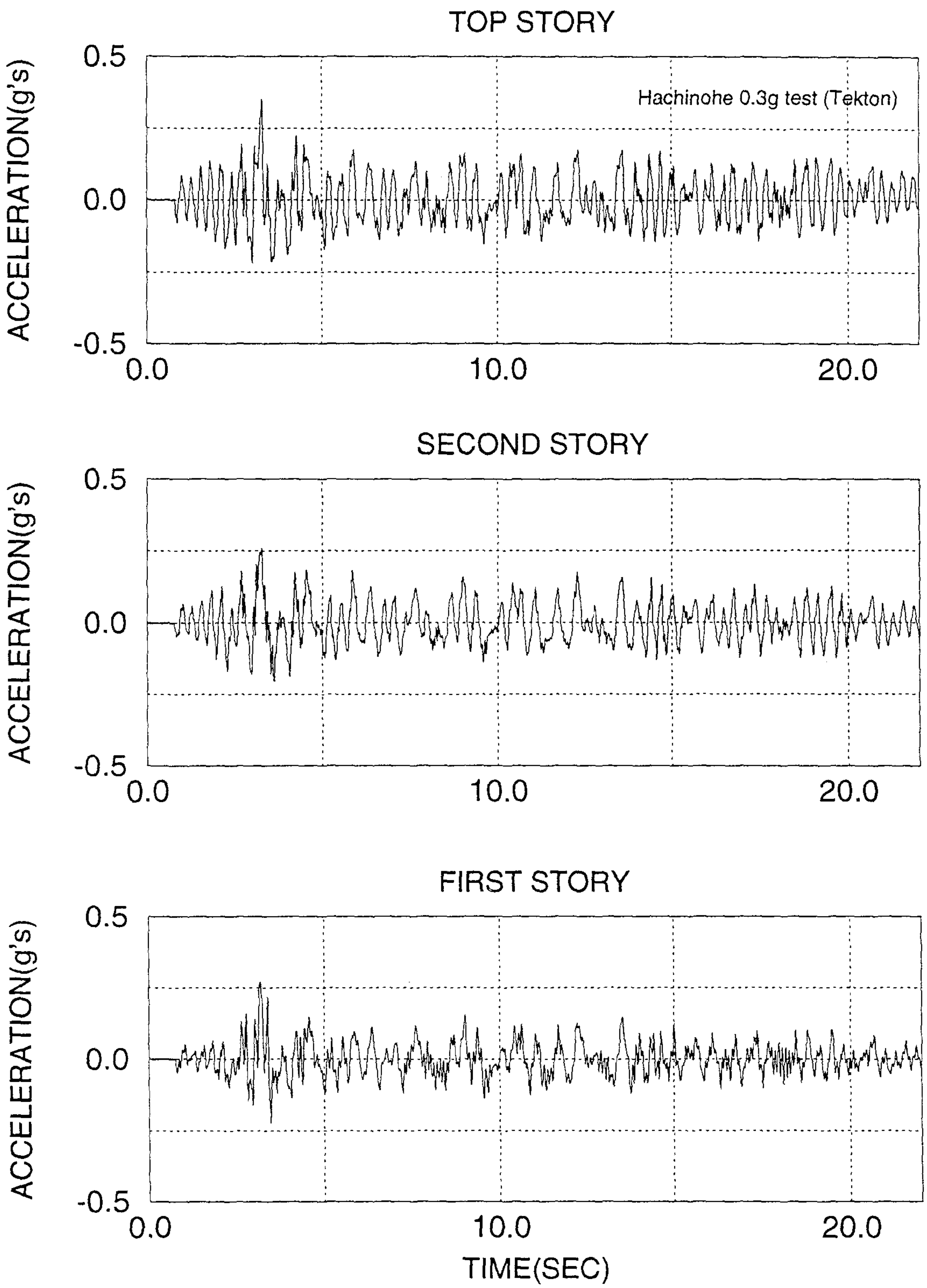

Figure 4-47 Acceleration Time History Response of the Model with Six Tekton Friction Dampers, Hachinohe Earthquake PGA 0.3g

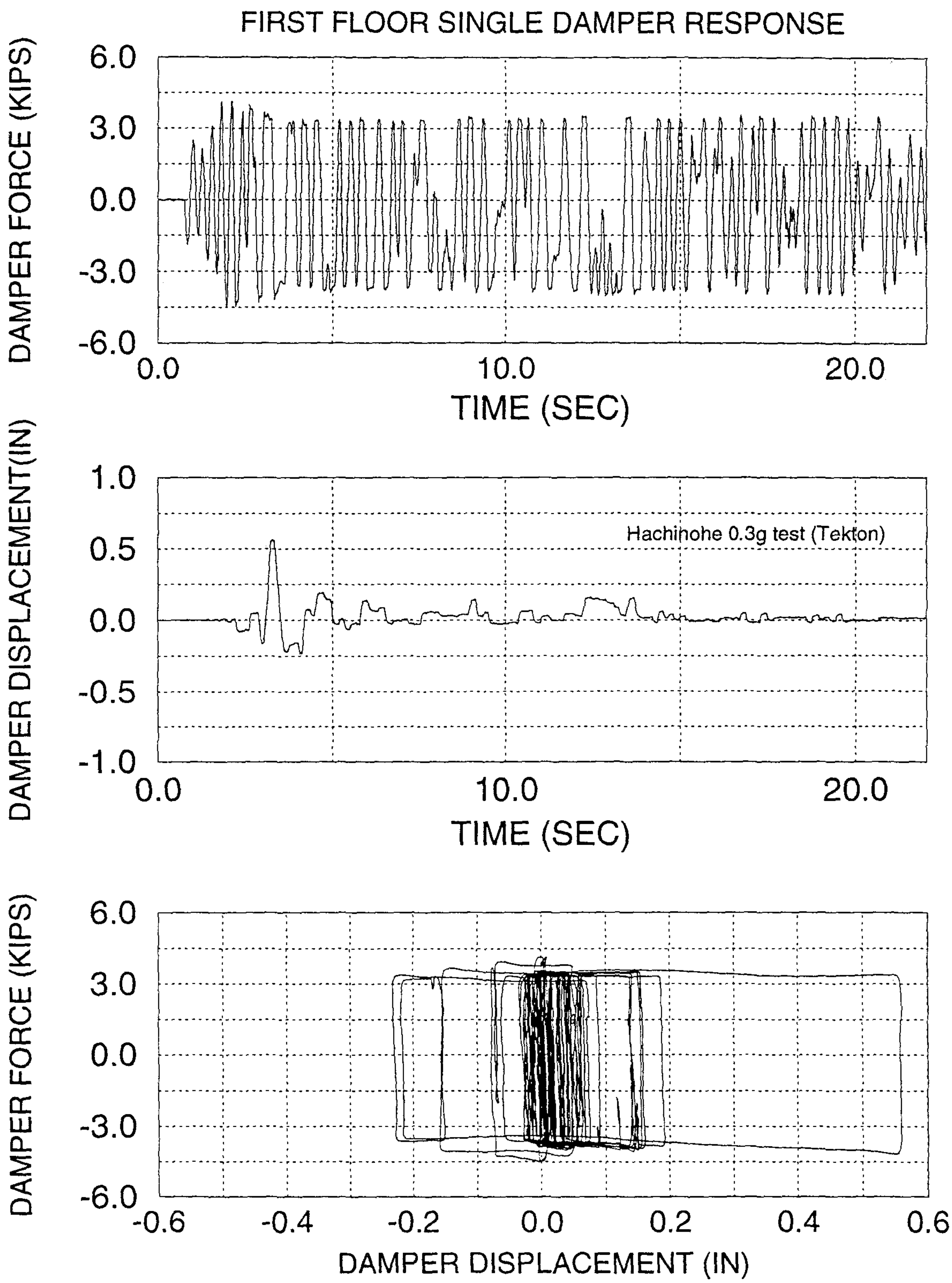

Figure 4-48 First Floor Single Damper Response, Hachinohe Earthquake PGA 0.3g

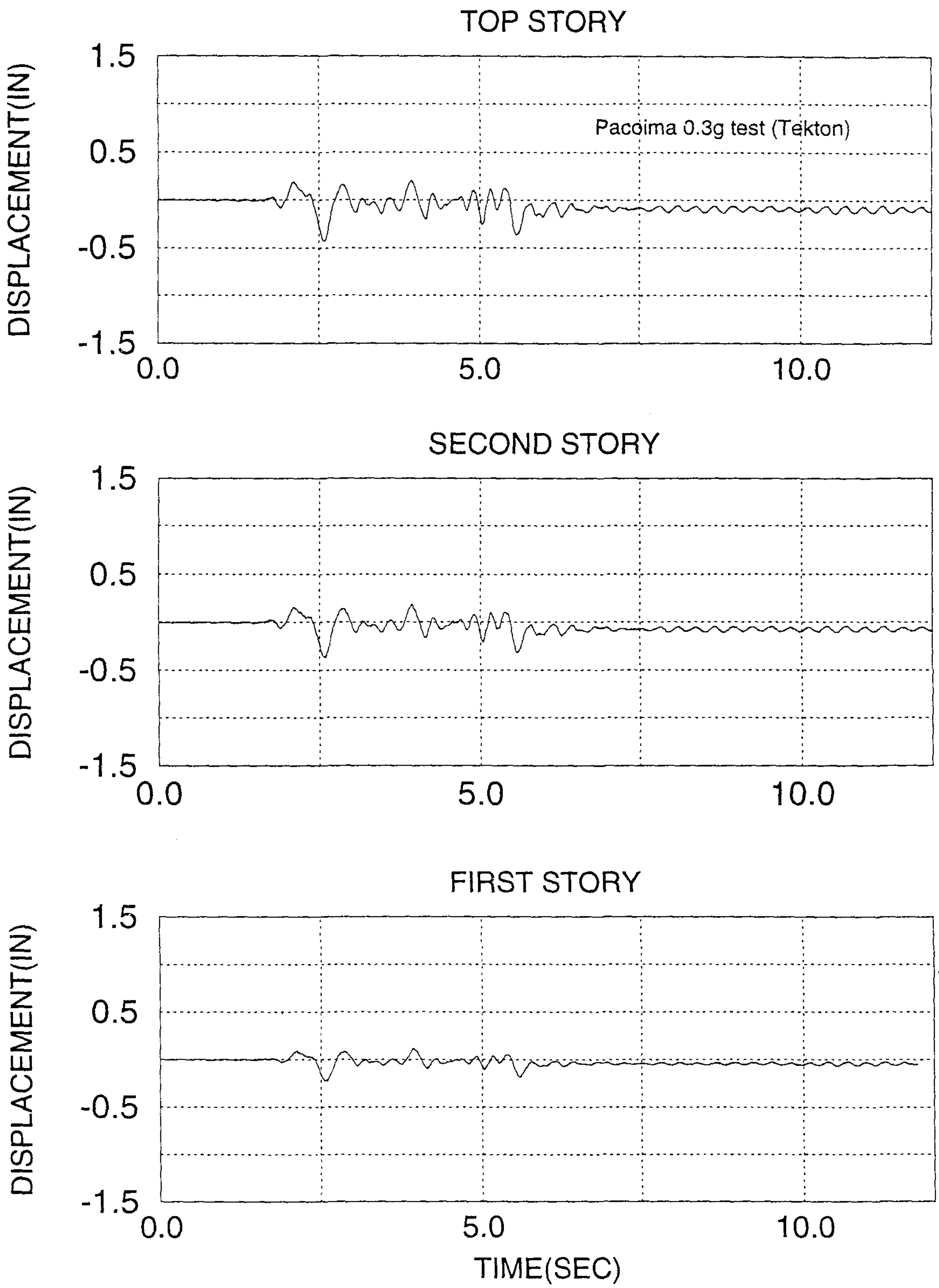

Figure 4-49 Displacement Time History Response of the Model with Six Tekton Friction Dampers, Pacoima Earthquake PGA 0.3g

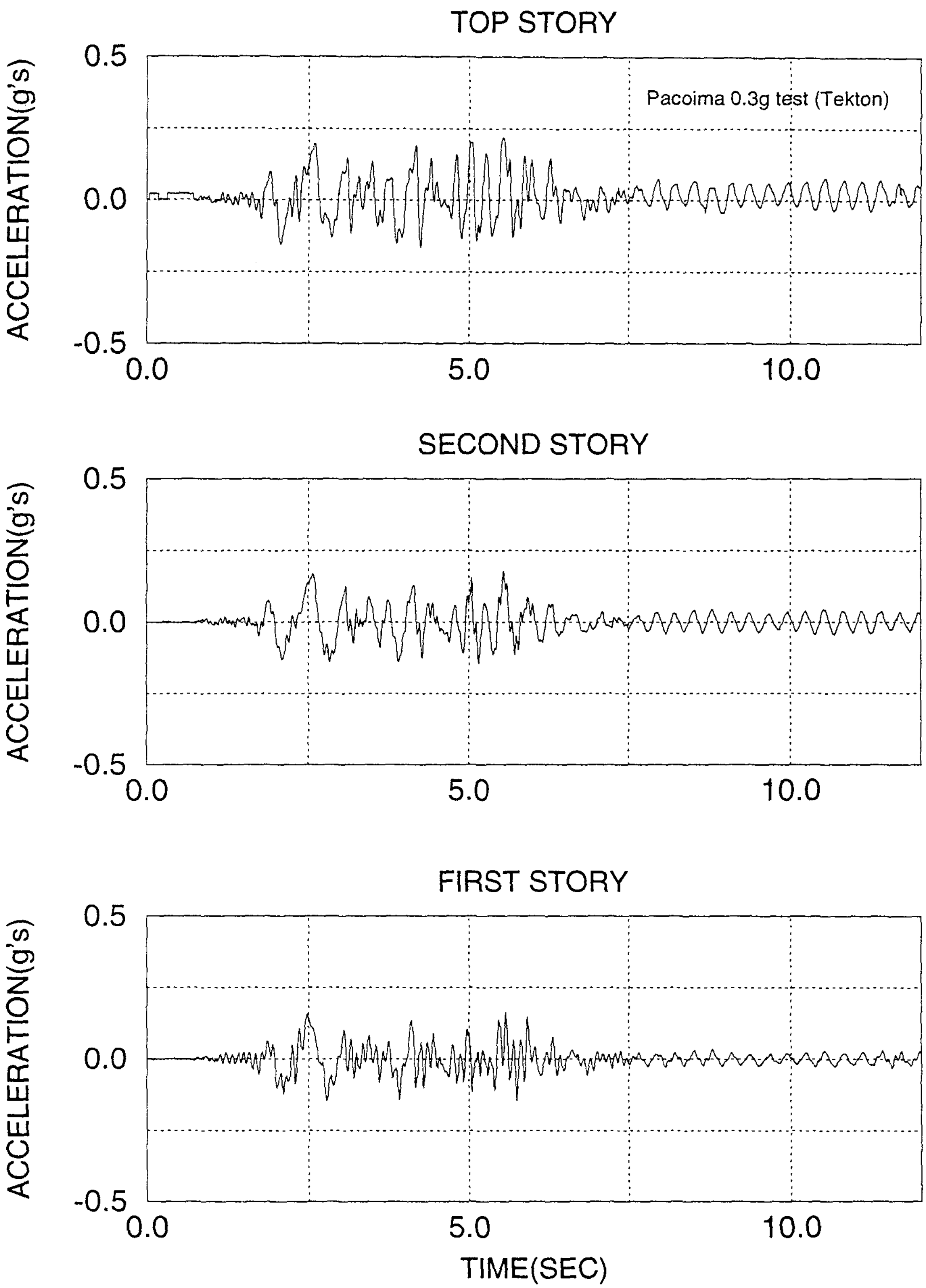

Figure 4-50 Acceleration Time History Response of the Model with Six Tekton Friction Dampers, Pacoima Earthquake PGA 0.3g

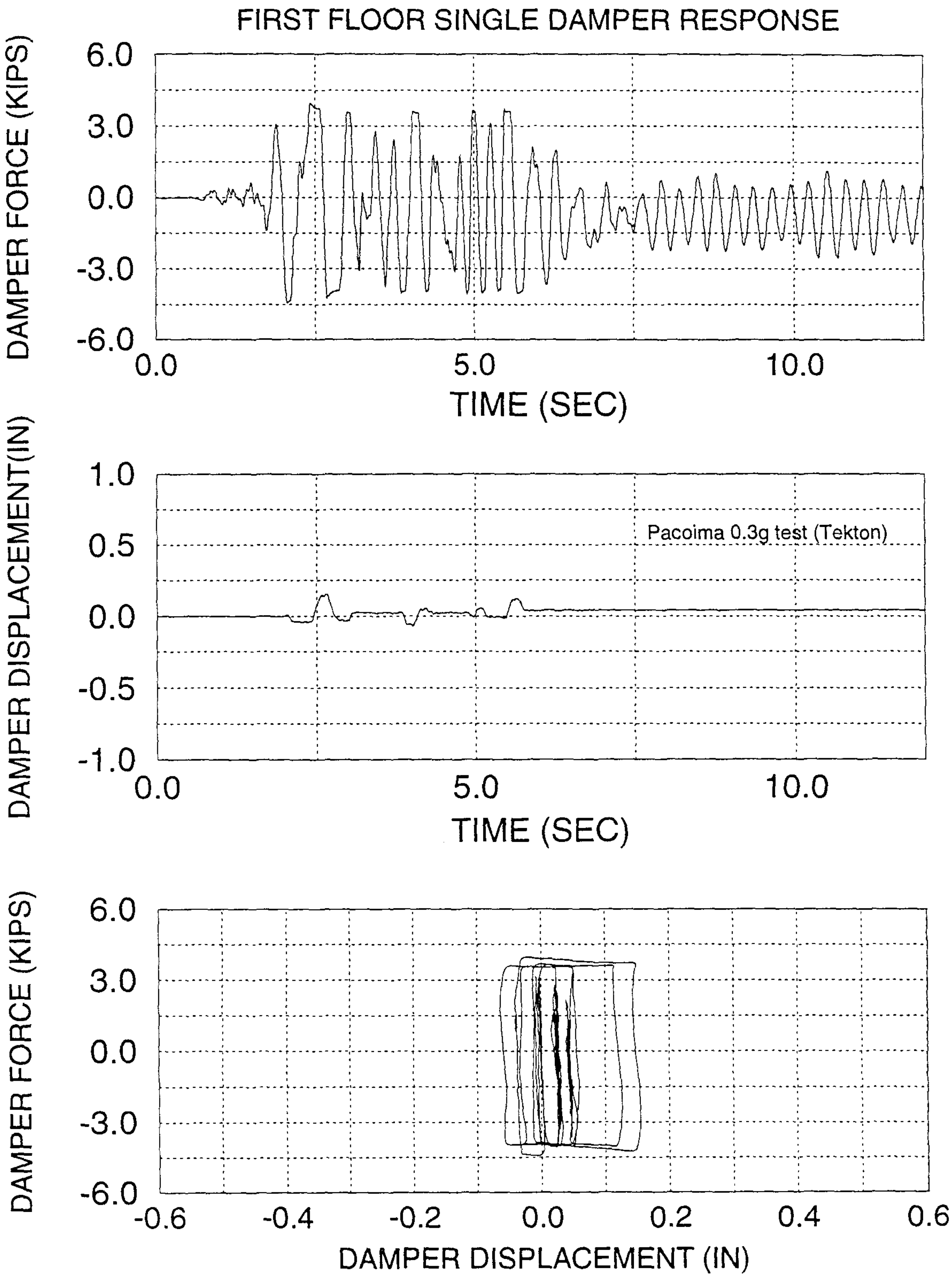

Figure 4-51 First Floor Single Damper Response, Pacoima Earthquake PGA 0.3g

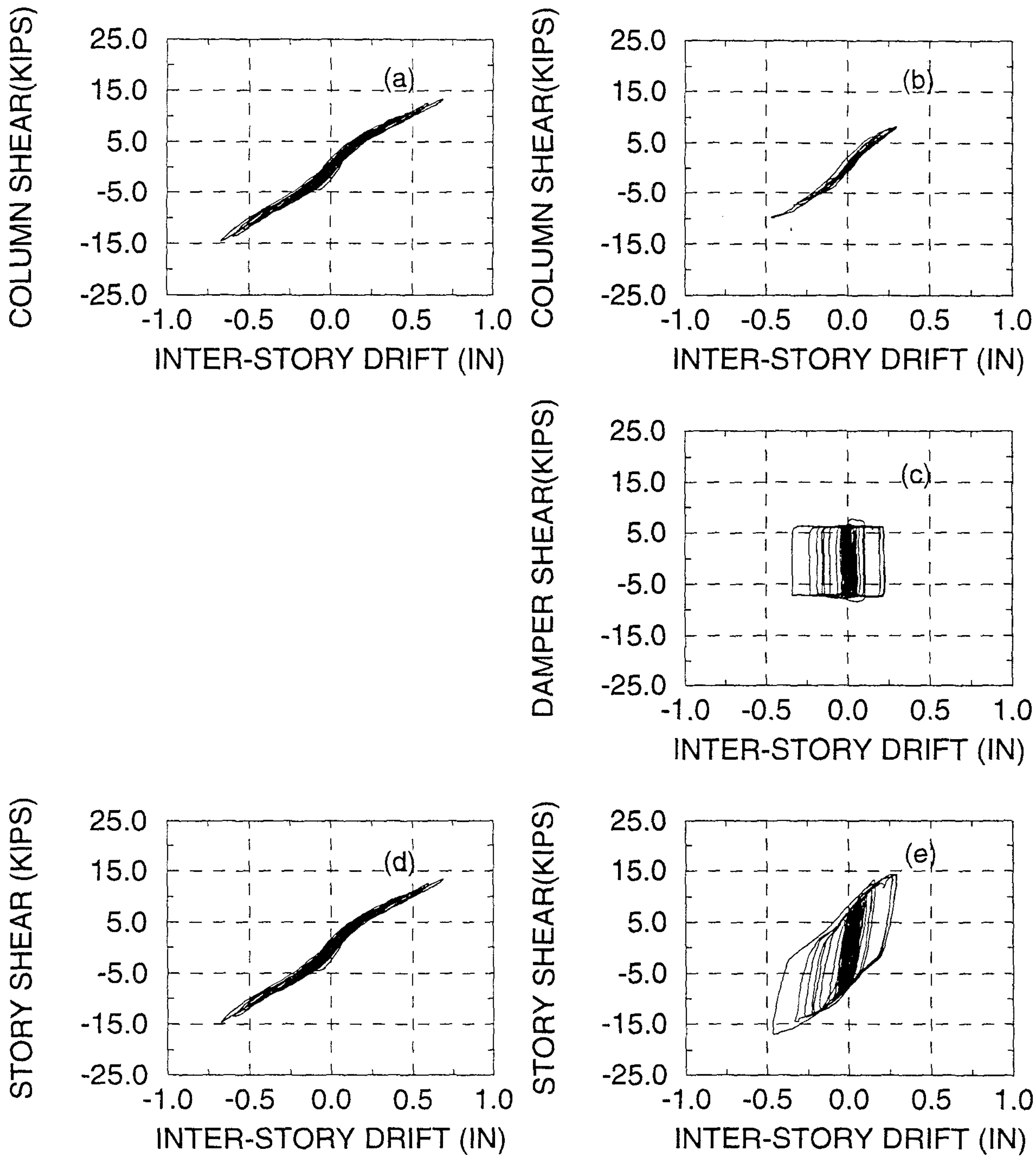

Figure 4-52 Forces in Structural Components at First Floor, from El-Centro PGA 0.3g Test (a) and (d) without Dampers; (b), (c) and (e) with Six Tekton Dampers

the second floor remains almost the same as without dampers. The distribution for forces during the response shows that while the overall response is improved, the local response may worsen or remain unaffected. It should be noted that while the deformations are substantially reduced at all floors for same level of excitation, the total base shear is only minimally influenced. The overall shear forces at severe excitation remain at the same level with minor increase. When the peak ground acceleration is increased, except for the Mexico City record, the long period excitation with high velocity maintains the internal forces increase for a longer time resulting in longer deformations and shear forces.

The friction damping devices seem to have limited influence where a monotonically increasing acceleration is predominant in the record, in particular if this increase has a long duration. Evaluations for such excitations are records obtained on soft soil (Mexico City 1985, Buchanest 1977, etc.) or linear fault records. For such cases, a different damping system may be required.

For a single ground record, the increase of peak ground acceleration (see Taft N21E experiment) produce a non-proportional increase in the displacement response. The damped response for 0.40g PGA is, however, smaller than the undamped response for 0.20g PGA.

Using damper at the first two floors produce better response at bottom floor and less at the top. The dampers have immediate influence on the local floor response. Similar response is obtained in using dampers at first floor only. The story forces are influenced also locally by the capacity diagram at each floor and by the local spectral demand (see

Section 6.2). This can be observed also from the typical time history responses in Fig. 4-30 to 4-33. While the total displacements are reduced at all floors the peak story absolute accelerations are not reduced, moreover, are increased at the top floor. The total energy balance (see Section 1, Eq. (1-1)) obtained from experimental data is displayed in Fig. 4-53 for $E_I = \int_0^t m(\ddot{u} + \ddot{u}_g)du_g$; $E_k = \frac{1}{2}m(\dot{u} + \dot{u}_g)^2$; $E_s = \frac{1}{2}ku^2$. While the total energy input is increased due to stiffening of the structure, the internal energy is redistributed such that 80% to 90% is taken by the supplemental dampers and dissipated, while hysteretic energy dissipation demand is reduced 85% to 95% in presence of dampers. The reduction of the demand for hysteretic energy dissipation is particularly important since it is preventing further deterioration of columns.

While the total shear forces at the base of the damped structure are increased in the presence of dampers. the force in the individual columns are smaller than in the undamped case. This indicates that the forces are partially transferred through the braces that protect the original columns (Table 4-5 and Fig. 4-52).

The axial force fluctuation is larger in the column (see Fig. 4-54), but not large enough to influence the flexural capacity of the columns (see Fig. 4-55). In taller structures, this is an important issue since the axial force may accumulate if a single bay of frame is braced. However, a proper redistribution of braces can eliminate or reduce the concentration and accumulation effects.

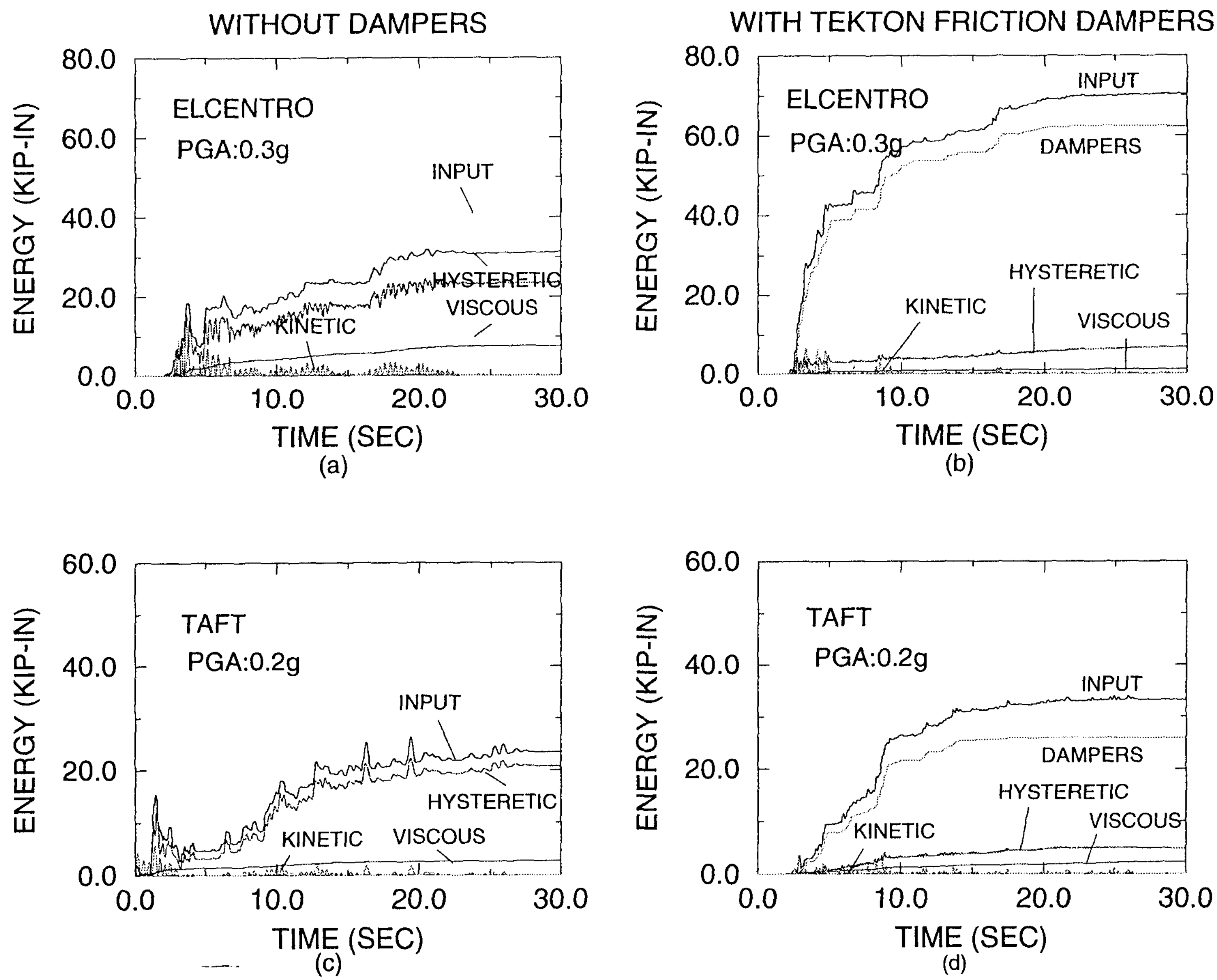

Figure 4-53 Energy Distribution in Structure w/o and with Six Tekton Friction Dampers

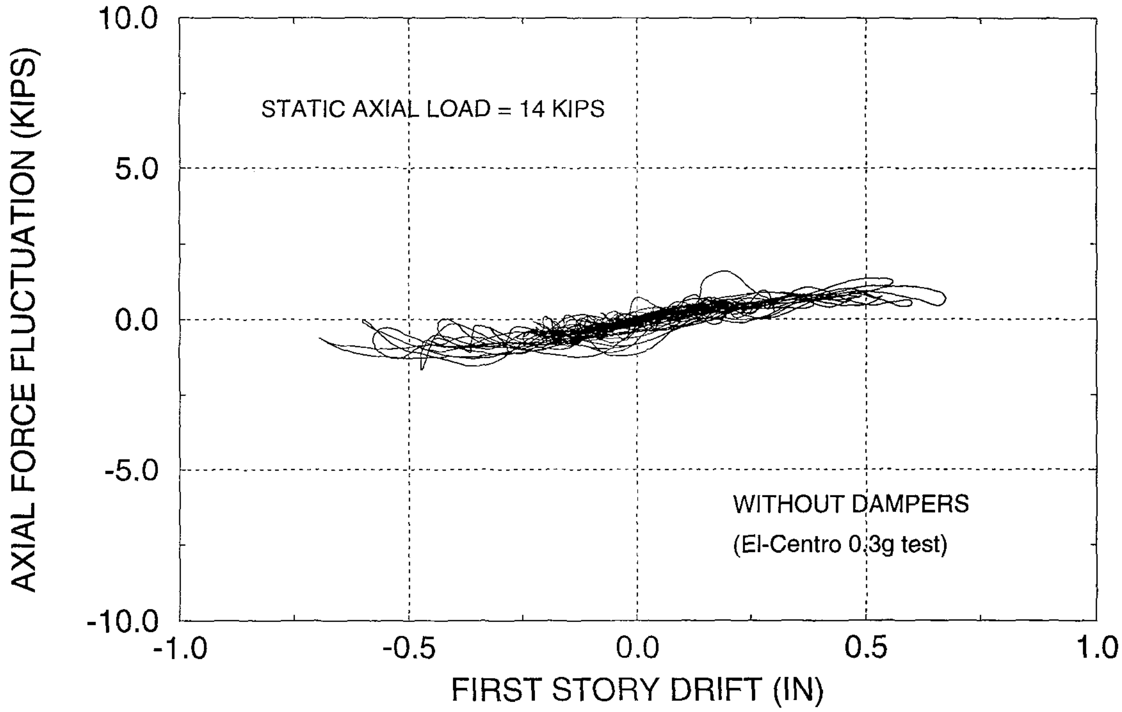

(a)

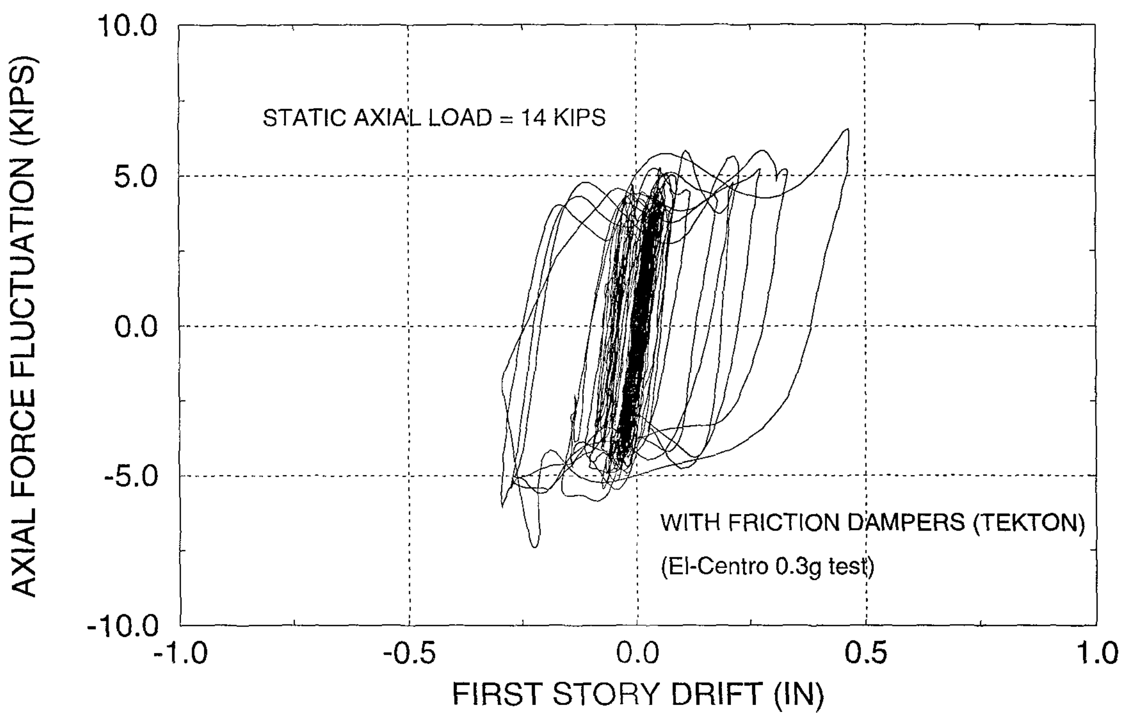

(b)

Figure 4-54 Axial Force Fluctuation in First Floor Interior Column for Simulated Earthquake El-Centro 0.3g, (a) w/o Dampers; (b) with Six Tekton Friction Dampers

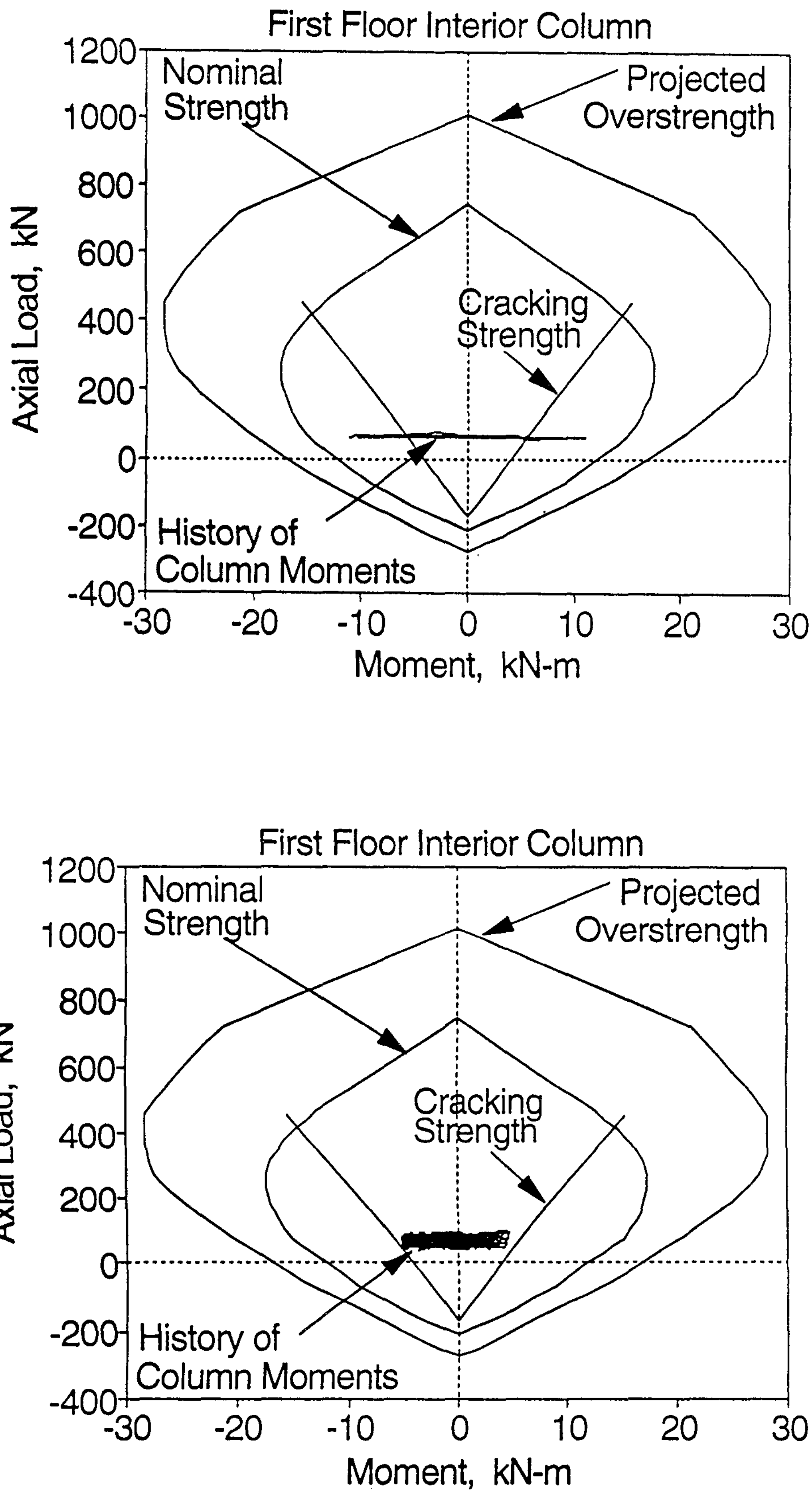

Figure 4-55 Forces in Column vs Structural Capacity for El-Centro PGA 0.3g
(a) without Dampers, (b) with Six Tekton Friction Dampers

4.8 Summary of the Experimental Study

The experiment indicated that the dampers show a small stiffness increase depending on the intensity of the earthquake and influence control deformation through damping. However, the forces transmitted to the foundation and the structure's accelerations are only minimally reduced and in some cases minimally increased. The energy dissipation capacity increase with the increase of intensity of the earthquake and the period of the structure varies with the intensity of the earthquake which will prevent possible resonant. The main benefit of the dampers in such inelastic structures consists in transferring of the energy dissipation needs from the columns to the dampers while controlling the lateral drifts and deformations. These results should be expected in all inelastic structures, as shown further by the analytical study and the approximated analyses.

SECTION 5

MODELING OF INELASTIC STRUCTURES WITH SUPPLEMENTAL DAMPERS

5.1 Modeling of Inelastic Structures

Inelastic analysis of structures to wind and earthquake loading is usually performed using step-by-step integration of equations of motion, which are representative to structures with variable stiffness due to cracking yielding, deterioration and secondary effects.

In this study the structure is modeled as a structural frame made of rigidly or semi-rigidly connected columns, beams, shear walls and braces (see Kunnath et al. 1992, Reinhorn et al. 1994). The structural members are modeled as macro-models with inelastic properties described by: (i) an extensive hysteretic model with stiffness and strength deterioration and pinching due to crack opening and closing (see Fig. 5-1); (ii) a non-symmetric distributed plasticity model obtained through a distributed flexibility model (see Fig. 5-2). The structure is modeled by the matrix equation:

$$\mathbf{M}\ddot{u} + \mathbf{C}\dot{u} + R(u) = -\mathbf{M}I\ddot{u}_g + F_w \qquad (5\text{-}1)$$

where u, $\dot{u}$, $\ddot{u}$ are the time dependent response, vector of displacement, velocity and acceleration respectively, $\ddot{u}_g$ is the ground acceleration; F_w is the wind force vector. **M** is the mass matrix, **C** is the inherent damping matrix of structure and R is the nonlinear resistance vector of the structure obtained from the addition of individual component's resistance. The resistance vector is a function of deformation based on models shown in Fig. 5-1 and 5-2 (Reinhorn et al. 1994).

The equation of motion can be written in incremental form as:

$$\mathbf{M}\Delta\ddot{u} + \mathbf{C}\Delta\dot{u} + \mathbf{K}\Delta u = -\mathbf{M}I\Delta\ddot{u}_g + \Delta F_w \quad \text{(5-2)}$$

where

$$\mathbf{K} = \frac{\Delta R(u)}{\Delta u} \quad \text{(5-3)}$$

is the instantaneous stiffness assumed constant during a specific incremental computation time step.

5.2 Modeling of Structure with Supplemental Dampers

The structure with supplemental dampers will have another dissipation term in the structure's equation:

$$\mathbf{M}\ddot{u} + \mathbf{C}\dot{u} + R(u) + F_D(u) = -\mathbf{M}\mathbf{I}\ddot{u}_g + F_w \quad \text{(5-4)}$$

where the supplemental damping forces F_D obtained from suitable transformation of braces forces to the corresponding degrees of freedom.

$$F_D(u) = \mathbf{D}F_{Di}(u_i) \quad \text{(5-5)}$$

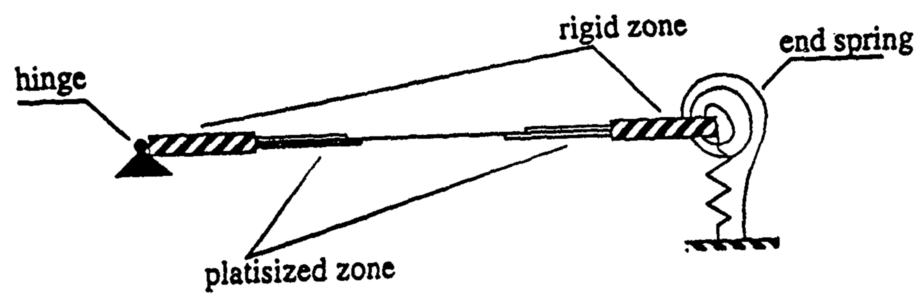

One dimensional schematic of triaxial hysteretic beam column element.

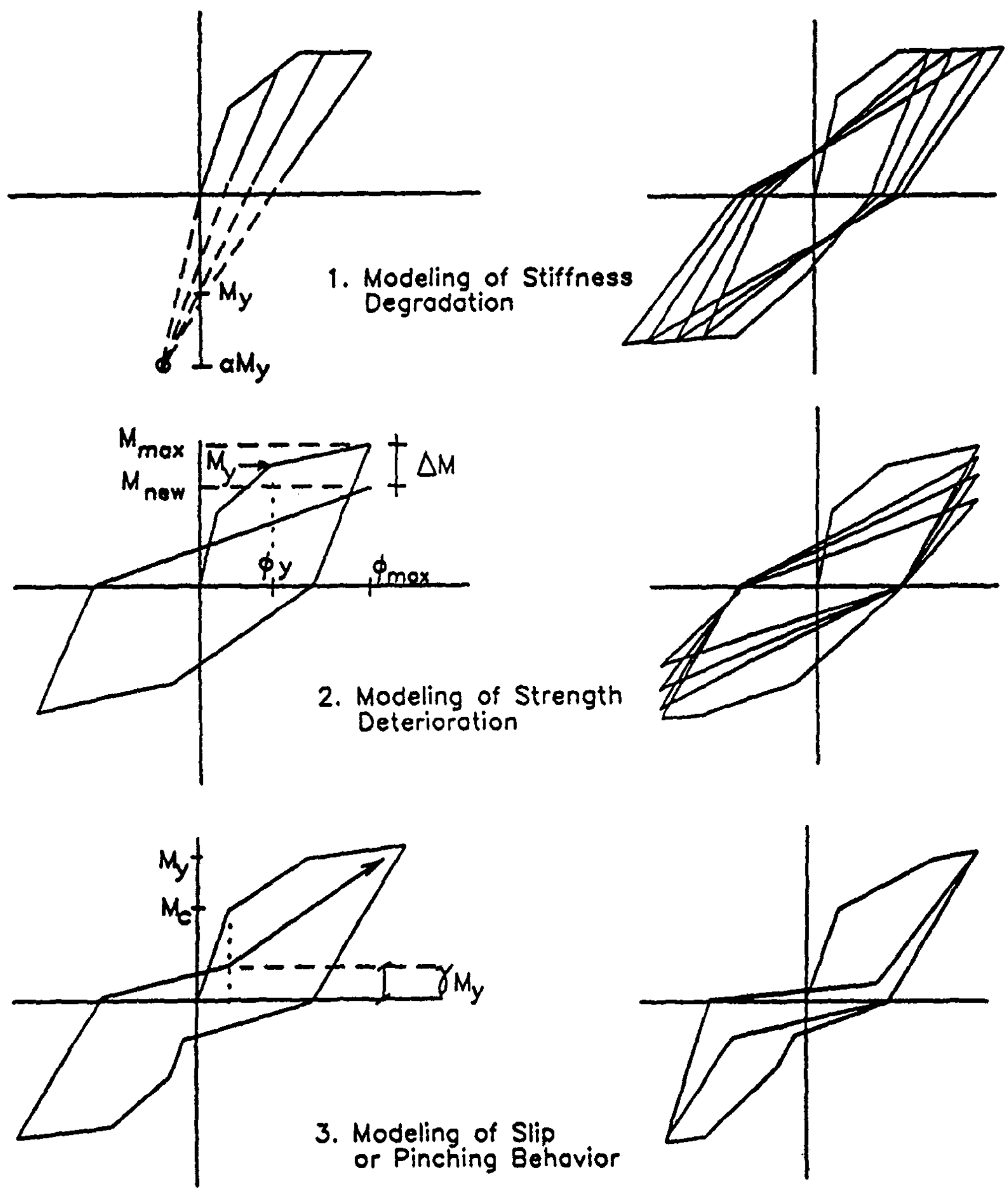

Figure 5-1 an Extensive Hysteretic Model with Stiffness and Strength Deterioration and Pinching Due to Crack Opening and Closing

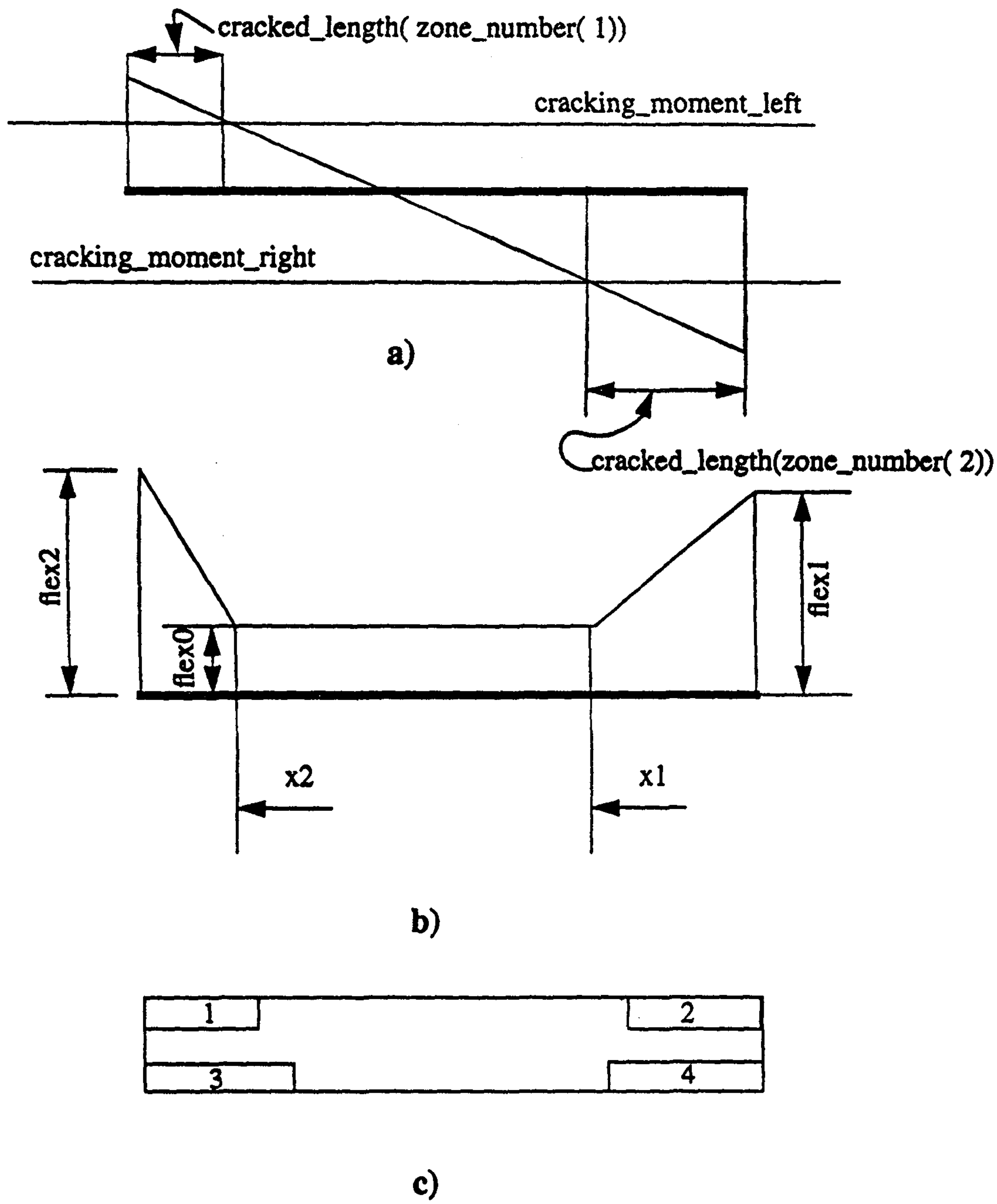

Figure 5-2 a Non-symmetric Distributed Plasticity Model Obtained through a Distributed Flexibility Model where **D** is a location matrix, F_{Di} is the vector of individual device forces, and u_i are the deformations and velocities of devices, i.

5.2.1 Modeling Using Bouc-Wen's Model

According to the discussion in Section 3.1.1, Bouc-Wen's models offer solutions in time domain, if solved simultaneously with the rest of the structure. According to these models:

$$F_D(u) = \mathbf{D}F_{Di}(u_i) \quad \text{(5-6)}$$

where D is the location matrix and the damping force F_i in each damper i is given in a differential form for Bouc-Wen's model:

$$F_D = k_0(\alpha U + (1-\alpha)ZU_y) \quad \text{repeat(3-1)}$$

Z is a nondimensional quantity given by:

$$\dot{Z} = \left(\dot{U} / U_y\right)\left\{A - Z^{\eta}\left[\gamma \operatorname{sgn}\left(\dot{U}Z\right) + \beta\right]\right\} \quad \text{repeat(3-2)}$$

The solution for models represented by differential forces is presented below.

5.2.2 Solution of Differential Equations

The solution is thought for the equations in incremental form:

$$\mathbf{M}\Delta\ddot{u} + \mathbf{C}\Delta\dot{u} + \mathbf{K}\Delta u + \mathbf{D}\Delta F_D = -\mathbf{MI}\ddot{u}_g + F_w \quad \text{(5-7)}$$

in which the incremental force, ΔF_D can be calculated using the semi-implicit Runge-Kutta method (Rosenbrook 1964):

$$\Delta F_{Dk} = R_1 k_k + R_2 l_k \qquad (5\text{-}8)$$

where $F_{D\,k}$ and $F_{D\,k\text{-}1}$ are the damper force at k-th and (k-1)-th time step, respectively. k_k and l_k are determined by solving following coupled equations:

$$k_k = \Delta t \left[f\left(F_k, u_k, \dot{u}_k\right)_{t-\Delta t} + a_1 \frac{\partial f\left(F_k, u_k, \dot{u}_k\right)_{t-\Delta t}}{\partial F} k_k \right] \qquad (5\text{-}9)\text{a}$$

$$l_k = \Delta t \left[f\left(F_k + b_1 k_k, u_k, \dot{u}_k\right)_{t-\Delta t} + a_2 \frac{\partial f\left(F_k + c_1 k_k, u_k, \dot{u}_k\right)_{t-\Delta t}}{\partial F} l_k \right] \qquad (5\text{-}9)\text{b}$$

or directly:

$$k_k = \Delta t \left[1 - a_1 \Delta t \frac{\partial f\left(F_k, u_k, \dot{u}_k\right)_{t-\Delta t}}{\partial F} \right]^{-1} f\left(F_k, u_k, \dot{u}_k\right)_{t-\Delta t} \Delta t \qquad (5\text{-}10)\text{a}$$

$$l_k = \Delta t \left[1 - a_2 \Delta t \frac{\partial f\left(F_k + c_1 k_k, u_k, \dot{u}_k\right)_{t-\Delta t}}{\partial F} \right]^{-1} f\left(F_k + b_1 k_k, u_k, \dot{u}_k\right)_{t-\Delta t} \Delta t \qquad (5\text{-}10)\text{b}$$

In above equations, the constant parameters R_1, R_2, a_1, a_2, b_1 and c_1 are obtained from the solution of the following equations:

$$R_1 + R_2 = 1 \qquad (5\text{-}11)\text{a}$$

$$R_1 a_1 + R_2 (a_2 + b_1) = \frac{1}{2} \quad \text{(5-11)b}$$

$$R_1 a_1^{\,2} + R_2 \left[a_2^{\,2} + (a_1 + a_2) b_1 \right] = \frac{1}{6} \quad \text{(5-11)c}$$

$$R_2 \left(a_2 c_1 + \frac{1}{2} b_1^{\,2} \right) = \frac{1}{6} \quad \text{(5-11)d}$$

In this study, a series of coefficients were selected (see Reinhorn et al. 1994) to obtain a fourth order truncation error $O(\Delta t^4)$ that satisfy Eq. (5-11), and they are: R_1 = 0.75; R_2 =0.25; a_1=a_2=0.7886751; b_1 = -1.1547005 and c_1 =0.

It should be noted that the incremental force ΔF_i requires information about u, $\dot{u}$ at the end of the incremental interval t+Δt. Therefore several iterations are required to solve Eq. (5-7) and (5-8) simultaneously.

5.2.3 Solution of Seismic Response of Structure

The solution of the equations of motion can be obtained from the algorithm outlined in Table 5-1. The algorithm in Table 5-1 will provide the solution for Bouc-Wen's models (Section 5.2.1).

5.2.4 Analytical Damage Evaluation

The solution presented in the preceding section was incorporated in an analytical platform, IDARC Version 3.2 (Reinhorn et al. 1992). In this platform, the inelastic

Table 5-1 Numerical Solution Algorithm

A. Equations

$$\Delta f_I + \Delta f_D + \Delta f_S + \Delta F_D = \Delta P$$

in which $\Delta f_I = \mathbf{M}\Delta\ddot{u}$; $\Delta f_D = \mathbf{C}\Delta\dot{u}$; $\Delta f_S = \bar{\mathbf{K}}\,\Delta u$ and

$$F_D = \bar{k}_D[\alpha u + (1-\alpha)Zu_y]$$

$$\dot{Z} = (\dot{u}/u_y)\{A - Z^\eta[\gamma \mathrm{sgn}(\dot{u}\,Z) + \beta]\}$$

B. Initial Condition

1. Form stiffness matrix $\bar{\mathbf{K}}$, mass matrix **M**, and damping matrix **C**.
2. Initialize u_0, $\dot{u}_0$ and $\ddot{u}_0$.
3. Select time step Δt, choose parameter α=0.25 and δ=0.5, calculate integration constants:

$$a_0 = \frac{1}{\alpha\Delta t^2};\ a_1 = \frac{\delta}{\alpha\Delta t};\ a_2 = \frac{1}{\alpha\Delta t};\ a_3 = \frac{1}{2\alpha} - 1;$$

$$a_4 = \frac{\delta}{\alpha} - 1;\ a_5 = \frac{\Delta t}{2}(\frac{\delta}{\alpha} - 2);\ a_6 = \Delta t(1-\delta);\ a_7 = \delta\Delta t.$$

4. Form effective stiffness matrix $\mathbf{K}^* = \bar{\mathbf{K}} + a_0\mathbf{M} + a_1\mathbf{C}$
5. Trianglarize $\mathbf{K}^*$: $\mathbf{K}^* = \mathbf{LDL}^T$

C. Step by Step Computation

1. Assume the pseudo-force (force from damper) $F^i_{D,t}$=0, $\dot{u}^i_t = 0$ solve for $F^i_{D,t+\Delta t}$ in the first iteration i=1 using Eq. (5-8)
2. Calculate the incremental effective load vector from time t to t + Δt:

$$\Delta P^* = \Delta P - \Delta F_D + 2\mathbf{C}_0\,\dot{u}_0 + \mathbf{M}[\frac{4}{\Delta t}\dot{u}_0 + 2\,\ddot{u}_0\,]$$

3. Solve for displacement increment from: $\mathbf{K}^*\Delta u = \Delta \mathbf{P}^*$

and $\Delta\dot{u} = \frac{2}{\Delta t}\Delta u - 2\,\dot{u}_0$; $\ddot{u}_t = \mathbf{M}^{-1}[P_t - f_{D,t} + f_{S,t} - F_{D,t}]$

4. Update the states of motion at time t + Δt:

$$u_{t+\Delta t} = u_t + \Delta u;\quad \dot{u}_{t+\Delta t} = \dot{u}_t + \Delta\dot{u}$$

5. Use $F^{i+1}_{D,t}$=0, $\dot{u}^{i+1}_t = 0$ and $\dot{u}^{i+1}_{t+\Delta t} = \dot{u}_{t+\Delta t}$ solve for $F^{i+1}_{D,t+\Delta t}$ using Eq. (5-8).
6. Compute Error = $\left|F^{i+1}_{D,t+\Delta t} - F^i_{D,t+\Delta t}\right|$
7. If error $\geq$ tolerance , return to C-1 for further iteration.
8. If error $\leq$ tolerance , no further iteration is needed. continue to next time step.

response is evaluated in terms of damage to members defined by the ratio of permanent curvature demand versus capacity expressed as (Reinhorn and Valles 1995):

$$\mathbf{M.I.} = \frac{\phi - \phi'}{\phi_u - \phi_u'} = \frac{\Delta\phi_a}{\Delta\phi_{u0}\left(1 - {E_h}/{4E_{h0}}\right)} = \frac{\Delta\phi_a}{\Delta\phi_u} \quad \text{...(5-12)}$$

where ϕ indicates the maximum deformation demand, ϕ' indicates the recoverable curvature due to elastic rebound, at maximum curvature, ϕ_u the ultimate curvature capacity and ϕ_u' the elastic rebound at same ultimate curvature, $\Delta\phi_a$ and $\Delta\phi_{u0}$ are the achieved maximum permanent curvature and the ultimate monotonic permanent curvature capacity, respectively. E_h is the cumulative energy dissipated by the member and E_{h0} is the energy dissipated monotonically at rupture (ultimate curvature capacity). If $\Delta\phi_a$ is the maximum permanent curvature in an event, then the index determined by Eq. (5-12) is defined as the "Event Damage Index" (Reinhorn and Valles 1995). If $\Delta\phi_a$ is the maximum residual curvature, the damage index is defined as the "Residual Damage Index". It should be noted that the ultimate dynamic permanent curvature capacity, $\Delta\phi_u$, is reduced during an earthquake as a function of the energy dissipation (Reinhorn and Valles 1995). Therefore the damage can be reduced by reducing the hysteretic energy dissipation demand, E_h.

5.2.5 Determining the Monotonic Strength Envelope

An inelastic monotonic envelope defines the force deformation strength of a structure or substructure and can be obtained through a pushover analysis. Static forces proportional to the story resistance are applied incrementally to the structure and the deformations are determined along with the internal force distribution. From the structures Eq. (5-1), neglecting the wind loading F_w:

$$R(u) = -\mathbf{M}\left(\ddot{u} + \ddot{u}_g I\right) - \mathbf{C}\dot{u} = F_i \quad \text{(5-13)}$$

Pre-multiplying both sides by a unit vector, $I^T = \{1,1,\ldots1\}^T$, Eq. (5-13) becomes:

$$I^T R(u) = -I^T\left(\mathbf{M}\ddot{u}_a + \mathbf{C}\dot{u}\right) = I^T F_i \quad \text{(5-14)}$$

where $\ddot{u}_a$ is the total absolute acceleration, $\ddot{u} + \ddot{u}_g I$.

The right hand side of the Eq (5-14) is the total base shear, BS:

$$BS = I^T F_i \quad \text{(5-15)}$$

Dividing Eq. (5-13) by (5-14) and using relationship of Eq. (5-15), the inertia forces are obtained as:

$$F_i = BS\frac{R(u)}{I^T R(u)} \quad \text{(5-16)}$$

The above force distribution is applied incrementally in the pushover analysis by increasing the base shear:

$$F_i^k = \left(BS^{k-1} + \Delta BS^k\right)\frac{R^{k-1}(u)}{I^T R^{k-1}(u)} \quad \text{(5-17)}$$

where k indicates the step of computation. The distribution of pushover force is based on previous computation step, since data is not available without iteration. The error, $ERR = BS^k - I^T R^k(u)$, involved in the above is minimal. However if the error is substantial, an iteration should be performed using Eq. (5-17) until solution converges. The deformation is obtained from the incremental analysis:

$$\mathbf{K}_k \Delta u^k = \Delta F_i^k \qquad (5\text{-}18)a$$

in which ΔF_i^k can be approximated as:

$$\Delta F_i^k = F_i^k - F_i^{k-1} \qquad (5\text{-}18)b$$

Solving for Δu^k one can determine the deformation increase. The increase in the internal forces is obtained from:

$$R^k(u) = \mathbf{K}_k \Delta u^k + R^{k-1}(u) \qquad (5\text{-}18)c$$

The stiffness $\mathbf{K}_{k+1}$ for next step is calculated from Eq. (5-3). The procedure determines the resistance envelope at any desired floor, or for the total structure characteristics.

5.2.6 Monotonic Strength Envelope with Braces

The structure stiffness will be enhanced in presence of dampers depending on different stages of the dampers, therefore instead of using the original stiffness of structure, **K** from Eq. (5-3), the enhanced stiffness **K**' (=**K**+Δ**K**) should be used, since it includes the contribution of dampers, $\mathbf{\Delta K}$. The $\mathbf{\Delta K}$ can be evaluated depending the stages of the dampers as:

$$\mathbf{\Delta K} = \mathbf{B}k_i \qquad \text{..........} (5\text{-}19)$$

where k_i is the stiffness of the damper i and:

$$B = \begin{bmatrix} N_j \cos^2\theta_j & -N_j \cos^2\theta_j & \cdot & \cdot & \cdot \\ -N_j \cos^2\theta_j & N_j \cos^2\theta_j + N_{j-1}\cos^2\theta_{j-1} & -N_{j-1}\cos^2\theta_{j-1} & \cdot & \cdot \\ \cdot & \cdot & \cdot & \cdot & \cdot \\ \cdot & \cdot & -N_3\cos^2\theta_3 & N_3\cos^2\theta_3 + N_2\cos^2\theta_2 & -N_2\cos^2\theta_2 \\ \cdot & \cdot & \cdot & -N_2\cos^2\theta_2 & N_2\cos^2\theta_2 + N_1\cos^2\theta_1 \end{bmatrix}$$

$$\text{..........} (5\text{-}20)$$

$$\begin{cases} k_i = k_{Di}, & F_{Di} < F_{Di,break-away} \\ k_i = 0, & F_{Di} > F_{Di,break-away} \end{cases} \qquad \text{..........} (5\text{-}21)$$

where N_j is the number of dampers or unit multiplier for dampers in brace level j with an angle of incidence of θ_j.

The performance of influence of dampers stiffening is evaluated in Sec. 5.3.

5.3 Validation of Structural Model with Friction Dampers

5.3.1 Time History Analysis

The performance of the structure model retrofitted with friction dampers was determined analytically through time history analysis. Bouc-Wen's model, with parameters from Section 2, was used to model the dampers for the test structure presented in Sections 3 and 4 subjected to several simulated earthquakes. The analytical and experimental displacements and the accelerations of the structure are compared in Fig. 5-3 and 5-4 for El-Centro earthquake and Fig. 5-5 and 5-6 for Taft earthquake. Similar results are obtained for all other earthquakes. The forces in the dampers calculated using Bouc-Wen's model are shown in Fig. 5-7. The computed maximum forces and displacements in the damper, as well as the total energy dissipated are in good agreement with the experimental results.

5.3.2 Monotonic Pushover Analysis

The validity of pushover analysis was verified also with experimental data. The analysis was performed according to the procedure obtained in Sec. 5.2. Fig. 5-8 indicated the variation of total structure resistance in terms of base shear (foundation reaction, Eq. 5-14 and 5-15) as a function of the displacement at the top of the structure. The stiffening effect at various stages of structural deformation is presented in Fig. 5-8. The initial strength resistance including the dampers (Eq. 5-25, i.e. $K+\Delta K$ in Fig. 5-8) can be up to 2.5 times larger than the original, and the final strength resistance (assume all dampers were at stage of slip) is equal to the resistance of the original structure plus a constant resistance from dampers.

Overall the pushover analysis is representative to the variation of total internal forces in structure due to the dynamic response. The introduction of dampers only increase the initial stiffness of the structure and once the dampers are slipping, the structure only increases certain strength without any stiffening. The increase of force demands in structure joints and foundation is limited. (see also Section 6).

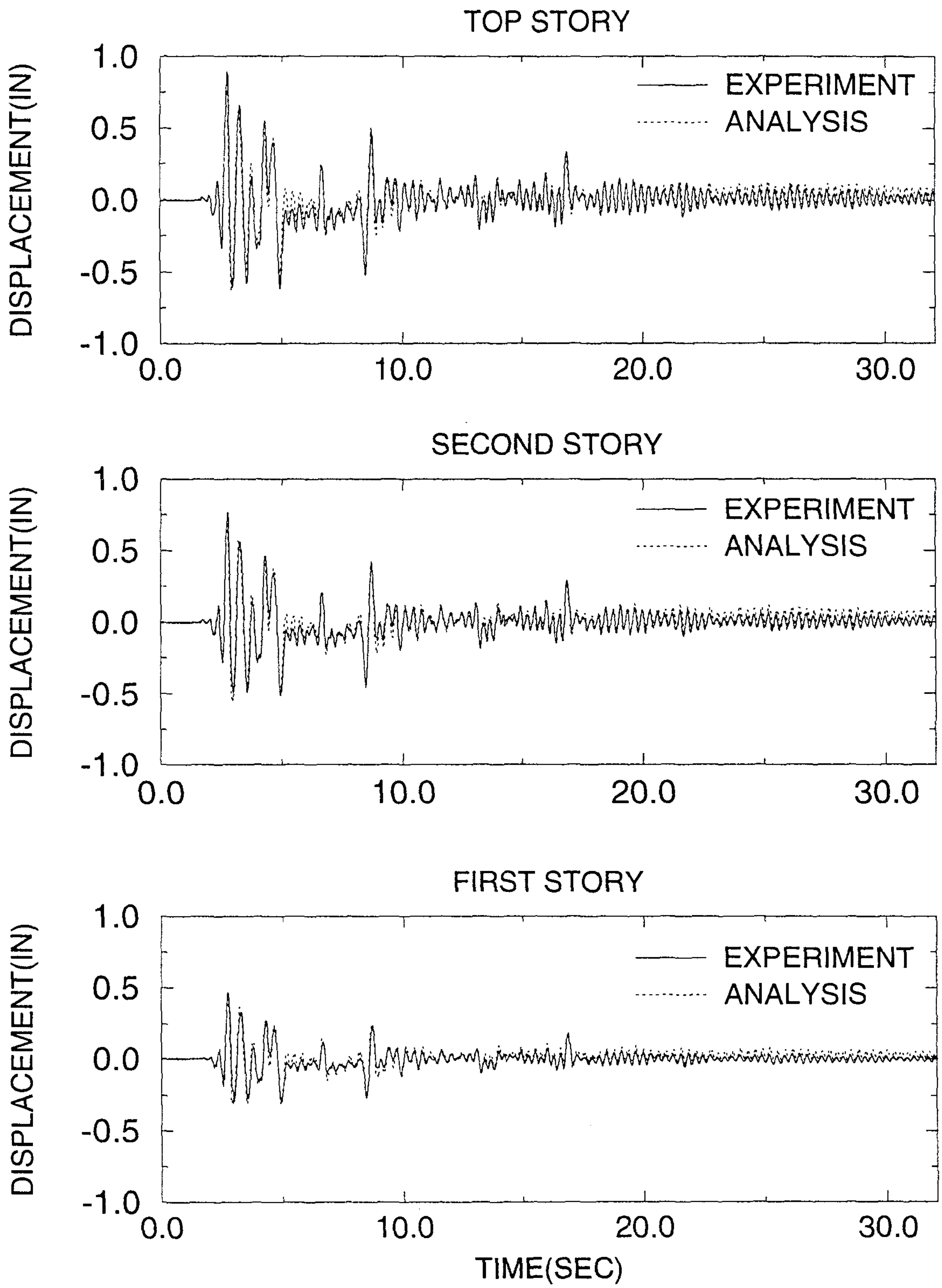

Figure 5-3 Comparison of Experimental and Analytical Displacement for El-Centro 0.3g (with Six Tekton Friction Dampers)

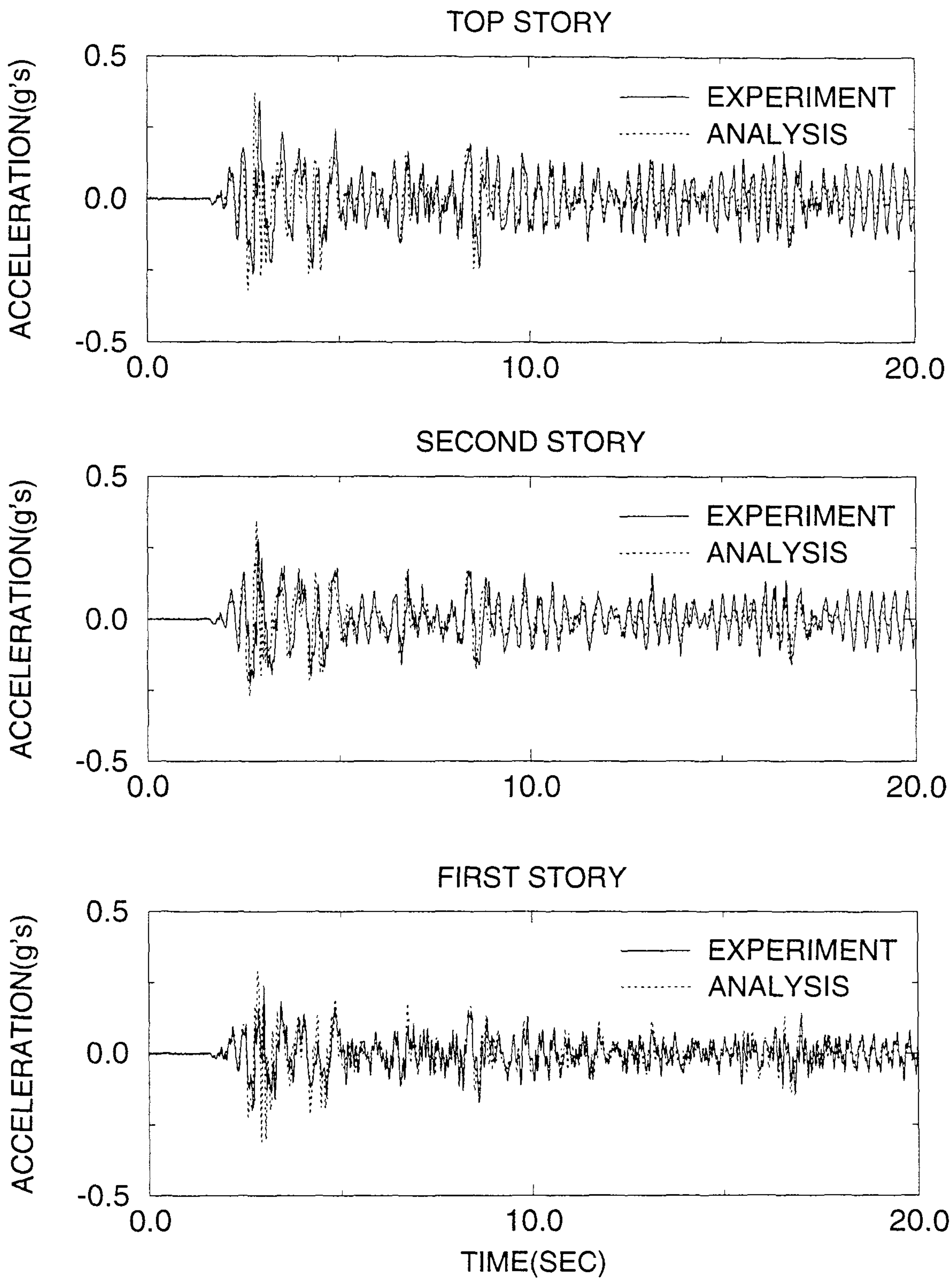

Figure 5-4 Comparison of Experimental and Analytical Acceleration for El-Centro 0.3g (with Six Tekton Friction Dampers)

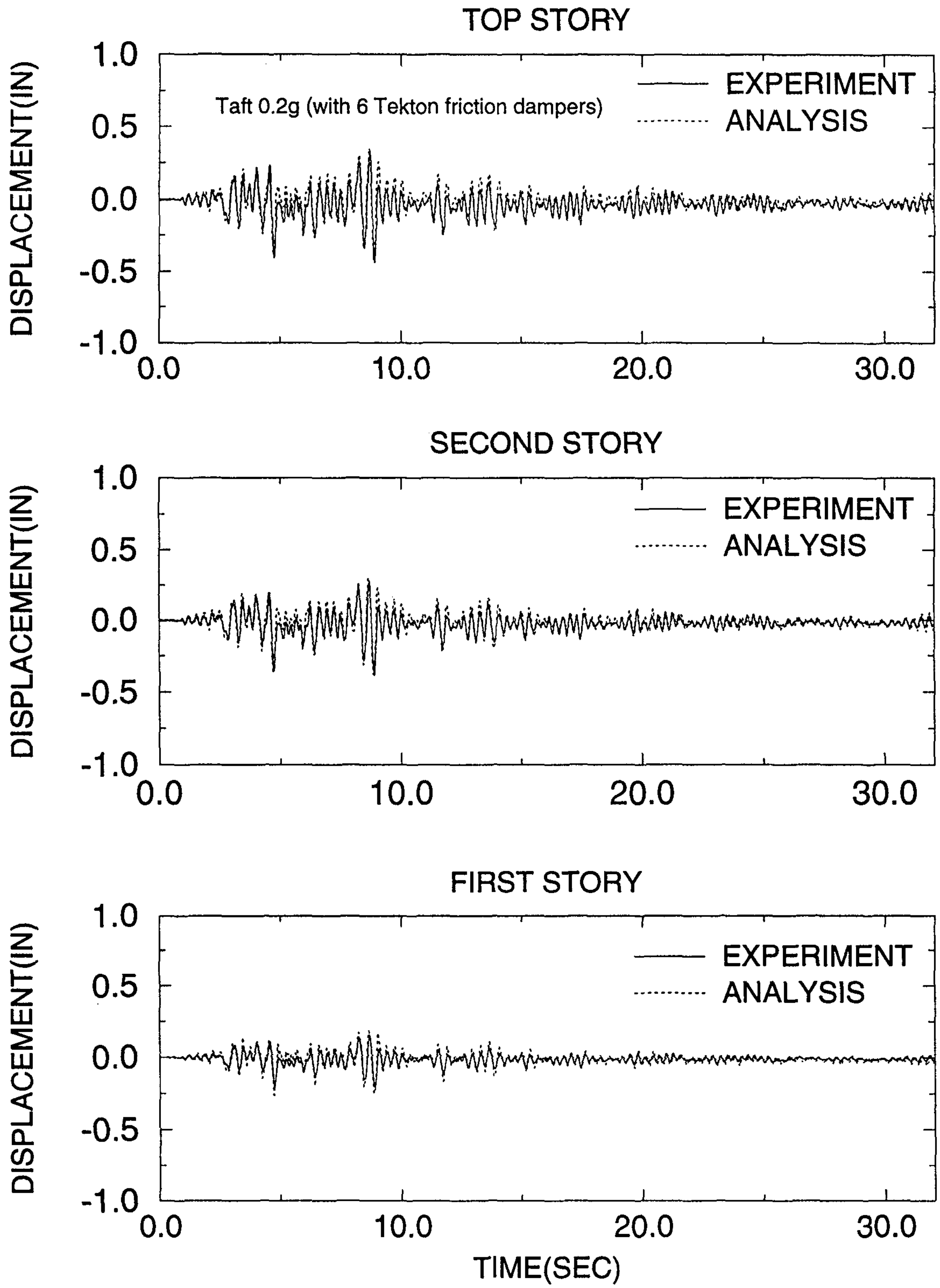

Figure 5-5 Comparison of Experimental and Analytical Displacement for Taft 0.2g (with Six Tekton Friction Dampers)

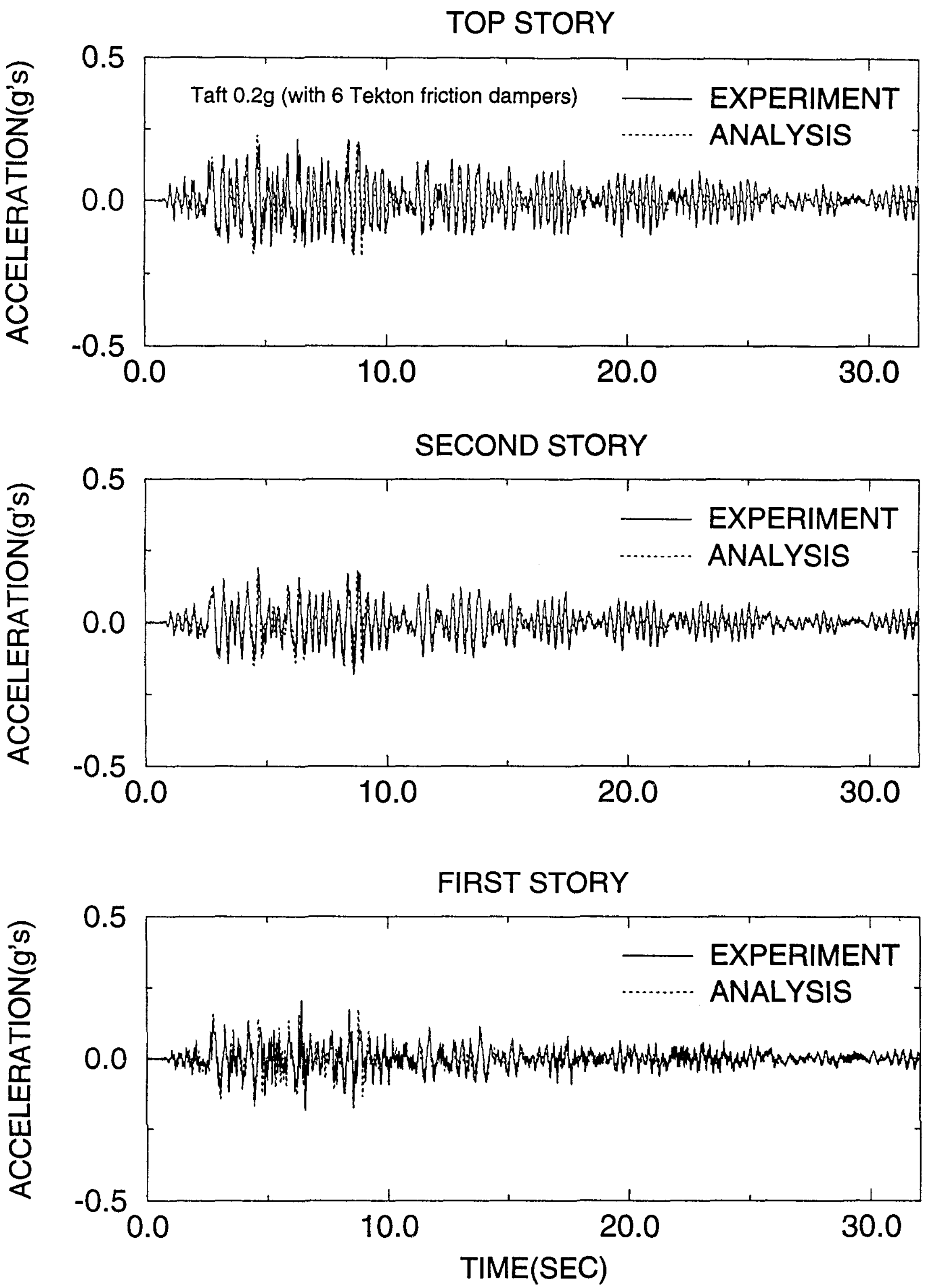

Figure 5-6 Comparison of Experimental and Analytical Acceleration for Taft 0.2g (with Six Tekton Friction Dampers)

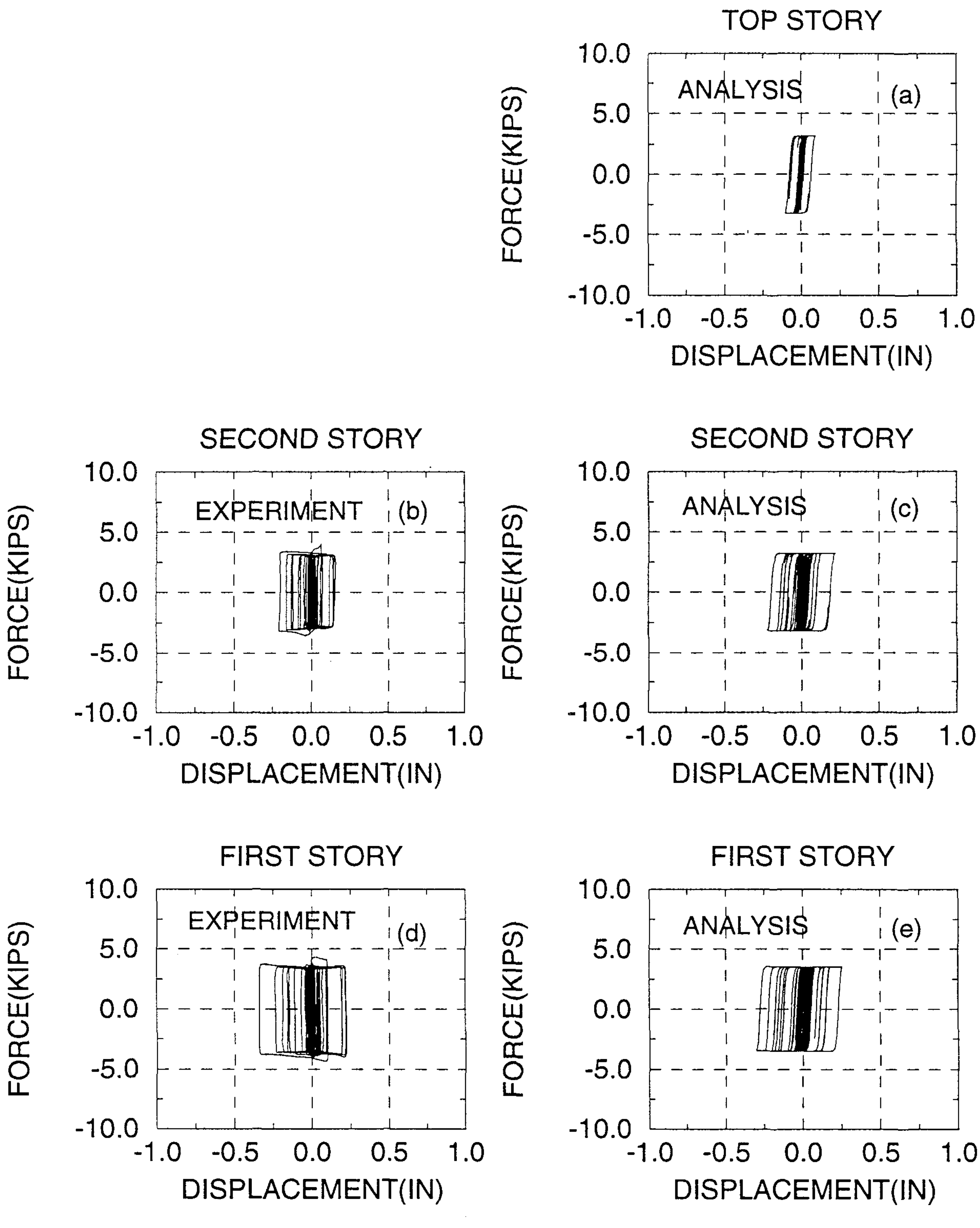

Figure 5-7 Comparison of Damper Forces for El-Centro Earthquake PGA 0.3g (with Six Tekton Friction Dampers)

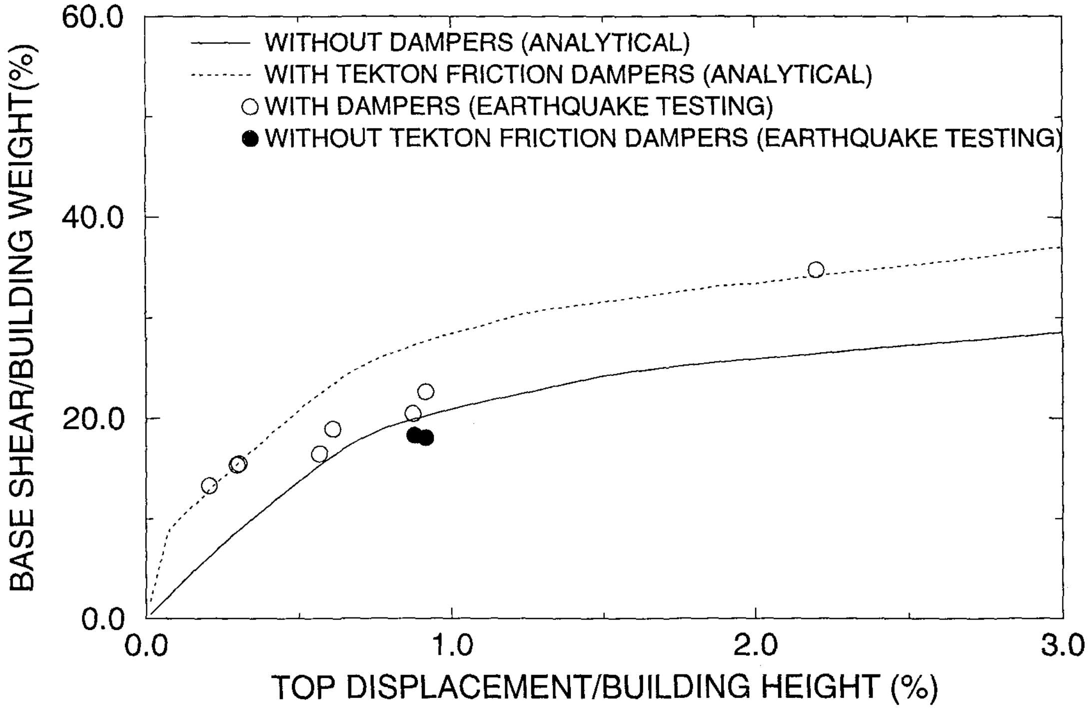

Figure 5-8 Structural Resistance in Presence of Friction Dampers

SECTION 6

SIMPLIFIED EVALUATION OF INELASTIC RESPONSE WITH SUPPLEMENTAL DAMPING

6.1 Response Spectra for Elastic Systems

The representation of structural response of elastic structures becomes more relevant using spectral approach monitoring simultaneously the acceleration (force) and displacement responses. The spectral representation of peak inertia forces versus the peak displacement response was suggested for evaluation of elastic structures (Kircher 1993a.) and for inelastic structures (Freeman 1993, Kircher 1993b).

6.1.1 Composite Response Spectra for Single Degree of Freedom (SDOF)

The acceleration response spectrum indicating the maximum acceleration, $S_a(T,\xi)$ is dependent on the period, T, and the damping of the SDOF oscillator, ξ. The maximum inertia force (or base shear, BS), is obtained:

$$BS = \left(W/g\right) S_a(T,\xi) \qquad \text{(6-1)a}$$

or

$$BS/W = S_a(T,\xi)/g \qquad \text{(6-1)b}$$

The displacement response spectrum can be obtained by direct computation, $S_d(T, \xi)$, or by transformation of acceleration spectra into a pseudo displacement spectrum:

$$PS_d(T,\xi) = S_a(T,\xi) \Big/ \left(2\pi/T\right)^2 \quad \text{..........} (6\text{-}2)$$

The plot of base shear spectra versus displacement response spectra are shown in Fig. 6-1 as composite response spectra. A line passing through origin with a slope of $(2\pi/T)^2$ will intersect the spectral line for ξ_1 at a point with coordinates indicating the response spectra of acceleration $S_a(T_1, \xi_1)$ and of displacement $PS_d(T_1, \xi_1)$. If $S_d(T_1, \xi_1)$ is used rather than $PS_d(T_1, \xi_1)$, then the line with slope of $(2\xi/T)^2$ will indicate only approximately the displacement.

6.1.2 Composite Spectra for Multi-Degree of Freedom (MDOF)

The acceleration response of any degree of freedom i due to a given spectral acceleration is:

$$\ddot{u}_k = \left\{ \sum_j \left[\Phi_{kj} \Gamma_j S_a\left(T_j, \xi_j\right) \right]^2 \right\}^{1/2} \quad \text{..........} (6\text{-}3)$$

in which Φ_{kj} is the modal shape j (mass normalized i.e. $\sum m_k \Phi_{kj}{}^2 = 1$ and Γ_j is the modal participation factor ($= \sum m_k \Phi_{kj}$).

$$u_k = \left\{ \sum_j \left[\Phi_{kj} \Gamma_j S_d\left(T_j, \xi_j\right) \right]^2 \right\}^{1/2} \quad \text{..........} (6\text{-}4)$$

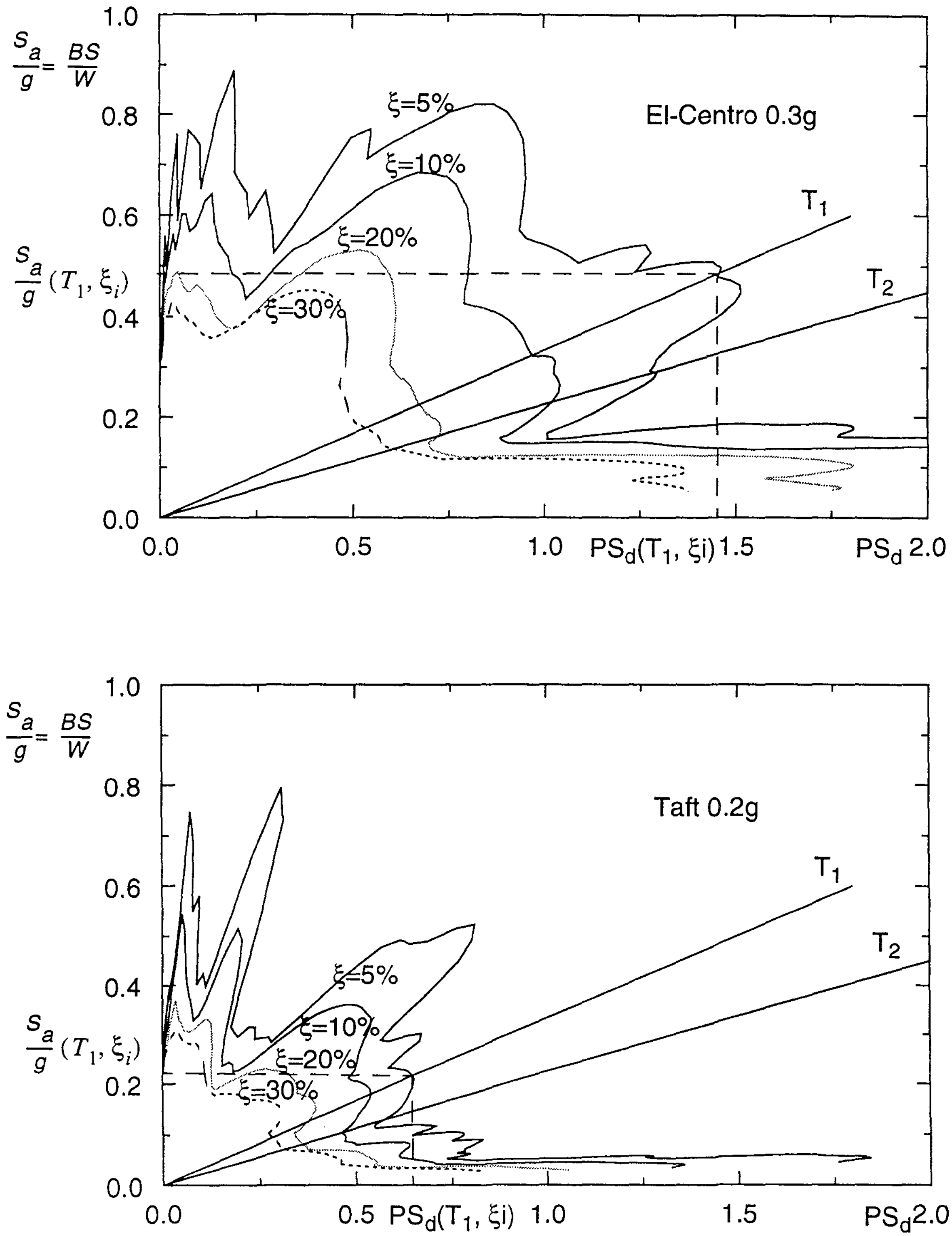

Figure 6-1 Composite Response Spectra for SDOF

The above definitions are based on SRSS superposition.

6.1.2.1 Composite Spectra for a Single Mode

For a single mode contribution, the modal component of acceleration and displacement, can be expressed for a single mode i setting j=1 in Eq.. (6-3) and (6-4). Varying the period, T_i from T_1 to T_2 range (selected for the description of the spectrum), then the composite spectral modal response can be defined as:

$$S_{u_k}^{(i)}(T,\xi) = \Phi_{ki}\Gamma_i S_d(T,\xi); \quad T_1 \le T \le T_2 \quad \text{(6-5)a}$$

$$S_{\ddot{u}_k}^{(i)}(T,\xi) = \Phi_{ki}\Gamma_i S_a(T,\xi); \quad T_1 \le T \le T_2 \quad \text{(6-5)b}$$

The composite spectra is defined as a function of $S_{\ddot{u}_k}/g$ vs S_{u_k} defined above, similarly with the spectra for SDOF (Fig. 6-1). The modal base shear is obtained from Eq. (6-5)b

$$BS/W = \Gamma_i^2\, S_a(T,\xi)/g \quad \text{(6-6)}$$

The composite spectra can be defined for the maximum base shear versus the maximum displacement response at any degree of freedom, k, by adjusting the index in Eq. (6-5). Charts similar to Fig. 6-1 can be developed for single mode.

6.1.2.2 Composite Spectra Including Higher Modes

The response in Eq. (6-3) can be written as:

$$\ddot{u}_k = \left\{ \sum_j \left[\Phi_{kj} \Gamma_j S_a \left(T_0 \left(\frac{T_j}{T_0} \right); \xi_0 \left(\frac{\xi_j}{\xi_0} \right) \right) \right]^2 \right\}^{1/2} \quad \text{...(6-7)}$$

$$u_k = \left\{ \sum_j \left[\Phi_{kj} \Gamma_j S_d \left(T_0 \left(\frac{T_j}{T_0} \right); \xi_0 \left(\frac{\xi_j}{\xi_0} \right) \right) \right]^2 \right\}^{1/2} \quad \text{...(6-8)}$$

in which the period T_j was expressed as a ratio (T_j/T_0) times T_0, the fundamental period, similarly the damping ratio ξ_j . Assuming that (T_j/T_0) is constant for any mode in respect to the first, independently of the value of T_0, it is possible to define a maximum peak for $\ddot{u}_k$ and u_k including the higher modes, by varying T_0 between two limits, T_1 and T_2 , defining as the spectral range. The composite spectrum, can be defined therefore by:

$$S_{u_k}(T,\xi) = \left\{ \sum_j \left[\Phi_{ki} \Gamma_i S_d \left(T,\xi,\frac{T_j}{T_0},\frac{\xi_j}{\xi_0} \right) \right]^2 \right\}^{1/2} \quad \text{...(6-9)a}$$

$$S_{\ddot{u}_k}(T,\xi) = \left\{ \sum_j \left[\Phi_{ki} \Gamma_i S_a \left(T,\xi,\frac{T_j}{T_0},\frac{\xi_j}{\xi_0} \right) \right]^2 \right\}^{1/2} \quad \text{...(6-9)b}$$

and plotted as the chart in Fig. 6-1.

Any other important response quantities can be derived from the definitions in Eq. (6-9). For example the base shear, BS can be determined:

$$BS/W = \left\{ \sum_j \left[\Gamma_i^2 S_a \left(T,\xi,\frac{T_j}{T_0},\frac{\xi_i}{\xi_0} \right) \right]^2 \right\}^{1/2} \quad \text{...(6-10)}$$

Using the expression in Eq. (6-10) and (6-9), one can develop a composite spectrum similar to Fig. 6-1 for SDOF.

Fig. 6-2 presents the composite spectra for the structural model studied in Section 3. The composite spectra based on single mode contribution (Eq. (6-6) and (6-5)b) is shown in Fig. 6-2a. The composite spectra based on three modes (Eq. (6-10) and Eq. (6-9)) is shown in Fig. 6-2(b) for comparison. Differences can be noted at high periods, however, for most purposes, the differences are minor otherwise.

6.2 Evaluation of Seismic Demand in Elastic Structures

6.2.1 Response without Supplemental Damping

The equation of motion of an elastic system is defined as:

$$\mathbf{M}\ddot{u} + \mathbf{C}\dot{u} + \mathbf{K}u = -\mathbf{M}\ddot{u}_g \quad \text{(6-11)}$$

or grouping the terms:

$$\mathbf{M}\left(\ddot{u} + \ddot{u}_g\right) + \mathbf{C}\dot{u} = -\mathbf{K}u \quad \text{(6-12)}$$

The extreme response requires that:

$$\left[\mathbf{M}\left(\ddot{u} + \ddot{u}_g\right) + \mathbf{C}\dot{u}\right]_{\max} = -\mathbf{K}u_{\max} \quad \text{(6-13)a}$$

If damping is indicated in the first term, (as shown in Eq. (6-13)), then this term indicates the inertia forces influenced by structure damping, i.e.

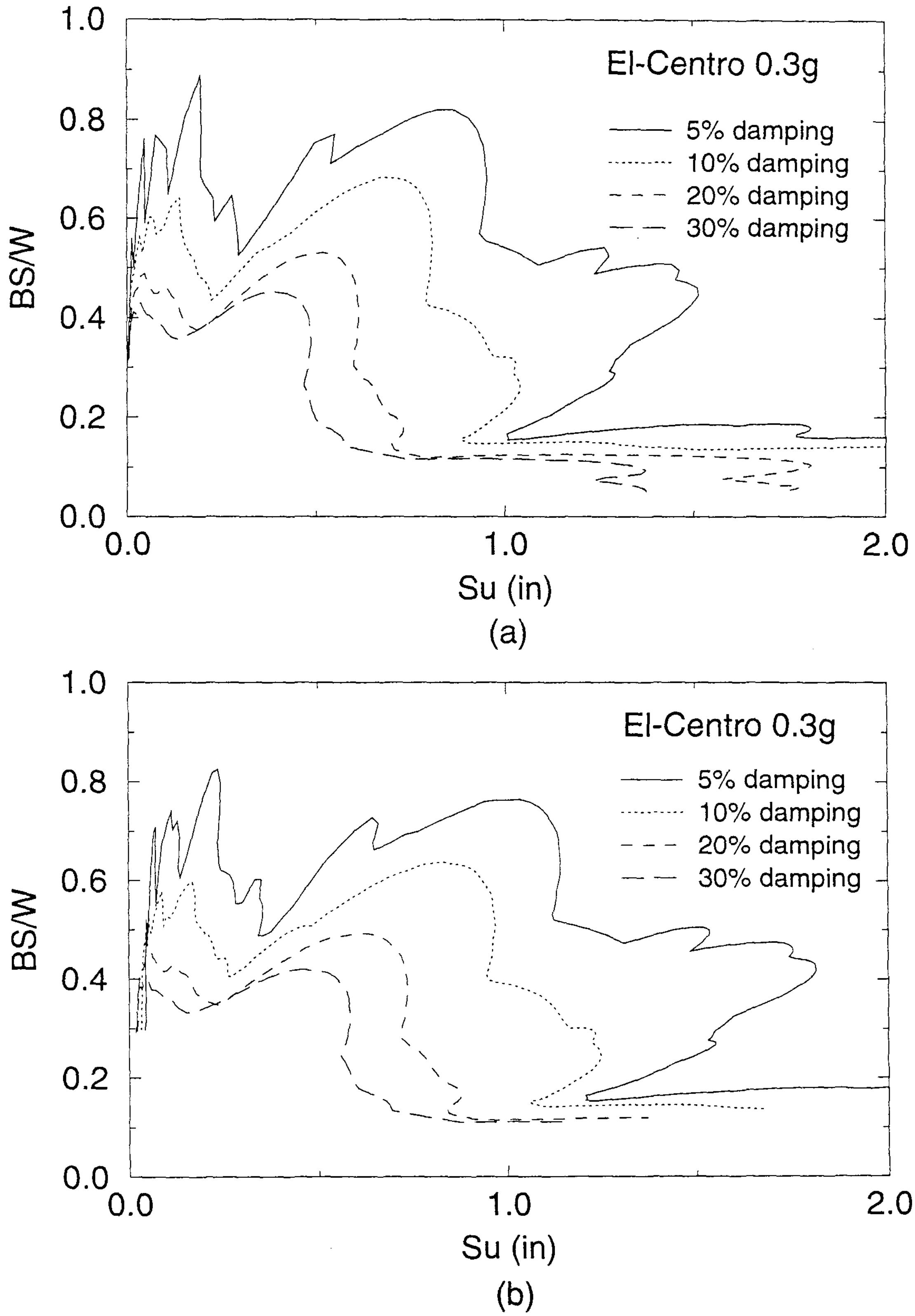

Figure 6-2 Composite Response Spectra for MDOF
(a) Single Mode Contribution, (b) Three Mode Contribution

$$\left[\mathbf{M}(\ddot{u}+\ddot{u}_g)+\mathbf{C}\dot{u}\right]_{\max} = -\mathbf{M}S_{\ddot{u}}(T_0,\xi_0) \quad \text{(6-14)}$$

The right side of Eq. (6-13) indicates:

$$Ku_{\max} = KS_u(T_0,\xi_0) \quad \text{(6-15)}$$

in which T_0 indicates the fundamental period.

Eq. (6-13) can be rewritten as:

$$MS_{\ddot{u}}(T_0,\xi_0) = KS_u(T_0,\xi_0) \quad \text{(6-16)}$$

Using the composite spectrum, Eq. (6-16) shows that the ratio of $S_{\ddot{u}}/S_u = \left(2\pi/T_0\right)^2$ is a line which intersects at the response quantities (see Fig. 6-1).

Therefore, to determine the actual response using the composite spectrum, an intersection of the spectral curve with the structure stiffness/mass properties line with the slope ($\tan\alpha = K/M = (2\pi/T_0)^2$) is required. The intersection point indicate the structural response in base shear and displacement terms (see point A in Fig. 6-3).

6.2.2 Response with Supplemental Damping

The friction damper force can be represented by Eq. (2-1) as:

$$F_D = k_D U, \quad for\ |F_D| \le \mu_{break-away} N \quad \text{(2-1)a, repeat}$$

$$F_D = \mu_{\min} N, \quad for\ \mu_{\min} N \le |F_D| < \mu_{break-away} N, \text{ after sliding occurred.} \quad \text{(2-1)b, repeat}$$

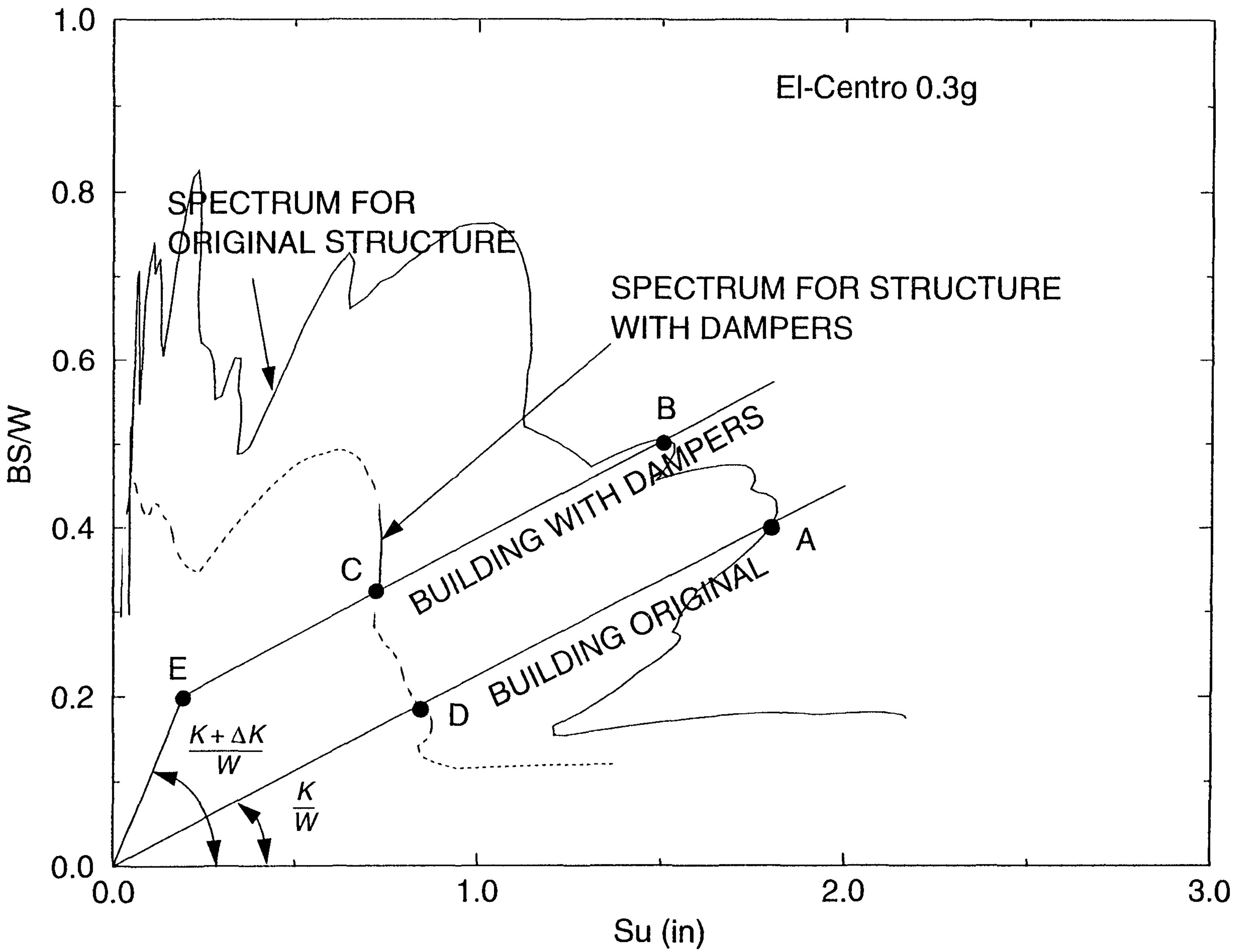

Figure 6-3 Response-Demand Using Composite Spectra

when added to Eq. (6-12), Eq. (6-13)a becomes:

$$\left[\mathbf{M}\left(\ddot{u}+\ddot{u}_g\right)+\mathbf{C}\dot{u}\right]_{\max} = -(\mathbf{K}+\Delta\mathbf{K})u_{\max}, \quad for\ |F_D| \le \mu_{break-away}N \text{ ....(6-13)b}$$

$$\left[\mathbf{M}\left(\ddot{u}+\ddot{u}_g\right)+\mathbf{C}\dot{u}\right]_{\max} = -\left(N\mu_{\min}+\Delta\mathbf{K}u_{\max}\right), \quad for\ \mu_{\min}N \le |F_D| \le \mu_{break-away}N \qquad \text{(6-13)b}$$

which indicates a change of initial slope in the stiffness/mass line in Fig. 6-3 to (K+ΔK)/W (and then with constant strength increase after slip C point) and a shift in the original spectral line from ξ_0 to $\xi_0 + \Delta\xi$ characteristics to the increase from C to C + ΔC.

It can be noted that the stiffening alone (K to K+ΔK) has the tendency to reduce deformations but increase the force (base shear) demand (point B) in Fig. 6-3. The increase in damping along with stiffness increase (C to C+ΔC) reduces both deformation and force demand (point C in Fig. 6-3).

6.3 Evaluation of Motion of Inelastic Structures

The equation of motion of an inelastic system (Eq. 5-1):

$$\mathbf{M}\ddot{u}+\mathbf{C}\dot{u}+\mathbf{R}(u) = -\mathbf{M}\ddot{u}_g \text{ ....(5-1)Repeat}$$

in which R(u) is the structure strength determined according to the procedure in section 5.2.5. Similarly with Eq. (6-13), the maximum response can be determined from:

$$\left[\mathbf{M}\left(\ddot{u}+\ddot{u}_g\right)+\mathbf{C}\dot{u}\right]_{\max} = MS_{\ddot{u}}(T,\xi) = R(u)_{\max} \text{ ....(6-17)}$$

Eq. (6-17) suggests that the maximum deformation is obtained at the intersection of the structure resistance R(u) with the acceleration spectral lines as shown in Fig. 6-4a. The spectral lines based on NEHRP, 1994 are used in Fig. 6-4 for an MDOF composite spectrum (see Section 6.1.2.2). for the test structure in Section 4. If the structure was elastic, the base shear would have been larger, while for the inelastic structure, the base shear response is smaller but accompanies by larger deformation.

6.3.1 Response Neglecting Hysteretic Damping

The structure dissipates energy during inelastic excursions (Bracci et al. 1992). Neglecting this energy, the damping in inelastic response will remain as the original, as shown in Fig. 6-4. However, neglecting the hysteretic damping, displacements and base shear larger than expected are produced if the response spectrum is a monotonically changing function.

6.3.2 Response Considering the Hysteretic Damping

The hysteretic energy dissipation can be interpreted as an increase in the "viscous" damping. In such case the response is obtained at the intersection of the elastic strength function R(u) with the composite spectral lines for an increased damping ratio $\xi_2 = \xi_1 + \Delta\xi$. An example of such response is shown in Fig. 6-5. The equivalent damping increase was measured from experiments using the equivalent frequency response for the structure subjected to three intensities ground shaking, i.e. Taft acceleration with PGA of 0.05g, 0,20g and 0.30g. The intersections of the composite spectra and the strength capacity

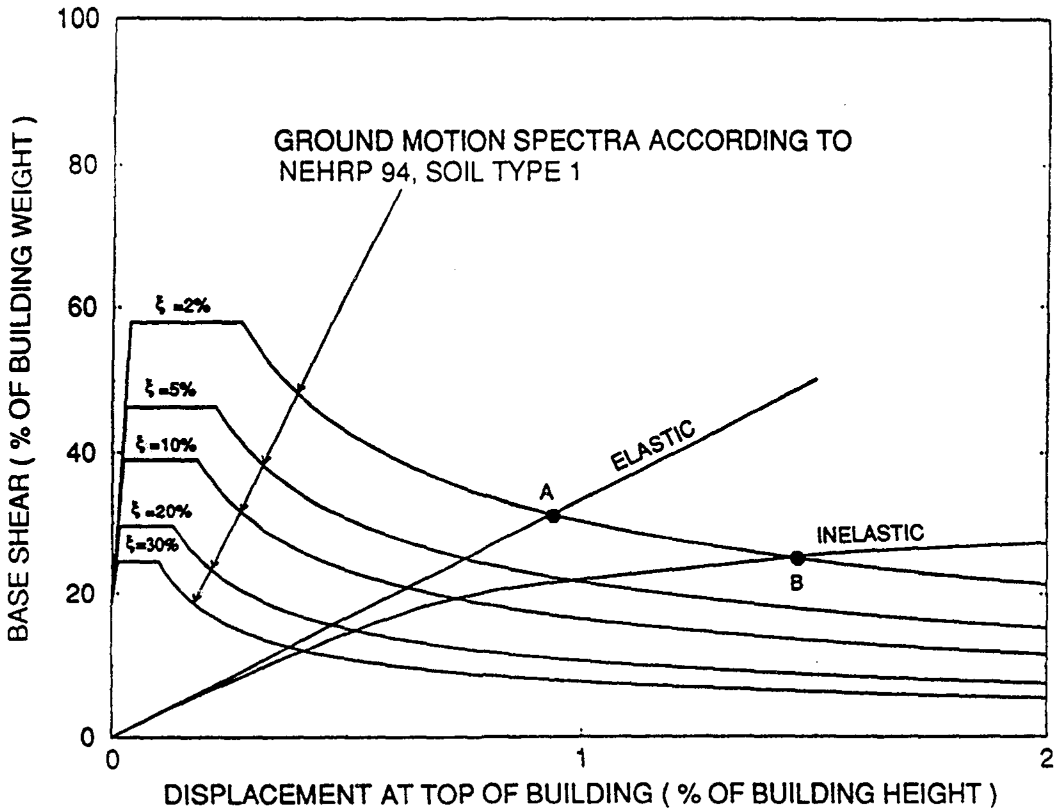

(a) Neglecting Hysteretic Damping

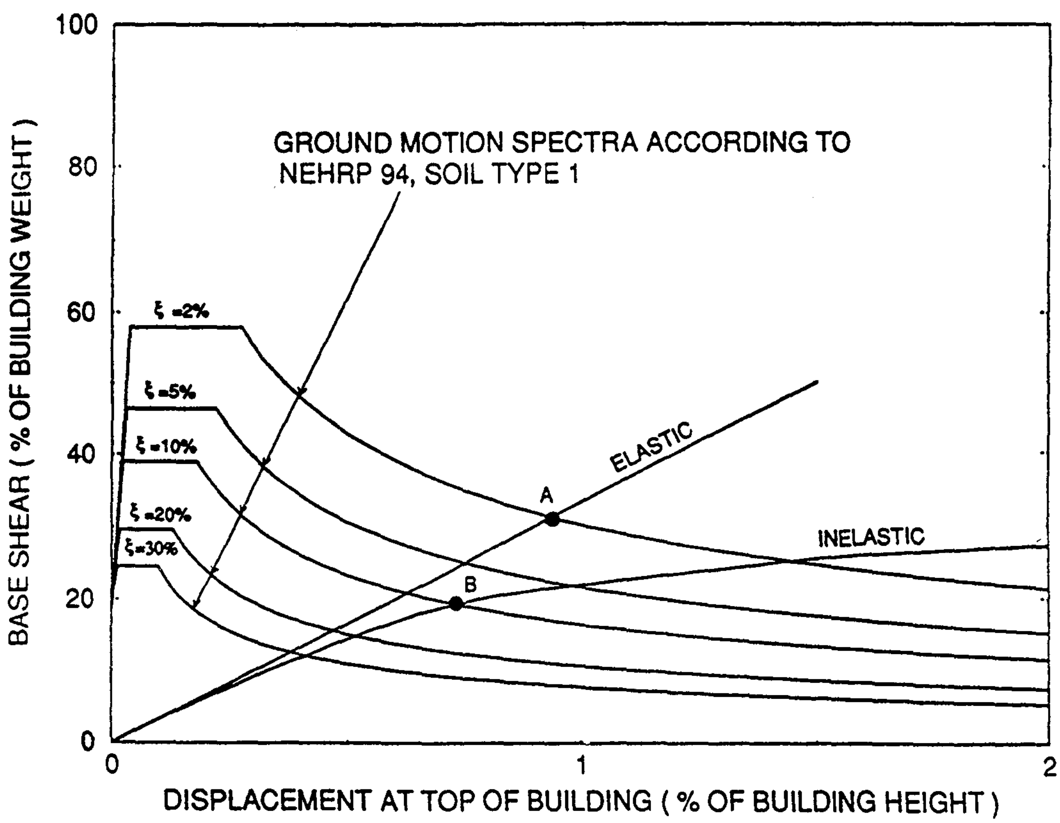

(b) Including Hysteretic Damping

Figure 6-4 Demand in Inelastic Structure Using Composite Spectra

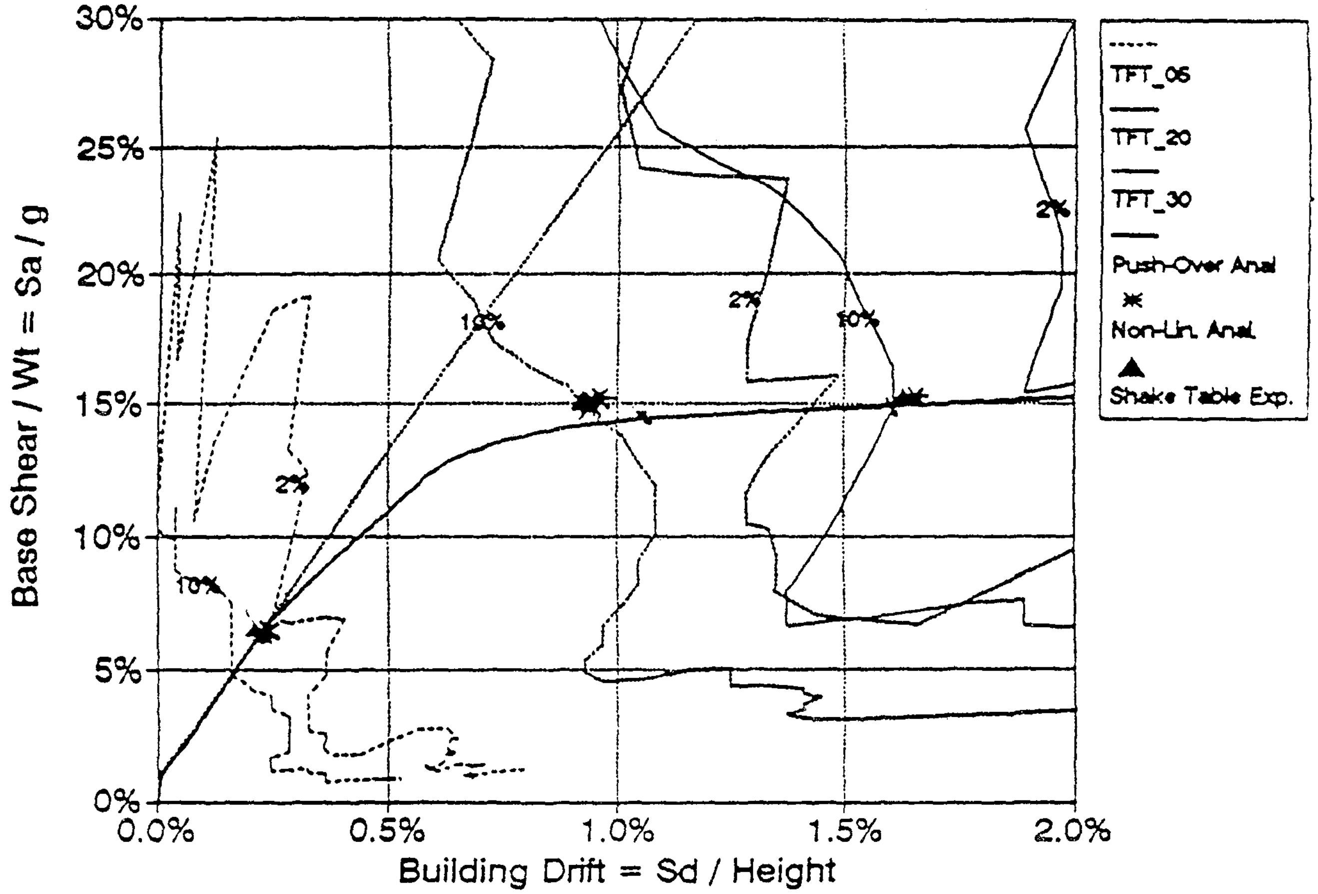

Figure 6-5 Composite Spectra vs Capacity of Structure for Taft 0.05g, 0.20g and 0.30g for 2% and 10% Critical Damping. Tested Damping Ratios 4.6%, 8.2% and 3% for above Motions, Respectively.

function, R(u) are very close to the experimental points. This indicates that the approach can determine the response of forces and displacements with an acceptable approximation.

6.3.2.1 Estimate of Equivalent Hysteretic Damping

For practical purpose however, the calculation of the equivalent damping is a complicated issue. The "viscous" equivalent damping depends on the hysteretic energy dissipation per cycle (Fig. 6-6):

$$E_{hc} = 4\gamma P_y\left(u_{\max} - u_y\right) \quad \text{(6-18)}$$

in which g is the ratio of the area enclosed in the hysteresis versus the area of the parallelogram $[4P_y(u_{max}-u_y)]$. This factor is influenced by bond slip or "pinching" in reinforced concrete elements (γ_c = 0.4 - 0.6) or by the Baussinger effects in steel structures [γ_s = 0.6 - 0.9]. The equivalent damping ratio is defined as:

$$\Delta\xi_{eq} = \frac{E_{hc}}{4\pi E^*_{pv}} \quad \text{(6-19)}$$

with the notation shown in Fig. 6-6. The equivalent increase in the damping ratio is therefore obtained as:

$$\Delta\xi_{eq} = \frac{2\gamma(\mu - 1)}{\pi\mu[1 + \alpha(\mu - 1)]} \quad \text{(6-20)}$$

in which m is the ductility defined as $\mu = u_{max}/\mu_y$. It is evident that the damping increase is a function of amplitude (ductility) per cycle. Earthquake response is neither cyclic nor

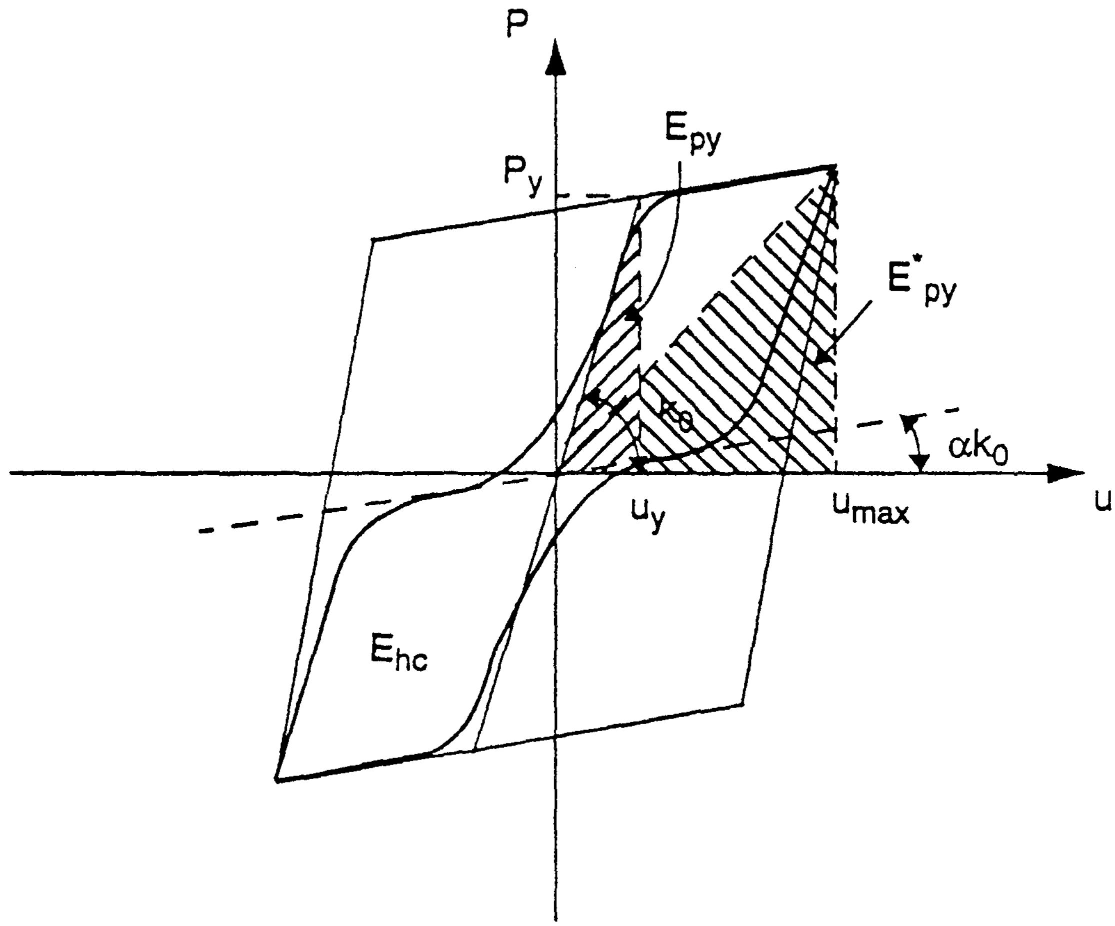

Figure 6-6 Cyclic Hysteretic Energy Dissipation

constant amplitude. Therefore the increase in damping can be determined only by approximations from response characteristics.

Using a linear model for which the maximum ductility is replaced by a rms., σ_μ , in Eq. (6-20) instead of μ_S , the equivalent damping is obtained as:

$$\Delta\xi_{eq} = \frac{2\gamma(\sigma_\mu - 1)}{\pi\sigma_\mu\left[1 + \alpha(\sigma_\mu - 1)\right]} \quad \text{.......(6-21)}$$

Assuming a probability density function such as a Gaussian distribution with a zero mean, the relation between the rms. (standard deviation) and the peak (assuming a probability of occurrence of 97.7%) is:

$$\mu_{max} = 2\sigma_\mu \quad \text{.......(6-22)}$$

Therefore the equivalent damping can be approximated from Eq. (6-21) with Eq. (6-22):

$$\Delta\xi_{eq} = \frac{4\gamma(\mu_{max} - 2)}{\pi\mu_{max}\left[2 + \alpha(\mu_{max} - 2)\right]} \quad \text{.......(6-23)}$$

which produces acceptable agreement for maximum deformation ductilities larger than 2. For smaller values the damping increase is negligible and should not be considered. Table 6-1 shows the damping increase for an reinforced concrete structure (γ=0.5) for various maximum ductilities. The damping obtained as shown above can estimate grossly the increase in damping in the test structure due to the hysteretic behavior. Further investigations might be necessary for improved results.

Table 6-1 Increase in effective damping ratio, $\Delta\xi_{eq}$ (for γ=0.5)

μ_{max}	2.00	2.05	2.10	2.20	2.50	3.00	3.50	4.00
α=0.02	0%	1%	2%	3%	6%	11%	13%	16%
α=0.10	0%	1%	2%	3%	6%	10%	13%	14%

6.4 Evaluation of Response of Inelastic Structure with Supplemental Damping

The suggested evaluation uses the composite spectrum approach outlined above. The response is obtained at the intersection of the composite spectrum lines with the inelastic resistance line obtained from push-over analysis, including the influence of supplemental dampers as presented in Section 5.3.2. The influence of stiffening and damping is evaluated below.

6.4.1 Influence of Damping Increase

If the damping devices have only damping characteristics, neglecting the initial stiffness increase, the structure resistance (capacity) remains as before retrofit (see Fig. 5-11, without dampers and Fig. 6-7). If the response without supplemental dampers is represented by point A (ξ = 10%) in Fig. 6-7, an increase in damping will shift the response to point B (ξ = 20%). The displacement response is reduced primarily with some reduction of base shear. However, the initial stiffness and strength increase is inevitable for friction devices. The capacity considering initial stiffness increase and strength increase has to be considered as follows.

6.4.2 Influence of Stiffening due to Supplemental Dampers

As previously outlined in Section 5.3.2, the dampers have a substantial contribution to stiffening at initial stage(see also Fig. 6-7). The influence of stiffening can be seen in the shift of point B to D in Fig. 6-7. The influence of stiffening and strengthening contributes to a further reduction of displacement response and increase in the base shear demand (although minor). A substantial stiffening and strengthening will increase the base shear demand substantially.

6.4.3 Influence of Dynamic Strength

It should be noted that the influence of supplemental damping in inelastic structures is to decrease the deformation of the structure and influence slightly the base shear demand, in many instance by a minor increase. However, it should be noted that the total shear includes the influence of the original structural elements, for which the capacity is indicated by the original line (point E in Fig. 6-7) at the maximum deformation response, and the influence of the dampers for which the forces are the difference between points D and E in same figure. Fig. 6-7 shows therefore that the forces in the original structural elements are reduced even in presence of stiffening. Moreover, the reduction in the deformation is also accompanied by a reduction of the demand for hysteretic energy dissipation which presents deterioration and extensive damage in structural elements (see also Section 4).

The minor increase in the base shear or in many cases the minor increase in the story shear forces may prove to be critical in the design of the load transfer path (i.e.

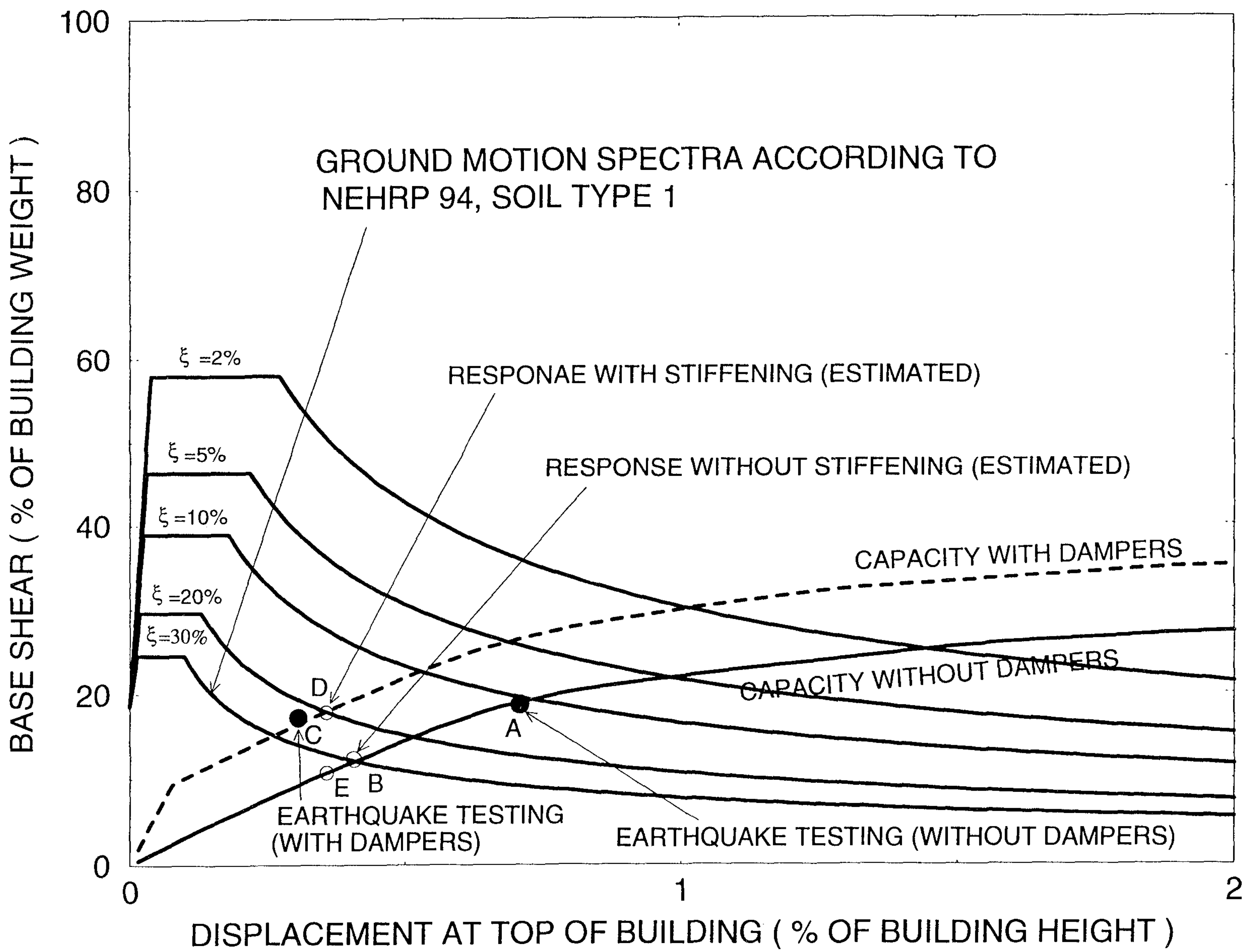

Figure 6-7 Influence of Supplemental Damping

connections, joints, foundations, etc.). Therefore, for design purposes, the maximum deformation demand can be determined conservatively including no stiffening, while the force demand can be determined conservatively from the capacity curve including stiffening and strengthening. The experimental study for the test structure shows this trend (see Fig. 6-8 and 6-9). The composite spectra was calculated using MDOF calculations (Section 6.1.2.2) while the response of the original structure is found on the original capacity curve, the response of the retrofitted structure with supplemental dampers fits the prediction from capacity curve with initial stiffening and strengthening after certain deformation (see Fig. 6-8 and 6-9), as already indicated in the discussion in Section 5.3.2.

The original structure (retrofitted by jacketing and damaged by prior tests) showed an "inherent" damping of 3% to 5% in mild inelastic response (ductilities below 2). The damping increase in the structure was entirely due to damping devices.

Although the composite spectrum diagram indicates adequately trends in the structural response, a better estimate of the damping characteristics, or a better estimate of the composite spectrum, is required in order to obtain a reliable estimation tool. The damping estimated through frequency analysis and through equivalent analytical tools (see Table 4-4) do not fit perfectly the damping increase showed in the composite spectra in Fig. 6-8 and 6-9. The experimental results show smaller "equivalent" damping than estimated by other means.

The composite spectrum is using information from the elastic response, while the structural response is inelastic. In the range of the experiment, the inelastic displacement

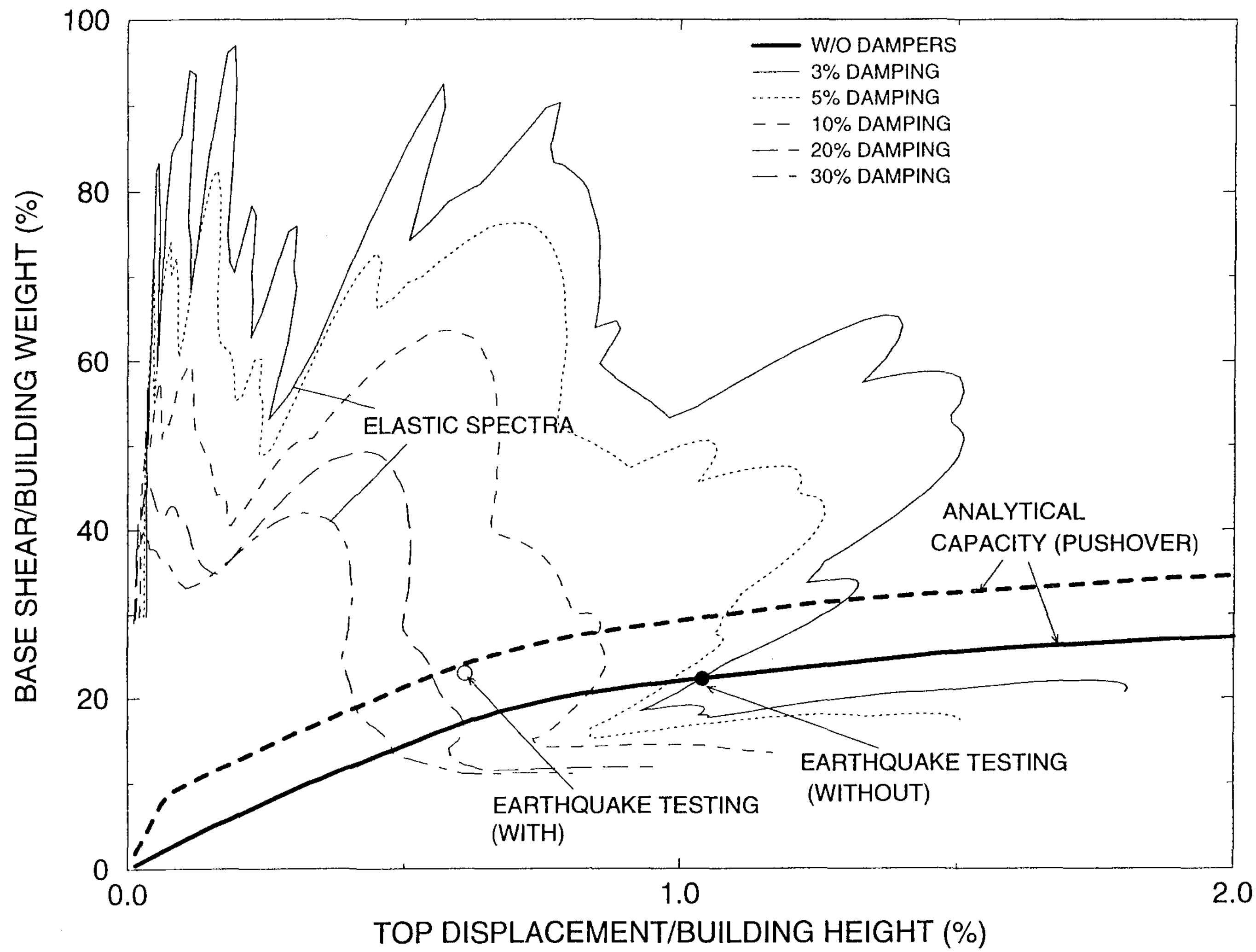

Figure 6-8 Evaluation of Structural Response for El-Centro Earthquake, PGA 0.3g

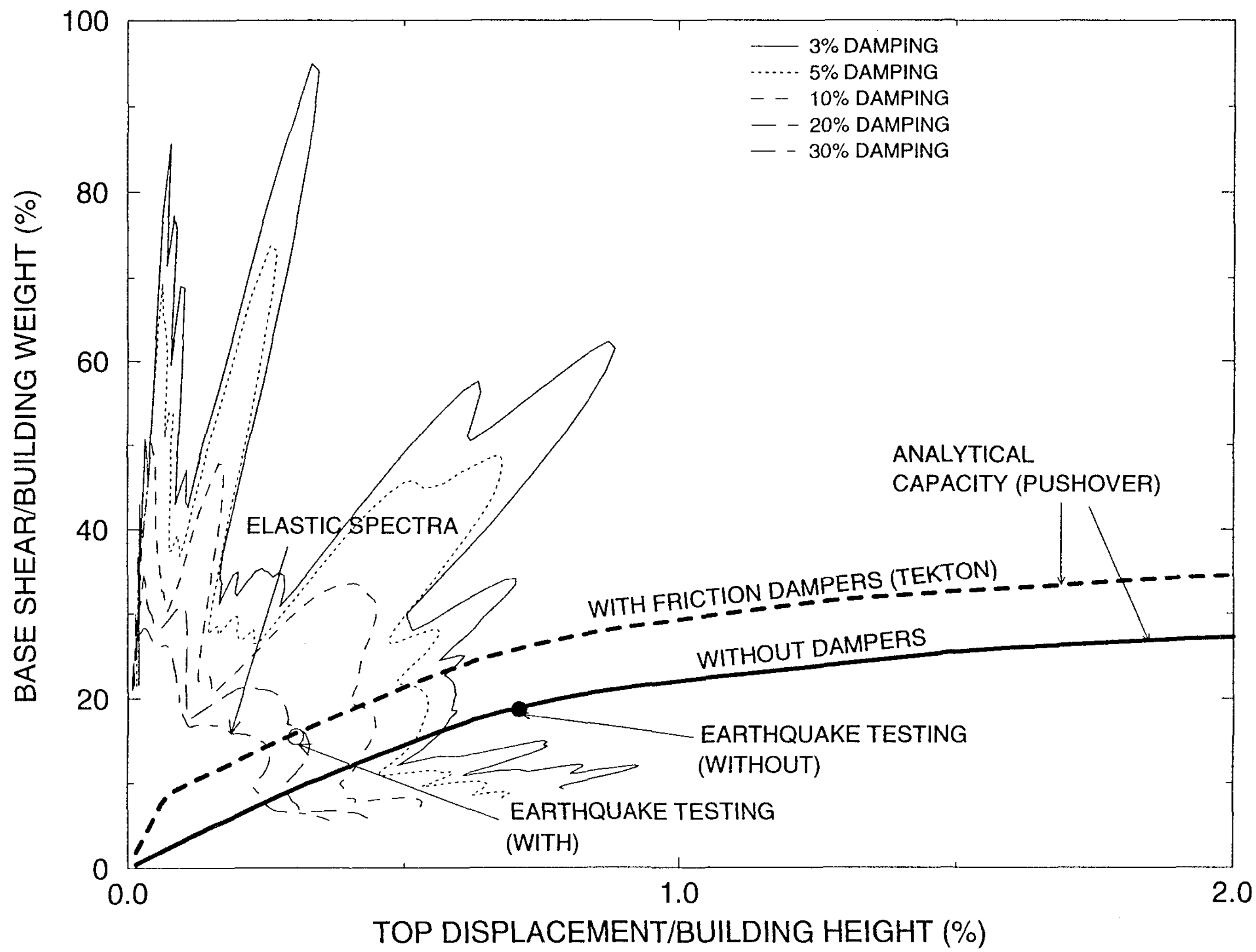

Figure 6-9 Evaluation of Structural Response for Taft Earthquake, PGA 0.2g

spectrum does not match perfectly the elastic one. This can be a probable reason for the above discrepancies.

It should be noted however, that using the spectral curves (developed according to NEHRP, 1994) instead of the individual motions used during testing, the estimate using approximated damping calculations (based on Table 4.3 column (5)) leads to results close to those from experiments (see Fig. 6-10 and 6-11). The spectral curves represent an average of multiple motions and the estimates are not affected by the response spectrum fluctuation when minor error in the estimate of structural parameters are present.

6.5 Evaluation of Experimental Response (Summary)

The experimental response of test structure was evaluated for the retrofit using friction dampers and the results are summarized in Table 4-4a and 4-4b and in Fig. 6-12. and Fig. 6-13 for the structure tested with and without dampers. The results for the other motions cannot be compared with the response without dampers since the unretrofitted structure could not be tested with such motions without the risk of complete collapse. The major findings from the comparison and the evaluation in view of the simplified composite-spectrum approach are presented below:

(a) The response related to displacements or drifts shows substantial reductions, from 30% to 60%, at all stories of the structure. This can be easily derived from the simplified composite spectrum approach presented in the previous section. The response

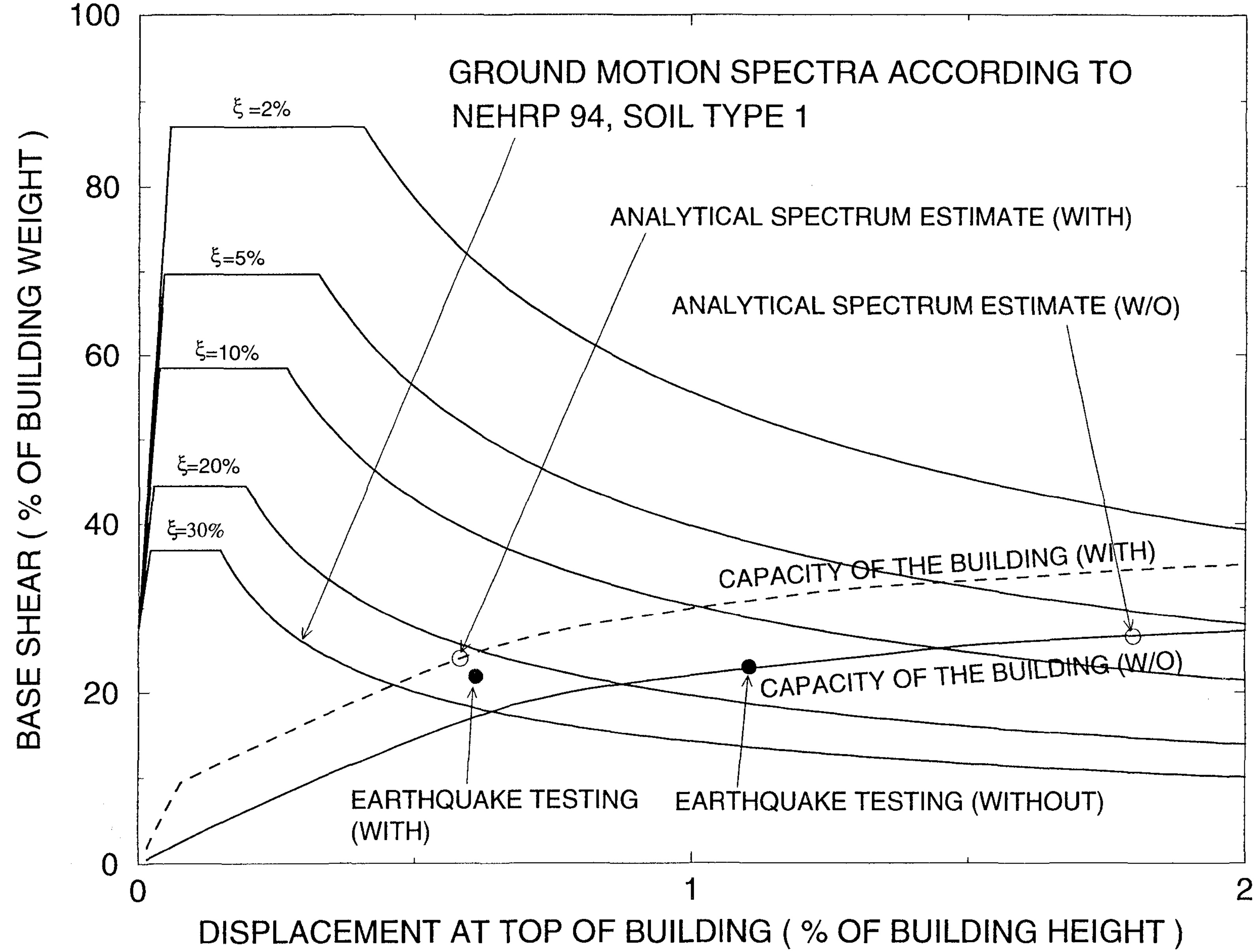

Figure 6-10 Evaluation of Response Using NEHRP Spectra (PGA=0.3g)

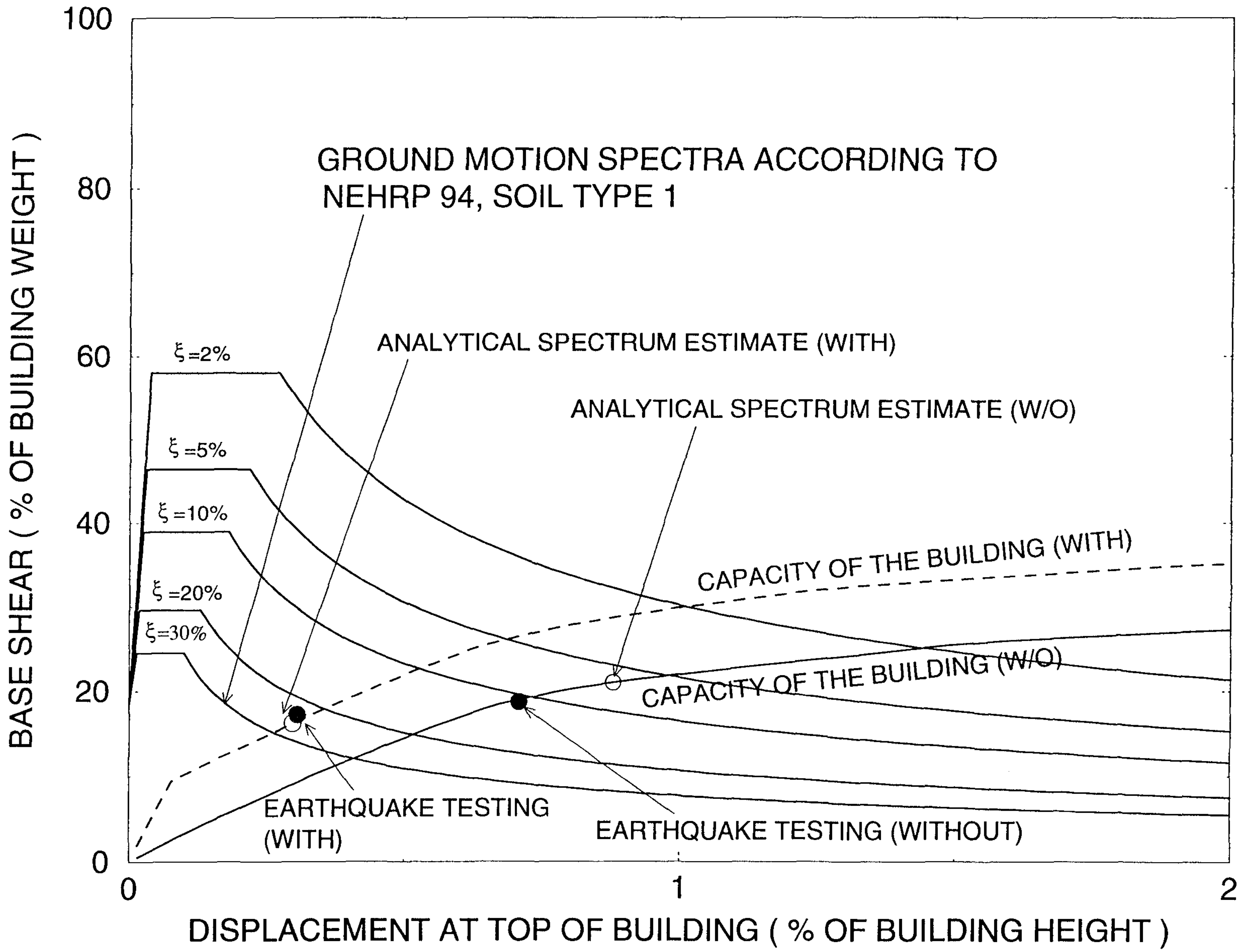

Figure 6-11 Evaluation of Response Using NEHRP Spectra (PGA=0.2g)

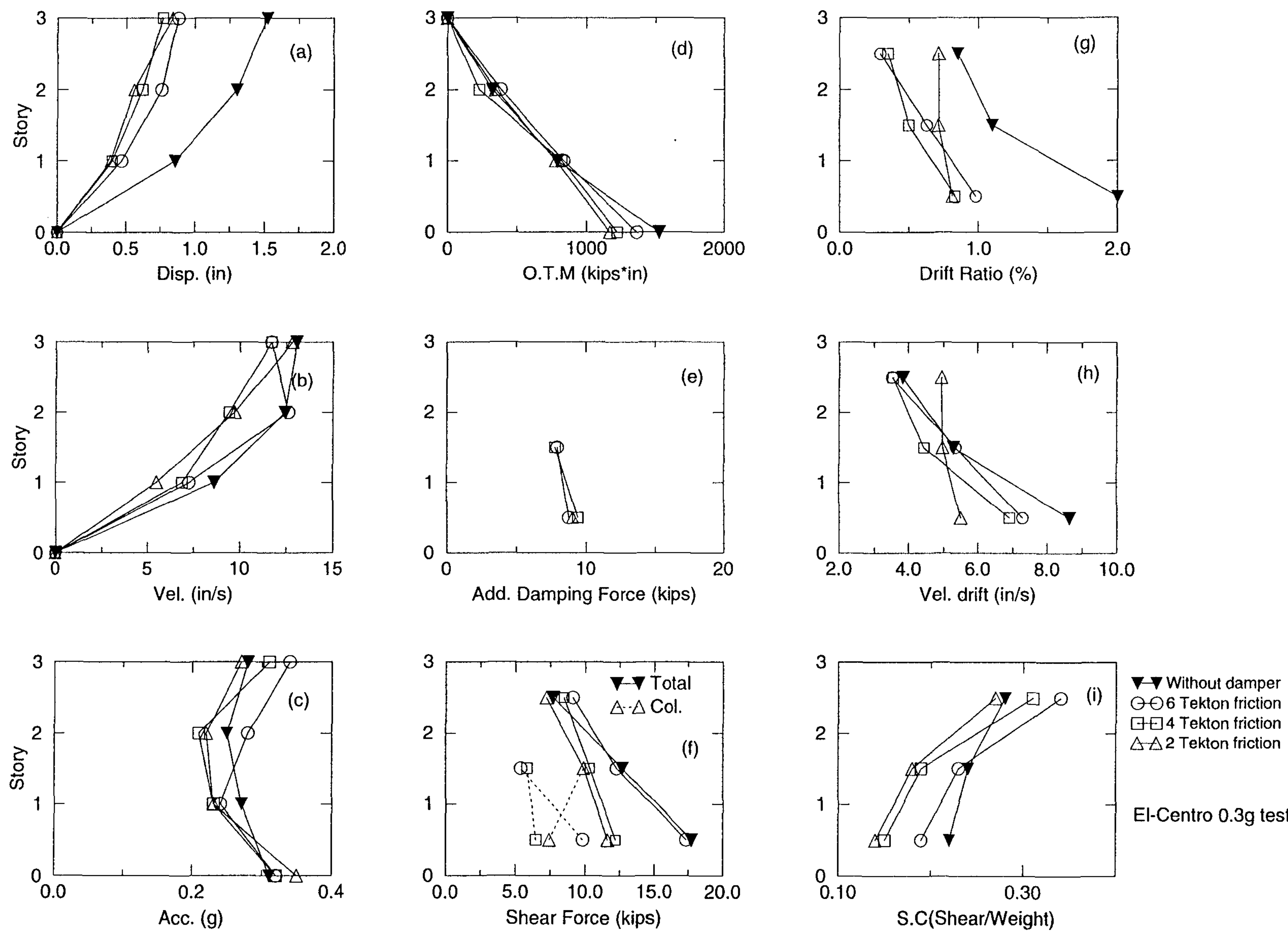

Figure 6-12 Summary of Experimental Response of Tested Structure Model (El-Centro, PGA 0.3g)

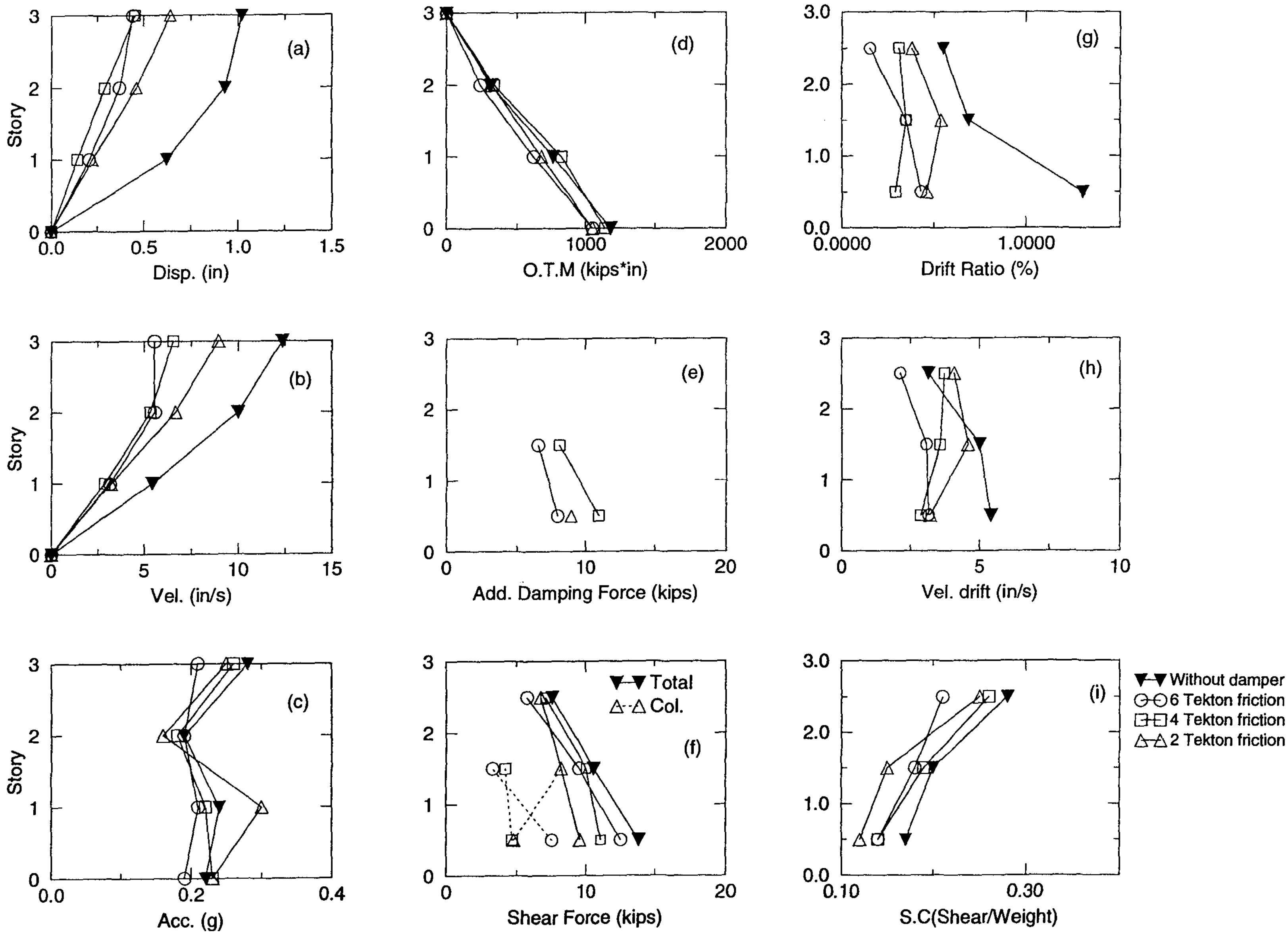

Figure 6-13 Summary of Experimental Response of Tested Structure Model (Taft, PGA 0.2g)

moves back on the capacity curve (see Fig. 6-7 which is flat in the inelastic range) to the increased damping spectra line, reducing substantially the displacements.

(b) The response related to accelerations (Fig. 6-12(c)), overturning moments (Fig. 6-12(d)), story forces (Fig. 6-12(f)) or story shear coefficients (Fig. 6-12(i)) show very little change, some reduced and some increased. The composite spectrum approach indicates this fact following the flat portion of the capacity diagram which has a small slope, on one hand, and is following stiffening patterns, on the other hand. The forces where increased limited amount since the friction dampers have only initial stiffness increase as shown in previous sections. The expected forces and accelerations can be derived from the composite spectrum provided good evaluation of expected damping is possible.

(c) The internal shear force (measured during the experiments) in the columns of the structure retrofitted with friction dampers are smaller than the forces in the unretrofitted structure, by a small amount (Fig. 6-12(f)). Although the total shear force is reduced insignificantly, the forces in the column alone are reduced more substantially 20% - 50%. This reduction is expected in view of the composite spectra and capacity curves as explained in Section 6.4.3 by Fig. 6-7, points A, B, C, D and E). The reduction of the shear forces in the columns depends primarily on the inelastic state at maximum response. If large inelastic excursions are expected, then the reduction in forces might be smaller than if smaller inelastic excursions occur, depending on the "flatness" of post-yielding capacity curve (compare reductions of 2nd story shears in structure, Fig. 6-12(f) and 6-13(f)).

(d) The forces in the friction dampers reach their maximum before the forces in columns do, and then keep a constant value for larger deformation. The connections and columns should be designed for combination of maximum forces and friction damper slip force and so does the foundation.

(e) A summary of testing results of the retrofitted structure with various damping devices (as indicated in the overall research program description in Section 1) is presented in Fig. 6-14 and 6-15. Fluid viscous devices, viscoelastic devices and special viscous walls were sized to fit a desired retrofit scheme. Although the designs were similar, due to construction constrains the resulting devices were different in damping capacity and stiffening characteristics, such that their influence can not be directly compared.

However, the trends of their influence on the structure can be evaluated and quantified using the capacity and composite spectrum approach. The influence of all devices is to reduce deformations and drifts (Fig. 6-10(a), (g)), while increasing or minimally reducing the overall structural forces (Fig. 6-14(d)(f)). The viscous devices (the subject of this report) have a minimal influence on the story forces among the other devices since their stiffening effect is minimal. The viscoelastic braces tested in the same structure have similar damping, but slightly higher stiffness that contributes to an overall increase of story forces.

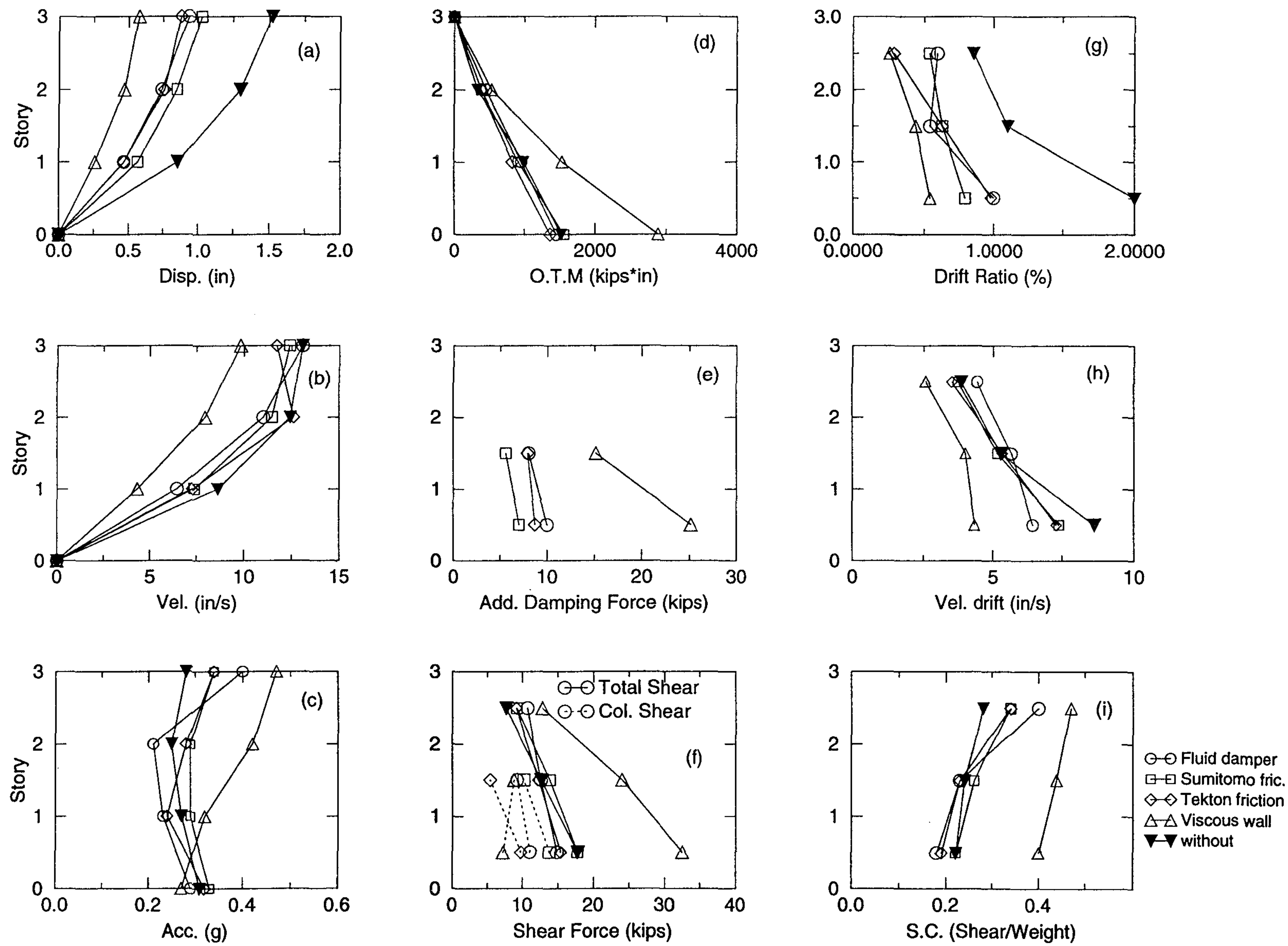

Figure 6-14 Summary of Experimental Response of Tested Structure Model with Various Dampers (El-Centro, PGA 0.3g)

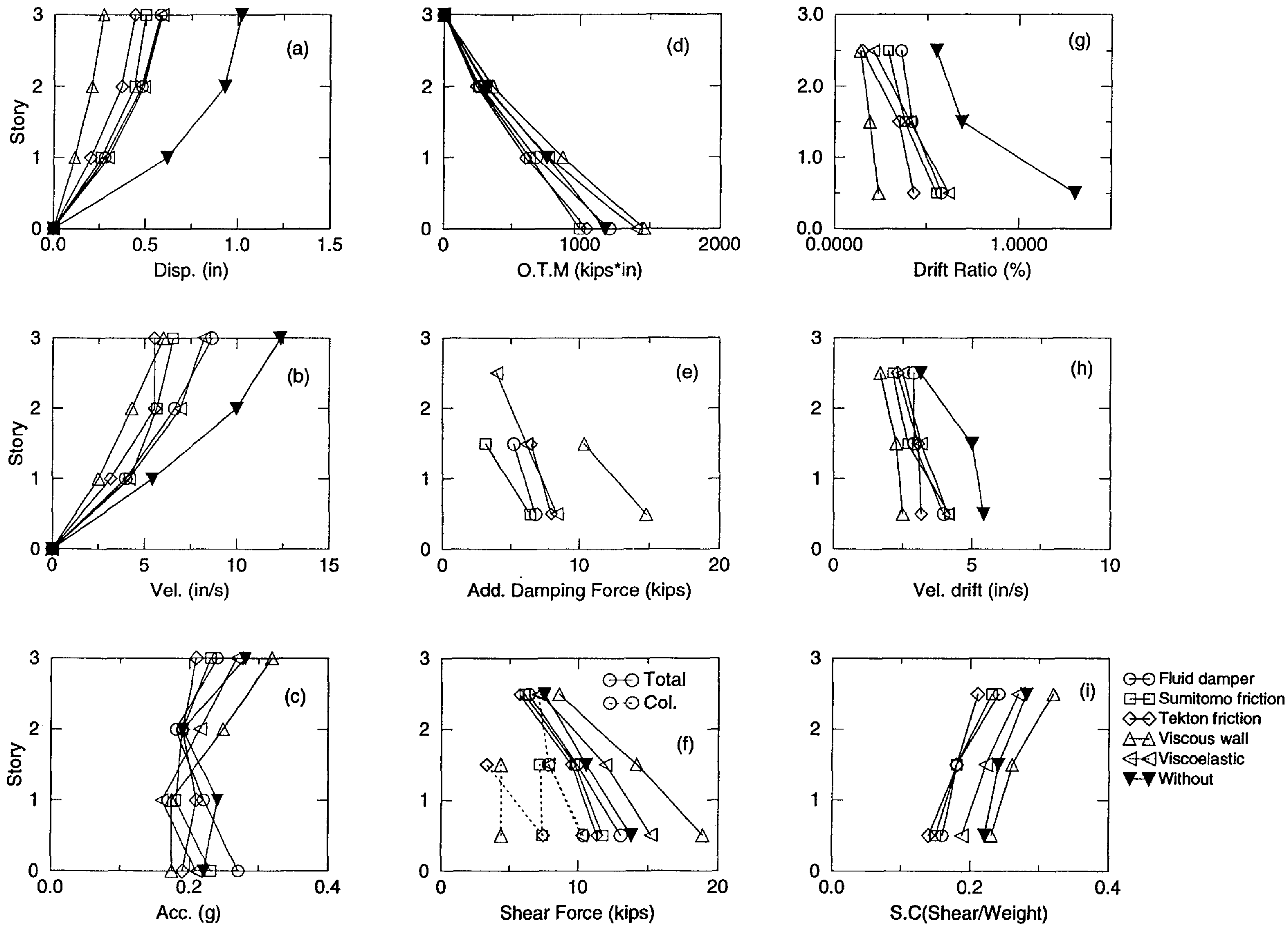

Figure 6-15 Summary of Experimental Response of Tested Structure Model with Various Dampers (Taft, PGA 0.2g)

The above trends validate the evaluation using the capacity and composite spectrum approach. Using this tool, it is possible to size damping devices and the structural components to achieve the desired goal of the retrofit, which is reduction of deformations and hysteretic energy dissipation demands that lead to damage. However, a complete nonlinear analysis is further necessary for the qualification of the final design.

SECTION 7

CONCLUSIONS

A combined experimental and analytical study of reinforced concrete structures retrofitted with friction dampers is presented herein. Shaking table tests of a 1:3 scale R/C frame structure with friction damping braces installed in the mid-bay of the frame with different configurations were conducted. A comprehensive component test program was also conducted on the friction dampers over a frequency range between essentially 1 Hz and 4 Hz. The inelastic behavior of the structure retrofitted using friction dampers incorporated in braces was investigated. The analytical modeling of friction damping devices was presented and models were implemented in IDARC2D, ver. 4.0 a platform for inelastic analysis for reinforced concrete structure with damping devices.

The important observations and conclusions of this study are summarized below:

(1) The retrofit of damaged R/C structure with friction damping braces produces satisfactory response during earthquakes. The damping enhancement contributes to the reduction of maximum deformations, primarily, and modifies only slightly the structural forces transmitted to the foundations.

(2) The dampers show stiffening characteristics at initial stage and show only strengthening afterwards. Stiffening and strengthening effects are almost not affected by frequency.

(3) The period of the structure varies with the intensity of the earthquake which will shift the structural frequency away from resonant frequency.

(4) Stiffening of structure from the damping devices leads to reduction of system's deformations. However, it may cause minor accelerations' increase (or total large shear increase). Strengthening of structure from damping devices increases the capacity of the structure.

(5) Although, total base shear could be increased somewhat, the internal shear forces in the original system retrofitted (i.e. columns, beams, etc.) are always reduced. The total structure shear includes the increased forces in dampers, synchronous with the forces in members, therefore subtracting this influence results in smaller forces in the original system. Therefore, the "structure's retrofit with dampers benefits in lowering the internal shear forces, although not in the same measure as the reduction of its deformations.

(6) The hysteretic behavior of dampers provides the main contribution to forces reduction of the structural response. However, the forces in dampers may transfer to columns so as to increase the axial force in the columns. A structural analysis should be made to determine the transfer load path.

(7) The corrosion problem of friction interfaces should be considered for long time period usage. The composition of the interfaces is of paramount importance for ensuring the longevity of the device.

(8) The dampers can be modeled by Bouc-Wen's model which is a smooth bilinear hysteretic model.

(9) The transfer load path and the influence of stiffening and strengthening of dampers can be obtained from a monotonic inelastic "push-over" analysis of structure as suggested herein. The dampers contribute their stiffening and strengthening properties to the increase in the overall capacity of structure. At large deformations the contribution comes from the strengthening property of the damper. At smaller deformation the contribution comes from stiffening property of the damper.

(10)The primary effect of dampers is the reduction of demand for hysteretic energy dissipation by the gravity load carrying structural members. Such a reduction that may be up to 80%-90%, leads to a substantial reduction of structural damage in the members due to low cycle fatigue (as reflected by the damage analysis) presented herein.

(11)Composite spectrum, acceleration/force versus deformation spectra combined with elastic analysis, can provide a good estimate of the peak structural response if interested with the "push-over" capacity curve. Although the accuracy of such estimate depends on the ability to determine the damping equivalent of inelastic (hysteretic) energy dissipation, The peak demands and the trends in the retrofit applications obtained from such approach can assist the design engineer in determining the initial design values. A more extensive nonlinear analysis is their required for final qualifications of design.

(12)The dampers size and position can also be determined using simple optimal structural control approach as presented by Gluck et al., 1995.

(13)Although the trends are similar for retrofit using other types of dampers, i.e. viscoelastic, fluid, etc., their modeling and general behavior has particular characteristic as shown in the other reports.

(14)Finally, the retrofit using these dampers may require minimal interference with the existing structural system and only minor enhancements of reinforcement in connections or local jacketing might be necessary.

SECTION 8

REFERENCES

1. Aiken, I.D. and Kelly, J.M. (1992). "Comparative Study of Four Passive Energy Dissipation Systems", *Bull. N.Z. Nat. Soc. for Earthquake Eng.*, 25(3), Sept., p.175-192.

2. Aiken, I.D. and Kelly, J.M. (1990). "Earthquake Simulator Testing and Analytical Studies of Two Energy-Absorbing System for Multistory Structures", Report No. *UCB/EERC-90/03*, University of California at Berkeley.

3. Arima, F., Miyazaki, M., Tanaka, H., and Yamazaki, Y. "A Study on Building with Large Damping Using Viscous Damping Walls", Proceedings, *Ninth world Conference on Earthquake Engineering*, International Association for Earthquake Engineering, Tokyo-Kyoto, Japan, 1988, vol. 5, p.821-826.

4. Bagley, R.L. and Torvik, P.J. (1983). "Fractional Calculus - A Different Approach to the Analysis of Viscoelastic Damped Structures", *AIAA Journal*, 21(5), p.741-748.

5. Boardman, P.R., Wood. B.J., and Carr, A.J., 1983, "Union House - A Cross Braced Structure with Energy Dissipators", *Bull. N.Z. Nat. Soc. for Earthquake Eng.*, 16(2), June, p.83-97.

6. Bracci, J.M., Reinhorn, A.M., and Mander, J.B. (1992a). "Seismic Resistance of Reinforced Concrete Frame Structures Designed only for Gravity Loads: Part I - Design and Properties of a One-Third Scale Model Structure", *Technical Report NCEER-92-0027*, National Center for Earthquake Engineering Research, SUNY/Buffalo.

7. Bracci, J.M., Reinhorn, A.M., and Mander, J.B. (1992b). "Seismic Resistance of Reinforced Concrete Frame Structures Designed only for Gravity Loads: Part II - Experimental Performance and Analytical Study of Structural Model", *Technical Report NCEER-92-0029*, National Center for Earthquake Engineering Research, SUNY/Buffalo.

8. Bracci, J.M., Reinhorn, A.M., and Mander, J.B. (1992c). "Evaluation of Seismic Retrofit of Reinforced Concrete Frame Structures: Part III - Experimental Performance and Analytical Study of Retrofitted Structural Model Structure", *Technical Report NCEER-92-0031*, National Center for Earthquake Engineering Research, SUNY/Buffalo.

9. Buckle, I.G. and Mayes, R. L., (1990). "Seismic Isolation: History, Application, and Performance - A World View", *Earthq. Spectra*, 6(2), p.161-201.

10. Chang, K.C., Soong, T.T., Oh, S-T. and Lai, M.L. (1991). "Seismic Response of a 2/5 Scale Steel Structure with Added Viscoelastic Dampers", Report No. *NCEER-91-0012*, National Center for Earthquake Engineering Research, Buffalo, N.Y.

11. Charleson, A.W., Wright, P.D., and Carr, A.J., (1993). "Union House - A Cross Braced Structure with Energy Dissipators", Bull. N.Z. Nat. Soc. for Earthquake Eng., Vol. 2, N.Z., Aug.

12. Ciampi, V., (1991). "Use of Energy Dissipation Devices, Based on Yielding of Steel, for Earthquake Protection of Structures", *Int. Meeting on Earthquake Protection of Buildings*, Ancona, Italy, June, p.41/D-58/D.

13. Constantinou, M.C., Reinhorn, A.M., Mokha, A. and Watson, R. (1991), "Displacement Control Device for Base-Isolated Bridges", *Earthquake Specta*, Vol. 7, No.2, 1991, p.179-200.

14. Constantinou, M.C. and Symans, M.D. (1992). "Experimental and Analytical Investigation of Seismic Response of Structures with Supplemental Fluid Viscous Dampers". *Technical Report NCEER-92-0032*, National Center for Earthquake Engineering Research, SUNY/Buffalo.

15. Craig, J.I., Goodno, B.J., Pinelli, J.-P., and Moor, C., (1992). "Modeling and Evaluation of Ductile Clading Connection Systems for Seismic Response Attenuation in Buildings", *Proc., 10WCEE*, Madrid, Spain, July, Vol. 7: 4183-4188.

16. Ferry, J.D. (1980). Viscoelastic Properties of Polymers. John Wiley & Sons, New York, NY.

17. Fiero, E., Perry, C., Sedarat, H., and Moor, C., (1992). "Modeling and Evaluation of Ductile Cladding Connection Systems for Seismic Response Attenuation in Buildings", *Proc., 10WCEE*, Madrid, Spain, July, Vol. 7: p.4183-4188.

18. Foutch, D.A., Wood, S.L., and Singh, J. (1993), "Seismic Retrofit of Non-ductile Reinforced Concrete Frames Using Viscoelastic Dampers", *Proceedings, ATC-17-1 Seminar on Seismic Isolation*, Passive Energy Dissipation, and Active Control, San Francisco, California, April 5, 1993, Vol. 1, p.605-616.

19. Freeman, S. (1994), "The Capacity Spectrum method for Determining the Demand Displacement", *ACI 1994 Spring Convention*, March 23, 1994.

20. Fujita, T. (editor) (1991). "Seismic Isolation and Response Control for Nuclear and Non-nuclear Structures", *Special Issue for the Exhibition of the 11th International Conference on Structural Mechanics in Reactor Technology*, SMIRT 11, Tokyo, Japan.

21. Gluck, N., Reinhorn, A. M., Gluck, M. and Levy, R. (1995), "Design of Supplemental Dampers for Control of Structures", *Journal of Struct. Eng.*, ASCE (in press).

22. Grigorian, C.E. and Popov, E.P., (1993). "Slotted Bolted Connections for Energy Dissipation", *ATC17-1*, Proc. of Seminar on Seismic Isolation, Passive Energy Dissipation, and Active Control, San Francisco, Calif., March 11-12, 1993, p.545-556.

23. Henry, R.W. (1985). "Analysis of Braced Frame Energy Absorbers", *Report No. 392*, Department of Civil Engineering, University of Auckland, Auckland, New Zealand.

24. Henry, R.W. (1986). "Braced Frame Energy Absorbers: A Test Programme". Department of Civil Engineering, University of Auckland, Auckland, New Zealand.

25. Hsu, S-Y. and Fafitis, A. (1992). "Seismic Analysis and Design of Frames with Viscoelastic Connections", *J. Struct. Engrg.*, ASCE, 118(9), p.2459-2474.

26. Kasai, K., Munshi, J.A., Lai, M.L. and Maison, B.F. (1993). "Viscoelastic Damper Hysteretic Model: Theory, Experimental, and Application", *Proceedings of Seismic Isolation*, Passive Energy, and Active Control, V.2, ATC17-1, San Francisco, CA, p.521-532.

27. Kelly, J.M., Skinner, M.S. and Beucke, K.E. (1980). "Experimental Testing of an Energy-Absorbing Base Isolation System". Report No. *UCB/EERC-80/35,* University of California, Berkeley.

28. Kelly, J.M., Skinner, R.I. and Heine, A.J., (1972). "Mechanisms of Energy Absorption in Special Devices for Use in Earthquake-Resistant Structures", *Bull. N.Z. Nat. Soc. for Earthquake Eng.*, 5(3), Sept, p.63-88.

29. Kelly, J.M. (1991). "A Long-Period Isolation System Using Low-Modulus High-Damping Isolators for Nuclear Facilities at Soft-Soil Site", Report No. *UCB/EERC-91/03*, EERC, Univ. of Calif., Berkeley, Calif.

30. Kircher, C.(1993a), "Status Report of Structure Engineers Association of California (SEAOC) Ad-Hoc Ground Motion Committee", *Presentation of at SEAOC Annual Convention*, Scottsdale, Arizona.

31. Kircher, C.(1993b), "Private Communication", with the authors, San Francisco, California.

32. Kobori, T., Yamada, T., Takenaka, Y., Maeda, Y., and Nishimura, I., (1988). "Effect of Dynamic Tuned Connector on Reduction of Seismic Response - Application to Adjacent Office Buildings", *Proc., 9WCEE,* Vol. 5, Tokyo/Kyoto, Japan, Aug., p. V-773-V-778.

33. Kunnath, S.K., Reihorn, A.M. and Lobo, R.F., "IDARC version 3.0: Inelastic Damage Analysis of Reinforced Concrete Structures", *Technical Report NCEER 92-0022*, August 31, 1992.

34. Li, C. and Reinhorn, A. M. (1995), "Experimental and Analytical Investigation of Seismic Retrofit of Structures with Supplemental Damping, Part II: Friction Damping Devices - Tekton", Report No. *NCEER-95-0009*, National Center for Earhtquake Engineering Research, Buffalo, NY.

35. Lin, R.C., Liang, Z., Soong, T.T., and Zhang, R.H. (1988). "An Experimental Study of Seismic Structural Response with Added Viscoelastic Dampers", *Technical Report NCEER-88-0018*, National Center for Earthquake Engineering Research, SUNY/Buffalo, June.

36. Lobo, R.F., Bracci, J.M., Shen, K.L., Reinhorn, A.M. and Soong, T.T. (1993). " Inelastic Response of Reinforced Concrete Structures with Viscoelastic Braces", Report No. *NCEER-93-0006*, National Center for Earthquake Engineering Research, Buffalo, N.Y.

37. Makris, N. and Constantinou, M.C. (1991). "Fractional-Derivative Maxwell Model Viscous Dampers", *ASCE Journal of Structural Engineering*, 117(9), p.2708-2724.

38. Miyazaki, M. and Mitsusaka, 1992, "Design of a Building with 20% or Great Damping", *Proc., 10WCEE*, Madrid, Spain, July.

39. Mokha, A., Constantinou, M.C., Reinhorn, A.M., and Zayas, V. (1991). "Experimental Study of Friction Pendulum Isolation System", *J. Struct. Engrg.*, ASCE, 117(4), p.1201-1217.

40. Popov, E.P., Takanashi, K., and Roeder, C.W., "Structural Steel Bracing System: Behavior under Cyclic Loading", *EERC Report 76-17*, Earthquake Engineering Research Center, University of California, Berkeley, Calif., 1976.

41. Popov, E.P., Kasai, K., and Engelhardt, M.D., (1987). "Advances in Design of Eccentrically Braced Frames", *Earthquake Spectra*, vol. 3, No. 1, 1987.

42. Reinhorn, A.M. and Li, C. (1995)a, "Experimental and Analytical Investigation of Seismic Retrofit of Structures with Supplemental Damping, Part III: Viscous walls", Report No. *NCEER-95-XXXX*, National Center for Earthquake Engineering Research, Buffalo, NY. (in press)

43. Reinhorn, A.M. and Valles, R. E. (1995), "Damage Evaluation in Inelastic Response of Structures: a Deterministic Approach", *Journal of Struct. Eng.*, ASCE (in press).

44. Reinhorn, A.M., Nagarajaiah, S., Constantinou, Tsopelas, P. and Li, R.(1994), "3D-BASIS-TABS: Version 2.0, Computer Program for Nonlinear Dynamic Analysis of Three Dimensional Base Isolated Structures. Report No. *NCEER-94-0018*, National Center for Earhtquake Engineering Research, Buffalo, NY.

45. Reinhorn, A.M. and Kunnath, A.K. (1994), ""IDARC version 3.2: Inelastic Damage Analysis of Reinforced Concrete Structures", User Manual, Dept. of Civil Engrg., SUNY/Buffalo.

46. Reinhorn, A.M. and Soong, T.T., et al., (1992). "Active Braceing System: A Full-scale Implementation of Active Control", Report No. *NCEER-92-0020*, National Center for Earhtquake Engineering Research, Buffalo, NY.

47. Robinson, W.H., and Cousins, W.J., (1987). "Recent Developments in Lead Dampers for Base Isolation", *Pacific Conf. on Earthquake Eng.*, Vol. 2, N.Z., Aug., p.279-283.

48. Robinson, W.H., and Greenbank, L.R., (1976). " An Extrusion Energy Absorber Suitable for the Protection of Structures During an Earthquake", *Int. Jnl. of Earthquake Eng. and Str. Dyn., Vol. 4.*

49. Roeder, C.W. and Popov, E.P., (1978). "Eccentrically Braced Frames for Earthquakes", *J. of Structural Division*, vol. 104. no. 3, p.391-412.

50. Rosen, S.L. (1982). Fundamental Principles of Polymeric Materials, John Wiley & Sons, New York, NY.

51. Rosenbrock, H.H.. (1964). "Some General Implicit Processes for the Numerical Solution of Differential Equations." Computer J., 18, 50-64.

52. Sakurai, T., Shibata, K., Watanabe, S., Endoh, A., Yamada, K., Tanaka, N., and Kobayashi, H., (1992). "Application of Joint Damper to Thermal Power Plant Buildings", *Proc., 10WCEE*, Vol. 7: 4149-4154, Madrid, Spain, July.

53. Shen, K.L. (1994). "Viscoelastic Dampers: Theory, Experimental and Application in Earthquake Engineering". Ph. D dissertation, Dept. of Civil Engrg., State Univ. of New York at Buffalo, Buffalo, NY.

54. Skinner, R.I., Tyler, R.G., Heine, A.J., and Robinson, W.J., (1980). "Hysteretic Dampers for the Protection of Structures from Earthquakes", *Bull. N.Z. Nat. Soc. for Earthquake Eng.*, 13(1), March, p.37-48.

55. Soong, T.T. (1990). Active Structural Control: Theory and Practice, Longman, John Wiley & Sons, Inc., New York.

56. Soong, T.T. and Constantinou, M.C. (Eds) (1994). "Passive and Active Structural Vibration Control in Civil Engineering", Springer-Verlag, Wien and New York.

57. Stiemer, S.F., Godden, W.G., and Kelly, J.M., (1981). "Experimental Behavior of a Special Piping System with Steel Energy Absorbers Subjected to Simulated Differential Seismic Input". Report NO. *UCB/EERC-81/09*, EERC, Univ. of California at , Berkeley, July.

58. Tsai, K.C., and Hong, C.-P., (1992). "Steel Triangular Plate Energy Absorber for Earthquake Resistant Buildings", *Proc., First World Congress on Constructional Steel Design*. Mexico.

59. Tyler, R.G. (1978). "Tapered Steel Energy Dissipators for Earthquake Resistant Structures", *Bulletin of New Zealand National Society for Earthquake Engineering*, 11(4), p.282-294.

60. Tyler, R.G. (1985). "Further Notes on Steel Energy-Absorbing Element for Braced Frameworks". *Bulletin of New Zealand National Society for Earthquake Engineering*, 18(3), 270-279.

61. Uang, C.M. and Bertero, V.V. (1990). "Evaluation of Seismic Energy in Structure", *Earthquake Engineering and Structural Dynamics*, Vol. 19, p.77-90.

62. Whittaker, A.S., Bertero, V.V., Aktan, H.M. and Giacchetti, R., 1989, "Seismic Response of a DMRSF Retrofitted with Friction-Slip Devices", *Proceedings of the 1989 EERI Annual Meeting*, San Francisco, Calif.

63. Williams, M.L. (1964). "Structural Analysis of Viscoelastic Materials", *AIAA Journal*, 2(5), p.785-808

64. Witting, P.R., and Cozzarelli, F.A., (1992). "Shape Memory Structural Dampers: Material Properties, Design and Seismic Testing", Report No. NCEER-92-0013, NCEER, State Univ. of New York at Buffalo, May.

APPENDIX A

A 1-1 Reinforcement Details

The following provides details of the reinforcing steel used in the model based on scale factor of 3 for geometric length similitude. Detailed information is presented by Bracci et al., (1992a), but is repeated here for sake of completion of this report.

The slab steel in the prototype structure was designed by the direct design method of the ACI 318/83. The design required #3 rebars at 6 in. spacing in different sections of the slab. To avoid excess labor in the construction of the 3-story model, a 2 in. square mesh composed of gauge 12 galvanized wires is chosen for acceptable similitudes of strength and geometric spacing length. Since the slab strength is not the main emphasis for this study, the slight disparities of slab steel placement due to the mesh are considered satisfactory for the experiment. Figure A-1 shows the layout details for the top and bottom reinforcing steel mesh in the slab. The longitudinal (direction of motion) and transverse (perpendicular to the direction of motion) beam reinforcement details for the model are shown in Fig. A-2. Figure A-3 shows the reinforcement details for the columns in the model based on the prototype design.

A 1.2 Model Materials

The following outlines the materials used in the construction of the model. It is to be noted that the materials used in the model are identical to materials in assumed prototype structure (Bracci et al., 1992 a). Therefore the scale factors were appropriately developed based on the principles of modeling the same acceleration and material.

A 1.2.1 Concrete properties

The concrete mix analysis and design was based on trial mixes from various recipes and a design mix was established for a 28 day target strength of 3500 psi, slump of 4 in., and maximum aggregate size of 1/2 in (#1 crushed stone). Table A-1 shows the mix formula for a one cubic yard batch of concrete.

The mix formulation is based on a saturated, surface dry concrete sand. The water : cement (: sand : stone) ratio is 0.5 : 1.0 (: 3.0 : 3.6). The full gradation analysis of the aggregates in the concrete mix is shown in Fig. A-4.

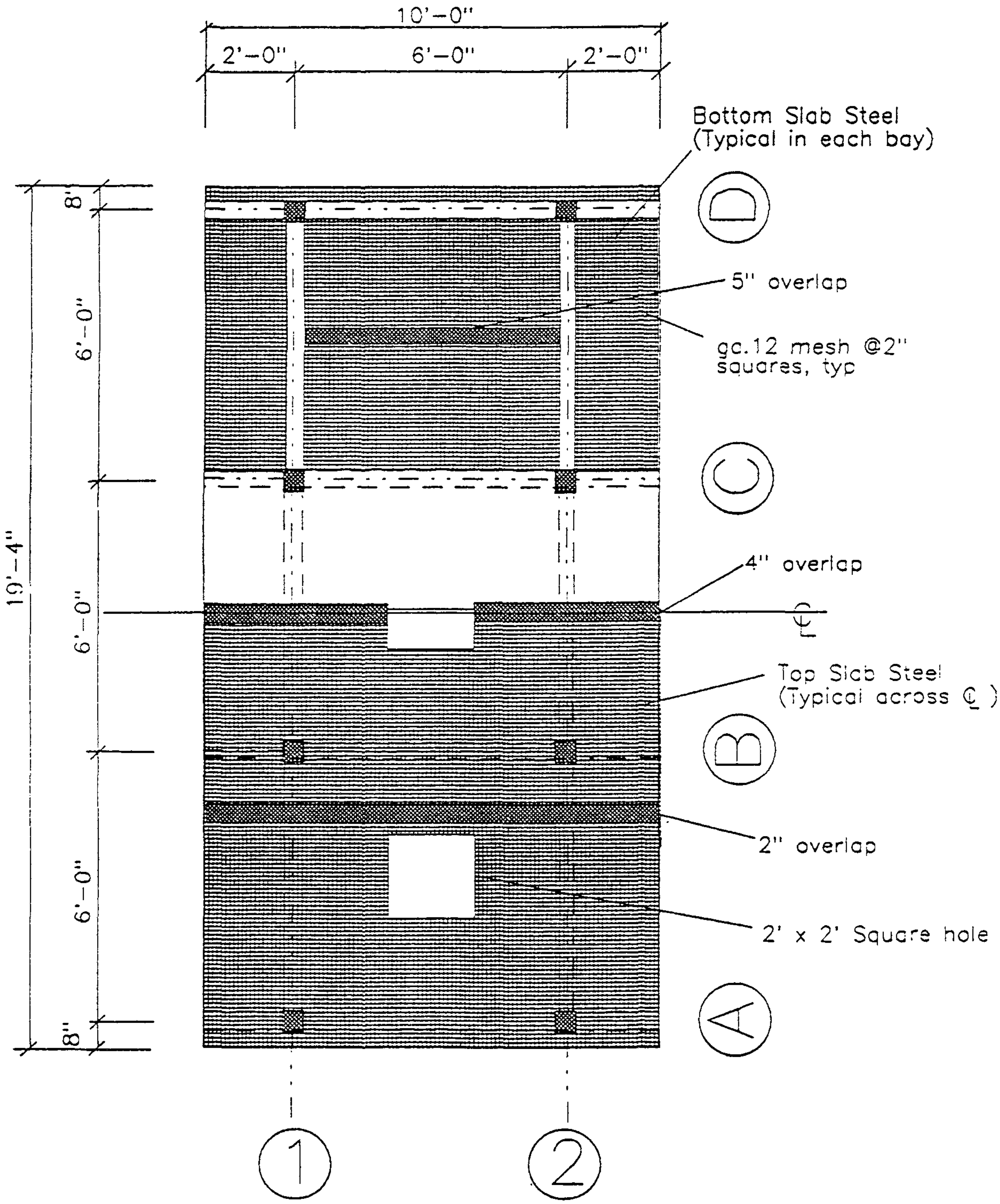

FIGURE A-1 Layout of Slab Steel Reinforcement

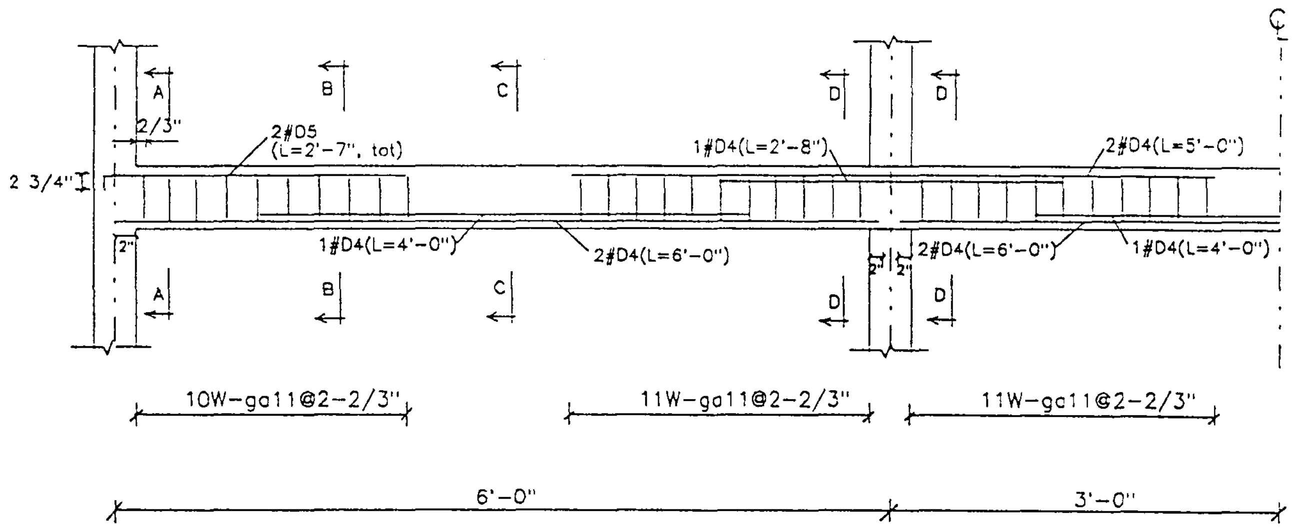

Longitudinal Beams (North-South)

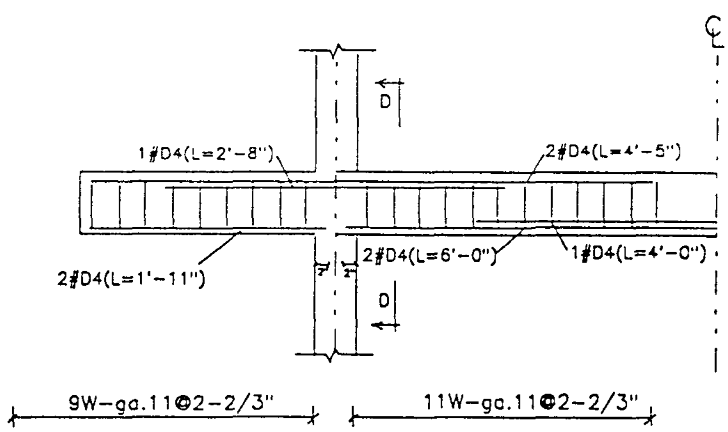

Transverse Beams (East-West)

FIGURE A-2a Details of the Beam Steel Reinforcement

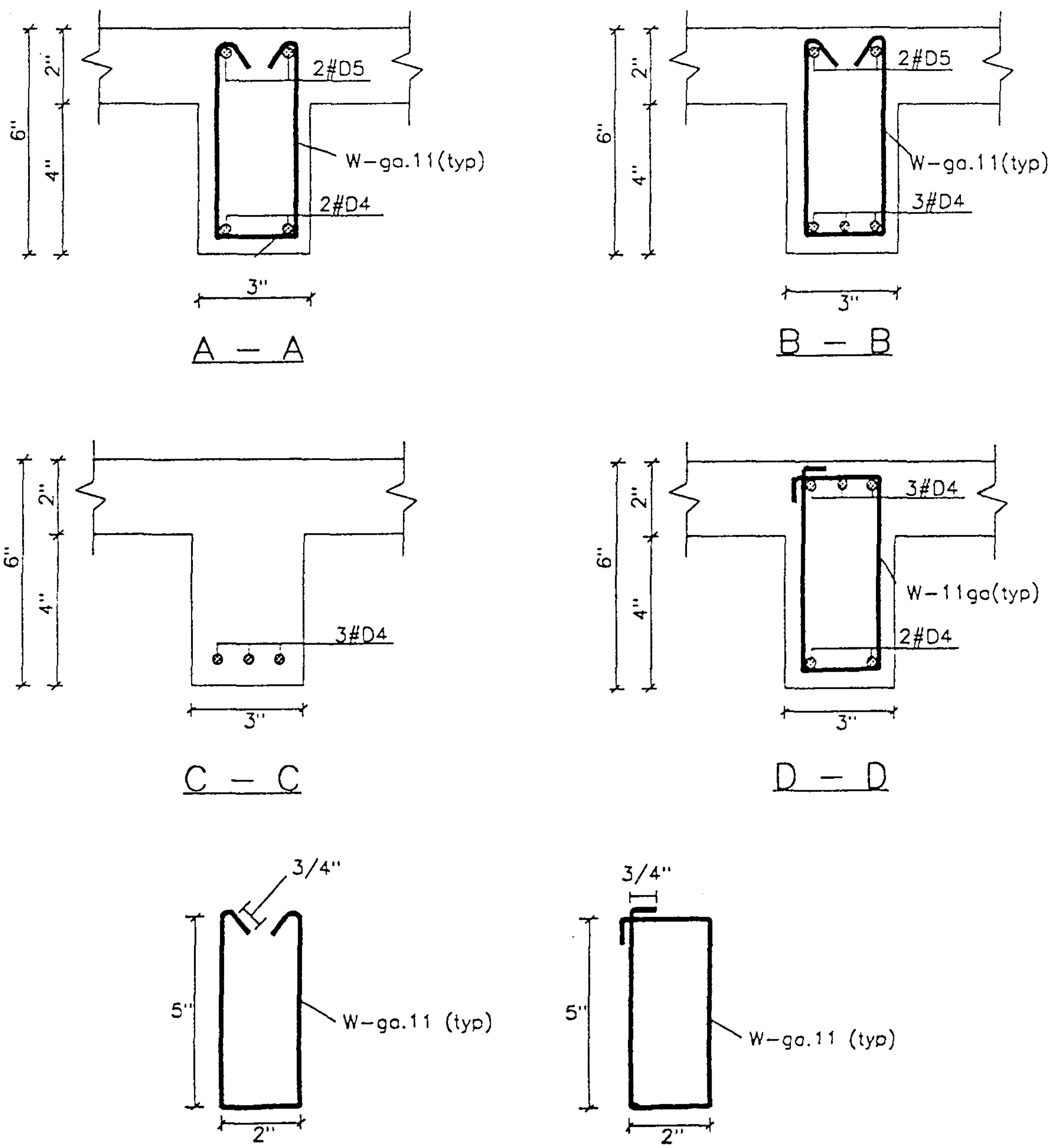

Beam Sections

FIGURE A-2b Details of the Beam Steel Reinforcement (Continued)

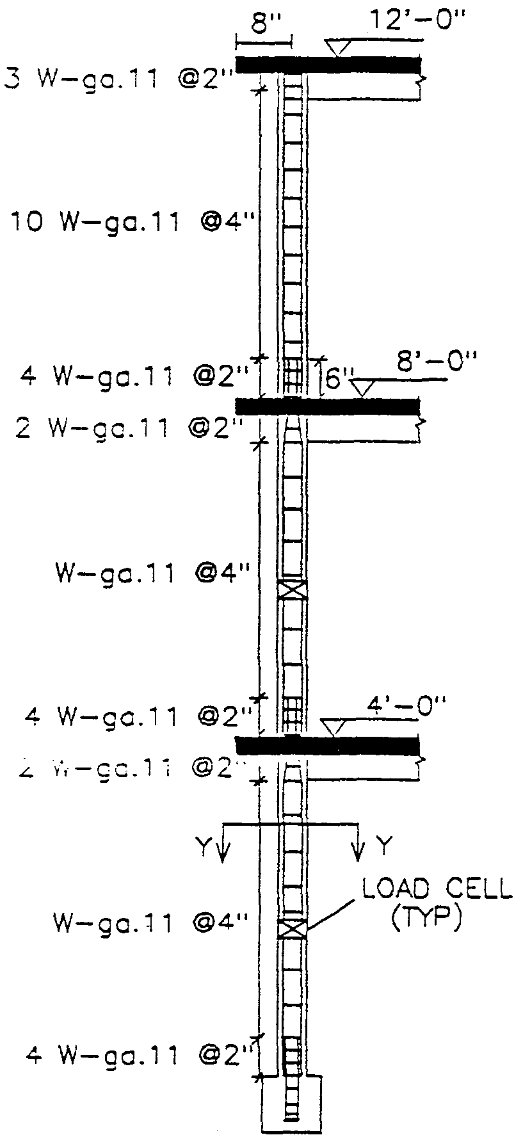

(a) Exterior Section

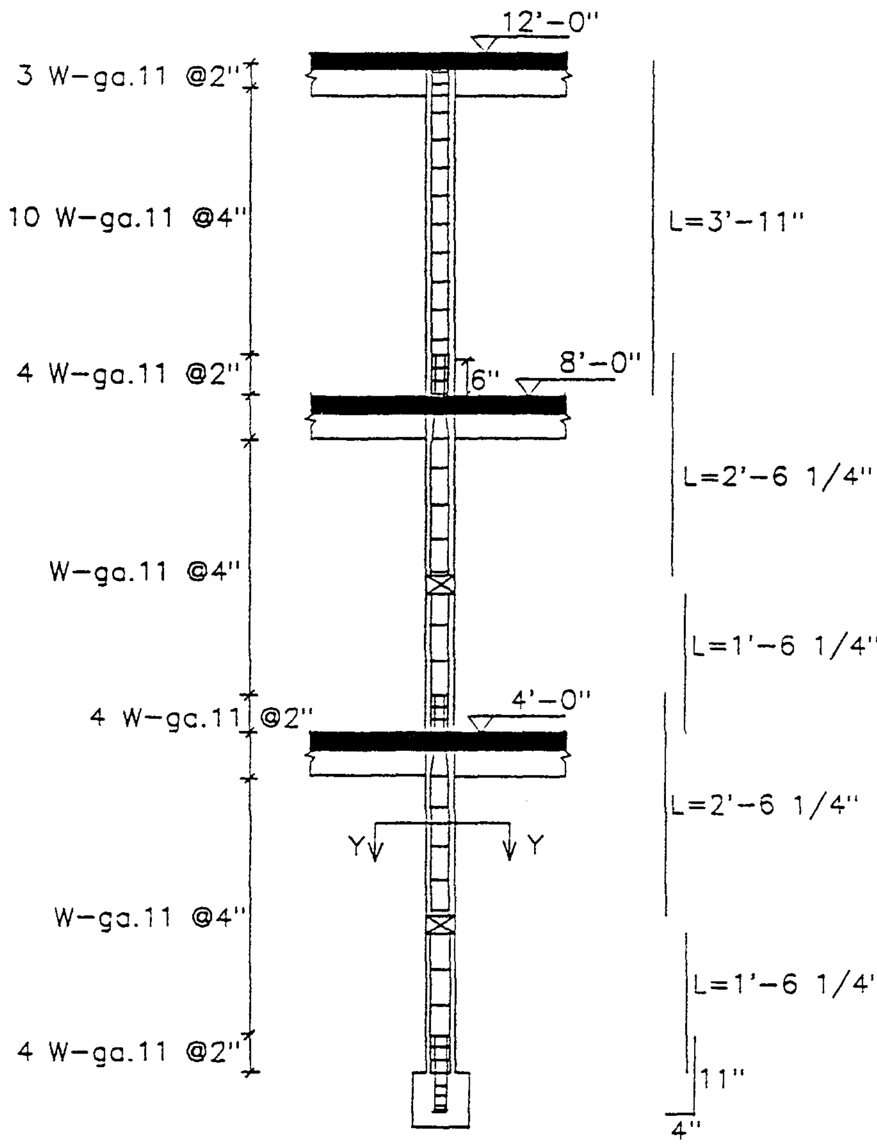

(b) Interior Section

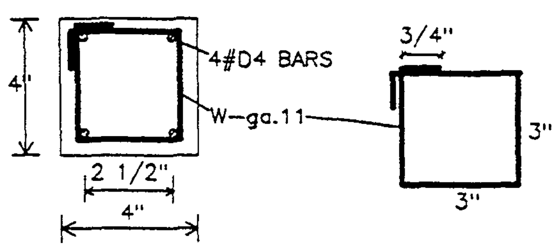

(c) Section Y-Y

FIGURE A-3 Details of the Column Steel Reinforcement

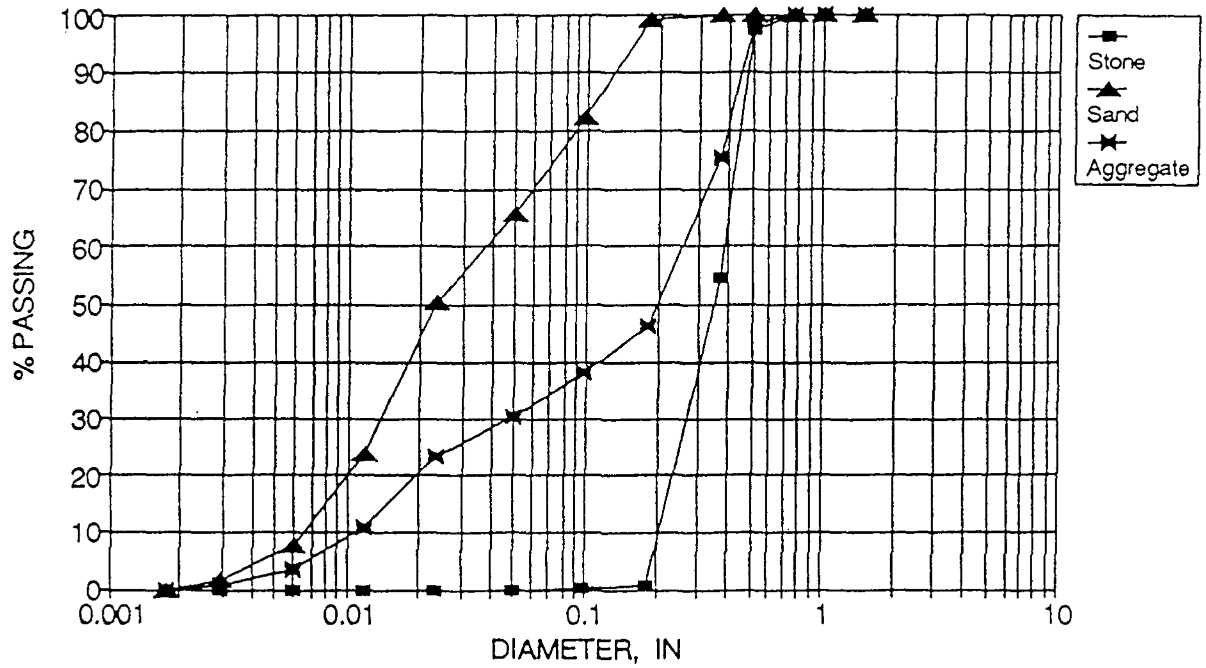

FIGURE A-4 Gradation Analysis of the Concrete Mix

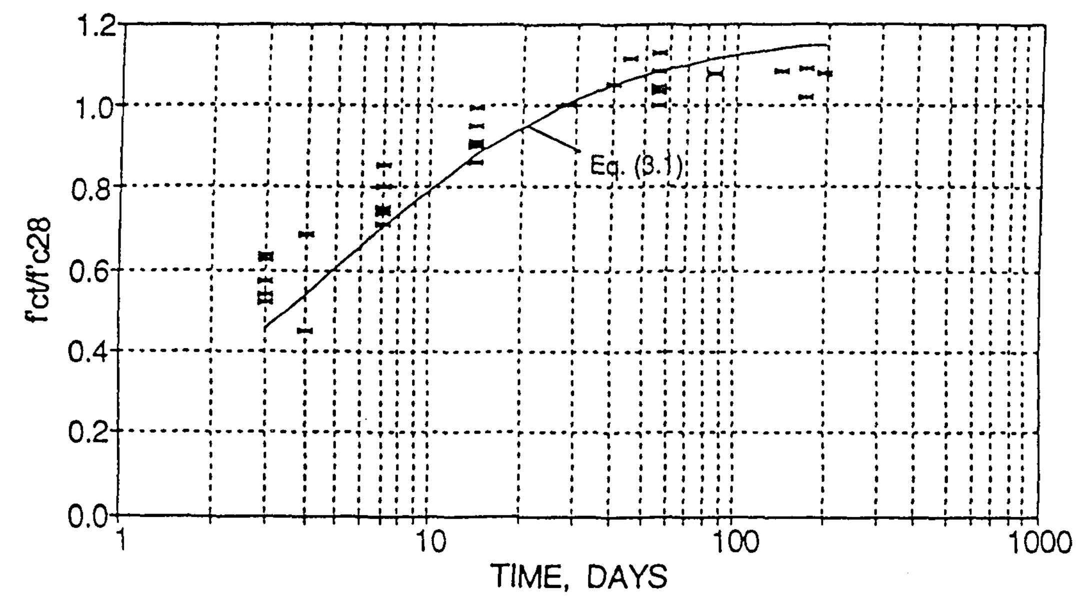

FIGURE A-5 Average Concrete Specimen Strength Versus Time

Table A-1 Mix Design Formula for the Model Concrete

Ingredient	Weight
Type I Cement	490 lb
Concrete Sand	1487 lb
#1 Crushed Stone	1785 lb
Water	242 lb
Superplasticizer	39.2 oz
Micro-Air	2.9 oz

A substantial variation can be observed in the mix strengths for the different components, even though all mixes had the same target strength (see Table A-2). The final strengths were very sensitive to moisture variations in the materials and the widely varying ambient temperatures at the time of construction. The variation of strength versus time is shown in Fig. 3-5, which indicates asymptotic stabilization of concrete strength.

Table A-2 Concrete Properties of the Model Structure

Pour Number and Location	f'_c (ksi)	E_c (ksi)	ε_{co} (strains)	ε_{spall} (strains)
1. Lower 1st Story Columns	3.38	2920	0.0020	0.011
2. Upper 2nd Story Columns	4.34	3900	0.0020	0.017
3. 1st Story Columns	4.96	3900	0.0021	0.009
4. Lower 2nd Story Column	4.36	3900	0.0026	0.014
5. Upper 2nd Story Column	3.82	3360	0.0022	0.020
6. 2nd Story Slab	2.92	2930	0.0015	0.020
7. 3rd Story Columns	3.37	3800	0.0019	0.020
8. 3rd Story Slab	4.03	3370	0.0021	0.012

The reinforcing steel uses a mix of #11 & #12 gage wires and D4, D5 annealed deformed bars. The summary of their properties is given in Table A-3

Table A-3 Reinforcing Steel Properties of the Model Structure

Bar	d_b (in)	A_b (in^2)	f_y (ksi)	E_s (ksi)	f_{max} (ksi)	ε_u
#12 ga.	0.109	0.0093	58	29900	64	0.13
	0.120	0.0113	56	29800	70	-
	0.225	0.0400	68	31050	73	0.15
	0.252	0.0500	38	31050	54	-

The D4 rebar was also annealed at different temperatures between 900^0 F and 1140^0 F to produce a yield strength between 49 and 73 ksi for yield force similitude with a #6 rebar. At a temperature of 1140^0 F, the average yield strength consistently reached was 68 ksi. Based on yield force similitude, the D4 rebar represented a #6 rebar with a yield strength of 55.6 ksi. Since a grade 40 steel has yield strengths between 40 and 60 ksi, the D4 rebar satisfied similitude with a #6 rebar. Both the original and annealed stress-strain relationships for the D4 and D5 rebars are shown in Fig. A-6.

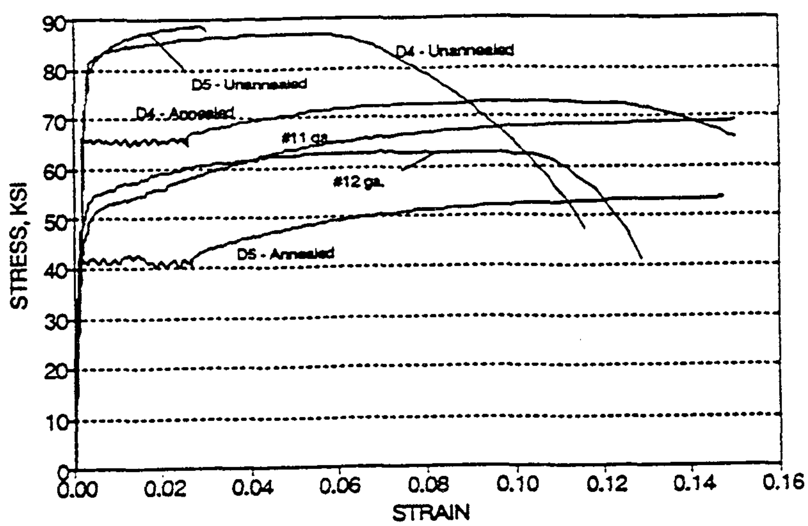

FIGURE A-6 Measured Representative Stress-Strain Relationships of the Reinforcing Steel

APPENDIX A-3

SCALING FACTORS FOR MODELING OF DYNAMIC BEHAVIOR

Quantity	General Case	Same Material and Acceleration (Model)	
		Required	Provided
Geometric Length, l	$\lambda_l = ?$	$\lambda_l = 3.00$	$\lambda_l = 3.00$
Elastic Modulus, E	$\lambda_E = ?$	$\lambda_E = 1.00$	$\lambda_E = 1.00$
Acceleration, a	$\lambda_a = ?\ (= 1/\lambda_l \cdot \lambda_E/\lambda_\rho)$	$\lambda_a = 1.00$	$\lambda_a = 1.00$
Density, ρ	$\lambda_\rho = \lambda_E/(\lambda_l\lambda_a)\ (= ?)$	$\lambda_\rho = 0.33$	$\lambda_\rho = 1.00$
Velocity, v	$\lambda_v = \sqrt{\lambda_l \cdot \lambda_a}$	$\lambda_v = 1.73$	$\lambda_v = 1.73$
Forces, f	$\lambda_f = \lambda_E\lambda_l^2$	$\lambda_f = 9.00$	$\lambda_f = 9.00$
Stress, σ	$\lambda_\sigma = \lambda_E$	$\lambda_\sigma = 1.00$	$\lambda_\sigma = 1.00$
Strain, ε	$\lambda_\varepsilon = 1.00$	$\lambda_\varepsilon = 1.00$	$\lambda_\varepsilon = 1.00$
Area, A	$\lambda_A = \lambda_l^2$	$\lambda_A = 9.00$	$\lambda_A = 9.00$
Volumn, V	$\lambda_A = \lambda_l^3$	$\lambda_A = 27.00$	$\lambda_A = 27.00$
Second Moment of Area, I	$\lambda_I = \lambda_l^4$	$\lambda_I = 81.00$	$\lambda_I = 81.00$
Mass, m	$\lambda_m = \lambda_\rho\lambda_l^3$	$\lambda_m = 9.00$	$\lambda_m = 27.00$
Impulse, i	$\lambda_i = \lambda_l^3 \cdot \sqrt{\lambda_\rho\lambda_E}$	$\lambda_i = 15.59$	$\lambda_i = 27.00$
Energy, e	$\lambda_e = \lambda_E\lambda_l^3$	$\lambda_e = 27.00$	$\lambda_e = 27.00$
Frequency, ω	$\lambda_\omega = 1/\lambda_l \cdot \sqrt{\lambda_E/\lambda_\rho}$	$\lambda_\omega = 0.58$	$\lambda_\omega = 0.33$
Time (Period), t	$\lambda_t = \sqrt{\lambda_l/\lambda_a}$	$\lambda_t = 1.73$	$\lambda_t = 1.73$
Gravitational Acceleration, g	$\lambda_g = 1.00$	$\lambda_g = 1.00$	$\lambda_g = 1.00$
Gravitational Force, fg	$\lambda_{fg} = \lambda_\rho\lambda_l^3$	$\lambda_{fg} = 9.00$	$\lambda_{fg} = 27.00$
Critical Damping, ξ	$\lambda_\xi = 1.00$	$\lambda_\xi = 1.00$	$\lambda_\xi = 1.00$

** Note for modeling with constant acceleration, λ_a becomes the independent variable (= 1.00) and λ_ρ becomes the dependent variable (= λ_E/λ_l).

APPENDIX B

INSTRUMENTATION

B 1. Load Cells

Special force transducers (load cells) to measure the internal force response of the model, which include axial loads, shear forces, and bending moments, were fabricated of mild steel and installed in the mid-story height of the first and second story columns and between fluid damper braces, shown in Fig.B-1 (designated by tag name LC# with measured force components N#, MX#, MY#, SX# and SY#). There were four actively wired load cells on the east side of the first and second story respectively, while there were four inactive ("dummy") load cells on the west side of the first and second story to maitain symmetry of stiffness in the model. The shear forces and bending moments were recorded in both the direction of motion and the transverse direction of motion. The load cells were designed such that the stiffness was similar to the concrete column.

Base on the yield strength of the steel, the axial, shear, and bending moment capacity ratings of the load cells are ±40 kips, ±5 kips, and ±40 kips-in respectively.

B 2. Displacement Transducers

Linear displacement sonic transducers (Temposonics™) were used to measure the absolute response displacements in the longitudinal (horizontal) direction of the base and each story level of the model during the shaking table tests. Fig.B-1 shows the location of the displacement transducers (designated by tag name D#) mounted on the east and west base and column-slab intersections on the north side of the model. The displacement transducers were also mounted between fluid damper braces to measure the displacement induced in dampers. The displacement transducers: have global displacement ranges of ±6 in., ±8 in., and ±10 in.; accuracy of ±0.05%

of the full scale displacement, 0.003, 0.004 and 0.005 in., respectively; were conditioned by a generic power supply and manufacturer amplifier-decoders; and were calibrated for the respective full scale displacement per 10 volts.

B 3. Accelerometers

Resistive accelerometers (Endevco™, ±25g) were used to measure the absolute story level accelerations of the model. Fig. 4-8) shows the location of each accelerometer with the respective tag name at the base, first, second, and third stories of the model in the direction of motion (designated by the name AH#), transverse to direction of motion (designated by tag name AT#), and for vertical motion (designated by tag name AV#). In the direction of motion, accelerometers were mounted on the east and west sides of the structure to detect any torsional response or out-of phase motions. The accelerometers were conditioned with 2310 Vishay Signal Conditioning Amplifiers, which filtered frequencies above 25 Hz., calibrated for an acceleration range of ±2 g per 10 volts, and have nonlinearities of ±1.0% of the recorded acceleration.

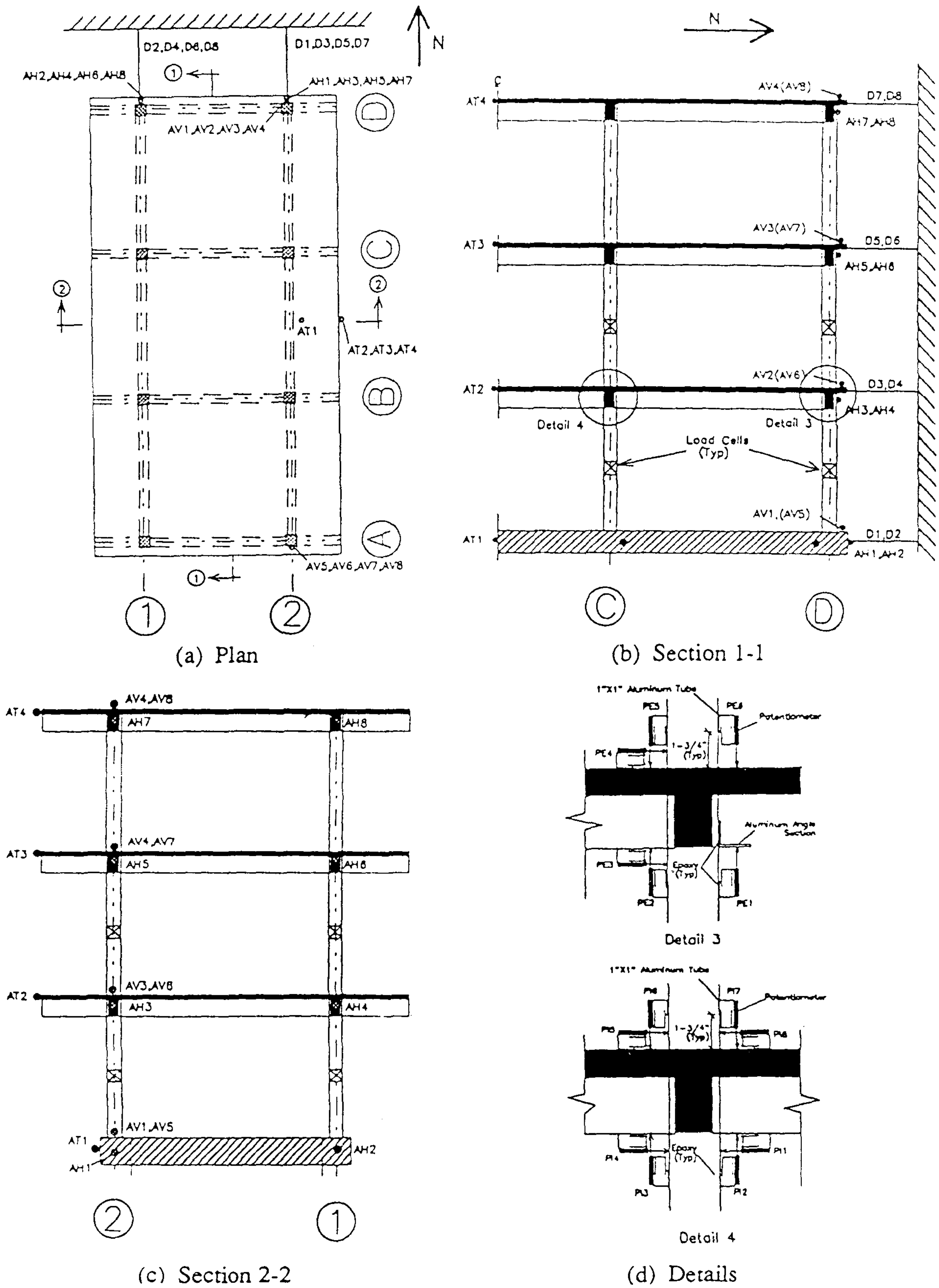

Figure B-1 Instrumentation Identification and Locations

NATIONAL CENTER FOR EARTHQUAKE ENGINEERING RESEARCH
LIST OF TECHNICAL REPORTS

The National Center for Earthquake Engineering Research (NCEER) publishes technical reports on a variety of subjects related to earthquake engineering written by authors funded through NCEER. These reports are available from both NCEER's Publications Department and the National Technical Information Service (NTIS). Requests for reports should be directed to the Publications Department, National Center for Earthquake Engineering Research, State University of New York at Buffalo, Red Jacket Quadrangle, Buffalo, New York 14261. Reports can also be requested through NTIS, 5285 Port Royal Road, Springfield, Virginia 22161. NTIS accession numbers are shown in parenthesis, if available.

NCEER-87-0001 "First-Year Program in Research, Education and Technology Transfer," 3/5/87, (PB88-134275).

NCEER-87-0002 "Experimental Evaluation of Instantaneous Optimal Algorithms for Structural Control," by R.C. Lin, T.T. Soong and A.M. Reinhorn, 4/20/87, (PB88-134341).

NCEER-87-0003 "Experimentation Using the Earthquake Simulation Facilities at University at Buffalo," by A.M. Reinhorn and R.L. Ketter, to be published.

NCEER-87-0004 "The System Characteristics and Performance of a Shaking Table," by J.S. Hwang, K.C. Chang and G.C. Lee, 6/1/87, (PB88-134259). This report is available only through NTIS (see address given above).

NCEER-87-0005 "A Finite Element Formulation for Nonlinear Viscoplastic Material Using a Q Model," by O. Gyebi and G. Dasgupta, 11/2/87, (PB88-213764).

NCEER-87-0006 "Symbolic Manipulation Program (SMP) - Algebraic Codes for Two and Three Dimensional Finite Element Formulations," by X. Lee and G. Dasgupta, 11/9/87, (PB88-218522).

NCEER-87-0007 "Instantaneous Optimal Control Laws for Tall Buildings Under Seismic Excitations," by J.N. Yang, A. Akbarpour and P. Ghaemmaghami, 6/10/87, (PB88-134333). This report is only available through NTIS (see address given above).

NCEER-87-0008 "IDARC: Inelastic Damage Analysis of Reinforced Concrete Frame - Shear-Wall Structures," by Y.J. Park, A.M. Reinhorn and S.K. Kunnath, 7/20/87, (PB88-134325).

NCEER-87-0009 "Liquefaction Potential for New York State: A Preliminary Report on Sites in Manhattan and Buffalo," by M. Budhu, V. Vijayakumar, R.F. Giese and L. Baumgras, 8/31/87, (PB88-163704). This report is available only through NTIS (see address given above).

NCEER-87-0010 "Vertical and Torsional Vibration of Foundations in Inhomogeneous Media," by A.S. Veletsos and K.W. Dotson, 6/1/87, (PB88-134291).

NCEER-87-0011 "Seismic Probabilistic Risk Assessment and Seismic Margins Studies for Nuclear Power Plants," by Howard H.M. Hwang, 6/15/87, (PB88-134267).

NCEER-87-0012 "Parametric Studies of Frequency Response of Secondary Systems Under Ground-Acceleration Excitations," by Y. Yong and Y.K. Lin, 6/10/87, (PB88-134309).

NCEER-87-0013 "Frequency Response of Secondary Systems Under Seismic Excitation," by J.A. HoLung, J. Cai and Y.K. Lin, 7/31/87, (PB88-134317).

NCEER-87-0014 "Modelling Earthquake Ground Motions in Seismically Active Regions Using Parametric Time Series Methods," by G.W. Ellis and A.S. Cakmak, 8/25/87, (PB88-134283).

NCEER-87-0015 "Detection and Assessment of Seismic Structural Damage," by E. DiPasquale and A.S. Cakmak, 8/25/87, (PB88-163712).

NCEER-87-0016 "Pipeline Experiment at Parkfield, California," by J. Isenberg and E. Richardson, 9/15/87, (PB88-163720). This report is available only through NTIS (see address given above).

NCEER-87-0017 "Digital Simulation of Seismic Ground Motion," by M. Shinozuka, G. Deodatis and T. Harada, 8/31/87, (PB88-155197). This report is available only through NTIS (see address given above).

NCEER-87-0018 "Practical Considerations for Structural Control: System Uncertainty, System Time Delay and Truncation of Small Control Forces," J.N. Yang and A. Akbarpour, 8/10/87, (PB88-163738).

NCEER-87-0019 "Modal Analysis of Nonclassically Damped Structural Systems Using Canonical Transformation," by J.N. Yang, S. Sarkani and F.X. Long, 9/27/87, (PB88-187851).

NCEER-87-0020 "A Nonstationary Solution in Random Vibration Theory," by J.R. Red-Horse and P.D. Spanos, 11/3/87, (PB88-163746).

NCEER-87-0021 "Horizontal Impedances for Radially Inhomogeneous Viscoelastic Soil Layers," by A.S. Veletsos and K.W. Dotson, 10/15/87, (PB88-150859).

NCEER-87-0022 "Seismic Damage Assessment of Reinforced Concrete Members," by Y.S. Chung, C. Meyer and M. Shinozuka, 10/9/87, (PB88-150867). This report is available only through NTIS (see address given above).

NCEER-87-0023 "Active Structural Control in Civil Engineering," by T.T. Soong, 11/11/87, (PB88-187778).

NCEER-87-0024 "Vertical and Torsional Impedances for Radially Inhomogeneous Viscoelastic Soil Layers," by K.W. Dotson and A.S. Veletsos, 12/87, (PB88-187786).

NCEER-87-0025 "Proceedings from the Symposium on Seismic Hazards, Ground Motions, Soil-Liquefaction and Engineering Practice in Eastern North America," October 20-22, 1987, edited by K.H. Jacob, 12/87, (PB88-188115).

NCEER-87-0026 "Report on the Whittier-Narrows, California, Earthquake of October 1, 1987," by J. Pantelic and A. Reinhorn, 11/87, (PB88-187752). This report is available only through NTIS (see address given above).

NCEER-87-0027 "Design of a Modular Program for Transient Nonlinear Analysis of Large 3-D Building Structures," by S. Srivastav and J.F. Abel, 12/30/87, (PB88-187950).

NCEER-87-0028 "Second-Year Program in Research, Education and Technology Transfer," 3/8/88, (PB88-219480).

NCEER-88-0001 "Workshop on Seismic Computer Analysis and Design of Buildings With Interactive Graphics," by W. McGuire, J.F. Abel and C.H. Conley, 1/18/88, (PB88-187760).

NCEER-88-0002 "Optimal Control of Nonlinear Flexible Structures," by J.N. Yang, F.X. Long and D. Wong, 1/22/88, (PB88-213772).

NCEER-88-0003 "Substructuring Techniques in the Time Domain for Primary-Secondary Structural Systems," by G.D. Manolis and G. Juhn, 2/10/88, (PB88-213780).

NCEER-88-0004 "Iterative Seismic Analysis of Primary-Secondary Systems," by A. Singhal, L.D. Lutes and P.D. Spanos, 2/23/88, (PB88-213798).

NCEER-88-0005 "Stochastic Finite Element Expansion for Random Media," by P.D. Spanos and R. Ghanem, 3/14/88, (PB88-213806).

NCEER-88-0006 "Combining Structural Optimization and Structural Control," by F.Y. Cheng and C.P. Pantelides, 1/10/88, (PB88-213814).

NCEER-88-0007 "Seismic Performance Assessment of Code-Designed Structures," by H.H-M. Hwang, J-W. Jaw and H-J. Shau, 3/20/88, (PB88-219423).

NCEER-88-0008 "Reliability Analysis of Code-Designed Structures Under Natural Hazards," by H.H-M. Hwang, H. Ushiba and M. Shinozuka, 2/29/88, (PB88-229471).

NCEER-88-0009 "Seismic Fragility Analysis of Shear Wall Structures," by J-W Jaw and H.H-M. Hwang, 4/30/88, (PB89-102867).

NCEER-88-0010 "Base Isolation of a Multi-Story Building Under a Harmonic Ground Motion - A Comparison of Performances of Various Systems," by F-G Fan, G. Ahmadi and I.G. Tadjbakhsh, 5/18/88, (PB89-122238).

NCEER-88-0011 "Seismic Floor Response Spectra for a Combined System by Green's Functions," by F.M. Lavelle, L.A. Bergman and P.D. Spanos, 5/1/88, (PB89-102875).

NCEER-88-0012 "A New Solution Technique for Randomly Excited Hysteretic Structures," by G.Q. Cai and Y.K. Lin, 5/16/88, (PB89-102883).

NCEER-88-0013 "A Study of Radiation Damping and Soil-Structure Interaction Effects in the Centrifuge," by K. Weissman, supervised by J.H. Prevost, 5/24/88, (PB89-144703).

NCEER-88-0014 "Parameter Identification and Implementation of a Kinematic Plasticity Model for Frictional Soils," by J.H. Prevost and D.V. Griffiths, to be published.

NCEER-88-0015 "Two- and Three- Dimensional Dynamic Finite Element Analyses of the Long Valley Dam," by D.V. Griffiths and J.H. Prevost, 6/17/88, (PB89-144711).

NCEER-88-0016 "Damage Assessment of Reinforced Concrete Structures in Eastern United States," by A.M. Reinhorn, M.J. Seidel, S.K. Kunnath and Y.J. Park, 6/15/88, (PB89-122220).

NCEER-88-0017 "Dynamic Compliance of Vertically Loaded Strip Foundations in Multilayered Viscoelastic Soils," by S. Ahmad and A.S.M. Israil, 6/17/88, (PB89-102891).

NCEER-88-0018 "An Experimental Study of Seismic Structural Response With Added Viscoelastic Dampers," by R.C. Lin, Z. Liang, T.T. Soong and R.H. Zhang, 6/30/88, (PB89-122212). This report is available only through NTIS (see address given above).

NCEER-88-0019 "Experimental Investigation of Primary - Secondary System Interaction," by G.D. Manolis, G. Juhn and A.M. Reinhorn, 5/27/88, (PB89-122204).

NCEER-88-0020 "A Response Spectrum Approach For Analysis of Nonclassically Damped Structures," by J.N. Yang, S. Sarkani and F.X. Long, 4/22/88, (PB89-102909).

NCEER-88-0021 "Seismic Interaction of Structures and Soils: Stochastic Approach," by A.S. Veletsos and A.M. Prasad, 7/21/88, (PB89-122196).

NCEER-88-0022 "Identification of the Serviceability Limit State and Detection of Seismic Structural Damage," by E. DiPasquale and A.S. Cakmak, 6/15/88, (PB89-122188). This report is available only through NTIS (see address given above).

NCEER-88-0023 "Multi-Hazard Risk Analysis: Case of a Simple Offshore Structure," by B.K. Bhartia and E.H. Vanmarcke, 7/21/88, (PB89-145213).

NCEER-88-0024 "Automated Seismic Design of Reinforced Concrete Buildings," by Y.S. Chung, C. Meyer and M. Shinozuka, 7/5/88, (PB89-122170). This report is available only through NTIS (see address given above).

NCEER-88-0025 "Experimental Study of Active Control of MDOF Structures Under Seismic Excitations," by L.L. Chung, R.C. Lin, T.T. Soong and A.M. Reinhorn, 7/10/88, (PB89-122600).

NCEER-88-0026 "Earthquake Simulation Tests of a Low-Rise Metal Structure," by J.S. Hwang, K.C. Chang, G.C. Lee and R.L. Ketter, 8/1/88, (PB89-102917).

NCEER-88-0027 "Systems Study of Urban Response and Reconstruction Due to Catastrophic Earthquakes," by F. Kozin and H.K. Zhou, 9/22/88, (PB90-162348).

NCEER-88-0028 "Seismic Fragility Analysis of Plane Frame Structures," by H.H-M. Hwang and Y.K. Low, 7/31/88, (PB89-131445).

NCEER-88-0029 "Response Analysis of Stochastic Structures," by A. Kardara, C. Bucher and M. Shinozuka, 9/22/88, (PB89-174429).

NCEER-88-0030 "Nonnormal Accelerations Due to Yielding in a Primary Structure," by D.C.K. Chen and L.D. Lutes, 9/19/88, (PB89-131437).

NCEER-88-0031 "Design Approaches for Soil-Structure Interaction," by A.S. Veletsos, A.M. Prasad and Y. Tang, 12/30/88, (PB89-174437). This report is available only through NTIS (see address given above).

NCEER-88-0032 "A Re-evaluation of Design Spectra for Seismic Damage Control," by C.J. Turkstra and A.G. Tallin, 11/7/88, (PB89-145221).

NCEER-88-0033 "The Behavior and Design of Noncontact Lap Splices Subjected to Repeated Inelastic Tensile Loading," by V.E. Sagan, P. Gergely and R.N. White, 12/8/88, (PB89-163737).

NCEER-88-0034 "Seismic Response of Pile Foundations," by S.M. Mamoon, P.K. Banerjee and S. Ahmad, 11/1/88, (PB89-145239).

NCEER-88-0035 "Modeling of R/C Building Structures With Flexible Floor Diaphragms (IDARC2)," by A.M. Reinhorn, S.K. Kunnath and N. Panahshahi, 9/7/88, (PB89-207153).

NCEER-88-0036 "Solution of the Dam-Reservoir Interaction Problem Using a Combination of FEM, BEM with Particular Integrals, Modal Analysis, and Substructuring," by C-S. Tsai, G.C. Lee and R.L. Ketter, 12/31/88, (PB89-207146).

NCEER-88-0037 "Optimal Placement of Actuators for Structural Control," by F.Y. Cheng and C.P. Pantelides, 8/15/88, (PB89-162846).

NCEER-88-0038 "Teflon Bearings in Aseismic Base Isolation: Experimental Studies and Mathematical Modeling," by A. Mokha, M.C. Constantinou and A.M. Reinhorn, 12/5/88, (PB89-218457). This report is available only through NTIS (see address given above).

NCEER-88-0039 "Seismic Behavior of Flat Slab High-Rise Buildings in the New York City Area," by P. Weidlinger and M. Ettouney, 10/15/88, (PB90-145681).

NCEER-88-0040 "Evaluation of the Earthquake Resistance of Existing Buildings in New York City," by P. Weidlinger and M. Ettouney, 10/15/88, to be published.

NCEER-88-0041 "Small-Scale Modeling Techniques for Reinforced Concrete Structures Subjected to Seismic Loads," by W. Kim, A. El-Attar and R.N. White, 11/22/88, (PB89-189625).

NCEER-88-0042 "Modeling Strong Ground Motion from Multiple Event Earthquakes," by G.W. Ellis and A.S. Cakmak, 10/15/88, (PB89-174445).

NCEER-88-0043 "Nonstationary Models of Seismic Ground Acceleration," by M. Grigoriu, S.E. Ruiz and E. Rosenblueth, 7/15/88, (PB89-189617).

NCEER-88-0044 "SARCF User's Guide: Seismic Analysis of Reinforced Concrete Frames," by Y.S. Chung, C. Meyer and M. Shinozuka, 11/9/88, (PB89-174452).

NCEER-88-0045 "First Expert Panel Meeting on Disaster Research and Planning," edited by J. Pantelic and J. Stoyle, 9/15/88, (PB89-174460).

NCEER-88-0046 "Preliminary Studies of the Effect of Degrading Infill Walls on the Nonlinear Seismic Response of Steel Frames," by C.Z. Chrysostomou, P. Gergely and J.F. Abel, 12/19/88, (PB89-208383).

NCEER-88-0047 "Reinforced Concrete Frame Component Testing Facility - Design, Construction, Instrumentation and Operation," by S.P. Pessiki, C. Conley, T. Bond, P. Gergely and R.N. White, 12/16/88, (PB89-174478).

NCEER-89-0001 "Effects of Protective Cushion and Soil Compliancy on the Response of Equipment Within a Seismically Excited Building," by J.A. HoLung, 2/16/89, (PB89-207179).

NCEER-89-0002 "Statistical Evaluation of Response Modification Factors for Reinforced Concrete Structures," by H.H-M. Hwang and J-W. Jaw, 2/17/89, (PB89-207187).

NCEER-89-0003 "Hysteretic Columns Under Random Excitation," by G-Q. Cai and Y.K. Lin, 1/9/89, (PB89-196513).

NCEER-89-0004 "Experimental Study of `Elephant Foot Bulge' Instability of Thin-Walled Metal Tanks," by Z-H. Jia and R.L. Ketter, 2/22/89, (PB89-207195).

NCEER-89-0005 "Experiment on Performance of Buried Pipelines Across San Andreas Fault," by J. Isenberg, E. Richardson and T.D. O'Rourke, 3/10/89, (PB89-218440). This report is available only through NTIS (see address given above).

NCEER-89-0006 "A Knowledge-Based Approach to Structural Design of Earthquake-Resistant Buildings," by M. Subramani, P. Gergely, C.H. Conley, J.F. Abel and A.H. Zaghw, 1/15/89, (PB89-218465).

NCEER-89-0007 "Liquefaction Hazards and Their Effects on Buried Pipelines," by T.D. O'Rourke and P.A. Lane, 2/1/89, (PB89-218481).

NCEER-89-0008 "Fundamentals of System Identification in Structural Dynamics," by H. Imai, C-B. Yun, O. Maruyama and M. Shinozuka, 1/26/89, (PB89-207211).

NCEER-89-0009 "Effects of the 1985 Michoacan Earthquake on Water Systems and Other Buried Lifelines in Mexico," by A.G. Ayala and M.J. O'Rourke, 3/8/89, (PB89-207229).

NCEER-89-R010 "NCEER Bibliography of Earthquake Education Materials," by K.E.K. Ross, Second Revision, 9/1/89, (PB90-125352).

NCEER-89-0011 "Inelastic Three-Dimensional Response Analysis of Reinforced Concrete Building Structures (IDARC-3D), Part I - Modeling," by S.K. Kunnath and A.M. Reinhorn, 4/17/89, (PB90-114612).

NCEER-89-0012 "Recommended Modifications to ATC-14," by C.D. Poland and J.O. Malley, 4/12/89, (PB90-108648).

NCEER-89-0013 "Repair and Strengthening of Beam-to-Column Connections Subjected to Earthquake Loading," by M. Corazao and A.J. Durrani, 2/28/89, (PB90-109885).

NCEER-89-0014 "Program EXKAL2 for Identification of Structural Dynamic Systems," by O. Maruyama, C-B. Yun, M. Hoshiya and M. Shinozuka, 5/19/89, (PB90-109877).

NCEER-89-0015 "Response of Frames With Bolted Semi-Rigid Connections, Part I - Experimental Study and Analytical Predictions," by P.J. DiCorso, A.M. Reinhorn, J.R. Dickerson, J.B. Radziminski and W.L. Harper, 6/1/89, to be published.

NCEER-89-0016 "ARMA Monte Carlo Simulation in Probabilistic Structural Analysis," by P.D. Spanos and M.P. Mignolet, 7/10/89, (PB90-109893).

NCEER-89-P017 "Preliminary Proceedings from the Conference on Disaster Preparedness - The Place of Earthquake Education in Our Schools," Edited by K.E.K. Ross, 6/23/89, (PB90-108606).

NCEER-89-0017 "Proceedings from the Conference on Disaster Preparedness - The Place of Earthquake Education in Our Schools," Edited by K.E.K. Ross, 12/31/89, (PB90-207895). This report is available only through NTIS (see address given above).

NCEER-89-0018 "Multidimensional Models of Hysteretic Material Behavior for Vibration Analysis of Shape Memory Energy Absorbing Devices, by E.J. Graesser and F.A. Cozzarelli, 6/7/89, (PB90-164146).

NCEER-89-0019 "Nonlinear Dynamic Analysis of Three-Dimensional Base Isolated Structures (3D-BASIS)," by S. Nagarajaiah, A.M. Reinhorn and M.C. Constantinou, 8/3/89, (PB90-161936). This report is available only through NTIS (see address given above).

NCEER-89-0020 "Structural Control Considering Time-Rate of Control Forces and Control Rate Constraints," by F.Y. Cheng and C.P. Pantelides, 8/3/89, (PB90-120445).

NCEER-89-0021 "Subsurface Conditions of Memphis and Shelby County," by K.W. Ng, T-S. Chang and H-H.M. Hwang, 7/26/89, (PB90-120437).

NCEER-89-0022 "Seismic Wave Propagation Effects on Straight Jointed Buried Pipelines," by K. Elhmadi and M.J. O'Rourke, 8/24/89, (PB90-162322).

NCEER-89-0023 "Workshop on Serviceability Analysis of Water Delivery Systems," edited by M. Grigoriu, 3/6/89, (PB90-127424).

NCEER-89-0024 "Shaking Table Study of a 1/5 Scale Steel Frame Composed of Tapered Members," by K.C. Chang, J.S. Hwang and G.C. Lee, 9/18/89, (PB90-160169).

NCEER-89-0025 "DYNA1D: A Computer Program for Nonlinear Seismic Site Response Analysis - Technical Documentation," by Jean H. Prevost, 9/14/89, (PB90-161944). This report is available only through NTIS (see address given above).

NCEER-89-0026 "1:4 Scale Model Studies of Active Tendon Systems and Active Mass Dampers for Aseismic Protection," by A.M. Reinhorn, T.T. Soong, R.C. Lin, Y.P. Yang, Y. Fukao, H. Abe and M. Nakai, 9/15/89, (PB90-173246).

NCEER-89-0027 "Scattering of Waves by Inclusions in a Nonhomogeneous Elastic Half Space Solved by Boundary Element Methods," by P.K. Hadley, A. Askar and A.S. Cakmak, 6/15/89, (PB90-145699).

NCEER-89-0028 "Statistical Evaluation of Deflection Amplification Factors for Reinforced Concrete Structures," by H.H.M. Hwang, J-W. Jaw and A.L. Ch'ng, 8/31/89, (PB90-164633).

NCEER-89-0029 "Bedrock Accelerations in Memphis Area Due to Large New Madrid Earthquakes," by H.H.M. Hwang, C.H.S. Chen and G. Yu, 11/7/89, (PB90-162330).

NCEER-89-0030 "Seismic Behavior and Response Sensitivity of Secondary Structural Systems," by Y.Q. Chen and T.T. Soong, 10/23/89, (PB90-164658).

NCEER-89-0031 "Random Vibration and Reliability Analysis of Primary-Secondary Structural Systems," by Y. Ibrahim, M. Grigoriu and T.T. Soong, 11/10/89, (PB90-161951).

NCEER-89-0032 "Proceedings from the Second U.S. - Japan Workshop on Liquefaction, Large Ground Deformation and Their Effects on Lifelines, September 26-29, 1989," Edited by T.D. O'Rourke and M. Hamada, 12/1/89, (PB90-209388).

NCEER-89-0033 "Deterministic Model for Seismic Damage Evaluation of Reinforced Concrete Structures," by J.M. Bracci, A.M. Reinhorn, J.B. Mander and S.K. Kunnath, 9/27/89.

NCEER-89-0034 "On the Relation Between Local and Global Damage Indices," by E. DiPasquale and A.S. Cakmak, 8/15/89, (PB90-173865).

NCEER-89-0035 "Cyclic Undrained Behavior of Nonplastic and Low Plasticity Silts," by A.J. Walker and H.E. Stewart, 7/26/89, (PB90-183518).

NCEER-89-0036 "Liquefaction Potential of Surficial Deposits in the City of Buffalo, New York," by M. Budhu, R. Giese and L. Baumgrass, 1/17/89, (PB90-208455).

NCEER-89-0037 "A Deterministic Assessment of Effects of Ground Motion Incoherence," by A.S. Veletsos and Y. Tang, 7/15/89, (PB90-164294).

NCEER-89-0038 "Workshop on Ground Motion Parameters for Seismic Hazard Mapping," July 17-18, 1989, edited by R.V. Whitman, 12/1/89, (PB90-173923).

NCEER-89-0039 "Seismic Effects on Elevated Transit Lines of the New York City Transit Authority," by C.J. Costantino, C.A. Miller and E. Heymsfield, 12/26/89, (PB90-207887).

NCEER-89-0040 "Centrifugal Modeling of Dynamic Soil-Structure Interaction," by K. Weissman, Supervised by J.H. Prevost, 5/10/89, (PB90-207879).

NCEER-89-0041 "Linearized Identification of Buildings With Cores for Seismic Vulnerability Assessment," by I-K. Ho and A.E. Aktan, 11/1/89, (PB90-251943).

NCEER-90-0001 "Geotechnical and Lifeline Aspects of the October 17, 1989 Loma Prieta Earthquake in San Francisco," by T.D. O'Rourke, H.E. Stewart, F.T. Blackburn and T.S. Dickerman, 1/90, (PB90-208596).

NCEER-90-0002 "Nonnormal Secondary Response Due to Yielding in a Primary Structure," by D.C.K. Chen and L.D. Lutes, 2/28/90, (PB90-251976).

NCEER-90-0003 "Earthquake Education Materials for Grades K-12," by K.E.K. Ross, 4/16/90, (PB91-251984).

NCEER-90-0004 "Catalog of Strong Motion Stations in Eastern North America," by R.W. Busby, 4/3/90, (PB90-251984).

NCEER-90-0005 "NCEER Strong-Motion Data Base: A User Manual for the GeoBase Release (Version 1.0 for the Sun3)," by P. Friberg and K. Jacob, 3/31/90 (PB90-258062).

NCEER-90-0006 "Seismic Hazard Along a Crude Oil Pipeline in the Event of an 1811-1812 Type New Madrid Earthquake," by H.H.M. Hwang and C-H.S. Chen, 4/16/90(PB90-258054).

NCEER-90-0007 "Site-Specific Response Spectra for Memphis Sheahan Pumping Station," by H.H.M. Hwang and C.S. Lee, 5/15/90, (PB91-108811).

NCEER-90-0008 "Pilot Study on Seismic Vulnerability of Crude Oil Transmission Systems," by T. Ariman, R. Dobry, M. Grigoriu, F. Kozin, M. O'Rourke, T. O'Rourke and M. Shinozuka, 5/25/90, (PB91-108837).

NCEER-90-0009 "A Program to Generate Site Dependent Time Histories: EQGEN," by G.W. Ellis, M. Srinivasan and A.S. Cakmak, 1/30/90, (PB91-108829).

NCEER-90-0010 "Active Isolation for Seismic Protection of Operating Rooms," by M.E. Talbott, Supervised by M. Shinozuka, 6/8/9, (PB91-110205).

NCEER-90-0011 "Program LINEARID for Identification of Linear Structural Dynamic Systems," by C-B. Yun and M. Shinozuka, 6/25/90, (PB91-110312).

NCEER-90-0012 "Two-Dimensional Two-Phase Elasto-Plastic Seismic Response of Earth Dams," by A.N. Yiagos, Supervised by J.H. Prevost, 6/20/90, (PB91-110197).

NCEER-90-0013 "Secondary Systems in Base-Isolated Structures: Experimental Investigation, Stochastic Response and Stochastic Sensitivity," by G.D. Manolis, G. Juhn, M.C. Constantinou and A.M. Reinhorn, 7/1/90, (PB91-110320).

NCEER-90-0014 "Seismic Behavior of Lightly-Reinforced Concrete Column and Beam-Column Joint Details," by S.P. Pessiki, C.H. Conley, P. Gergely and R.N. White, 8/22/90, (PB91-108795).

NCEER-90-0015 "Two Hybrid Control Systems for Building Structures Under Strong Earthquakes," by J.N. Yang and A. Danielians, 6/29/90, (PB91-125393).

NCEER-90-0016 "Instantaneous Optimal Control with Acceleration and Velocity Feedback," by J.N. Yang and Z. Li, 6/29/90, (PB91-125401).

NCEER-90-0017 "Reconnaissance Report on the Northern Iran Earthquake of June 21, 1990," by M. Mehrain, 10/4/90, (PB91-125377).

NCEER-90-0018 "Evaluation of Liquefaction Potential in Memphis and Shelby County," by T.S. Chang, P.S. Tang, C.S. Lee and H. Hwang, 8/10/90, (PB91-125427).

NCEER-90-0019 "Experimental and Analytical Study of a Combined Sliding Disc Bearing and Helical Steel Spring Isolation System," by M.C. Constantinou, A.S. Mokha and A.M. Reinhorn, 10/4/90, (PB91-125385).

NCEER-90-0020 "Experimental Study and Analytical Prediction of Earthquake Response of a Sliding Isolation System with a Spherical Surface," by A.S. Mokha, M.C. Constantinou and A.M. Reinhorn, 10/11/90, (PB91-125419).

NCEER-90-0021 "Dynamic Interaction Factors for Floating Pile Groups," by G. Gazetas, K. Fan, A. Kaynia and E. Kausel, 9/10/90, (PB91-170381).

NCEER-90-0022 "Evaluation of Seismic Damage Indices for Reinforced Concrete Structures," by S. Rodriguez-Gomez and A.S. Cakmak, 9/30/90, PB91-171322).

NCEER-90-0023 "Study of Site Response at a Selected Memphis Site," by H. Desai, S. Ahmad, E.S. Gazetas and M.R. Oh, 10/11/90, (PB91-196857).

NCEER-90-0024 "A User's Guide to Strongmo: Version 1.0 of NCEER's Strong-Motion Data Access Tool for PCs and Terminals," by P.A. Friberg and C.A.T. Susch, 11/15/90, (PB91-171272).

NCEER-90-0025 "A Three-Dimensional Analytical Study of Spatial Variability of Seismic Ground Motions," by L-L. Hong and A.H.-S. Ang, 10/30/90, (PB91-170399).

NCEER-90-0026 "MUMOID User's Guide - A Program for the Identification of Modal Parameters," by S. Rodriguez-Gomez and E. DiPasquale, 9/30/90, (PB91-171298).

NCEER-90-0027 "SARCF-II User's Guide - Seismic Analysis of Reinforced Concrete Frames," by S. Rodriguez-Gomez, Y.S. Chung and C. Meyer, 9/30/90, (PB91-171280).

NCEER-90-0028 "Viscous Dampers: Testing, Modeling and Application in Vibration and Seismic Isolation," by N. Makris and M.C. Constantinou, 12/20/90 (PB91-190561).

NCEER-90-0029 "Soil Effects on Earthquake Ground Motions in the Memphis Area," by H. Hwang, C.S. Lee, K.W. Ng and T.S. Chang, 8/2/90, (PB91-190751).

NCEER-91-0001 "Proceedings from the Third Japan-U.S. Workshop on Earthquake Resistant Design of Lifeline Facilities and Countermeasures for Soil Liquefaction, December 17-19, 1990," edited by T.D. O'Rourke and M. Hamada, 2/1/91, (PB91-179259).

NCEER-91-0002 "Physical Space Solutions of Non-Proportionally Damped Systems," by M. Tong, Z. Liang and G.C. Lee, 1/15/91, (PB91-179242).

NCEER-91-0003 "Seismic Response of Single Piles and Pile Groups," by K. Fan and G. Gazetas, 1/10/91, (PB92-174994).

NCEER-91-0004 "Damping of Structures: Part 1 - Theory of Complex Damping," by Z. Liang and G. Lee, 10/10/91, (PB92-197235).

NCEER-91-0005 "3D-BASIS - Nonlinear Dynamic Analysis of Three Dimensional Base Isolated Structures: Part II," by S. Nagarajaiah, A.M. Reinhorn and M.C. Constantinou, 2/28/91, (PB91-190553).

NCEER-91-0006 "A Multidimensional Hysteretic Model for Plasticity Deforming Metals in Energy Absorbing Devices," by E.J. Graesser and F.A. Cozzarelli, 4/9/91, (PB92-108364).

NCEER-91-0007 "A Framework for Customizable Knowledge-Based Expert Systems with an Application to a KBES for Evaluating the Seismic Resistance of Existing Buildings," by E.G. Ibarra-Anaya and S.J. Fenves, 4/9/91, (PB91-210930).

NCEER-91-0008 "Nonlinear Analysis of Steel Frames with Semi-Rigid Connections Using the Capacity Spectrum Method," by G.G. Deierlein, S-H. Hsieh, Y-J. Shen and J.F. Abel, 7/2/91, (PB92-113828).

NCEER-91-0009 "Earthquake Education Materials for Grades K-12," by K.E.K. Ross, 4/30/91, (PB91-212142).

NCEER-91-0010 "Phase Wave Velocities and Displacement Phase Differences in a Harmonically Oscillating Pile," by N. Makris and G. Gazetas, 7/8/91, (PB92-108356).

NCEER-91-0011 "Dynamic Characteristics of a Full-Size Five-Story Steel Structure and a 2/5 Scale Model," by K.C. Chang, G.C. Yao, G.C. Lee, D.S. Hao and Y.C. Yeh," 7/2/91, (PB93-116648).

NCEER-91-0012 "Seismic Response of a 2/5 Scale Steel Structure with Added Viscoelastic Dampers," by K.C. Chang, T.T. Soong, S-T. Oh and M.L. Lai, 5/17/91, (PB92-110816).

NCEER-91-0013 "Earthquake Response of Retaining Walls; Full-Scale Testing and Computational Modeling," by S. Alampalli and A-W.M. Elgamal, 6/20/91, to be published.

NCEER-91-0014 "3D-BASIS-M: Nonlinear Dynamic Analysis of Multiple Building Base Isolated Structures," by P.C. Tsopelas, S. Nagarajaiah, M.C. Constantinou and A.M. Reinhorn, 5/28/91, (PB92-113885).

NCEER-91-0015 "Evaluation of SEAOC Design Requirements for Sliding Isolated Structures," by D. Theodossiou and M.C. Constantinou, 6/10/91, (PB92-114602).

NCEER-91-0016 "Closed-Loop Modal Testing of a 27-Story Reinforced Concrete Flat Plate-Core Building," by H.R. Somaprasad, T. Toksoy, H. Yoshiyuki and A.E. Aktan, 7/15/91, (PB92-129980).

NCEER-91-0017 "Shake Table Test of a 1/6 Scale Two-Story Lightly Reinforced Concrete Building," by A.G. El-Attar, R.N. White and P. Gergely, 2/28/91, (PB92-222447).

NCEER-91-0018 "Shake Table Test of a 1/8 Scale Three-Story Lightly Reinforced Concrete Building," by A.G. El-Attar, R.N. White and P. Gergely, 2/28/91, (PB93-116630).

NCEER-91-0019 "Transfer Functions for Rigid Rectangular Foundations," by A.S. Veletsos, A.M. Prasad and W.H. Wu, 7/31/91.

NCEER-91-0020 "Hybrid Control of Seismic-Excited Nonlinear and Inelastic Structural Systems," by J.N. Yang, Z. Li and A. Danielians, 8/1/91, (PB92-143171).

NCEER-91-0021 "The NCEER-91 Earthquake Catalog: Improved Intensity-Based Magnitudes and Recurrence Relations for U.S. Earthquakes East of New Madrid," by L. Seeber and J.G. Armbruster, 8/28/91, (PB92-176742).

NCEER-91-0022 "Proceedings from the Implementation of Earthquake Planning and Education in Schools: The Need for Change - The Roles of the Changemakers," by K.E.K. Ross and F. Winslow, 7/23/91, (PB92-129998).

NCEER-91-0023 "A Study of Reliability-Based Criteria for Seismic Design of Reinforced Concrete Frame Buildings," by H.H.M. Hwang and H-M. Hsu, 8/10/91, (PB92-140235).

NCEER-91-0024 "Experimental Verification of a Number of Structural System Identification Algorithms," by R.G. Ghanem, H. Gavin and M. Shinozuka, 9/18/91, (PB92-176577).

NCEER-91-0025 "Probabilistic Evaluation of Liquefaction Potential," by H.H.M. Hwang and C.S. Lee," 11/25/91, (PB92-143429).

NCEER-91-0026 "Instantaneous Optimal Control for Linear, Nonlinear and Hysteretic Structures - Stable Controllers," by J.N. Yang and Z. Li, 11/15/91, (PB92-163807).

NCEER-91-0027 "Experimental and Theoretical Study of a Sliding Isolation System for Bridges," by M.C. Constantinou, A. Kartoum, A.M. Reinhorn and P. Bradford, 11/15/91, (PB92-176973).

NCEER-92-0001 "Case Studies of Liquefaction and Lifeline Performance During Past Earthquakes, Volume 1: Japanese Case Studies," Edited by M. Hamada and T. O'Rourke, 2/17/92, (PB92-197243).

NCEER-92-0002 "Case Studies of Liquefaction and Lifeline Performance During Past Earthquakes, Volume 2: United States Case Studies," Edited by T. O'Rourke and M. Hamada, 2/17/92, (PB92-197250).

NCEER-92-0003 "Issues in Earthquake Education," Edited by K. Ross, 2/3/92, (PB92-222389).

NCEER-92-0004 "Proceedings from the First U.S. - Japan Workshop on Earthquake Protective Systems for Bridges," Edited by I.G. Buckle, 2/4/92, (PB94-142239, A99, MF-A06).

NCEER-92-0005 "Seismic Ground Motion from a Haskell-Type Source in a Multiple-Layered Half-Space," A.P. Theoharis, G. Deodatis and M. Shinozuka, 1/2/92, to be published.

NCEER-92-0006 "Proceedings from the Site Effects Workshop," Edited by R. Whitman, 2/29/92, (PB92-197201).

NCEER-92-0007 "Engineering Evaluation of Permanent Ground Deformations Due to Seismically-Induced Liquefaction," by M.H. Baziar, R. Dobry and A-W.M. Elgamal, 3/24/92, (PB92-222421).

NCEER-92-0008 "A Procedure for the Seismic Evaluation of Buildings in the Central and Eastern United States," by C.D. Poland and J.O. Malley, 4/2/92, (PB92-222439).

NCEER-92-0009 "Experimental and Analytical Study of a Hybrid Isolation System Using Friction Controllable Sliding Bearings," by M.Q. Feng, S. Fujii and M. Shinozuka, 5/15/92, (PB93-150282).

NCEER-92-0010 "Seismic Resistance of Slab-Column Connections in Existing Non-Ductile Flat-Plate Buildings," by A.J. Durrani and Y. Du, 5/18/92.

NCEER-92-0011 "The Hysteretic and Dynamic Behavior of Brick Masonry Walls Upgraded by Ferrocement Coatings Under Cyclic Loading and Strong Simulated Ground Motion," by H. Lee and S.P. Prawel, 5/11/92, to be published.

NCEER-92-0012 "Study of Wire Rope Systems for Seismic Protection of Equipment in Buildings," by G.F. Demetriades, M.C. Constantinou and A.M. Reinhorn, 5/20/92.

NCEER-92-0013 "Shape Memory Structural Dampers: Material Properties, Design and Seismic Testing," by P.R. Witting and F.A. Cozzarelli, 5/26/92.

NCEER-92-0014 "Longitudinal Permanent Ground Deformation Effects on Buried Continuous Pipelines," by M.J. O'Rourke, and C. Nordberg, 6/15/92.

NCEER-92-0015 "A Simulation Method for Stationary Gaussian Random Functions Based on the Sampling Theorem," by M. Grigoriu and S. Balopoulou, 6/11/92, (PB93-127496).

NCEER-92-0016 "Gravity-Load-Designed Reinforced Concrete Buildings: Seismic Evaluation of Existing Construction and Detailing Strategies for Improved Seismic Resistance," by G.W. Hoffmann, S.K. Kunnath, A.M. Reinhorn and J.B. Mander, 7/15/92, (PB94-142007, A08, MF-A02).

NCEER-92-0017 "Observations on Water System and Pipeline Performance in the Limón Area of Costa Rica Due to the April 22, 1991 Earthquake," by M. O'Rourke and D. Ballantyne, 6/30/92, (PB93-126811).

NCEER-92-0018 "Fourth Edition of Earthquake Education Materials for Grades K-12," Edited by K.E.K. Ross, 8/10/92.

NCEER-92-0019 "Proceedings from the Fourth Japan-U.S. Workshop on Earthquake Resistant Design of Lifeline Facilities and Countermeasures for Soil Liquefaction," Edited by M. Hamada and T.D. O'Rourke, 8/12/92, (PB93-163939).

NCEER-92-0020 "Active Bracing System: A Full Scale Implementation of Active Control," by A.M. Reinhorn, T.T. Soong, R.C. Lin, M.A. Riley, Y.P. Wang, S. Aizawa and M. Higashino, 8/14/92, (PB93-127512).

NCEER-92-0021 "Empirical Analysis of Horizontal Ground Displacement Generated by Liquefaction-Induced Lateral Spreads," by S.F. Bartlett and T.L. Youd, 8/17/92, (PB93-188241).

NCEER-92-0022 "IDARC Version 3.0: Inelastic Damage Analysis of Reinforced Concrete Structures," by S.K. Kunnath, A.M. Reinhorn and R.F. Lobo, 8/31/92, (PB93-227502, A07, MF-A02).

NCEER-92-0023 "A Semi-Empirical Analysis of Strong-Motion Peaks in Terms of Seismic Source, Propagation Path and Local Site Conditions, by M. Kamiyama, M.J. O'Rourke and R. Flores-Berrones, 9/9/92, (PB93-150266).

NCEER-92-0024 "Seismic Behavior of Reinforced Concrete Frame Structures with Nonductile Details, Part I: Summary of Experimental Findings of Full Scale Beam-Column Joint Tests," by A. Beres, R.N. White and P. Gergely, 9/30/92, (PB93-227783, A05, MF-A01).

NCEER-92-0025 "Experimental Results of Repaired and Retrofitted Beam-Column Joint Tests in Lightly Reinforced Concrete Frame Buildings," by A. Beres, S. El-Borgi, R.N. White and P. Gergely, 10/29/92, (PB93-227791, A05, MF-A01).

NCEER-92-0026 "A Generalization of Optimal Control Theory: Linear and Nonlinear Structures," by J.N. Yang, Z. Li and S. Vongchavalitkul, 11/2/92, (PB93-188621).

NCEER-92-0027 "Seismic Resistance of Reinforced Concrete Frame Structures Designed Only for Gravity Loads: Part I - Design and Properties of a One-Third Scale Model Structure," by J.M. Bracci, A.M. Reinhorn and J.B. Mander, 12/1/92, (PB94-104502, A08, MF-A02).

NCEER-92-0028 "Seismic Resistance of Reinforced Concrete Frame Structures Designed Only for Gravity Loads: Part II - Experimental Performance of Subassemblages," by L.E. Aycardi, J.B. Mander and A.M. Reinhorn, 12/1/92, (PB94-104510, A08, MF-A02).

NCEER-92-0029 "Seismic Resistance of Reinforced Concrete Frame Structures Designed Only for Gravity Loads: Part III - Experimental Performance and Analytical Study of a Structural Model," by J.M. Bracci, A.M. Reinhorn and J.B. Mander, 12/1/92, (PB93-227528, A09, MF-A01).

NCEER-92-0030 "Evaluation of Seismic Retrofit of Reinforced Concrete Frame Structures: Part I - Experimental Performance of Retrofitted Subassemblages," by D. Choudhuri, J.B. Mander and A.M. Reinhorn, 12/8/92, (PB93-198307, A07, MF-A02).

NCEER-92-0031 "Evaluation of Seismic Retrofit of Reinforced Concrete Frame Structures: Part II - Experimental Performance and Analytical Study of a Retrofitted Structural Model," by J.M. Bracci, A.M. Reinhorn and J.B. Mander, 12/8/92, (PB93-198315, A09, MF-A03).

NCEER-92-0032 "Experimental and Analytical Investigation of Seismic Response of Structures with Supplemental Fluid Viscous Dampers," by M.C. Constantinou and M.D. Symans, 12/21/92, (PB93-191435).

NCEER-92-0033 "Reconnaissance Report on the Cairo, Egypt Earthquake of October 12, 1992," by M. Khater, 12/23/92, (PB93-188621).

NCEER-92-0034 "Low-Level Dynamic Characteristics of Four Tall Flat-Plate Buildings in New York City," by H. Gavin, S. Yuan, J. Grossman, E. Pekelis and K. Jacob, 12/28/92, (PB93-188217).

NCEER-93-0001 "An Experimental Study on the Seismic Performance of Brick-Infilled Steel Frames With and Without Retrofit," by J.B. Mander, B. Nair, K. Wojtkowski and J. Ma, 1/29/93, (PB93-227510, A07, MF-A02).

NCEER-93-0002 "Social Accounting for Disaster Preparedness and Recovery Planning," by S. Cole, E. Pantoja and V. Razak, 2/22/93, (PB94-142114, A12, MF-A03).

NCEER-93-0003 "Assessment of 1991 NEHRP Provisions for Nonstructural Components and Recommended Revisions," by T.T. Soong, G. Chen, Z. Wu, R-H. Zhang and M. Grigoriu, 3/1/93, (PB93-188639).

NCEER-93-0004 "Evaluation of Static and Response Spectrum Analysis Procedures of SEAOC/UBC for Seismic Isolated Structures," by C.W. Winters and M.C. Constantinou, 3/23/93, (PB93-198299).

NCEER-93-0005 "Earthquakes in the Northeast - Are We Ignoring the Hazard? A Workshop on Earthquake Science and Safety for Educators," edited by K.E.K. Ross, 4/2/93, (PB94-103066, A09, MF-A02).

NCEER-93-0006 "Inelastic Response of Reinforced Concrete Structures with Viscoelastic Braces," by R.F. Lobo, J.M. Bracci, K.L. Shen, A.M. Reinhorn and T.T. Soong, 4/5/93, (PB93-227486, A05, MF-A02).

NCEER-93-0007 "Seismic Testing of Installation Methods for Computers and Data Processing Equipment," by K. Kosar, T.T. Soong, K.L. Shen, J.A. HoLung and Y.K. Lin, 4/12/93, (PB93-198299).

NCEER-93-0008 "Retrofit of Reinforced Concrete Frames Using Added Dampers," by A. Reinhorn, M. Constantinou and C. Li, to be published.

NCEER-93-0009 "Seismic Behavior and Design Guidelines for Steel Frame Structures with Added Viscoelastic Dampers," by K.C. Chang, M.L. Lai, T.T. Soong, D.S. Hao and Y.C. Yeh, 5/1/93, (PB94-141959, A07, MF-A02).

NCEER-93-0010 "Seismic Performance of Shear-Critical Reinforced Concrete Bridge Piers," by J.B. Mander, S.M. Waheed, M.T.A. Chaudhary and S.S. Chen, 5/12/93, (PB93-227494, A08, MF-A02).

NCEER-93-0011 "3D-BASIS-TABS: Computer Program for Nonlinear Dynamic Analysis of Three Dimensional Base Isolated Structures," by S. Nagarajaiah, C. Li, A.M. Reinhorn and M.C. Constantinou, 8/2/93, (PB94-141819, A09, MF-A02).

NCEER-93-0012 "Effects of Hydrocarbon Spills from an Oil Pipeline Break on Ground Water," by O.J. Helweg and H.H.M. Hwang, 8/3/93, (PB94-141942, A06, MF-A02).

NCEER-93-0013 "Simplified Procedures for Seismic Design of Nonstructural Components and Assessment of Current Code Provisions," by M.P. Singh, L.E. Suarez, E.E. Matheu and G.O. Maldonado, 8/4/93, (PB94-141827, A09, MF-A02).

NCEER-93-0014 "An Energy Approach to Seismic Analysis and Design of Secondary Systems," by G. Chen and T.T. Soong, 8/6/93, (PB94-142767, A11, MF-A03).

NCEER-93-0015 "Proceedings from School Sites: Becoming Prepared for Earthquakes - Commemorating the Third Anniversary of the Loma Prieta Earthquake," Edited by F.E. Winslow and K.E.K. Ross, 8/16/93.

NCEER-93-0016 "Reconnaissance Report of Damage to Historic Monuments in Cairo, Egypt Following the October 12, 1992 Dahshur Earthquake," by D. Sykora, D. Look, G. Croci, E. Karaesmen and E. Karaesmen, 8/19/93, (PB94-142221, A08, MF-A02).

NCEER-93-0017 "The Island of Guam Earthquake of August 8, 1993," by S.W. Swan and S.K. Harris, 9/30/93, (PB94-141843, A04, MF-A01).

NCEER-93-0018 "Engineering Aspects of the October 12, 1992 Egyptian Earthquake," by A.W. Elgamal, M. Amer, K. Adalier and A. Abul-Fadl, 10/7/93, (PB94-141983, A05, MF-A01).

NCEER-93-0019 "Development of an Earthquake Motion Simulator and its Application in Dynamic Centrifuge Testing," by I. Krstelj, Supervised by J.H. Prevost, 10/23/93, (PB94-181773, A-10, MF-A03).

NCEER-93-0020 "NCEER-Taisei Corporation Research Program on Sliding Seismic Isolation Systems for Bridges: Experimental and Analytical Study of a Friction Pendulum System (FPS)," by M.C. Constantinou, P. Tsopelas, Y-S. Kim and S. Okamoto, 11/1/93, (PB94-142775, A08, MF-A02).

NCEER-93-0021 "Finite Element Modeling of Elastomeric Seismic Isolation Bearings," by L.J. Billings, Supervised by R. Shepherd, 11/8/93, to be published.

NCEER-93-0022 "Seismic Vulnerability of Equipment in Critical Facilities: Life-Safety and Operational Consequences," by K. Porter, G.S. Johnson, M.M. Zadeh, C. Scawthorn and S. Eder, 11/24/93, (PB94-181765, A16, MF-A03).

NCEER-93-0023 "Hokkaido Nansei-oki, Japan Earthquake of July 12, 1993, by P.I. Yanev and C.R. Scawthorn, 12/23/93, (PB94-181500, A07, MF-A01).

NCEER-94-0001 "An Evaluation of Seismic Serviceability of Water Supply Networks with Application to the San Francisco Auxiliary Water Supply System," by I. Markov, Supervised by M. Grigoriu and T. O'Rourke, 1/21/94.

NCEER-94-0002 "NCEER-Taisei Corporation Research Program on Sliding Seismic Isolation Systems for Bridges: Experimental and Analytical Study of Systems Consisting of Sliding Bearings, Rubber Restoring Force Devices and Fluid Dampers," Volumes I and II, by P. Tsopelas, S. Okamoto, M.C. Constantinou, D. Ozaki and S. Fujii, 2/4/94, (PB94-181740, A09, MF-A02 and PB94-181757, A12, MF-A03).

NCEER-94-0003 "A Markov Model for Local and Global Damage Indices in Seismic Analysis," by S. Rahman and M. Grigoriu, 2/18/94.

NCEER-94-0004 "Proceedings from the NCEER Workshop on Seismic Response of Masonry Infills," edited by D.P. Abrams, 3/1/94, (PB94-180783, A07, MF-A02).

NCEER-94-0005 "The Northridge, California Earthquake of January 17, 1994: General Reconnaissance Report," edited by J.D. Goltz, 3/11/94, (PB193943, A10, MF-A03).

NCEER-94-0006 "Seismic Energy Based Fatigue Damage Analysis of Bridge Columns: Part I - Evaluation of Seismic Capacity," by G.A. Chang and J.B. Mander, 3/14/94, (PB94-219185, A11, MF-A03).

NCEER-94-0007 "Seismic Isolation of Multi-Story Frame Structures Using Spherical Sliding Isolation Systems," by T.M. Al-Hussaini, V.A. Zayas and M.C. Constantinou, 3/17/94, (PB193745, A09, MF-A02).

NCEER-94-0008 "The Northridge, California Earthquake of January 17, 1994: Performance of Highway Bridges," edited by I.G. Buckle, 3/24/94, (PB94-193851, A06, MF-A02).

NCEER-94-0009 "Proceedings of the Third U.S.-Japan Workshop on Earthquake Protective Systems for Bridges," edited by I.G. Buckle and I. Friedland, 3/31/94, (PB94-195815, A99, MF-MF).

NCEER-94-0010 "3D-BASIS-ME: Computer Program for Nonlinear Dynamic Analysis of Seismically Isolated Single and Multiple Structures and Liquid Storage Tanks," by P.C. Tsopelas, M.C. Constantinou and A.M. Reinhorn, 4/12/94.

NCEER-94-0011 "The Northridge, California Earthquake of January 17, 1994: Performance of Gas Transmission Pipelines," by T.D. O'Rourke and M.C. Palmer, 5/16/94.

NCEER-94-0012 "Feasibility Study of Replacement Procedures and Earthquake Performance Related to Gas Transmission Pipelines," by T.D. O'Rourke and M.C. Palmer, 5/25/94, (PB94-206638, A09, MF-A02).

NCEER-94-0013 "Seismic Energy Based Fatigue Damage Analysis of Bridge Columns: Part II - Evaluation of Seismic Demand," by G.A. Chang and J.B. Mander, 6/1/94, (PB95-18106, A08, MF-A02).

NCEER-94-0014 "NCEER-Taisei Corporation Research Program on Sliding Seismic Isolation Systems for Bridges: Experimental and Analytical Study of a System Consisting of Sliding Bearings and Fluid Restoring Force/Damping Devices," by P. Tsopelas and M.C. Constantinou, 6/13/94, (PB94-219144, A10, MF-A03).

NCEER-94-0015 "Generation of Hazard-Consistent Fragility Curves for Seismic Loss Estimation Studies," by H. Hwang and J-R. Huo, 6/14/94, (PB95-181996, A09, MF-A02).

NCEER-94-0016 "Seismic Study of Building Frames with Added Energy-Absorbing Devices," by W.S. Pong, C.S. Tsai and G.C. Lee, 6/20/94, (PB94-219136, A10, A03).

NCEER-94-0017 "Sliding Mode Control for Seismic-Excited Linear and Nonlinear Civil Engineering Structures," by J. Yang, J. Wu, A. Agrawal and Z. Li, 6/21/94, (PB95-138483, A06, MF-A02).

NCEER-94-0018 "3D-BASIS-TABS Version 2.0: Computer Program for Nonlinear Dynamic Analysis of Three Dimensional Base Isolated Structures," by A.M. Reinhorn, S. Nagarajaiah, M.C. Constantinou, P. Tsopelas and R. Li, 6/22/94, (PB95-182176, A08, MF-A02).

NCEER-94-0019 "Proceedings of the International Workshop on Civil Infrastructure Systems: Application of Intelligent Systems and Advanced Materials on Bridge Systems," Edited by G.C. Lee and K.C. Chang, 7/18/94, (PB95-252474, A20, MF-A04).

NCEER-94-0020 "Study of Seismic Isolation Systems for Computer Floors," by V. Lambrou and M.C. Constantinou, 7/19/94, (PB95-138533, A10, MF-A03).

NCEER-94-0021 "Proceedings of the U.S.-Italian Workshop on Guidelines for Seismic Evaluation and Rehabilitation of Unreinforced Masonry Buildings," Edited by D.P. Abrams and G.M. Calvi, 7/20/94, (PB95-138749, A13, MF-A03).

NCEER-94-0022 "NCEER-Taisei Corporation Research Program on Sliding Seismic Isolation Systems for Bridges: Experimental and Analytical Study of a System Consisting of Lubricated PTFE Sliding Bearings and Mild Steel Dampers," by P. Tsopelas and M.C. Constantinou, 7/22/94, (PB95-182184, A08, MF-A02).

NCEER-94-0023 "Development of Reliability-Based Design Criteria for Buildings Under Seismic Load," by Y.K. Wen, H. Hwang and M. Shinozuka, 8/1/94, (PB95-211934, A08, MF-A02).

NCEER-94-0024 "Experimental Verification of Acceleration Feedback Control Strategies for an Active Tendon System," by S.J. Dyke, B.F. Spencer, Jr., P. Quast, M.K. Sain, D.C. Kaspari, Jr. and T.T. Soong, 8/29/94, (PB95-212320, A05, MF-A01).

NCEER-94-0025 "Seismic Retrofitting Manual for Highway Bridges," Edited by I.G. Buckle and I.F. Friedland, to be published.

NCEER-94-0026 "Proceedings from the Fifth U.S.-Japan Workshop on Earthquake Resistant Design of Lifeline Facilities and Countermeasures Against Soil Liquefaction," Edited by T.D. O'Rourke and M. Hamada, 11/7/94, (PB95-220802, A99, MF-E08).

NCEER-95-0001 "Experimental and Analytical Investigation of Seismic Retrofit of Structures with Supplemental Damping: Part 1 - Fluid Viscous Damping Devices," by A.M. Reinhorn, C. Li and M.C. Constantinou, 1/3/95.

NCEER-95-0002 "Experimental and Analytical Study of Low-Cycle Fatigue Behavior of Semi-Rigid Top-And-Seat Angle Connections," by G. Pekcan, J.B. Mander and S.S. Chen, 1/5/95.

NCEER-95-0003 "NCEER-ATC Joint Study on Fragility of Buildings," by T. Anagnos, C. Rojahn and A.S. Kiremidjian, 1/20/95, (PB95-220026, A06, MF-A02).

NCEER-95-0004 "Nonlinear Control Algorithms for Peak Response Reduction," by Z. Wu, T.T. Soong, V. Gattulli and R.C. Lin, 2/16/95.

NCEER-95-0005 "Pipeline Replacement Feasibility Study: A Methodology for Minimizing Seismic and Corrosion Risks to Underground Natural Gas Pipelines," by R.T. Eguchi, H.A. Seligson and D.G. Honegger, 3/2/95, (PB95-252326, A06, MF-A02).

NCEER-95-0006 "Evaluation of Seismic Performance of an 11-Story Frame Building During the 1994 Northridge Earthquake," by F. Naeim, R. DiSulio, K. Benuska, A. Reinhorn and C. Li, to be published.

NCEER-95-0007 "Prioritization of Bridges for Seismic Retrofitting," by N. Basöz and A.S. Kiremidjian, 4/24/95, (PB95-252300, A08, MF-A02).

NCEER-95-0008 "Method for Developing Motion Damage Relationships for Reinforced Concrete Frames," by A. Singhal and A.S. Kiremidjian, 5/11/95.

NCEER-95-0009 "Experimental and Analytical Investigation of Seismic Retrofit of Structures with Supplemental Damping: Part II - Friction Devices," by C. Li and A.M. Reinhorn, 7/6/95.